ERRATA

Page	Paragraph	Line	
vi		7	"conference" for "confrence"
xvii	6	3	"Trondheim" for "Troudheim"
1	1	1	"a certain" for "certain"
1	3	4	"interest to researchers" for "interest researchers"
1	4	3	"called" for "called as"
1	4	4	"the 1980s" for "1980s"
2	2	6	“cross-sections” for “cross-section”
2	3	3	“remains at” for “still stays in”
4	1	2	"a certain" for "certain"
4	4	5	"there is still controversy" for "there are still controversies"
5	1	1	"the tensile" for "tensile"
5	1	3	"the advancement" for "the advance"
5	4	3	"a certain" for "certain"
7	3	3	"believes" for "believe"
8	2	2	"de Ruvo 1986" for "Ruvo 1986"
8	2	3	"the sheet" for "sheet"
8	3	4	“with the beating” for “with beating”
9	2	3	"wall affects swelling" for "wall affect swelling"
10	3	6	"a small" for "small"
11	3	5	"determine" for "determines"
12	2	6	"applies only to perfectly random sheets" for "apples only to perfect random of sheets"
13	3	3	"bears" for "bear"
14	1	2	"lead to" for "lead"
15	1	10	"the network and," for "the network"
17	1	1	"Räisänen" for "Raisanen"
17	3	3	Insert “l_f is fibre length” between “$x \in (0, l_f)$,” and “and”
19	2	12	"Räisänen" for "Raisanen"
19	3	13	"depending" for "depend"
23	1	6	Delete "the" before Page's
24	4	1	“Kärenlampi 1995a; Kärenlampi 1995b” for “Kärenlampi 1995; Kärenlampi 1995”
25	2	3	“$n_p / n_f = f(\phi / \beta)$” for “$n_f / n_p = f(\phi / \beta)$”
29	2	3	"de Ruvo 1986" for "Ruvo 1986"
29	2	9	"provided" for "provide"
29	2	11	"exists" for "exist"
34	2	6	"a routine" for "routine"
36	3	6	"the following" for "following"
38	3	8	“determined” for “determine d”
39	4	1	"attempted" for "attempt"
43	2	2	"In other words," for "In other word,"
45	1	2	"stress is transferred" for "stress transferred"
45	2	6	Delete “paper by using the second ad hoc premise.”
46	3	1	Add “(greater than 200kg/m^3)” after “reasonably high density”
48	1	1	“a ratio, *r*,” for “a ratio”
48	3	2	“dry zero span strength” for “zero span strength”
48	3	8	"wider distribution" for "larger distribution"
50	2	1	"the number of" for "the number"
51	2	4	Delete "its"

51	2	3	"A_{bf}" for "A_b"
53			Replace "a" with "b" in Equation 3.9
56	3	8	“a technique” for “technique”
56	3	10	"RBA that have been" for "RBA that been"
56	3	11	"model for the number of" for "model for number of"
56	4	5	"equation is derived" for "equation are derived"
57	2	2	"fibre-fibre contacts per unit" for "fibre-fibre contact per unit"
59	2	5	“(Li and Parker 1999)” for “(Li 1999)”
63	3	7	Delete "into block"
73	1	3	"by the routine confocal" for "by the route confocal"
82	3	2	"Table 5-1" for "Figure 5-1"
84	2	1	Delete “is” between “AD” and “can”
84	2	2	“and using” for “according to its definition by”
84	5	1	"100g OD" for "100g"
85	2	4	“in (Li and Johnston at al. 1999)” for “in (Li 1999)”
92	4	3	“A_{bm}” for “ A_s ”
92	4	4	“Subsection 4.4.1.5” for “Subsection 4.4.5”
93	Equation 6.2		“ $f_m = \frac{\pi^2 (t/P)(1-\pi t/P)}{1-(\delta_D/r)^2}$ ” for “ $f_m = \frac{\pi^2 (t/P)(1-t/P)}{1-(\delta_D/r)^2}$ ”
96	Figure 6-4		Insert paragraph break between the caption and “Table 6-1”
98	2	3	“shifts” for “skews”
100	2	3	"layers" for "layer"
100	1	13	Add “(vertical distance between two neighbouring contacts)” after “distance” “
101	2	1	"fibre cross-sections" for "fibre cross-section"
103	2	15	“for the number” for “for number”
104	2	7	“and total number” for “and number”
104	2	14	"the number …is affected by" for "number…is affect by"
104	2	10	“total numbers” for “properties”
104	2	18	“on the number of” for “on number of”
104	Table 7-1		*“Ncm”* for *“Nc”*
109	1	1	"rejects responded to wet" for "reject to wet"
109	1	3	“shifted” for “skewed”
111	Figure 7-5		“Frequency of the free fibre length” for “Probability” on both x and y axes.
111	1	1	“frequency of the free fibre length” for “probability”
111	1	2	“frequency” for “probability”
113	1	8	“from the literature” for “from literature”
114	1	1	“measured number of fibre-fibre contacts, *Ncm*, and” for “measure number of fibre-fibre contacts and”
114	2	1	“the new model, *Ncp*, are” for “the new model are”
114	2	18	“on the number” for “on number”
122	2	2	Add “b is fibre bond strength per unit bonded area,” after “ A is the average fibre cross sectional area (m^2),”
123	2	1	“shear bond strength per unit bonded area” for “bond strengths”
125	1	4	"fibre morphology have on" for "fibre morphology on"
125	3	3	"the Page equation" for "Page equation"
138	5	2	"the following equation" for "the follow equation"
153	2	7	"at a very" for "at very"
153	3	2	"contact" for "contacts"

160	1	"Kärenlampi, P. (1995a)" for "Kärenlampi, P. (1995)"
160	4	"Kärenlampi, P. (1995b)" for "Kärenlampi, P. (1995)"

.

ADDENDUM

p 9 Figure 2-2: Add at the end of the caption: "(The arrows indicate the stress direction)"

p 15 Figure 2-5: Change the caption to "Load distribution in a fibre predicted by Cox's shear lag model, where L is the fibre length and l is the distance over which the stress is transferred into the fibre."

p 16 Figure 2-6: Add at the end of the caption ", where l is the position along the fibre and l_f is the total fibre length"

p 18 para 4 line 2: replace "Working with very thin sheets that were treated as two-dimensional sheets," for "Working with very thin, two-dimensional sheets,"

p 20 para 3 line 5: Replace "This type of model is called a strength…" for "We call this type of model strength…"

p 20 para 3 line 7: Replace "This type of model is called a pull-out…" for "We call this type of model pull-out…"

p 25 para 2: Replace "the mean axial force required to pull a fibre from the sheet across the rupture line (β)" for "bond strength (β)"

p 25 para 4 line 2: Add "b is bond strength per unit bonded area," at the end of the line

p 61 para 3: Add at the end of the paragraph: "The saturation of the fibres is not a problem for measurements of paper embedded in resin but must be considered when preforming measurements on individual fibres."

p 63 para 2: Add at the end of the paragraph: "Spherical aberration is not a significant effect in this study because our measurement distance inside the sample was only about 10μm and the difference of RI between resin and fibre is very small."

p 67 para 1 line 7: Add "Manual adjustment of the threshold will introduce operator bias. However, as the measured results (see Subsection 4.5.1) showed that the bias was not significant in this study." after "manually adjusting the threshold".

p 72 Figure 4-9: The arrows from left to right should be labelled as "1, 2, 3, 4 and fibre of interest".

p 86 para. 1: Delete the last sentence and add: "The fibre lengths of both accepts and rejects are similar to that of the starting stock."

p 99 para 1 line 4: "This suggests…" for "This indicates…"

p 111 in Figure 7.5: Replace "RejP_1 for "Rej-Po" and replace "RejP_5" for "Rej-P_H"

p 113 end paragraph: Add "In Table 7-2, *Ncm* is now the number of contacts per metre of fibre length."

Quantitative Study of Paper Structure at the Fibre Level for Development of a Model for the Tensile Strength of Paper

Jihong He
Masters of Pulp and Papermaking Engineering
Pulp and Paper Research Institute of China (Beijing China)

Submitted in fulfilment of the requirements for the
Degree of Doctor of Philosophy

Australian Pulp and Paper Institute
Department of Chemical Engineering
Monash University

July 2005

Declaration

I hereby declare that this thesis contains no material which has been accepted for the award of any other degree or diploma in any university, and to the best of my knowledge and belief contains no material previously published or written by another person, except where due reference is made.

JIHONG HE

Date _____

Summary

A new combined technique of resin embedding and confocal laser scanning microscopy is developed for quantitative analysis of paper structure at the fibre level. Fibre dimensions, fibre orientation and fibre collapse have been measured simultaneously in paper by using the new technique and image analysis. This technique is validated by comparing the measured values of fibre wall areas by the new technique in paper with those measured by the routine confocal microscopy technique on freely dried fibres on glass slides. For the first time, a technique is available for quantitative analysis of paper structure at the fibre level.

This technique has been used to study the mechanisms of densification of the paper structure in wet pressing. New parameters are defined for the purpose of quantifying the changes in the transverse dimensions of fibres in paper in wet pressing. It was found that fibre twist, fibre collapse and gap closure are the major types of movement of fibres in paper in wet pressing. Fibre twist, fibre collapse and gap closure occur simultaneously at low pressing pressures, and the gap closure is the predominant mechanism in paper structure densification at low pressing pressures. Increasing pressing pressure only increases the apparent density slightly and the density increase is mainly contributed by the additional twist and collapse of the fibres at the high pressing pressure.

Based on the above new technique, a new technique for measuring properties of fibre-fibre contacts is developed. Properties of fibre-fibre contacts, including the free fibre segment length, number and nature of fibre-fibre contacts and out-of-plane angle of fibre segments are measured in paper. It is the first technique that can determine all of the parameters associated with the fibre-fibre contacts simultaneously in paper. For the first time, data of fibre-fibre contacts in 'real' paper is available for testing models of fibre-fibre contacts. This study shows that the out-of-plane deflection angles of the free fibre segments have no regular trend with the pressing intensity. However, the out-of-plane deflection distance has been reduced by wet pressing since the free fibre length has been reduced. The experimental data seems to fit a two-parameter Weibull probability density function, even if no theoretical basis is given for using the Weibull density function.

This thesis presents a new model that relates the fibre cross-sectional dimensions and the apparent density of paper to the number of fibre-fibre contacts per unit length of fibre. It is the first model that considers the effects of fibre cross-sections on the fibre-fibre contacts and it is also the first time such a model has been fully verified with experimental data. The model is also converted into two expressions for RBA, which is verified with measured results by two different methods.

This thesis also presents a new analytical model for tensile strength of paper based on the assumption that the macroscopic fracture of paper is trigger by the failure of fibres lying in the direction of the applied load. The new model relates the tensile strength to the zero-span strength of the component fibres through a factor r. The value of r is the ratio of the peak load and the average load in the fibres. It is the first analytical model that attempts to predict the start point of paper failure under load. It is shown that the shear lag analysis does not seem to apply to the fracture of paper.

Model structures of a fibre of interest connecting the fibre network matrix were constructed by using the experimental data and the Weibull density function. Simulations of load distribution on the fibre of interest suggest that the value of r is a 'dynamic value', which is determined by the way that the fracture of paper is triggered. It is shown that bond breakage occurs before the sheet fracture, and it significantly affects the value of r. The simulation model is still at very preliminary stage. It can not predict the correct values of r. However, a very good correlation is shown between the tensile index calculated by the peak average load from the bond breakage model and the measured tensile index, although the predicted value is only 1/3 of the measured value. This indicates the promise of the bond breakage model. Further modifying the bond breakage model by including fibre fracture is expected to provide better prediction of the sheet fracture and therefore better calculation of r value for testing the simple fibre fracture model. This project has built up a solid base for further refining the bond breakage model in the future study.

Acknowledgements

I would like to thank my supervisor Dr. Warren Bachelor for his guidance, flexibility and great support which allowed me to make most of my time to finish this thesis and develop my career in the paper industry. Thanks also go to my co-supervisor Professor "Bob" Johnston. He has also been a great supervisor and one who is always willing to advise and to help.

Thank you to Richard Markowski for your assistance in many experiments including pulping, fibre fractionation and paper testing. Thank you also for your friendship.

I would like to thank Andrew Conn for his excellent assistance in writing those macros for image analysis. Thanks Loi Nguyen for providing wood chips and assistance in pulping. Thank you John Barnard and Gamini Ganegoda from the Chemical Engineering Department Workshop for helping build the heating rig for the Nitrogen Adsorption test. I would also like to thank Roy Harrip and Gamini for your assistance in solving computer associated problems.

Thank you to all APPI staff and students for your friendship. The good memories we shared will remain in my mind forever.

I want to thank my beautiful wife Ying and my son Eric for their unconditional love and patience during my long hours away and for the pure joy that they bring to me everyday.

This work is funded by the Australian Research Council (ARC). I gratefully appreciate the funding received from ARC. I also appreciate a small fund received from Visy Paper for part of this work.

TABLE OF CONTENTS

LIST OF FIGURES

LIST OF TABLES

Publications and Conference Papers

Publications

Warren Bachelor and Jihong He, *A new method for determining the relative bonded area,* Tappi Journal. 4(6) P.23-28 (2005)

Jihong He, Warren Bachelor and Bob Johnston, *A microscopic study of fibre-fibre contacts in paper*, Appita Journal, 57(4), 292-298, (2004)

Jihong He, Warren Bachelor and Bob Johnston, *The behavour of fibre in wet pressing.* Tappi Journal, 2(12), P.27-31, (2003)

Jihong He, Warren Bachelor and Bob Johnston, *A New Approach for Quantitative Analysis of Paper Structure at Fibre Level*. Appita Journal 56(5), 366-370, (2003)

Conference Papers

Jihong He, Warren Bachelor and Bob Johnston, *A new analytical model for fibre-fibre contacts in paper and expressions for RBA,* presented at the 2003 international paper physics conference, Canada, September.

Jihong He, Warren Bachelor and Bob Johnston, *Comparison of analytical models for the tensile properties of paper with experimental results,* presented at the 2004 international paper physics conference, Troudheim, Norway, June.

1 Introduction

Every paper grade used in daily life needs certain strength to satisfy not only the end uses but also the converting operations. Papermakers have been making great efforts to produce papers with greater strength to meet the increasing requirements of modern life. For example, the increase in the already very high speed of printers is one of the major driving forces.

A sheet of paper is a network made of millions of fibres bonded together through hydrogen bonds at the crossing points. The strength of the paper is determined by both the properties of the component fibres and the network. These properties include fibre length, fibre strength, fibre-fibre bond strength, bond area, dimensions of the fibre cross-section, fibre-fibre contacts and the sheet density. It is essential to understand the relationship between the strength of paper and the fundamental properties in order to be able to make stronger paper products. Fundamental studies for the tensile strength of paper always try to develop models to describe this relationship.

The difficulty for modelling tensile strength of paper is that paper has a complex structure and the component fibres have properties with certain statistical distributions. This is also evidenced by the enormous work attracted by this topic in the past 50 years. Today this topic is still of interest of researchers.

Two types of methods have been used for developing models for tensile strength of paper: the analytical method and simulation method. Correspondingly models developed by these two methods are called as analytical models or closed-form models and simulation models. Most of the models developed before 1980s are analytical models. In later studies, particularly in recent years, computer simulation has been increasingly employed for modelling the tensile strength of paper.

It has been well recognized that some parameters, including fibre length, fibre strength, fibre-fibre bonded area, bond strength, the dimensions of fibre cross-section and fibre orientation, are important for the tensile strength of paper. A general understanding of the relationship between the tensile strength of paper and these fundamental parameters

has been established based on previous studies. For example, it is well known that longer and stronger fibres usually make stronger sheets. However, the mechanism through which these fundamental parameters contribute to the tensile strength of paper is still inadequately understood. The mechanism, by which the fracture of paper is triggered, is still the subject of research.

The other aspect of modelling the tensile strength of paper is verification of the models developed. The work is only completed when the model has been fully verified by experimental data. A complete set of data is essential for the model verification. However, some of the parameters mentioned above are very difficult to measure. New techniques need to be developed for measuring parameters such as dimensions of fibre cross-section in paper, fibre-fibre contacts in paper and relative bonded area.

The complexity and importance of paper structure makes it always a challenging topic in paper physics. Although enormous work has been done in this area, most of our knowledge in paper structure still stays in qualitative level. No techniques are available for measuring some important quantities of paper structure such as the number of fibre-fibre contacts and the dimensions of fibres in paper. Data of these quantities are critically important for understanding the mechanism by which fibres develop strength of paper. Such data is also desired for testing the previous models of the tensile strength of paper. Clearly, further study in modelling the tensile strength of paper requires quantitative study of paper structure at the fibre level.

The objective of this thesis is to quantitatively study the paper structure at the fibre level to provide valuable data and knowledge for development of a new model for the tensile strength of paper. The project starts with the development of a new technique to quantitatively analyse the paper structure at the fibre level. By using this technique, fibre cross-sectional dimensions, fibre collapse and fibre orientation will be measured directly in paper. This technique will also be used to study the mechanisms of densification of the paper structure in wet pressing. Based on this technique, a technique will be developed to measure the properties associated with fibre-fibre contacts, including the nature of the contacts, number of fibre-fibre contacts, free fibre length and out-of-plane angle. A new model for the number of fibre-fibre contacts will be presented and fully verified with experimental data. Model structures of a fibre of

interest connecting to the fibre network will be constructed based on the experimental data and the load distribution along the length of a fibre will be simulated for no bond breakage, as well as with bond breakage. All of the experimental data and data from simulations will be used for testing the final model for the tensile strength of paper.

Chapter 2 reviews the literature in both studies in paper structure and modelling the tensile strength of paper. Chapter 3 presents a new simple fibre fracture model for the tensile strength of paper and a new model for the number of fibre-fibre contacts. The new techniques for quantitative study of the paper structure are discussed in Chapter 4. Chapter 5 illustrates the important experimental methods used in this thesis. Chapter 6 discusses the mechanisms of densification of the paper structure in wet pressing. In Chapter 7, the new model for number of fibre-fibre contacts is verified with experimental data and the distribution of the free fibre length is also discussed. Tests of the simple fibre fracture model for the tensile strength of paper is discussed in Chapter 8. Firstly, the Page equation is tested with experimental data obtained in this thesis, and then the application of the shear lag analysis for calculation of load distribution along the length of a fibre is discussed. Finally, a new direct load transfer theory is presented and simulations of load distribution along the fibre based on the new load transfer theory are discussed. Chapter 9 summarises the conclusions drawn from the work in this thesis and gives the recommendations for future work.

2 Literature review

2.1 Introduction

Paper is a complex network of fibres that are bonded together through hydrogen bonds at points where fibres cross each other. Every paper grade needs certain strength for both converting operation and end use. Tensile strength is the most commonly used parameter for describing the mechanical properties of a sheet of paper. In other words, the tensile strength of paper is the most important strength property of paper. The tensile strength of a sheet is determined by the properties of the fibre network and the properties of the fibres comprising the network. A better understanding of the relationship between the tensile strength of paper and the fundamental properties of its component fibres and paper structure is important for both paper research and production.

After years of theoretical and experimental research, it has been found that the important parameters for tensile strength of paper include fibre length, fibre strength, bond strength, relative bonded area (RBA), the number of fibre-fibre contacts, dimensions of fibre cross-section and apparent density.

Numerous researchers have attempted to develop models, either using analytical or simulation methods, to relate the tensile strength of paper to the properties of fibres and the structure of paper. Models of this relationship are critical, because they allow for the prediction of the behaviour of paper with structures outside the range of previous experimental data.

Modelling tensile strength always has to answer two questions. The first question is what is the mechanism by which load is transferred from one fibre to its adjacent fibres? This controls the load distribution along the axis of the fibre. The second question is what is the trigger of the fracture of paper (macroscopic fracture)? The trigger could be the failure of fibre-fibre bonds or the failure of fibre segments in the sheet. There are still controversies over both these questions.

Another important aspect for the modelling tensile strength of paper is model verification. However, some of the parameters are very difficult to measure. This makes the studies incomplete and to some extent hinders the advance of these studies.

In this chapter, the important properties of fibre and paper structure for tensile strength of paper are briefly outlined. This chapter reviews previous theories for stress transfer between fibres and the initiation of the fracture of paper. The important parameters in stress transfer are also discussed. This chapter also reviews the important analytical models for tensile strength developed in previous studies. These models are compared with each other and the assumptions they make are discussed. Verification of these models by experimental work is also discussed. Measurement of those parameters that are difficult to measure is discussed extensively.

2.2 Fibres and fibre network

In this section the important parameters of the fibres and the fibre network are discussed.

2.2.1 Fibres

Fibres are the basic component for paper. A sheet of paper consists of millions of fibres. These fibres should have a certain length and strength in order to form a fibre network with certain strength. A fibre also has transverse dimensions including fibre wall thickness, fibre width, wall area and lumen area.

The importance of transverse dimensions of wood pulp fibres has been long recognized. In early studies, fibre coarseness, defined as the mass of per unit fibre length, was commonly used for characterization of fibre cross-section. The effects of fibre coarseness of softwood pulp fibres on paper physical properties have been investigated intensively by Seth (Seth 1990) and Paavilainen (Paavilainen 1993). Both authors emphasized the importance of the effect that fibre coarseness has on paper physical properties. For a given sheet grammage, finer fibres being more numerous, make more

fibre-fibre contacts per unit area, and therefore make stronger sheets. Paavilainen (Paavilainen 1993) showed that the effect of fibre coarseness on the tensile strength of paper is more significant than that of fibre length. She believed that, to obtain high paper strength, the abilities of the pulp fibres to form strong bonds and high intrinsic fibre strength are more important than the number of load-bearing fibres.

A later study found that fibre coarseness alone is insufficient to define and predict pulp quality, as two fibres of similar coarseness can have quite different wall thicknesses if their perimeters are different (Seth 1997). The dimensions of fibre cross-sections should be characterised directly.

The shape of the fibre is also critical because it is not constant. Never-dried fibres tend to collapse under wet pressing. The more collapsed the fibres are, the better the bonds (larger bonding area) they will form. Fibres will flatten out as they collapse to be wider and therefore have greater potential bonding areas.

The transverse dimensions of fibres affect the degree of fibre collapse therefore the conformability of fibres. Several studies have been conducted to quantify the degree of fibre collapse (Kibblewhite 1991; Jang 1995; Jang 1998). Jang (Jang 1998) found a geometrical factor, $LP/2\pi t$, that controls the degree of fibre collapse, where LP is the total lumen perimeter (uncollapsed and collapsed) and t is fibre wall thickness. Jang (Jang 2001) has also presented a new theory on fibre collapse. This will be discussed in detail in Chapter 6.

2.2.2 Fibre network

We normally think of paper as a heterogeneous network of fibres bonded together by hydrogen bonds. The heterogeneity and the fact that there are always distributions for the fibre properties make the paper structure difficult to characterize. Scientists attempt to do this, however, in terms of network parameters. Network parameters attempt to define the structure in terms of the dimensions, physical properties, geometrical orientations of the fibres and the nature and extent of the bonding between fibres. The often used network parameters can be roughly divided into macroscopic and

microscopic parameters. The former includes sheet density and formation, while the latter includes bond nature, bond area, bond strength, number of fibre-fibre bonds per unit length of fibre, relative bonded area (*RBA*) and fibre orientation. The features of these parameters are briefly discussed as follows.

2.2.2.1 Sheet density

The sheet density is simply defined as the mass per unit volume, or basis weight divided by calliper. The sheet density is the simplest measure of paper structure. There is generally a strong linear relationship between sheet density and the bonding degree of the network (El-Hosseiny 1979).

Wet pressing significantly affects sheet density. An understanding of the mechanisms of densification of paper in wet pressing is an important topic of paper structure analysis. Szikla believe that increasing fibre bonding is the dominant mechanism in the densifying effect of wet pressing (Szikla 1989). Gorres et al (Gorres 1993) conclude that there are two mechanisms controlling the relationship between the density of paper and the wet pressing pressure. Fibre collapse and deflection of free fibre segments are the predominant mechanisms at low pressing pressure, while at high pressure all spaces within the sheet which can be filled by such deflections have been filled, therefore completion of fibre collapse and perhaps other effects then predominate. They claimed that a second effect is needed to explain the continuing increase in density at high pressure where fibres are totally collapsed. The understanding of the mechanisms of the densification of paper structure in wet pressing is still incomplete. Sophisticated techniques for analysis of paper structure at the fibre level are essential for a better understanding of the densification of paper structure.

It was first noted many years ago that tensile strength is often a linear function of the apparent density (Clark 1943). A linear relationship is also very often seen in later studies, no matter whether the density of paper was changed by refining or by wet pressing (Luner 1961; Seth 1990; Kibblewhite 1993). No generally accepted explanation is known for this.

Even though the apparent density of paper is not a well-defined quantity, it would be useful for practical applications to understand how density affects paper strength (Niskanen 1993). Thus, a model for tensile strength that includes apparent density is called for.

Niskanen (Niskanen 1993) proposed that the tensile index of paper is a linear function of sheet density at reasonably high densities. De Ruvo and his co-workers (Ruvo 1986) proposed that the tensile index depends on how efficiently the structure of sheet utilises the component fibres. The efficiency normally increases with beating of the fibres and with increasing intensity of wet pressing of the wet web. An increase in density can improve stress distribution in the sheet allowing the fibres to participate more homogeneously in the bearing of load. However, no analytical expression for this has been determined and so the concept has only qualitative predictive capability.

2.2.2.2 Bond nature and bond area

Page et al, (Page 1962) in a piece of classic research, studied fibre-fibre bonds by direct observation using polarized illumination. They found that fibre-fibre bonds in paper could be divided into two main types in terms of bond nature, i.e. simple bonds and obstructed bonds, as schematically shown in Figure 2-1.

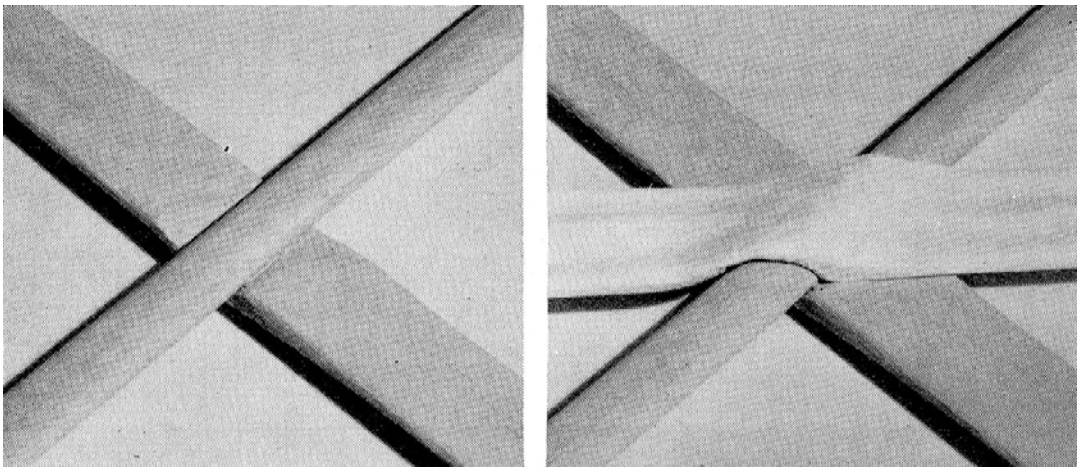

Figure 2-1 Models illustrating, on the left, simple and, on the right, obstructed fibre-fibre bonds (Page 1962).

Fibre-fibre bonds form gradually as the solids content of paper increases. Page et al believed that there are two possible mechanisms by which fibre-fibre bonds may form

(Page 1962). Collapse of one fibre on to another may occur because of the large forces of wet pressing and surface tension. Alternatively, the contact areas may be developed by the accumulation of dissolved and suspended material in the residual water in the regions of a crossing. Campbell's (Campbell 1959) description for bond formation is that surface tension forces, such as colloidal interactions and mechanical interlocking of fibrils, pull fibres closer together when water is removed from the wet web. This is the Campbell effect. However, the solids content at which actual inter-fibre bonds form is not exactly known, since the Campbell effect changes gradually into hydrogen bonds. Lyne and Gallay (Lyne 1954) suggested that hydrogen bonds begin to form in the range of 10 to 25% solids content.

Fibres shrink during drying. The amount of shrinkage depends on the swelling degree of the wet fibre wall (Laivins 1993). The internal fibrillation and chemical composition of the fibre wall affect swelling. Lignin reduces and hemicellulose increases swelling.

Fibres shrink primarily in the lateral direction (Weise and Paulapuro 1996). The competition between the lateral shrinkage tendency and longitudinal stiffness of fibres creates shear stresses in the bond area, especially at its periphery, as shown in Figure 2-2 (Van Den Akker 1962). The shear stresses at inter-fibre bonds generate axial compressive forces on the crossing fibres and may even cause deformations in bonded fibre segments. These deformations are sometimes called microcompressions (Page 1962). They modify the mechanical properties of the bonded segments in comparison with the freely dried fibres. The mechanical properties of the fibres in a paper sheet are therefore related to the presence of inter-fibre bonds.

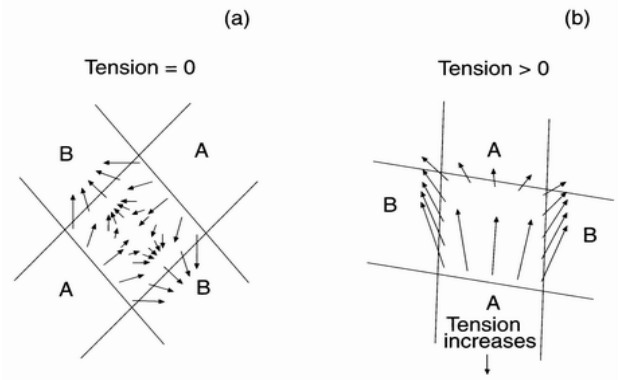

Figure 2-2 Schematic of the stress of a shrinking bond area: a free bond (a) and the same configuration under external load (b) (Van Den Akker 1962).

No simple definition for the bond area is available because the overlap area of two fibres is not necessarily completely bonded. It is believed that fibres in optical contact may not necessarily form bonds because the distance for optical contact is two or more orders of magnitude greater than the distance necessary for hydrogen bonding.

Nanko and Ohsawa (Nanko 1989) did an excellent study on the structure of fibre bonds of a bleached hardwood kraft pulp by using a transmission electron microscope. They identified four major features in the bond: the bonding layer, wrinkles, skirt and covering layer, as illustrated in Figure 2-3 (Nanko 1989).

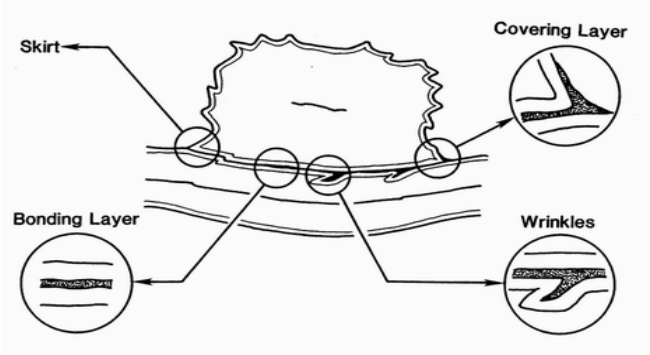

Figure 2-3 Structural features of fibre bonds according to Nanko and Ohsawa (Nanko 1989).

The major variables that may affect the bonding size (or the bonding area) include furnish, beating, pressing and drying conditions. The fibre width is a controlling factor for the bond size. Furthermore, the surface topography and plasticity of fibres in different furnishes will have a major effect. Beating significantly increases the bond size of both simple and obstructed bonds. Wet pressing has similar effects to beating. Dry tension, has only small effect on the bond size and, if anything, tends to reduce it.

2.2.2.3 Fibre-fibre bond strength

The strength of a fibre-fibre bond usually refers to its shear strength. This is the maximum load that the bond can carry when the bonded fibres are displaced relative to one another parallel to the bonding area (Niskanen 1998). The bond strength is fibre dependent. A summerwood fibre bond has higher bond strength than a springwood

fibre bond although the former has smaller bond area. A typical springwood fibre bond can bear less than half a gram before fracture (Stratton 1990).

Another often used parameter is specific bond strength, which is defined as the strength per unit bonding area. However, Button (Button 1979) concluded that the specific bond strength could not characterize the bonding capacity of the fibres. He showed with a bond model that the stress distribution within the bond is nonuniform when the bond is loaded. He also showed experimentally that the bond strength is almost independent of bond length or area but increases as the square root of the thickness of the bonded fibres. This result can explain why the summerwood bonds are stronger than the springwood bonds.

2.2.2.4 Fibre-fibre contacts

The fibre-fibre contact is the most important fundamental parameter for a paper structure. The properties related to fibre-fibre contacts include number of fibre-fibre contacts per unit length of fibre, the nature of the contacts, the free fibre length and its distribution and the out-of-plane deflection angles of fibre segments in the paper. These variables as a whole determines the arrangement of fibres in a network, therefore they determine the mechanical behaviour of the fibre network under external stress.

Fibres are brought together to form fibre-fibre contacts during the densification of a sheet in wet pressing. For a random sheet, the number of fibre-fibre contacts is determined by the sheet density and the cross-sectional shape of fibres in the sheet. One has to know both to determine the number of fibre-fibre contacts in the sheet. There are still no techniques available for quantifying the shape of fibres in a sheet. Therefore it is crucial to develop new techniques to measure the cross-sectional dimensions of fibres in sheets in order to further study the number of fibre-fibre contacts in sheet.

Free fibre length is a critical parameter for paper structure. Different parameters have been used to represent a free fibre length. The free fibre length has been defined as the distance between the centres of fibre crossings (Kallmes and Corte 1960); the intercrossing distance represented by the distance between the centres of bonded

crossings (Kallmes 1963); and the projected interbond distance, which is the distance between the projection of the bonds on the fibre axis (Page 1962). Kallmes and Bernier (Kallmes 1963) have shown that these three definitions of a free fibre length will have different absolute values but will produce similar distributions of free fibre length.

The distribution of free fibre length is also critical for modelling the structure of paper. Kallmes and Bernier (Kallmes and Corte 1960; Kallmes 1963) have shown that a 2-dimensional sheet has a negative exponential distribution of free fibre length. However, the measurements of Page *et al*. (Page 1962) clearly cannot be fitted to a negative exponential distribution. Dent (Dent 2001) recently showed that the negative exponential distribution apples only to perfect random of sheet made of infinitely long fibres. He proposed that a random sheet of fibres of finite length has a general gamma distribution of the free fibre length. This model is based on a 2-dimensional model and has not been verified by experimental data.

The arrangement of fibres in the z-direction can be layered or felted. Differences in the mechanical properties in the z-direction of the sheets are attributed to the differences in interwoven structure or z-directional fibre arrangement in the sheets. A felted sheet structure should give better out-of-plane or z-directional strength than a layered structure because fibres are stronger than bonds (Niskanen 1998). The out-of-plane-angle is then an important quantity for describing the fibre arrangement in the z-direction. A felted sheet will have a higher out-of-plane-angle than a layered structure. However, there are still no effective techniques available for measuring the out-of-plane-angle in a sheet. New microscopy and image analytical techniques can provide new information.

2.2.2.5 Relative bonded area

The relative bonded area (RBA) is the fraction of the total available fibre surface that is bonded and is a quantity that has found widespread application in theories of paper mechanical properties. The standard definition of relative bonded area is $RBA = (A_t - A)/A_t$ where A_t is the total area available for bonding and A is the unbonded area in the sheet after is has been formed. The RBA is a derived property. It is

determined by a combination of the number of fibre-fibre bonds, bond area and area of fibre surfaces.

It is believed, in general, that refining and wet pressing can increase the *RBA* of a sheet therefore increase the tensile strength of the sheet. According to Page's theory (Page 1969), the relationship between *RBA* and tensile strength of paper can be illustrated as Figure 2-4. Such a relationship has also been shown by experimental work by many other researchers (Ingmanson and Thode 1959; El-Hosseiny and Abson 1983; Retulainen and Ebeling 1993).

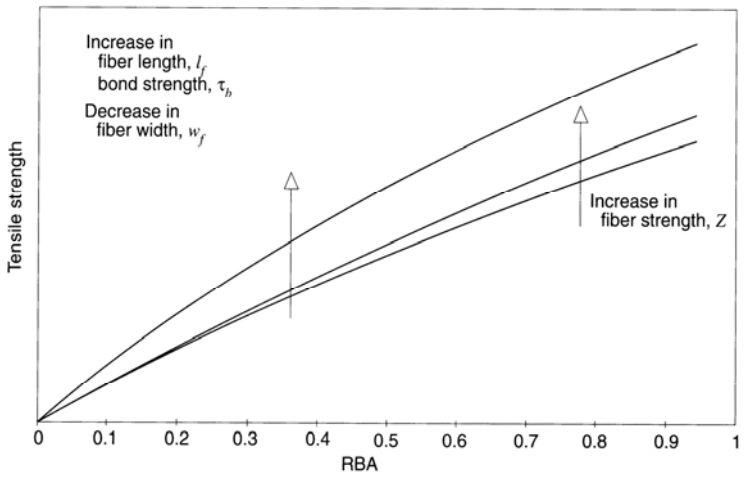

Figure 2-4 The relationship between tensile strength and *RBA* according to the Page equation (Niskanen 1998).

2.2.2.6 Formation

Formation is the variability of the basis weight of paper. Good formation is important for the mechanical properties of the final sheet (Lyne 1954). We expect that uniform paper bear higher stresses than non-uniform paper. Variations in local basis weight have been explained by the tendency of the fibres in a suspension to flocculate forming relatively dense assemblies known as flocs (Radvan 1980). Longer fibres have a greater tendency to floc due to the greater tendency for mechanical entanglement (Roberts 1996). Curled fibres entangle more easily to flocs and settle more rapidly out of suspension, both of which affect the formation of the sheet (Page 1985). Niskanen (Niskanen 1993) has emphasised, in his review paper, the importance of the formation for tensile strength. However, analytical methods can do little to consider the effects of

the formation on the tensile strength of paper. It is believed that computer simulations, in combination with new measurements and effective data analysis will lead fruitful results in this aspect. This project will not consider the effects of the formation on the tensile strength.

2.3 Mechanisms of stress transfer and stress distribution in fibre

As discussed above, paper is usually seen as a network of fibres with finite length. When the paper is loaded, the load has to be transferred somehow from one fibre to its neighbouring fibres. Whatever assumptions are made in network theories it is still necessary to consider how the loads may be transferred from one fibre to another. The mechanism by which load is transferred determines to a great extent the mechanical properties of the paper, and the load transfer mechanism itself is determined by the fundamental properties of fibre and paper structure.

The major variables that determine the mechanism of stress transfer include fibre length, bond stiffness and sheet density. Previous theories attempted to relate the mechanism of stress transfer to these fundamental parameters. These theories are reviewed in this subsection.

Cox (Cox 1952) contributed the first model for stress transfer. The Cox model is established based on an ideal structure in which each fibre is considered as embedded in a continuous solid medium of resin. The resin matrix as a whole is strained homogeneously, but locally this state of uniform stress and strain is disturbed by the transfer of load to the fibres. When the resin matrix is strained the stress is transferred to fibres via the shear stresses in the interface region between the fibre and matrix. The Cox model is often called the shear lag model and this model was the theoretical basis for later studies (Page, Seth et al. 1979; Aström, Saarinen et al. 1994; Räisänen 1996; Räisänen 1997). Ochiai and Hojo (Ochiai 1994), and more recently Johnston (Johnston 1995) reported modified shear lag models that account for the whole stress-strain curve for a fibre reinforced composite.

When the shear lag model is applied to a fibre network, it predicts that stress is transferred from each fibre to its adjacent fibres in the regions of the fibre ends. If we consider sheets of different degrees of bonding, it is expected that the higher the degree of bonding, the shorter the length over which transfer of stress would occur (Figure 2-5). The stress in a fibre is at its maximum at the centre and diminishes to zero at the ends. For constant grammage and fibre coarseness, reduction in fibre length increases the number of fibre ends in the sheet, and decreases the number of fibre-fibre contacts per fibre. Since stress is only transferred across a fibre end, the distribution of stress in the network is more uneven if there are more fibre ends. Thus, an increase in fibre length improves the stress distribution in the network, therefore enhances the tensile strength.

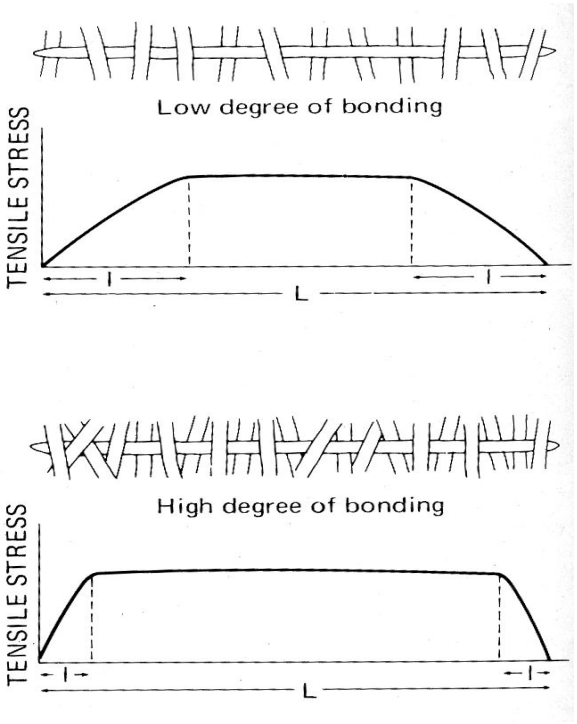

Figure 2-5 Load distribution in a fibre predicted by the Cox's shear lag model (Page, Seth et al. 1979).

The finite element method (FEM) has been successfully used for analysis of stress transfer in fibre network. Rigdahl et al. (Rigdahl 1984) simulated a simple fibre network (a completely square lattice) using FEM. They analysed the effects of the fibre ends, the sheet density and the bond stiffness on the stress transfer. They found that the axial stress is low close to the fibre ends. It increases rather sharply with increasing distance from the ends and tends to reach a plateau level. If, however, a neighbouring fibre has an end beside the fibre under consideration, this will give rise to a relatively

sharp peak in the stress distribution, as shown in Figure 2-6. Rigdahl et al stated that these stress peaks are of great significance for the mechanical properties of paper structures, especially for the **onset** of rupture. The cause of the appearance of the stress peaks is that the load carried by a fibre close to its end must be redistributed to the next fibres. They concluded that the fibre ends are very pronounced in stress transfer and therefore the strength of the paper.

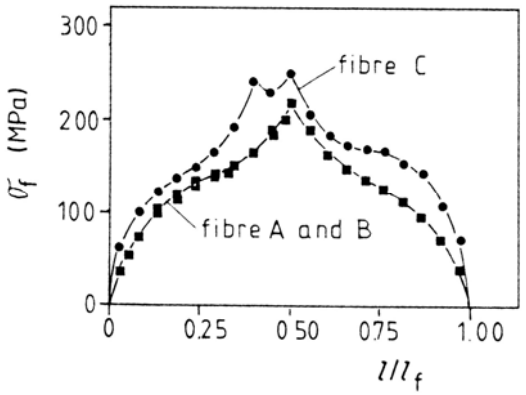

Figure 2-6 Load distribution according to Rigdahl's simulation (Rigdahl 1984).

In the same study, Rigdahl et al also found that a decrease in sheet density reduces the efficiency of stress transfer. The reduction is mainly due to a decrease, with decreasing density, of the number of crossing fibres that transfer the stress between fibres in the network structure. Another important finding by Rigdahl et al is that the bond stiffness does not significantly affect the stress transfer between the fibres unless it is rather low.

The findings of Rigdahl et al (Rigdahl 1984) emphasise the importance of the fibre length (longer fibres have less fibre ends in the network) and the number of fibre-fibre contacts for stress transfer in a paper structure. These findings are significant for the understanding of the mechanisms of stress transfer in paper structure, although the model used is rather simple.

In a later computer simulation study, Aström et al (Aström, Saarinen et al. 1994) analysed the stress transfer mechanisms in fibres constructed within the effective medium approximation first developed by Cox. Their computer simulations showed that the shear lag model holds for random fibre networks at high densities.

Raisanen et al. (Räisänen 1997), in a more recent study, extended the shear lag model to flexible bonds in simulations of random fibre networks. They analysed the stress transfer mechanisms by using a force balance approximation. In the force balance approximation, fibre stress is allowed to be transferred from one longitudinal fibre directly to the next one. In other words, the stress of a given fibre may at any bond be 'taken up' by the crossing fibre, therefore there should be stress fluctuations along the fibres. They concluded that the shear lag model does not apply to random fibre networks.

The shear lag type models give an expression for the stress distribution along a fibre in a sheet as follows (Aström, Saarinen et al. 1994):

$$\sigma_f(x,k) = E\varepsilon_x\left(1 - \frac{\cosh\left[k\left(\frac{1}{2} - \left(x/l_f\right)\right)\right]}{\cosh(k/2)}\right) \qquad 2.1$$

where E is the elastic modulus of the fibre and ε_x is strain of the sheet in the x direction (the direction of the longitudinal axis of the fibre), x is the distance from one fibre end, $x \in (0, l_f)$, and k is a factor determined by the stress transfer mechanism.

The average load in the fibre is obtained by integrating Equation 2.1 and dividing by l_f. Therefore:

$$\overline{\sigma_f} = E\varepsilon_x\left(1 - \frac{2\tanh(kl_f/2)}{kl_f}\right) \qquad 2.2$$

The value of k has been determined by different methods. It was determined analytically by Cox (Cox 1952) and by Page et al (Page and Seth 1980). It has also been determined by computer simulations in more recently studies by Aström et al (Aström, Saarinen et al. 1994) and by Raisanen et al (Räisänen 1997). Determination of the value of k will be discussed in detail in Chapter 9.

2.4 Initiation of the fracture of paper

Fracture here means the macroscopic fracture of paper in a tensile strength test. The tensile strength is the maximum load that occurs at the moment macroscopic rupture begins. Once the rupture has been initiated, it proceeds rapidly during the tensile testing. Therefore the mechanism by which the fracture of paper is initiated is of critical importance for the tensile strength of paper. One has to determine what initiates the fracture of paper before attempting to predict the tensile strength. The fracture of paper can be triggered either by fracture of fibre segments or by fracture of bonds in the paper. Correspondingly, two viewpoints exist - the fibre-fracture triggered viewpoint and the bond-fracture triggered viewpoint.

Page (Page 1969) and Kallmes et al (Kallmes 1977) believed that the fracture of paper is initiated by the failure of the fibres oriented in the direction of the applied load. Cox (Cox 1952) has shown theoretically that the tensile strength of a random two-dimensional sheet does not exceed one third of the strength of its component fibres. On the other hand, other researchers (Van Den Akker 1958) (Niskanen 1993) believed that fibre bonds control the tensile strength of paper. They assumed that paper fails when the external stress equals the bond yielding threshold.

While Page (Page 1969) has provided some evidence supporting the fibre-fracture triggered viewpoint, Van Den Akker (Van Den Akker 1958) has shown that many bonds fail before macroscopic failure has commenced, and many fibres rupture only after the macroscopic failure has commenced. However, none of this evidence is strong enough to support one viewpoint and against the other.

The best way to answer the question is direct observation of the fracture process of a sheet. Working with very thin, two-dimensional sheets, Corte el al (Corte 1961) were able to detect the failure of individual bonds when a sheet was strained. However, such observation is only limited to very thin sheets. Page et al (Page 1962) observed individual fibre bonds of normal sheets under a light microscope. They found that in contrast to the thin sheets studied by Corte et al, the bonds ruptured only partially when paper was strained to failure. The partial rupture of the bonds can be explained not only

by the irregular shape of the bonded area (Page 1962) but also by the stress distribution induced by drying (Van Den Akker 1962).

Giertz and Roedland (Giertz 1979) measured the local strains as a function of the external elongation of a paper sheet. They also observed that the bonds did not rupture completely. The bonds that yielded at small strain often did not deform more at higher strain. When the external load was removed, permanent elongation was found to have taken place primarily in the bonded areas of fibres. In summary, the bonded fibre segments seemed capable of governing the load-elongation behaviour of paper. In addition to this, many researchers have shown that typical single fibres can elongate plastically, much like paper (Dumbleton 1972; Seth 1983). Seth and Page (Seth 1983) showed experimentally that the plasticity of paper is mainly caused by the plasticity of fibres and the effect of bond breakage is usually small. Page recently also showed that most of the work done in plastic deformation is due to the deformation of the fibres (Page 2002). The computer simulations of Raisanen et al. (Räisänen 1996) support Seth and Page's viewpoint.

In summary, there is still no sufficient evidence showing that the macroscopic fracture of paper is triggered by rupture of fibre segments or bonds in the paper. However, it is clear that, before macroscopic fracture, when paper is stretched, fibre segments become permanently elongated and fibre-fibre bonds rupture, both in small steps. The partial bond ruptures and the related yielding of fibre segments relax the local stresses, and this will increase the stresses in neighbouring elements. One can adopt the viewpoint that the plasticity of paper is mainly caused by the plasticity of the bonded fibre segments in the paper. The partial rupture of bonds will relax the stresses in those bonds and this can increase the stresses in nearby fibre segments. The stresses in fibre segments increase as the external stress increases and the number of partially ruptured bonds increase. When the stresses in the fibre exceed its strength, the fibre breaks and triggers the macroscopic fracture of the paper. Once the rupture has been initiated, it proceeds rapidly in the fibre network. Fibres break or pull-out depends on the bonding degree of the fibres.

2.5 Important models for tensile strength

Modelling tensile strength (or elastic properties) of paper has long been an interesting topic in paper physics. Over the past 50 years, a large number of attempts have been made using either analytical methods or computer simulations to develop models for tensile strength. In early years, models developed by analytical methods were confined to a simple and uniform network. However, they produced results of great interest and value. These models are referred to as analytical models (or closed-form models) and usually given by explicit expressions. During 1970s and 1980s, the arrival of computers with considerable computation capacity enabled scientists to study more complicated fibre networks by computer simulations. The models developed by computer simulations are referred to as simulation models. The rapid development in computer science in 1990s further enhanced the studies in paper network simulations, and resulted in more powerful simulation models, taking into account more and more variables, which were believed to be important

Numerous models for tensile strength have been developed in previous studies. Only the most often cited models are reviewed and discussed here.

2.5.1 Analytical models

The analytical models reviewed here can be roughly divided into two groups according to the assumptions they made. One group of models, including the Cox model, Kallmes-Bernier-Perez model, Page equation and Allan-Neogi model, are based on the assumption that the tensile strength of paper is dominated by the strength of the component fibres. We call this type of models fibre strength dominated models. The other group of models assume that a structure of paper can be treated as a fibre reinforced composite. We call this type of model a pull-out model. Examples of this type of model are the Kane and Shallhorn and Karnis models.

2.5.1.1 Cox Model

Cox (Cox 1952) contributed the first model for the elastic modulus of paper. The Cox model considers paper as a perfect homogenous plane consisting of long straight thin fibres oriented either at random or according to some statistical distribution. Each fibre is assumed to extend throughout the whole body of the material and to be loaded only at the ends. This ideal paper allows for no stress transfer between fibres and the strain in every fibre is equal to the local strain of the sheet in the fibre direction. This implies that the relation between the strain in a fibre and the strain in the paper is purely geometrical. From an analysis of strains and stresses in fibres, Cox related the stiffness of paper to the stiffness of fibres through a distribution function of fibre orientation. The distribution function of fibre orientation, f, used by Cox in his analysis is as follows:

$$\pi f(\theta) = 1 + a_1 \cos 2\theta + a_2 \cos 4\theta + b_2 \sin 4\theta \qquad \textbf{2. 3}$$

where θ is the angle of fibre with respect to the horizontal strain, and a_1, a_2 and b_2 are coefficients.

Cox found, for a general situation, the stiffness of paper was affected by fibre orientation in a rather complex manner. If the paper is random, the coefficients, a_1, a_2 and b_2, all become zero, and the relationship between the elastic modulus of paper and the elastic modulus of the fibres is given by the following equation:

$$E_p = 1/3 E_f \qquad \textbf{2. 4}$$

where E_p is the elastic modulus of the paper and E_f is the elastic modulus of fibre, where sheet and fibre moduli are normalised for grammage and coarseness respectively.

This model does not give an explicit expression for the tensile strength of sheet, however for a random sheet, assuming failure occurs when the paper failure strain reaches the fibre failure strain, the tensile strength can be predicted as:

$$T = E_p \varepsilon_f = 1/3 E_f = 1/3 \sigma_f \qquad \textbf{2. 5}$$

Where T is the breaking length of the sheet (km), ε_f is the failure strain of fibre and σ_f is the breaking length of the fibre (km).

Cox verified this model with resin-bonded board in his study. Page and Seth (Page, Seth et al. 1979; Page and Seth 1980; Page and Seth 1980) tested the Cox model with paper and found the Cox model predicts modulus correctly only in the case of strongly bonded handsheets of long straight fibres.

2.5.1.2 Kallmes-Bernier-Perez Model

The Kallmes-Bernier-Perez model (referred to as the KBP model) was first developed by Kallmes and Perez (Kallmes and Perez 1965), and was later extended by Kallmes, Bernier and Perez (Kallmes 1977; Kallmes 1978). Kallmes et al. attempted to describe the whole load-elongation curve of paper. Kallmes et al. made some assumptions that are the same as those made in the Cox model. They assumed that the component fibres of a paper are purely elastic and the axial elastic modulus of each fibre is much greater than its lateral shear modulus. The strain of the sheet is assumed to be uniform. It is also assumed there are no variations of strain along the length of fibre, and that the strain in a fibre is equal to the local strain of the sheet in the fibre direction. The stress and strain in a fibre are related to the stress and strain in the sheet through geometrical analysis. To include fibre orientation, Kallmes et al used a distribution function of $1+a_1\cos 2\theta$ that is the first two terms of the four-term expansion function used in the Cox model (Cox 1952). However, the a_1 coefficient in the function was not determined. When Kallmes el al used the model in practice they set the a_1 coefficient to be zero by assuming the paper was random in fibre orientation.

Kallmes et al. suggested that fibre segments (the distance between two bonds) in paper can be divided into two types: 'inactive' or 'passive' type and 'active' type. The passive segments take no loads when the sheet is strained, and the active segments are those that take loads and are also referred to as load-bearing elements. Before the paper is strained, passive segments of fibres already exist, which were induced by the defects in fibres, such as curl and kinks, and they will not contribute to the tensile strength of paper. Kallmes et al proposed that during the process of paper straining, bond failure

occurs, which causes the plasticity of paper. The difference between the load actually developed by a sheet under strain and that which would have been developed elastically is due to the complete removal of the passive fibre segments as load-bearing elements. In other words, a fraction of passive fibre segments is generated due to bond failure prior to sheet failure. This actually implies that the load in a sheet is taken by progressively fewer fibres during the process of straining, which is also one of the Page's assumptions (Page 1969). In the case of well-bonded sheet, Kallmes et al. assumed that the failure of paper is initiated by the failure of fibres oriented in the direction of maximum sheet strain. In the case of weakly bonded sheet, Kallmes et al. assumed that the failure of sheet is caused by failure of bonds at lower strain.

The fraction of passive fibre segments due to bond failure is given by:

$$f_b = c\frac{driving\ force}{resistance} \qquad \textbf{2. 6}$$

The driving force setting up shear stresses in contact areas is the axial load developed in the fibres. The force that is resisting bond failure is equal to the shear strength of the contact areas. The constant c in Equation 2.6 was not determined by Kallmes et al.

Based on the above considerations, a well-bonded sheet ruptures when the sheet strain is equal to the fibre failure strain. Then the tensile strength of a sheet whose rupture is initiated by fibre failure is given by:

$$T_f = \frac{W}{w}t(1-f_f)\left[\frac{1}{3}-\frac{\pi e}{4}-\frac{ct}{36s\lambda\omega RBA_f}(5-4\pi e)\right] \qquad \textbf{2. 7}$$

where T_f is the tensile strength of a strongly bonded sheet (kN/m), W is the basis weight of the sheet (g/m^2), w is the coarseness of fibre (mg/m), t is the strength of fibre (kN), f_f is the proportion of passive or macro-curled fibres at sheet failure, s is the shear strength of the inter-fibre bonds (N/m^2), λ is the length of a fibre (m), ω is the width of the fibre (m), RBA_f is the degree of bonding of sheets at its final failure and e is the eccentricity of the fibre network, which defines the degree of bias of the fibre-orientation distribution and c is the constant from Equation 2.6.

For a weakly bonded sheet, the point of final rupture is defined as the maximum point on the load-elongation curve and the tensile strength is given by:

$$T_b = \frac{1}{16}\frac{W}{w}\frac{s\lambda\omega RBA_f}{c}(1-f_f)\frac{(4-3\pi e)^2}{(5-4\pi e)} \qquad \textbf{2. 8}$$

Kallmes et al. believe that the failure of paper can be initiated by either fibre failure or bond failure, however, the mechanism by which the paper ruptures is determined by the degree of bonding (RBA_f) at the moment of the incipient sheet failure. A concept of 'critical degree of bonding' (RBA_{cr}) is defined explicitly by setting the strain of the sheet at the maximum point of the load-elongation curve equal to the fibre failure strain. When RBA_f is greater than RBA_{cr} sheet failure is initiated by fibre failure, otherwise, bond failure initiates sheet failure.

There are a number of criticisms that can be made of the KBP model. The basic idea of the Kallmes et al. is that the plasticity of paper is caused entirely by the failure of inter-fibre bonds. Seth and Page (Seth 1983), whose experiments show that the plasticity of paper is mainly caused by the plasticity of the fibres themselves and that the effect of breakage of bonds is usually small, argue against this viewpoint. Seth and Page's viewpoint is also supported by the recent simulation study of Räisänen et al (Räisänen 1996). Another criticism is that straining the sheet actually straightens fibres, reducing the number of passive segments. A final criticism is – how do you measure the proportion of passive fibres?

Kärenlampi (Kärenlampi 1995; Kärenlampi 1995) extended the KBP model by accounting for the distributions of fibre properties. The three nested integrals in the Kärenlampi model, however, are quite difficult to solve. This was overcome by Feldman et al. (Feldman, Jayaraman et al. 1996) by generating random fibres crossing the failure line of the paper and numerically evaluating the stresses.

2.5.1.3 Page Equation

The Page equation (Page 1969) is based on two important assumptions. The first assumption is that during the straining process the load is taken by progressively fewer

fibres crossing the rupture line, which is also one of Kallmes et al's (Kallmes 1977; Kallmes 1978) assumptions. The paper will break catastrophically when the fibres lying in the direction of the loading reach their rupture strain. According to Page, this implies that the fibres across the failure line can be divided into two fractions. One fraction (n_f) is composed of fibres that take the load at failure and then break, the other fraction (n_p) consists of fibres that pull out intact due to prior bond breakage and hence carry no load at paper failure. Using this assumption in combination with the relationship between finite-span tensile strength and zero span tensile strength (Z) and the Cox (Cox 1952) result of a Poisson's ratio of one third for random sheets, the breaking length of a sheet (T) (km) was expressed as the following equation:

$$T = 8n_f Z / 9(n_f + n_p) \qquad \textbf{2. 9}$$

The second assumption assumes that the number of fibres pulled out to the number of fibres broken is only dependent on the ratio of fibre strength (ϕ) and bond strength (β) i.e. $n_f / n_p = f(\phi / \beta)$. The simplest form of the function, $n_f / n_p = \phi / \beta$, was chosen in the Page equation:

$$\frac{1}{T} = \frac{9}{8}\left[\frac{1}{Z} + \frac{1}{Z}\frac{\phi}{\beta}\right] \qquad \textbf{2. 10}$$

After substitution of the bond strength and the fibre strength in Equation 2.10, Page gave the model for tensile strength as:

$$\frac{1}{T} = \frac{9}{8Z} + \frac{12A\rho g}{bPL(RBA)} \qquad \textbf{2. 11}$$

where Z is the zero span breaking length (km), A is the average fibre cross section area (m^2), ρ is the density of the fibre (g/m^3), g is the acceleration due to gravity (m/s^2), P is the perimeter of the fibre cross section (m), L is the length of the fibre (m) and RBA is the relative bonded area.

Verification and the validity of the Page equation and the KBP model have been discussed elsewhere (El-Hosseiny and Abson 1983; Williams 1983) and are also discussed in section 2.6.4. One point that should be noted is that both Page and Kallmes et al. believe that the failure of fibres oriented in the direction of sheet strain initiates the failure of the well-bonded sheet.

2.5.1.4 Allan-Neogi Model

Allan and Neogi (Allan and Neogi 1974) attempted to find an even more fundamental equation than the Page equation. The Allan-Neogi model makes a similar assumption as the first premise of Page's theory i.e. the fibres that have already debonded before the sheet reaches the peak stress do not contribute to the strength. Using this assumption in combination with the concept of zero span tensile strength and a Poisson ratio of 1/3 for a random sheet gives the following expression for sheet strength:

$$T = Z(1 - f_p) = Z(1 - \frac{14\sigma_f}{9b\sigma_b l}) \qquad \textbf{2. 12}$$

where T is the breaking length of the sheet (km), Z is the zero-span tensile strength (km), f_p is the fraction of fibres pulled out cross the failure line, σ_f is the tensile strength of a fibre (N), σ_b is the bond strength per unit bond length (N/m) and l is the fibre length (m).

2.5.1.5 Kane Model

The Kane (Kane 1959a; Kane 1959b) model is a pull-out model assumes that paper is a thin, randomly orientated, fibre reinforced web whose tensile strength is gained either by the load to pull out fibres, and/or breaking fibres crossing the failure line. The behaviour of fibres at the failure of paper sheet depends on the length of fibres embedded into the fibrous matrix (referred to as the effective length by Kane). The critical event is described by the definition of the critical fibre length (λ_c). According to Kane's theory, fibres crossing the separation line pull out if the fibre's embedded length is less than half the critical length, and break if the fibre's embedded length is greater than half the critical length.

The theory also assumes that all fibres crossing the separation line pull out for the case of weakly bonded sheets while fibres break or pull out in the case of strongly bonded sheets. This results in two expressions for the tensile strength of paper.

For weakly bonded sheets tensile failure load is expressed as:

$$T = PN_a\lambda_{ma} = P\left(\frac{2n_a\lambda_a l}{\pi}\right)\left(\frac{\lambda_a}{4}\right) = \frac{Pn_a\lambda^2{}_a\, l}{2\pi} \qquad \textbf{2. 13}$$

where T is the tensile failure load of weakly bonded sheet according to Kane model (N), P is the constant of proportionality which is a function of the static friction between unbonded fibre contacts and the bonding between fibres (N/m), N_a is the number of fibres that cross the line of separation, λ_{ma} is the mean embedded length of N_a fibres (m), n_a is the number of fibres per unit area in the plane of the sheet (m^{-2}), λ_a is the length of a fibre (m), and l is the length of the fracture line (m).

For strongly bonded sheets $(\lambda_a > \lambda_c)$ the tensile failure load is given by:

$$T = PN_b\lambda_{mb} + CN_c = \frac{Pn_a\lambda^2{}_c\, l}{2\pi} + \frac{4cn_a(\lambda_a - \lambda_c)l}{2\pi} \qquad \textbf{2. 14}$$

where N_b is the number of fibres of embedded length less than half the critical length crossing the line of separation, λ_{mb} is the mean embedded length of the N_b fibres (m), N_c is the number of fibres of embedded length greater than half the critical length that cross the line of separation, C is the tensile strength of a fibre (N) and $\lambda_c (= 2C/P)$ is the critical fibre length (m).

The Kane model calculates the tensile failure load of a sheet by accumulating the forces required for pulling out fibres and breaking fibres that cross the failure line without accounting for the fibre orientation. The model actually assumes that fibres are perpendicular to the line of separation.

The Kane model gives a definition of the critical fibre length to describe the fibre behavior at sheet failure. However, the proportionality "*P*" used in the critical length calculation is not well defined. Moreover, the fibre behaviour at sheet failure, as described by the critical length, may only be true for thin paper.

2.5.1.6 Shallhorn and Karnis Model

Like the Kane model, the Shallhorn and Karnis Model (Shallhorn and Karnis 1979) is also a pull-out model. The Shallhorn and Karnis model considers paper as a continuum, in which all fibres have identical properties, and all are aligned in the direction of the applied load. The tensile strength of paper is calculated by summing the forces required either to pull out fibres totally or to break and pull out fibres across the failure line of the sheet. Whether the fibres will pull out or break depends on the length embedded in the matrix.

Johnston et al. (Johnston 1997) extended the Shallhorn-Karnis model to incorporate fibre length and orientation distributions. Johnston et al. showed that mean fibre length alone is a poor predictor of sheet strength. El-Hosseiny et al. (El-Hosseiny and Abson 1983) also found the ratio of fibre length to fibre strength is a more powerful predictor than length alone.

2.5.2 Simulation Models

Simulation methods have been widely used to study the strength properties in recent years. With the help of computer, a fibre network is first generated and its properties are then analyzed by means of the finite element method. Simulation studies attempt to describe the stress-strain behaviour of paper at the fibre level, something that is believed to be insoluble by conventional analytical techniques (Aström and Niskanen 1991; Heyden and Gustafsson 1998).

In the earliest studies, the network models are very simple in structure. For example, Rigdahl's (Rigdahl 1984) model is a two-dimensional mesh. As computer capacity has increased, more complicated network models have been simulated. Many models are random two-dimensional networks in which fibres are modelled as linear elastic beams of identical length. Heyden et al. (Heyden and Gustafsson 1998) introduced curled fibres and studied the effect of curl on the elastic stiffness of networks. Räisänen et al. (Räisänen 1996) introduced elastic-plastic fibres in the network, and found the shape of the stress-strain curve of the network is similar to that of a single fibre. Niskanen et al

(Niskanen 1997) made a novel approach to study the three-dimensional network structure of paper. The KCL-Pakka model combined different furnishes and filler into a random fibre network with a porous planar structure very similar to that of real paper. From the generated structure, all paper properties were simply related to the network geometry.

2.5.3 Comparison Between Models

Many researchers have compared these analytical models with one to the other. Williams (Williams 1983) showed that the Page equation is a limiting form of the KBP model. De Ruvo et al (Ruvo 1986) showed that the limiting form of the Page equation is of the shear lag analysis type and shows a direct resemblance to the KBP model. Niskanen (Niskanen 1993) showed that the Shallhorn-Karnis model could be derived from the two premises of the Page equation. More recently, Jayaraman and Kortschot (Jayaraman and Kortschot 1998) reviewed the analytical models for tensile strength of paper. They compared all of the six analytical models reviewed here and found that a striking similarity exists between the expressions for the weakly bonded paper provide by the Kane model, the KBP model and the Shallhorn-Karnis model, and that an impressive resemblance also exist between the expressions for the strongly bonded paper provided by the Kane model, the KBP model, the Allan-Neogi model and the Shallhorn-Karnis model, outside of the numerical constants. In summary, these analytical models for the tensile strength of paper are in general very similar to each other.

The complexity of the structure of paper and the wide distributions of fibre properties makes it difficult to model paper tensile strength. Thus, the modeling always starts from some assumptions. These assumptions simplify the structure of paper and idealize the properties of its component fibres, but are the major limitations of the network models.

The Page equation (Page 1969) and the KBP model (Kallmes 1977) have a common assumption that the fracture of paper is initiated by the failure of the fibres oriented in the direction of the applied load. On the other hand, some researchers (Van Den Akker 1958) believed that fibre bonds control the tensile strength of paper. Paper fails when

the external stress equals the bond yielding threshold. This viewpoint is encouraged by the experimental observation that many bonds fail before macroscopic failure has commenced, and many fibres rupture only after the macroscopic failure has commenced (Van Den Akker 1958). However, this observation gives no information about the 'trigger' of the rupture of the paper. There is still a controversy over whether bond or fibre failure initiates the rupture of paper.

All of the closed-form models, reviewed here except the KBP model, focus on calculation of forces required for breaking or pulling out of fibres only at the moment of sheet rupture. The KBP model (Kallmes 1977) tried to describe the stress-strain curve of sheet with the basic idea that the breakage of fibre-fibre bonds is solely responsible for the plastic behaviour of the sheet. Seth and Page (Seth 1983) argued against this point by showing experimentally that the plasticity of paper is mainly caused by the plasticity of fibre and the effect of breakage of bonds is usually small. The computer simulations of Räisänen et al. (Räisänen 1996) support Seth and Page's viewpoint.

2.6 Experimental verification of models

It is essential to verify the models in order to fully realize the potential of the models. Verification of the models with experimental data is also important for further refining the models. Therefore it is important to be able to measure the quantities involved in the models. Table 2-1 gives the variables that are required to calculate strength from a given model. Some of the quantities can be easily measured. However, most of the quantities are very difficult to measure. This subsection discusses the techniques for measurement of all of these quantities.

Table 2-1 Variables need for calculating sheet strength from a given model

	Variable	Nature of Measurement	Method of Measurement
Fibre properties	Fibre length	Easy to measure	Various commercial fibre analysers
	Fibre strength	Difficult to measure directly	Zero-span, single fibre measurements
	Fibre shape	Difficult to measure directly	Coarseness (indirect measurement), Microscopic methods (direct measurement)
Fibre network properties	Apparent sheet density	Easy to measure	Standard methods
	Fibre-fibre contacts	Difficult to measure	Microscopic methods
	Relative bonded area (RBA)	Difficult to measure	Optical method, Nitrogen adsorption, Microscopic methods
	Bond strength	Very difficult to measure	No reliable method exists

2.6.1 Easily measured quantities

2.6.1.1 Fibre length

Several methods have been employed for length measurement of wood fibres. In early studies, fibre length has been successfully measured by optical microscopy. This method was found to be too tedious. Fibre length has also been measured by using classifiers, such as the Bauer-McNett fractionator (Clark 1985). This is a series of cascading vertical screens, which separate stirred holding tanks of pulp. Most fibres pass through the coarser screens and as the screens get finer, the fibres that pass through them are generally shorter in length. The Bauer-McNett readings are traditionally translated into values of fibre length measurement by calculations using TAPPI method T-233.

The Kajaani Fibre Analyser is the most widely used device for measuring the distributions of fibre length (Bentley 1994). The Kajaani Fibre length Analyser measures single fibres which are drawn from a dilute 0.01% consistency through a narrow capillary, under suction. The fibres pass through a beam of polarised light.

Cellulose fibres, being birefringent to polarised light, create an interval of birefringence as they pass through. The interval is related to the fibre length of the fibres. The method is fast as it can measure thousands of fibres in a short space of time, and it can report statistical information on the fibre distributions. The significant difference between the Kajaani analyser and the Bauer-McNett classifier is that the former measures the number of fibres in each fraction whereas the latter measures the fraction weights. Bentley et al. (Bentley 1994) found that the precision of measurement of the two methods is comparable, generally to within ±3 - 4%. In recent years, several other instruments to measure fibre length have also been developed, such as the FQA (Robertson, Olson et al. 1999), FibreMaster (Mohlin, Dahlbom et al. 1996) and CyberSizer (Lehto 2004).

2.6.1.2 Sheet density

The sheet density is usually calculated based on the measurements of the grammage and thickness of the sheet. The thickness is defined as the thickness of sheet under standard conditions of platen size and pressure. Some researchers have questioned the accuracy of the measurement of the thickness, and hence, the calculation of sheet density (Taylor 1964; Fellers 1986; Yamauchi 1987). They put forward several reasons for this. First, paper is compressible and the thickness, thus density, depends on the load applied during the measurement. Second, the surface roughness of paper affects the thickness measurement, which introduces an error in the density. The "density" and the compressibility of the surface regions are different from those in the bulk. Although these do affect the measurement of paper thickness, and therefore the calculation of density, the standard methods for measuring the sheet density are still commonly used. In this project, the APPITA standard method AS/NZS 1301.426s-94: 1992 was used for measuring sheet density.

2.6.2 More difficult to measure quantities

2.6.2.1 Fibre strength

Many attempts were made at measuring single fibre strength. Mark and Gillis (Mark 1994) presented an excellent summary of the techniques used to measure single fibre strength. The procedure for handling the samples is usually tedious and time consuming. More recently, Denis (Denis 1996) showed that there were difficulties in obtaining reliable and statistically valid results when measuring the single fibre strength of eucalypt fibres.

Due to the difficulties of measuring single fibre strength, the zero span tensile strength is the most commonly used method to determine the strength of fibres in the sheet (Van Den Akker 1958; Page 1969; Boucai 1971; Kallmes 1977). It has been shown that the zero-span tensile test provides a valid measure of fibre strength (Van Den Akker 1958) provided that the sheet grammage is kept at 60g/m^2 or under (Batchelor 2003). The zero-span tensile test indicates the strength of fibres while they are in the sheet. This is also important as the degree of drying restraint strongly influences fibre strength and it is difficult to replicate sheet drying conditions when preparing single fibres for testing. Another possible advantage of the zero-span test is that it is affected by distributions in fibre strength (El-Hosseiny and Bennett 1985). That is, the larger the distribution in fibre strength, the more the zero-span tensile strength will be reduced below the strength based on the expected average. A larger distribution of fibre strength should also have a similar effect on paper strength.

2.6.2.2 Fibre shape

In early studies, researchers used fibre coarseness to describe the cross-sections of fibres (Seth 1990; Paavilainen 1993). By measuring the total length of a known weight of sample, an average of coarseness of the fibres can be calculated. The coarseness can be adequately measured on most fibre length analysers but not the Kajaani F200 (Seth 1997), as the Kajaani F200 does not reliably count all particles.

In later studies, researchers tend to directly measure fibre wall area, fibre wall thickness, fibre lumen area, fibre width and thickness to characterize the cross-sections of the fibres. The first reliable measurement of fibre cross-sectional dimensions seems to be contributed by Kibblewhite and Bailey (Kibblewhite 1988). They used a technique of embedding fibres vertically in a resin block and sectioning the block to expose the cross-sections of the fibres. The cross-sections of the fibres were then measured in either a SEM or light microscope. The fibre cross-section parameters they measured were width, thickness, cross-section wall area, fibre wall thickness and the fractions of wall and lumen areas.

In recent studies, the most commonly used technique is confocal laser scanning microscopy combined with image analysis. This technique has been used for measurement of fibre transverse dimensions and shapes of different pulp fibres (Jang 1992; Jang 1995; Seth 1997; Xu, Filonenko et al. 1997; Conn 1999). Nowadays, the measurement of fibre transverse dimensions and shapes using a confocal microscope combined with image analysis has become routine process.

The above studies measured the fibre transverse dimensions either on fibres freely dried on glass or embedded in resin. The measured dimensions were then used to predict the structure and physical properties of the paper made with the pulp. It is more important to measure the fibre transverse dimensions in a real paper structure since the shape of the fibres in a sheet dried under restraint may be different from that of freely dried fibres on glass slides. The shape of fibres in a sheet can also be changed significantly by the papermaking process, such as wet pressing, for example.

Several researchers have attempted to measured fibre dimensions in paper. Gorres, et al. (Gorres 1993) measured the transverse dimensions of fibres in very thin fibre networks pressed on glass slides. Hasuike et al (Hasuike 1992) have re-constructed the 3-D structure of paper, from a series of cross-sectional images of the paper, by using computer tomography. The sample size examined by this technique was quite small (0.2x0.2mm), therefore may not be fully representative. Recent studies also generated 3-D images of paper structure by using synchrotron x-ray source (Christine 2002). Although the authors did not measure the dimensions of individual fibres in the sheet, it seems that the quality of the images is not good enough for such measurements.

Dickson (Dickson 2000a) obtained quality images of paper cross-sections by employing a combined technique of resin embedding and laser scanning confocal microscopy. Dickson measured the dimensions of the fibres in the sheet cross-sections. However, the orientations of the fibres are still unknown, thus the shapes of the fibres are still unknown. It appears that new techniques that can measure fibre dimensions directly in paper sheet are called for.

2.6.2.3 Fibre-fibre contacts

As has been discussed before, fibre-fibre contacts in paper, including the number of fibre-fibre contacts per unit length of fibre, the nature of contacts, the free fibre length and its distribution and the out-of-plane deflection angle of a fibre segment, are the most important fundamental properties of a paper structure. Most previous studies of fibre-fibre contacts focused on the development of models for the number of fibre-fibre contacts using statistical methods either based on analysis of model structures of paper (Kallmes and Corte 1960; Kallmes 1961) or fibre assemblies (Komori and Makishima 1977; Pan 1993; Komori and Itoh 1994). These models have provided valuable knowledge for understanding of the fibre-fibre contacts in paper. However, verification of these models is always problematic because there is little experimental data on the properties of fibre-fibre contacts in paper. There is always a requirement for new techniques for measuring comprehensive data of fibre-fibre contacts directly in a sheet.

Some techniques have been used for measuring fibre-fibre contacts directly in a sheet, including examining the paper plane (x-y plane) of very thin fibre networks by their magnified projected images (Kallmes and Corte 1960), examining the x-y plane of a normal sheet under vertical illumination in polarized light (Kallmes 1961; Page 1962), and examining serial cross-sections of paper embedded in resin (Yang 1978). The technique of Page *et al.* (Page 1962) and the technique of Kallmes *et al.* (Kallmes 1961) can only measure fibres on the paper surface, and can only measure interbond distances between bonds on one side of the fibre. Page *et al*. (Page 1962) estimated the interbond distances within the sheet by superimposing two sets of measurements, one set representing the upper surface of the fibre and the other the lower surface. Yang *et al.* (Yang 1978) examined a series of images of paper cross-section acquired at different

depths from the paper cross-sectional surface, and measured the probability of fibre-fibre contacts with a given fibre cross-section. This technique overcomes the limitations of only measuring the surface fibres, however, it cannot measure the interbond distances. In a later study, a new technique of evaluating the 3-dimensional geometric arrangement of fibres in a paper sheet was developed based on the measurement of the locations of fibre segments in the successive cross-sections of the sheet (Hasuike 1992). The relative coordinate positions of fibre peripheries in the sections were recorded by a digitising system attached to a computer. Using this technique, the authors measured the possibility of fibre-fibre contacts with respect to a given fibre cross-section and the number of fibre-fibre contacts per unit length of fibre. The sample size examined by this technique was quite small (0.2x0.2mm), and therefore may not be fully representative. It appears that a more powerful technique is required for measurement of fibre-fibre contacts directly in a paper sheet

2.6.2.4 Relative bonded area (*RBA*)

The measurement of *RBA* is always problematic. Traditionally, the Ingmansson and Thode pressing /beating/ extrapolation method (Ingmanson and Thode 1959) was often used for *RBA* measurement.

This method measures the Kubelka-Munk light scattering coefficient, S (m^2/kg), of paper made from pulps with different beating degrees or of paper pressed under different wet pressing pressures. The results of light scattering coefficient are then plotted against the tensile strength of the paper. The light scattering coefficient, S_0, of the unbonded sheet is obtained by extrapolating the plot to zero tensile strength of paper. *RBA* is then calculated from following equation:

$$RBA = \frac{(S_0 - S)}{S_0} \qquad \textbf{2. 15}$$

The scattering coefficient S is the reflectance of a single sheet backed by a black cavity. The principle of the light scattering coefficient method is that a fibre surface element appears bonded if there is another fibre surface at a distance smaller than half the wavelength of the light used in the measurement. Two such fibre surfaces can form an optical contact. The Ingmansson and Thode pressing/beating/ extrapolation method

relies on at least two presumptions. Firstly, it is implicitly assumed that the light scattering properties of the sheet can be used to distinguish between bonded and unbonded areas even though the wavelength of light is at least one hundred times the bond length for hydrogen bonding. The second assumption is that the value, S_0, determined by extrapolating the plot of tensile strength and light scattering coefficient is equal to the scattering coefficient of an unbonded sheet.

Ingmansson and Thode's study (Ingmanson and Thode 1959), showed that the relationship between S and tensile strength was independent of the degree of beating, and the data for various degrees of wet pressing at all refining intervals fell on one common curve. They concluded that the total dry fibre surface area available for fibre bonding, which is effective in developing tensile strength, remains constant with refining time and is unaffected by production of fines or the degree of fibrillation. In contrast, Swanson and Steber (Swanson 1959) found the plot of tensile strength and the scattering coefficient data obtained with various degrees of wet pressing and at different beating intervals did not fall on one common curve. Instead, the data points seemed to form separate curves for each refining interval rather than a single common curve. Nordman and Gustafsson (Nordman 1951) also noted separate curves for the scattering coefficient-tensile strength relationship for a variety of pulps beaten in the Valley beater. They suggested that this was due to the fibrillar structure of some pulps being retained during drying. Tensile strength can also change in beating in part for other reasons than an increase in RBA.

Niskanen (Niskanen 1998) has also criticised the method on the grounds that the tensile strength will fall to zero long before the bonding completely disappears in the network. The method is also completely unsuitable for measuring bonding in machine made papers, since a range of sheets with different strengths cannot be obtained.

Since the extrapolation of tensile strength usually does not give a reliable value for S_0, some other studies worked on forming unbonded sheets and measuring S_0 directly (Parsons 1942; Ratliff 1949; Keeny 1952; Braaten 2000). Parsons (Parsons 1942) was the first to make an unbonded sheet. The sheet was formed in a non-polar liquid and suffered from poor formation. Ratliff (Ratliff 1949) improved the technique but still the

sheets were formed in a non-polar liquid. Keeny (Keeny 1952) first formed sheets from water in an ordinary sheet former and then displaced the water by an alcohol and a non-polar liquid. These techniques are usually laborious and involve using hazardous chemicals. Drying the sheets from the non-polar liquid avoided forming inter and intra-fibre bonds. The non-polar liquid dried unbonded sheets avoid the formation of inter fibre bonds but the intrafibre bonds as well. Too high a scattering coefficient was yielded because of the intra-fibre scattering. A freeze drying technique has also been used to form unbonded sheets (Merchant 1957; Braaten 2000). Although the freeze-dried unbonded sheets were dried in a water base the inter-fibre bonds and intra-fibre bonds could not form. The additional intra-fibre scattering still results in an overestimate for the value of S_0.

El-Hosseiny and Abson (El-Hosseiny 1979) have tried to relate scattering coefficient to density. They found that for a wider range of pulps, scattering coefficient was linearly related to sheet density. This in turn was used to estimate *RBA*. However, this method has not been further applied.

Nitrogen adsorption is another important technique that has been used to measure fibre surface area to calculate *RBA*. Haselton (Haselton 1954; Haselton 1955) is the first to propose the use of gas adsorption as a method of measurement of the surface area and bonded area of papers. After comparing bonded areas calculated by four methods he concluded that a value closest to the true bonded area could be obtained by applying a correction factor to the regular optical values. When nitrogen adsorption is employed for area studies, the surface area accessible to nitrogen molecules of approximately 4.3Å thickness (N_2 diameter is 16.3 $Å^2$) is determine d. The bonded area in the external and internal portions of fibres is believed to be separated by distances of 4 to 5Å or less. Therefore, it is reasonable to believe that nitrogen is not absorbed on areas involved in bonding and that adsorption methods may provide an excellent tool for the measurement of the unbonded internal and external area of cellulose materials. The Brunauer, Emmett and Teller (B.E.T.) theory (Brunauer 1938) was used to calculate the volume of gas required to form a monolayer on a given adsorbent. The BET equation is given as:

$$\frac{p/p_0}{v(1-p/p_0)} = \frac{1}{v_m c} + \frac{c-1}{v_m c}(p/p_0) \qquad \textbf{2. 16}$$

where p/p_0 is relative pressure, v is the volume of adsorbed gas (cm^3/g STP) per gram of adsorbent at a certain relative pressure, v_m (cm^3 STP) is the volume of gas per gram of sample required to form a monolayer, and c is a constant.

The plot of $\frac{p/p_0}{v(1-p/p_0)}$ against p/p_0 should therefore be a straight line with slope $s=(c-1)/v_m c$ and intercept $i=1/v_m c$. Solution of the two simultaneous equations gives v_m and c. Multiplying the number of gas molecules corresponding to v_m by the cross-sectional area of each molecule gives the area of the solid accessible to the gas.

$$A=\frac{Nv_m L}{22{,}400}x10^{-20} \qquad \textbf{2. 17}$$

where A (m^2/g) is the specific area of the sample, N is Avogadro's number and L (m^2) is the molecular cross-sectional area of the gas absorbed.

Another group of researchers attempt to measure *RBA* by analysis of sheet cross-sections (Yang 1978; Paavilainen 1994; Niskanen 2002). These measurements are time consuming, involving a great amount of microscopy work. Niskanen and Rajatora (Niskanen 2002) compared their measured values of *RBA* with those reported by Yang et al (Yang 1978) and Paavilainen (Paavilainen 1994). The comparison showed that their values of *RBA* were smaller than the values measured by the other two studies. Niskanen and Rajatora (Niskanen 2002) emphasised the importance of the threshold separation for any measurement of *RBA* by analysis of cross-sections of paper. The values of *RBA* reported by these studies are, in general, smaller than those measured by indirect methods, for example in (Retulainen and Ebeling 1993; Braaten 2000).

Although numerous studies have been conducted on *RBA* measurement, the requirement still exists for new and reasonable simple techniques that can determine *RBA* with reasonably accuracy.

2.6.3 Very difficult to measure quantity

2.6.3.1 Bond strength

The bond strength, defined as the strength per unit bonded area, is a straightforward concept, but it is a parameter that is extremely difficult to measure. Numerous studies have focused on measurement of the strength of fibre-fibre bonds.

Earlier researchers (Nordman 1957; Nordman 1965; Skowronski 1991) focused on sheet measurements. Nordman (Nordman 1957) defined a so-called "Nordman Bond Strength" (NBS) as the ratio of the irreversible work of straining the sheet to the change in the scattering coefficient. Subsequent work by Nordman et al (Nordman 1965) revealed that the bond strength appears to be a characteristic of pulp. They found that the bonding strength of fibres was essentially constant in pulps of low hemicellulose content, while for high hemicellulose content pulps it appeared to increase with beating and decreased with wet pressing. Over the years many researchers have used the NBS in their studies. While some evidence supports it, other evidence contradicts it. Page (Page 2002) has shown that the Nordman procedure for determination of bond strength is fundamentally flawed as the work of straining a sheet is not consumed by bond breakage. It is consumed by the fibres as they deform plastically. Fibre-fibre bonds break because, when a sheet is strained, shear stresses are induced at the perimeter of each bond site. The bond breakage is seen as a strain-induced phenomenon rather than an energy-induced phenomenon.

Several investigators have directly measured the shear strength of individually prepared single fibre-fibre, fibre-shive, or fibre-cellulose-film crossings (McIntosh 1962; Page 1962; Schniewind 1964; Mohlin 1974). Such measurements are tedious, and the results suffer from large variability because of damage during testing, failure by peeling rather than shear, and errors in measuring the bonded area in the crossings. Moreover, these methods measure the strength of the bond structure rather than the shear strength of the interface, as pointed out in Uesaka's review (Uesaka 1984) of the measurement of fibre-fibre bond properties. Baum (Baum 1993) made a similar point. Since the S1 and S2 layers of the fibre cell wall have very different fibril angles, the two layers may respond differently to bonding stresses. This suggests that the S1-S2 interface may be a weak

zone. If the failure between two bonded fibres originates within one of the cell walls, rather than area between the fibres, as indicated in Figure 2-7, the meaning of bond strength becomes obscure. Nanko's (Nanko 1989) work suggests that such events are not rare. More recently, Stratton and Colson (Stratton 1993) also have reported similar fibre wall damage during bond failure. In addition to the above concerns, a single fibre-fibre bond test may not be able to represent the bonds in a sheet because fibres in the sheet will likely have properties markedly different from fibres dried outside the network (Baum 1993).

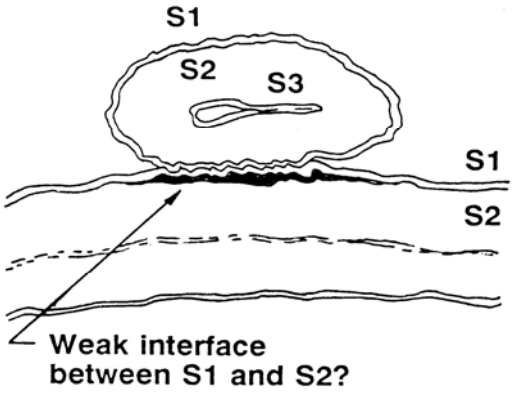

Figure 2-7 A schematic diagram illustrating a weak S1-S2 interface (Baum 1993).

In summary, as pointed out by Niskanen (Niskanen 1993) in his review paper, the microscopic interpretation of bond strength is still unclear.

2.6.4 Attempts at partial verification of models

Many attempts have been made to verify the models developed in previous studies. It is not necessary to review the verifications of every model. We will only discuss the verifications of the Page equation and the KBP model. The major point we will try to make is that it is usually very difficult to fully verify a model for tensile strength.

Page (Page 1969) tested his model by using data from the literature that indeed showed linear relationships between $1/T$ and $1/L$ and between $1/T$ and $1/RBA$ (refer to Equation 2.11). He further verified the model by calculating the zero-span tensile strength of the paper from the intercepts on the ordinates of these graphs. This was done by finding the values of $1/T$ for the cases $1/L = 0$ or $1/RBA = 0$ from these

graphs and calculating zero-span strength, Z, from the expression $Z = 9T/8$. The calculated values of Z have shown quite reasonable agreement with the measured values. Obviously, such verification of the model is quite limited.

Kallmes *et al* tested the KBP model by using data mainly from Seth and Page's work (Seth and Page 1975). They compared the calculated values of zero-span strength with the predicted values. The zero-span strength was calculated by arbitrarily setting the ratio of the proportion of active fibres at sheet failure to that at initiation of sheet strain equal to 1. The comparisons showed good agreements. Interestingly, they used the same data of Ingmanson and Thode (Ingmanson and Thode 1959) (which has also been used by Page) to show that the relationship between T/Z and RBA is linear when RBA is less than RBA_{cr} and non-linear when RBA is greater than RBA_{cr} thereby partially verifing the theory.

In fact, all of the models developed in previous studies have never been completely verified because some quantities, as discussed above, are very difficult to measure. It is of critical importance to develop new techniques to measure those parameters that were not able to be measured in previous studies.

2.7 Summary

Paper obtains its tensile strength from the strength of the fibres bonded together through hydrogen bonds in the network. How efficiently the fibre network uses the strength of the fibres depends on the properties of the network and the fibres. These properties include fibre length, bond area, fibre-fibre contacts, relative bonded area, sheet density and formation. One should note that these properties are not necessarily independent. Some of the relationships between them will be discussed in detail in later chapters.

Modelling the tensile strength of paper has to answer two questions. What are the mechanisms by which the stress is transferred from one fibre to other fibres bonded with it? What initiates the macroscopic fracture of paper? Many researchers have attempted to answer these two questions. Cox developed the shear-lag model based on an effective medium approximation for a fibre in equilibrium with average surroundings.

The shear lag model was later applied to fibre networks by Page and Seth. This model predicts that stresses transferred from one fibre to its adjacent fibres via shearing the bonds in the regions of the fibre ends. Therefore, the stress along the length of the fibre is at its maximum at the centre and diminishes to zero at the ends. The shear lag model has been shown to be valid for random fibre networks at high densities by computer simulations. There is still a controversy over the initiation of the macroscopic fracture of the paper. Two viewpoints exist – the bond failure triggered and the fibre fracture triggered. Some researchers tried to answer the question by providing some indirect evidence. Others tried to directly observe the fracture process of the paper. However, there is still no satisfactory evidence to support one viewpoint against the other. Kallmes *et al* described the initiation of the macroscopic fracture in their analysis of the zero-span tensile strength of paper. They concluded that it is the rupture of comparable fibres that triggers the final catastrophic failure of a sheet in a conventional tensile test. When the first fibres of a sheet fail in a conventional tensile test, a large amount of energy is released in an impact-type manner to their immediate neighbours. One can readily visualise that these fibres, or the bonds between them, fail in turn, causing further failures. In other words, the rupture of the first fibres triggers the catastrophic final failure of the sheet. This rupture once initiated at a point in the sheet, is propagated rapidly in two directions. The above mechanism for the initiation of the fracture of paper is quite reasonable although the authors could not provide direct proof for it. One question that needs to be answered is how we get fibre fracture if bond failure is the trigger.

Studies of modelling tensile strength of paper would only be completed when the final model has been fully verified with experimental data. In other word, verification of the models is a critical part of such studies. However, verification of the previous models is always problematic because some of the quantities involved in these models are very difficult to measure, such as bond strength, fibre dimensions in paper, relative bonded area and fibre-fibre contacts etc. As has been discussed, although numerous attempts have been made to develop new techniques for measuring these quantities, there are still, to the best of our knowledge, no techniques available for measuring these quantities with reasonable accuracy. It appears that development of new techniques, especially microscopic techniques, for measuring these quantities is of first importance for any further studies of modelling tensile strength of paper. Such techniques are not

only important for providing experimental verifications of the final model, but also important for better understanding the paper structure.

3 Theory

3.1 Introduction

As was discussed in Chapter 2, to model the tensile strength of paper, the following questions must be answered. What are the mechanisms by which the stress transferred from one fibre to other fibres bonded with it? What initiates the macroscopic fracture of paper?

Although numerous studies have been conducted to observe the fracture process of paper, no agreement has been reached as to what initiates the macroscopic fracture of paper. The Page equation (Page 1969) and the KBP model (Kallmes 1977) made a common assumption that the fracture of paper is initiated by the failure of the fibres oriented in the direction of the applied load. The Page equation linked the fibre strength to the zero-span tensile strength of paper by using the second ad hoc premise. The KBP model calculated the sheet strength by making another assumption that paper fails when the sheet strain reaches the failure strain of the fibres. It is clear that both models ignore the load distribution along the axis of a fibre in the sheet, as they used the average load in the fibre to predict the fracture of the paper under stress. Other workers (Van Den Akker 1958; Niskanen 1998) have proposed that it is the failure of the bonds that triggers paper fracture.

In fact, all of the previous analytical models for tensile strength of paper fail to predict the initiation of the fracture of paper. They assumed that all bonds or segments reach the failure threshold simultaneously. This is only true when the sheet is purely homogeneous. In reality, however, the stresses in fibres are not uniform because of the stress transfer. The stress distribution in a fibre in a network will also depend on the local structure of the network.

In section 3.2 of this Chapter, a new simple analytical model for the tensile strength of paper is presented. In the new model, an expression is developed relating paper strength to the stress distribution along the loaded fibres in the paper. This stress distribution function will obviously be determined by the local network structure, including the

positions and nature of the crossing fibres. The new model adopts the assumption made by the Page equation and the KBP model that the fracture of paper is initiated by the failure of the fibres oriented in the direction of the applied load, but considers the load distribution in these fibres. In other words, the local bonding structure of the paper is considered when calculating the paper strength.

In Chapter 8, several attempts are made to fit the theory to the data using stress distributions along the fibre given by different shear lag models. One of the key inputs required in the shear lag models is the distance between the fibre-fibre contacts along the fibre. In section 3.3 a new theory for the number of fibre-fibre contacts in a network will be presented. This theory will be tested against the experimental data in Chapter 7 as well as being used as input for the shear lag calculations in Chapter 8.

3.2 Model for tensile strength of paper

3.2.1 Fibre network model

We consider here a random fibre network with reasonably high density and tensile strength. The plasticity of the network is mainly caused by stretch of the fibres in it. When the fibre network is loaded, the stresses are transferred from one fibre to its adjacent fibres by the mechanism of the form predicted by the shear lag model.

3.2.2 Criteria for fracture

The tensile strength is the maximum load that occurs at the moment that macroscopic rupture begins. Once the rupture has been initiated, it proceeds rapidly during the tensile testing. Therefore, the initiation of the macroscopic fracture of the fibre network is critically important for the tensile strength of paper. We assume that the macroscopic fracture of the fibre network is triggered by the fracture of the most stressed fibre segments in it. The highest stressed fibre segments most likely exist in the fraction of fibres that are oriented in the direction of the applied load. We assume that once the peak load in these fibres exceeds the strength of these fibres, they will break and trigger

the macroscopic fracture of the network. This rupture, once initiated at a point in the sheet, is propagated rapidly in two directions.

3.2.3 Theory

We start with a cross-sectional slice through the sheet taken perpendicular to the stress-direction (See Figure 3-1). For a unit area of the sheet with apparent density, ρ_a, under some stress, σ, then the average stress in the fibre wall, $\sigma_{f,av}$ is

$$\sigma_{f,av} = \frac{\rho}{\rho_a}\sigma \qquad \textbf{3. 1}$$

where ρ is the density of the cell wall material. This equation holds true not matter what the fibre orientation distribution is.

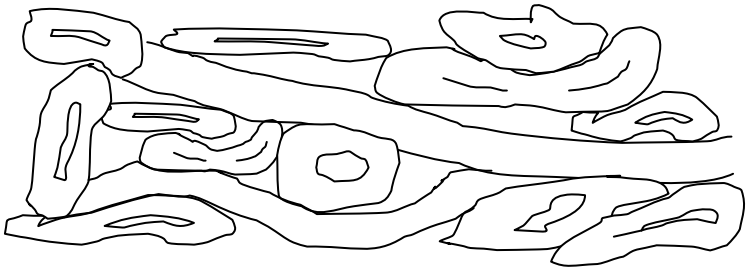

Figure 3-1 Cross-sectional image of the fibre network

Cox's (Cox 1952) result is that for sheets with randomly orientated fibres, the stress in the fibres lying parallel to the loading direction is 3 times larger than if all of the fibres had been aligned with the stress direction. As the fibres that are most heavily loaded are the ones that break first when fracture begins, we consider only the loads on the fibres in the 0^o (parallel to applied stress) position. If we denote these fibres with the superscript, *o*, then

$$\sigma^o_{f,av} = 3\frac{\rho}{\rho_a}\sigma \qquad \textbf{3. 2}$$

Any fibre cutting a sheet cross-section will do so at a random place along the fibre. Accordingly, unless the stress is completely uniformly distributed along the fibre, the actual stress in the fibre at that point will differ from the average. We define the

maximum stress in a fibre as being related to the average stress by a ratio where the value of r will depend on the fibre length and the degree of bonding. Accordingly

$$\sigma^{o}_{f,\max} = 3r\frac{\rho}{\rho_a}\sigma \qquad \textbf{3. 3}$$

If we assume that the fracture of the sample begins when the fibres begin to break and we designate this stress as σ_b, then this must be related to the breaking stress of the fibres, $\sigma_{f,b}$ by

$$\sigma_b = \frac{\sigma_{f,b}\rho_a}{3r\rho} \qquad \textbf{3. 4}$$

3.2.4 Estimation of fibre breaking stress

There are two possible methods of measuring the fibre breaking stress- measuring single fibre strength or measuring the zero-span strength. Measuring the zero-span strength is preferable as in the zero-span test the fibres are measured in the sheet. This is not insignificant, as the mechanical properties of the fibres will depend on how they have been dried. In other words we would not expect that the strength of fibres which have been allowed to freely dry to be the same as fibres which have been dried under restraint in the sheet. The other advantage of the zero-span test is that it is affected by distributions in fibre strength (El-Hosseiny and Bennett 1985). That is, the larger the distribution in fibre strength, the more the zero-span tensile strength will be reduced below the strength based on the expected average. This is also likely to be true for paper tensile strength.

From zero-span theory, for a randomly oriented sheet, the zero-span strength, σ_z, will be 3/8 of the strength measured if all of the fibres had been oriented in the direction of applied stress (Van Den Akker 1958). Therefore Equation 3.4 can be rewritten as:

$$\sigma_b = \frac{1}{r}\frac{\rho_a}{\rho}\frac{8}{9}\sigma_z \qquad \textbf{3. 5}$$

3.2.5 Estimation of r

In the model for tensile strength, r is defined as the ratio of the maximum load to the average load in the fibre. For any axial load distribution, an example of which is shown in Figure 3-2, r is by definition:

$$r = \frac{F_{\max} L}{A} \qquad \textbf{3. 6}$$

Where $F_{\max}$ is the peak axial load in the fibre, L is the length of the fibre and A is area under the load distribution curve that when divided by L is equal to average load in the fibre.

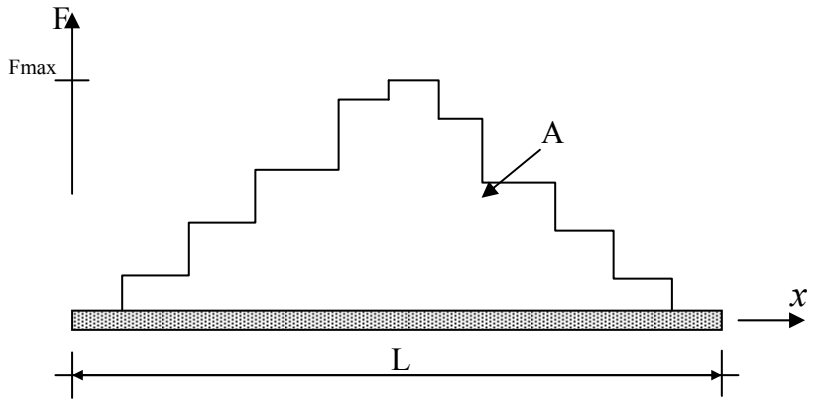

Figure 3-2 Axial force along length of fibre

In general, the value of r is believed to be a function of fibre length and number of fibre-fibre contacts. In the model for tensile strength, Equation 3.5, r describes the efficiency that the paper network uses the strength of the fibres in the paper. Thus although there is no expression for bonded area and fibre length in the expression for the breaking strength of the paper, these will appear in the expression for r.

The problem will be easily solved if the axial load distribution in the fibre is known. Simulation of a fibre network with Finite Element Method (FEM) is believed to be the best way to determine the axial load distribution in the fibre, provided the network is simulated in sufficient detail. However, it is impossible to do such a simulation in this project due to the limited time range.

As a start for estimating the value of r, we will use the shear lag model to analyse the stress distribution along the axis of a fibre. The shear lag model (Cox 1952), as discussed in Chapter 2, predicts that stress is transferred from each fibre to its adjacent fibres in the regions of the fibre ends. The stress in a fibre is at its maximum at the center and diminishes to zero at the ends. The application of the shear-lag model and other methods to determine r is discussed in Chapter 8.

3.3 Model for number of fibre-fibre contacts and expressions for relative bonded area (RBA)

As discussed above, a model for number of fibre-fibre contacts in paper is required for determination of the value of r in the new model for tensile strength of paper (Equation 3.5).

Fibre-fibre contacts have long been an interesting topic in the study of paper physics with numerous attempts to develop analytical models for the number of fibre-fibre contacts. Corte and Kallmes (Corte 1962) presented the first important model for number of fibre crossings in a three dimensional random fibre network. An expression equivalent to this model was proposed some years later by Komori and Makishima (Komori and Makishima 1977). Komori and Makishima's model was later modified by Pan (Pan 1993) by allowing for the reduction in free fibre length due to existing contacts. Pan's work was criticized and corrected by Komori and Itoh (Komori and Itoh 1994). Later a similar model was also derived independently by Dodson (Dodson 1996). More recently Dent (Dent 2001) showed that the 'general gamma' distribution can statistically describe 'non-random' as well as 'random' structures. These models use statistical analysis to predict the possible number of fibre-fibre contacts that a certain number of fibres could make in a given volume. They ignore the effects of fibre cross-sectional properties on the fibre-fibre contacts, so cannot model the effects of fibre collapse. In fact, however, the fibre width, fibre height and the fibre collapse degree all affect the fibre-fibre contacts. It is necessary to include these parameters in any model of fibre-fibre contacts.

Because the measurement of the number of fibre-fibre contacts is usually very difficult, it has always been problematic to obtain effective data to verify different models for the number of fibre-fibre contacts. In this subsection, we first present a new analytical model for the number of fibre-fibre contacts, which relates the cross-sectional properties of the fibres in the sheet to the number of fibre-fibre contacts per unit length of fibre. The model is further used to derive expressions for the Relative Bonded Area (*RBA*) for the purpose of verifying the model for number of fibre-fibre contacts by using data of *RBA*.

3.4 The new model for number of fibre-fibre contacts

3.4.1 Model paper structure

We start with the model fibre cross-section shown in Figure 3-3. A fill factor, f_h, is defined as the ratio of the fibre wall area, A_f, to the area of the smallest rectangular bounding box, A_b, that can completely enclose the irregular shape of the fibre and with its one side parallel to the paper plane. Here D_h and D_w are the minimum dimensions of the rectangular bounding box.

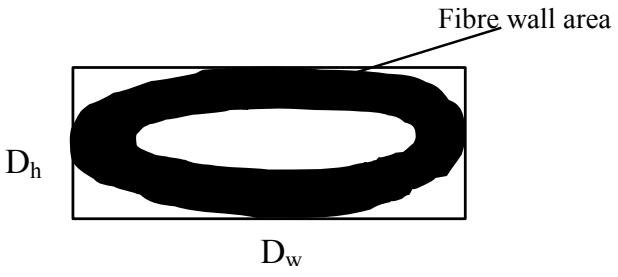

Figure 3-3 The bounding box surrounding a model fibre

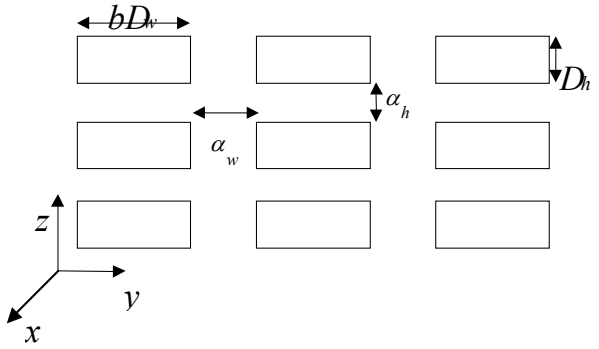

Figure 3-4 Idealized cross-sectional matrix of fibres

A paper sheet cross-section is then idealized as a regular matrix as shown in Figure 3-4, in which only the bounding boxes of the fibres are shown. The factor, b, here is an angle factor and accounts for the fibres in general not cutting the $y-z$ plane at right angles. In the situation depicted, z is the direction through the sheet thickness and the y axis can be selected to be any direction within the plane of the sheet. The apparent density of the sheet, ρ_a, is (ignoring the effect of surfaces)

$$\rho_a = \frac{\rho f_h D_h b D_w}{(D_h + \alpha_h)(bD_w + \alpha_w)} \qquad \textbf{3. 7}$$

where ρ is the density of the cell wall material, and α_h and α_w are the packing variables giving the spacing of the fibres within each layer and between the layers, respectively. In this equation, f_h, D_h and D_w can be relatively readily determined by confocal microscopy, leaving b, α_w and α_h to be estimated theoretically.

3.4.2 Determination of b, α_w and α_h

To determine b, we need to determine the average angle that a fibre makes in crossing the *y*-axis. If the distribution of fibre angle is random (as in a standard handsheet) then the average angle to any given plane perpendicular to the *x*-axis is:

$$\theta_{av} = \frac{\int_0^{\pi/2} \theta \cos\theta \; d\theta}{\int_0^{\pi/2} \cos\theta \; d\theta} \qquad \textbf{3. 8}$$

Here the factor $\cos\theta$ is the probability density function for the number of fibres having angle θ to any given plane. For a sheet with random fibre orientation, the theoretical value of θ_{av} given by Equation 3.8 is $\pi/2-1$, or 32.7°. Equation 3.8 could be made general for a machine made paper by replacing $\cos\theta$ with a function $F(\theta)$, which would include the distribution information. The value of b is then given by $b = 1/\cos\theta_{av}$.

The idealized matrix presented in the previous section represents the fibres sitting in their idealized positions and not actually in contact with each other. Letting Figure 3-5 and Figure 3-6 depict the idealized *x-y* and *x-z* models, then $2\Delta L$ is the distance along the fibre axis between the fibre crossing midpoints and from geometry the following relationship can be derived.

$$\sin\theta_{av} = \frac{\alpha_w + aD_w}{2\Delta L} \qquad \textbf{3. 9}$$

The layer-layer separation is determined by α_h. Figure 3-6 shows fibres within a single layer crossing each other. As a strong theoretical basis for determining layer-layer separation is lacking, we assumed that $\alpha_h = \beta D_h$. Here β is a packing factor that will be determined experimentally.

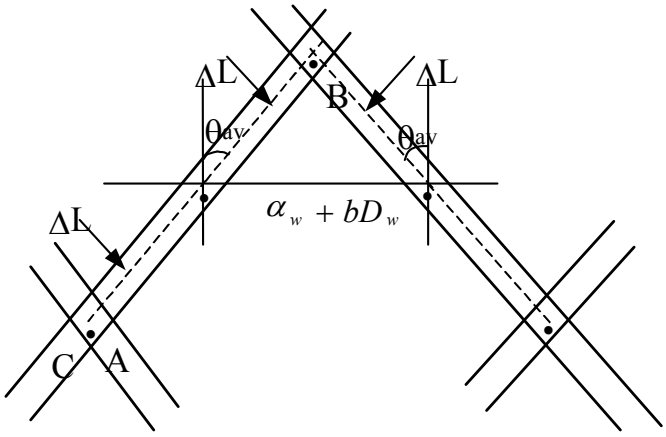

Figure 3-5 Fibre-Fibre crossing within a layer (*x-y* Projection)

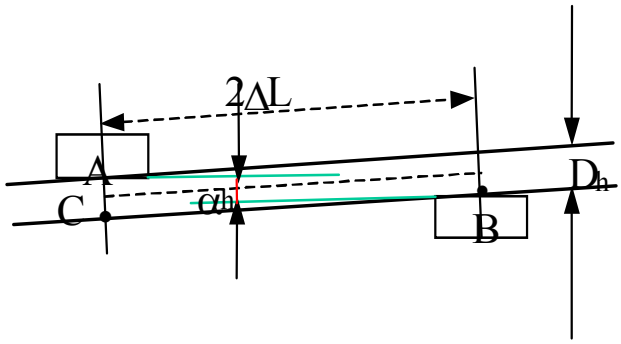

Figure 3-6 Side view of fibre-fibre contacts in one layer (x-z Projection)

3.4.3 Apparent density and Number of fibre-fibre contacts

Substituting the expressions for b, α_h and α_w into Equation 3.9, we obtain the following expression for the apparent density:

$$\rho_a = \frac{\rho f_h D_w}{(1+\beta)\Delta L \sin 2\theta_{av}} \qquad \textbf{3. 10}$$

Now if we assume that an equal number of fibre-fibre contacts on a fibre come from the layers above and below a given layer then the number of fibre-fibre contacts per unit length of fibre, N_c is given by:

$$N_c = \frac{3(1+\beta)}{2} \frac{\rho_a}{\rho f_h} \frac{\sin 2\theta_{av}}{D_w} \qquad \textbf{3. 11}$$

There is very little data that can be used to check the validity of this expression. One such set of data is the work of Elias (Elias 1967) in which data was obtained for the number of contacts per mm of fibre length for mats of glass fibres with a diameter of 7.22 μm and varying lengths, that were pressed at different pressures. When this data was taken into Equation 3.11, β was found to be –0.6, as shown in Table 2-1. The value of β is negative meaning that fibres from any given layer have deflected up and down into its neighbouring layers.

Table 3-1 Calculated value of β by Equation 3.11 using Elias' data

Fibre length (mm)	Diameter (μm)	Mean No. contacts per mm	Solid fraction	Calculated value of β
2.26	7.22	3.2	0.0310	-0.57
2.26	7.22	5.0	0.0488	-0.57
2.26	7.22	5.6	0.0545	-0.57
1.09	7.22	6	0.0739	-0.66
4.55	7.22	4.7	0.0575	-0.66

*For the cylindrical glass fibres, the fill factor, f, is given by $\pi/4$.

The fact that the calculated value of β is approximately constant is an important indicator that Equation 3.11 could provide an accurate predictor of the number of fibre-fibre contacts.

3.5 Expressions for *RBA*

Equation 3.11 can be used to provide theoretical expressions for the RBA. Two different expressions for the RBA were given in consideration of the two different methods used for RBA determination.

If the RBA is measured by nitrogen adsorption, then the total surface area of a unit length of fibre can be assumed to be $2(D_w + D_h)$. If the area of each fibre contact is A_c, then the Relative Bonded Area for nitrogen adsorption, RBA_{N_2}, can be written as:

$$RBA_{N_2} = \frac{N_c A_c}{2(D_w + D_h)} \qquad \textbf{3. 12}$$

One critical assumption is that the sheets are thick enough so that the exclusion of the effect of the surfaces of the sheet from this calculation does not introduce significant error. The second critical assumption is that if the fibres are purely ribbon-like, the projected area of each contact may be expressed as $A_c = D_w^2/\sin 2\theta_{av}$. However, in a real sheet, the actual area of each contact could differ from the idealized situation of two rectangles with width, D_w, therefore a factor, R, should be taken into account for

calculating A_c i.e. $A_c = R(D_w^2 / \sin 2\theta_{av})$. When this is substituted in Equation 3.12 together with the expression for N_c from Equation 3.11 then we obtain

$$RBA_{N_2} = \frac{3(1+\beta)}{2}\frac{R}{2}\frac{1}{(1+\delta)}\frac{\rho_a}{\rho f_h} \qquad \textbf{3. 13}$$

in which $\delta = D_h / D_w$.

For the *RBA* measured by scattering coefficient we assume that only the top and bottom surfaces contribute to the measured scattering coefficient, from which it can be shown that

$$RBA_{sc} = \frac{3(1+\beta)}{2}\frac{R}{2}\frac{\rho_a}{\rho f_h} \qquad \textbf{3. 14}$$

The model for number of fibre-fibre contacts presented in this chapter can be validated directly with data for number of fibre-fibre contacts measured in paper, and can also be validated indirectly with data for *RBA* measured by nitrogen adsorption method and by scattering coefficient method. Techniques for measuring the number of fibre-fibre contacts directly in paper and for measuring the *RBA* are required. A new microscopic technique for quantitative analysis of paper structure at the fibre level has been developed and validated and is presented in Chapter 6. Based on this new technique, technique for measuring the fibre-fibre contacts directly in paper has also been developed. This is discussed in Chapter 7. These new techniques together with new techniques for measuring the *RBA* that has been developed in this project are then used for obtaining data for validation of the new model for number of fibre-fibre contacts in paper. This is discussed in Chapter 8.

3.6 Summary

This chapter has presented a new analytical model for tensile strength of paper based on the assumption that the macroscopic fracture of paper is trigger by the failure of fibres lying in the direction of the applied load. The new model relates the tensile strength to the zero-span strength of the component fibres through a factor r. The sheet density only comes in as the equation are derived for stresses and not as tensile index. In other words it corrects for the void volume in the sheet. The value of r is the ratio of the peak load and the average load in the fibres, and r is believed to be a function of

number of fibre-fibre contacts and fibre length. It is the first analytical model that attempts to predict the start point of paper failure under load.

A new model that relates the fibre cross-sectional dimensions and the apparent density of paper to the number of fibre-fibre contact per unit length of fibre has been presented in this chapter. It is the first model that considers the effects of fibre cross-sections on the fibre-fibre contacts.

The model for number of fibre-fibre contacts will be fully verified in Chapter 7. The experimental verification for the model for tensile strength of paper will be presented in Chapter 8.

4 A New Microscopic Technique for Quantitative Analysis of Paper Structure at the Fibre Level

4.1 Introduction

Chapter 2 has reviewed how researchers have attempted to describe the strength properties of paper in terms of the structural properties of the fibre network and the mechanical properties of the fibres (Cox 1952; Page 1969; Kallmes 1977). Fibre dimensions and 3-dimensional orientation have been shown to be very important for paper strength in these studies. However, no technique is available to obtain quantitative data of fibre dimensions and this 3-dimensional orientation in situ to fully verify these network models. In recent studies on the paper mechanics, it has also been shown that better understanding of the structure of paper at the fibre level is required. This project starts from analysis of paper structure as the basis for development of a new model for the tensile strength of paper.

It is essential to expose and image the internal structure of paper for structure analysis and many techniques have been used for doing this. The most commonly used technique to expose internal structure is thin sectioning (microtomy). Some examples of the successful use of thin sectioning to study paper structure, using both transmitted light and electron microscopy are given in references (Page 1965; Quackenbush 1971; Nanko 1989; Szikla 1989). The main problem of thin sectioning is that the sample structure can be distorted during mechanical sectioning. Its use for quantitative analysis of paper structure is therefore problematical.

Williams et al (Williams 1994) and Williams and Drummond (Williams 2000) recently developed a new technique in which samples were embedded in resin and the cross-sections of the samples were then exposed by grinding the block surface using progressively finer abrasive papers. In order to get proper topographic contrast for scanning electron microscope (SEM) viewing, chemicals were used to etch away a layer of the supporting resin from the block surface. The Williams et al technique avoids exposing the sample to the compressive and shear forces developed during the thin sectioning. However, great care must be taken during surface resin removal with

chemicals to avoid swelling of the exposed fibres and paper surface. In addition to this, the SEM can only obtain the image of the cross-sectional surface, and this may not be free of artifacts of sample preparation. Using this technique, Forseth and Helle (Forseth 1997) quantified the change in fibre lumen area in paper during moistening. In their study, only fibres cut more or less parallel to the fibre length direction were measured to prevent overestimation of the fibre wall thickness.

Confocal laser scanning microscopy has been commonly used in qualitative analysis of paper structure in recent years (Li 1997; Moss 1997; Ting 1997). The major feature of the CLSM is its optical sectioning capability, which can be used to obtain three-dimensional images of fibre and paper non-destructively. However, the signal intensity diminishes rapidly with increasing depth in the sample (Li 1999). Therefore these studies, which looked through the in-plane surface of the samples, could not obtain a complete view of a sheet cross-section. (Li 1997; Moss 1997; Ting 1997).

More recently, Dickson (Dickson 2000a; Dickson 2000b) conducted successful quantitative analysis of paper cross-sections using a combination of the sample preparation technique developed by Williams and Drummond (Williams 2000) and the confocal laser scanning microscopy technique. Complete cross-sections of paper were imaged with CLSM just below the cross-sectional surface to avoid the artifacts on the surface (Dickson 2000a). Dickson quantified the profile properties of the paper cross-section including the wall area, the total pore area, interfibre pore area and lumen area. The dimensions of individual fibres in the sheet were not measured in any of these studies.

Fibre orientation has often been measured by tracing a fraction of dyed fibres in a sheet (Perkins 1981; Rigdahl 1983). The fibre orientation measured by this technique is the in-plane orientation and the fibres traced are always limited to the paper surface. Another technique is to split a sheet into thin, transparent layers and then measure the fibre orientation with image analysis in all these layers (Erikkila 1998). This technique allows the in-plane fibre orientation in different layers to be measured but not the out-of-plane fibre orientation. A more accurate and relatively easy technique is still required for measurement of overall fibre orientation.

In this chapter, we present a new method for quantifying paper structure. The dimensions and orientations of individual fibres in a sheet are measured simultaneously using a combination of resin embedding and confocal laser scanning microscopy. This is the first technique that can simultaneously obtain all this information directly in situ. Based on this technique, we further developed a technique for measuring the properties of fibre-fibre contacts including the nature of fibre contact, the number of fibre-fibre contacts, the length of free fibre segment and the out-of-plane angle of each free fibre segment. This work is presented in Chapter 7. This is also the first technique that can simultaneously measure all these quantities directly in paper.

4.2 Basic idea of the new technique

The basic idea of this new technique is to examine the individual fibres in paper directly by using a confocal microscope. Paper samples were arranged vertically and embedded in resin. The sample cross-section was exposed by grinding the resin block with abrasive paper. It is critically important that the sample is thoroughly penetrated by the resin to provide sufficient support to the paper structure. Once quality images of the paper cross-section was obtained, measurement of fibre dimensions, fibre orientation and fibre-fibre contacts was carried out in these images by using different macros written in the commercial software package Optimas 6.1.

4.3 Experimental equipment and methods

4.3.1 Confocal microscope

A confocal laser scanning microscope (CLSM) was used to measure the cross-sectional dimensions of fibres on glass slides and in paper. The CLSM used in this project was the Optiscan F900e that was fitted to an Olympus BH2 optical microscope. The CLSM can operate in either reflectance or fluorescence mode. In reflectance mode the image is the light that has been reflected from the sample while in fluorescence mode, fluorescence excited by the incident laser beam is detected. To use the fluorescence

mode, the sample must either be naturally fluorescent or fluorescent dye must be added. This mode was used for all of the confocal work presented in this thesis.

The Optiscan F900e uses an optic fibre to deliver the laser light through the optic system of the microscope and to collect the light signal from the excited fluorescent dye contained in the fibres.

Figure 4-1 schematically shows the principle of the confocal microscope. The laser used was an Argon-Ion laser operating at a wavelength of 480nm. The signal from the excited fluorescent dye is passed back through the optical path and through a small aperture, the confocal pinhole, before reaching an electronic detector or photo-multiplier tube (PMT). The PMT converts the light into a digital image displayed on a computer monitor. Because of the confocal pinhole, only light returning from on or very near the focal plane is permitted to pass through to the PMT. Light returning from other than the specific optical plane is blocked. This process creates an extremely thin optical section that can be positioned within a specimen to potentially provide a sharp image with a significantly higher resolution than a conventional microscope.

For optimum performance in the confocal microscopy, it is necessary to keep to a minimum, the degree of refractive index mismatch between the object being investigated and its surrounding medium. If there is a large refractive index mismatch between the fibres then the refraction of light from irregular surfaces in the object will cause lower levels of signal to be sent back to the PMT, something that will affect the image quality. This will be compounded when attempting to obtain images below the sample surface (scanning inside the sample). Therefore, full saturation of the fibre samples with oil of similar refractive index (RI) and removal of the air trapped in the fibres are essential for obtaining quality images. The immersion oil used had an RI of 1.51. It was specially designed for oil objective lenses.

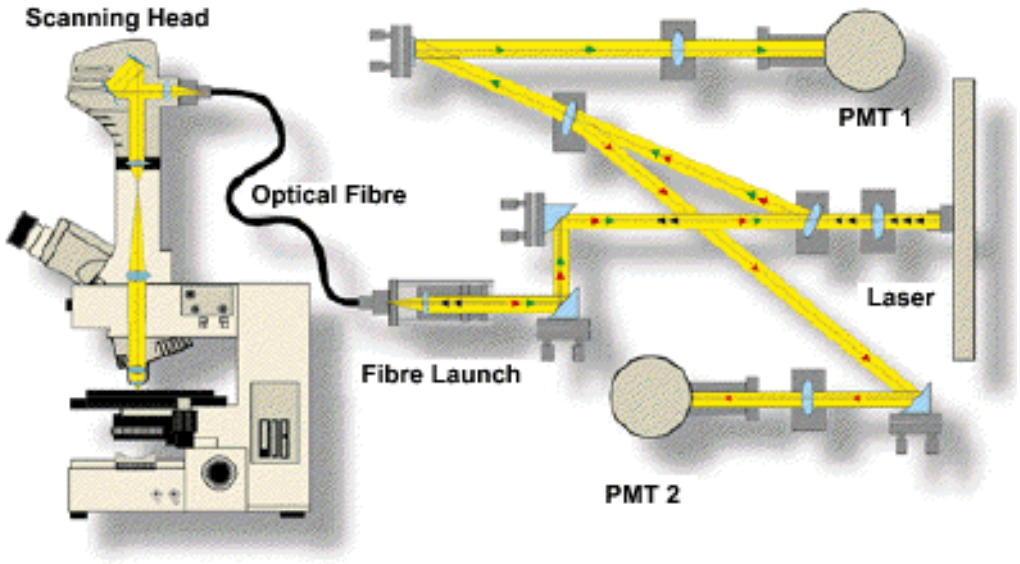

Figure 4-1 Schematic showing the basic principle of the optical system of the Optiscan F900e system (From Optiscan Pty Ltd)

4.3.2 Sample preparation

Recycled pulp of commercial plaster line board and laboratory made never dried radiata pine kraft pulp (kappa no. 95) (refer to Appendix A for details of these pulp) were used in the experiments for development and validation of the new technique.

4.3.2.1 Staining of pulp fibres and handsheet formation

The fibres were stained in a stock divider at a consistency of 1.5 % prior to handsheet formation. The dye (Acridine Orange) was added at a rate of 0.0005% w/w water. From each pulp, three sets of square handsheets were made on a Moving Belt Sheet Former (Xu and Parker 2000). Each set of the handsheets from each pulp were pressed dynamically using the Sheet Roll Press at one of three pressing levels, viz P_1, P_2 and P_3 (see Subsection 5.2.1). The handsheets made from the recycled pulp were denoted as R_0, R_L and R_H, and those made from the kraft pulp were denoted correspondingly as Kp_0, Kp_L and Kp_H.

4.3.2.2 Sample embedding – Initial technique

The sample embedding technique presented in this subsection was used only at the beginning of the project when the new microscopic technique was verified. It was found that it could be improved during verification of the new technique. The improved technique will be discussed in the next subsection.

The resin used for sample embedding was Epofix (from **(Struers)).** This resin met the following criteria:

a. no reaction with fibres
b. good penetration into the fibres
c. refractive index of the resin block is 1.57, which is close to the fibre refractive index 1.53.

Samples were first placed directly in 100% resin and degassed overnight so that the resin could penetrate into the paper structure and expel gas in the paper. The samples were then taken out of the resin and put on a plate for about 5 minutes to allow the resin at the sample surfaces to drain away. The samples were then put into a plastic mould, and a pre-degassed mixture of resin and hardener (15 parts of resin and 2 parts of hardener) was poured into the mould and the whole sample was put into a vacuum apparatus and left until the resin cured into block. It is very important to ensure that all gas is removed from the samples and the internal structure of the paper is thoroughly penetrated by the mixture of resin and hardener. The cross-sections of the samples were then exposed by abrading the block surface with a range of abrasive papers of decreasing roughness (P400, P600, P800 P1200, P1500 and P2400). Figure 4-2 shows an embedded sample ready for examination in the confocal microscope.

4.3.2.3 Sample embedding – improved technique

As will be discussed later in this chapter, the embedding technique outlined in the above subsection may not provide a thorough penetration of the resin and hardener mixture into the sample structure. A new rig, a vacuum impregnation apparatus, as illustrated in

Figure 4-3, was designed and used to improve the sample embedding technique. The improved technique was used in the subsequent experimental work.

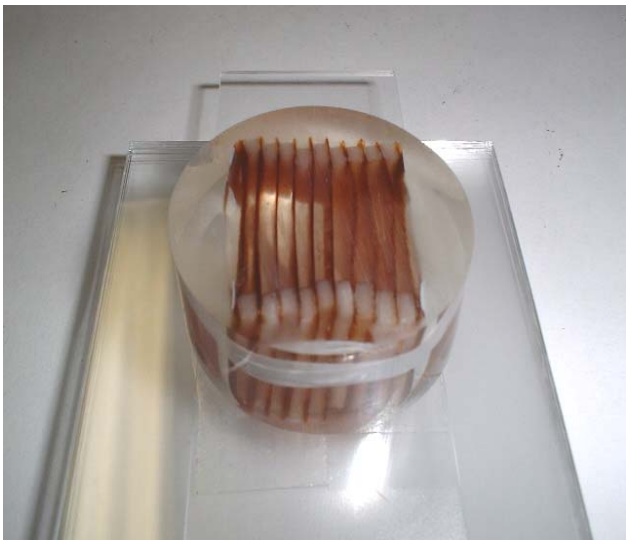

Figure 4-2 Embedded sample ready for examination in confocal microscope

The pre-cut sample was vertically put into the mould. The sample and the mould were then put into the container. Valve 2 is closed and valve 1 is opened. The vacuum is applied for at least for 4 hours to first remove air trapped in the sample structure. Then valve 1 is closed and valve 2 is opened to suck the resin and hardener mixture into the mould. A vacuum impregnation is created with this procedure, which can provide a thorough penetration of the mixture into the sample structure. When enough resin mixture has been sucked into the mould, valve 2 is closed and valve 1 is opened to apply vacuum to the whole system for at least another 4 hours to further remove air in the sample and the resin mixture.

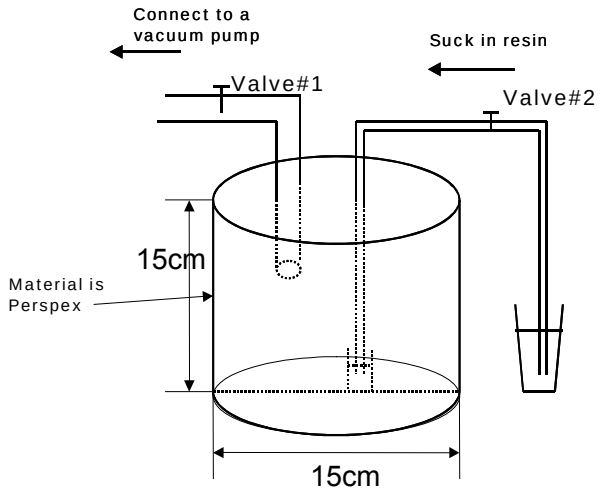

Figure 4-3 Schematic drawing of the vacuum impregnation apparatus

4.4 Quantitative analysis of paper structure

4.4.1 Measurements of fibre orientation and shape

4.4.1.1 Imaging and image analysis

Imaging was performed with the Optiscan C900e confocal laser scanning microscope using a 60×oil immersion lens (see Figure 4-4). The inspection area of each image frame was 100×100 μm with a resolution of 512×512 pixels.

For each region of interest, a group of images of the region was captured at different depths from the cross-sectional surface. Fifty groups of cross-sectional images of each sample were captured and processed for measurement of fibre orientation and fibre cross-sectional dimensions. A typical group of cross-sectional images of the paper is given in Figure 4-5. The images shown in Figure 4-5 were obtained using the initial embedding technique as discussed in subsection 4.3.2.2. The data used for verification of the new technique in this chapter were measured in images of samples embedded using the initial embedding technique. In the rest of the project, the improved embedding technique was used for sample preparation. The image with 0-depth was

captured just below the exposed surface of the sample. The depths of the other images are measured with respect to the 0-depth image. It can be seen that the image brightness decreases with increasing depth. The maximum scanning depth used in this study was 10μm. Scanning deeper led to a rapid deterioration of image quality.

Figure 4-4 Picture showing a sample on the stage of a confocal microscope

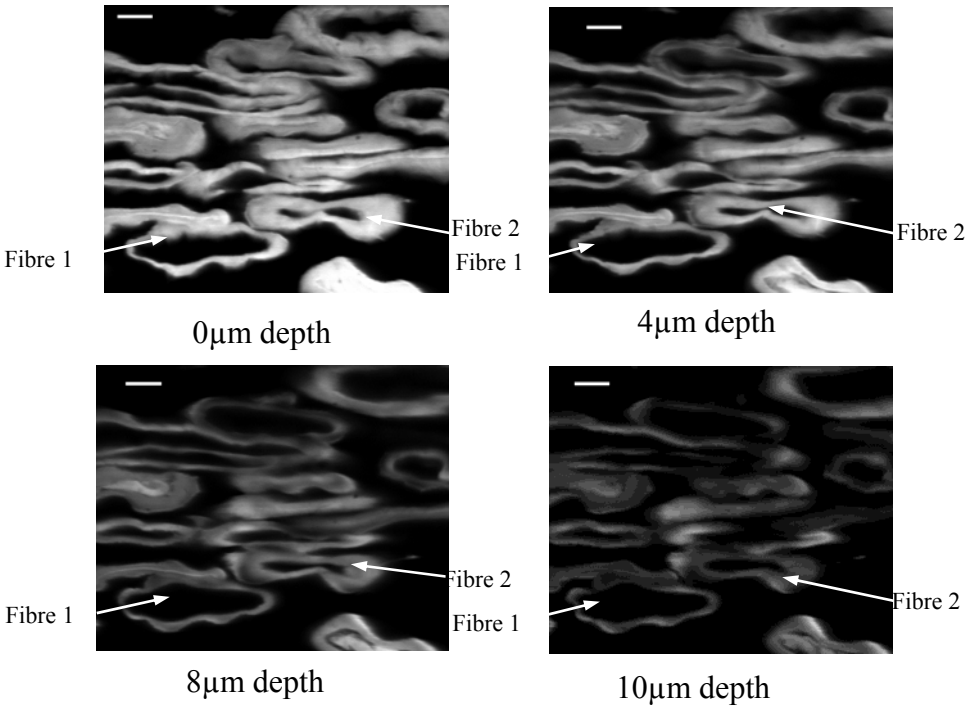

the scale bar is 10μm

Figure 4-5 Cross-sectional images of paper acquired at depth of 0, 4, 8 and 10μm (for the explanation of the depth see text).

The image analysis was conducted using the commercial image analysis software (OPTIMAS 6.1). The analysis sequence used was: 1) select a region of interest; 2) smooth the image with a 3×3 Gaussian filter; 3) adjust the threshold level; and 4) extract features including fibre wall area, mass centre of fibre cross-sectional area, fibre width (D_w) and fibre hight (D_h). A macro was written in the software for performing the above process automatically (see Appendix D**).** The boundary of a fibre was identified by manually adjusting the threshold. For those fibres that touched each other, a line was drawn between them to separate the fibres but keep the features of the fibre of interest unchanged. The following subsections discuss the quantities of paper structure were measured directly in the paper cross-section by using the new microscopic technique. Some of the quantities are defined for the first time in this project.

4.4.1.2 Fibre orientation

Fibre orientation was measured by following the positions of individual fibres in sheet cross-sections scanned at 0μm depth and 10μm depth. The position of the mass centre of the fibre cross-section was determined by the distance from the mass centre to a reference point in the Y and Z directions. As shown in Figure 4.6, the mass centre of the fibre cross-section in the 0-depth image is (Y_1, Z_1), and in the 10μm depth image is (Y_2, Z_2). The angle θ that the fibre makes to the X direction (the plane of the paper) can then be calculated from geometry. For example, in Figure 4-5, the position of fibre 1 has no apparent change when scanning down from 0-depth inside the sample to 10μm deep. This indicates fibre 1 is almost perpendicular to the exposed surface. However, the position of fibre 2 shifts markedly indicating that fibre 2 sits at an angle other than 90^o to the exposed surface of the sample.

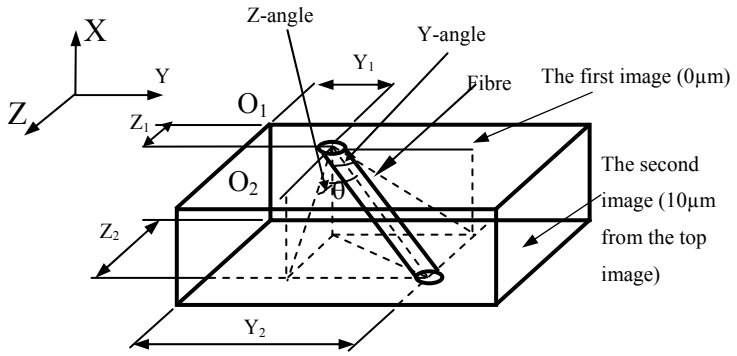

Figure 4-6 Depiction of Measurement of fibre orientation in paper.

4.4.1.3 Fibre in and out of plane angle

The fibre orientation angle, θ, measured by using the above method is the overall angle. As shown in Figure 4-6, if needed the out of plane angle (the Z-angle), and the in-plane angle (the Y-angle) can also be calculated from geometry.

4.4.1.4 Fibre wall area

For the work in this Chapter, the wall areas of fibres from both pulps were measured from both the 0μm and 4μm depth images. In the rest of the project, when the improved sample embedding technique was used, the fibre dimensions were measured in images acquired just below the sample surface. If the fibre is not perpendicular to the paper cross-section, the wall area will be enlarged by a factor of $1/\cos\theta$. The measured wall area of each individual fibre has been corrected by this factor.

The fibre wall areas of the two pulps were also measured on freely dried fibres on glass sides using the confocal laser scanning microscope following a procedure described by (Xu, Conn et al. 1998). Details of sample preparation and image analysis for this measurement is given in Appendix B. These results were compared with the fibre wall areas measured in situ on fibres in paper sheets for the purpose of verification of the new technique.

4.4.1.5 Fill factor, Shape factor and twist angle

As discussed in Chapter 3, the fill factor is defined for the purpose of modelling the structure of paper. The fill factor, f_h, is defined as the ratio of the fibre wall area, A_f, to the area of the smallest rectangle bounding box, A_{bf}, that can completely enclose the irregular shape of the fibre and with its one side parallel to the paper plane (see Figure 3-3). The fill factor was calculated by the measured fibre wall area divided by the area of the rectangular bonding box for each individual fibre. The rectangular bonding box was generated automatically by running the macro (refer to Appendix D).

In order to quantify the degree of fibre collapse, an additional shape factor is defined. As shown in Figure 4-7, the shape factor, f_m, is defined as the ratio of the fibre wall area, A_f, to the area of the smallest rectangular bounding box, A_{bm}, that can completely enclose the irregular shape of the fibre. The two axes of the rectangular box are then defined as the major and minor axes of the fibre cross-section. When the fibre is in a cross-section of paper, the angle between the major axis of the fibre and the paper plane is defined as the twist angle of the fibre cross-section.

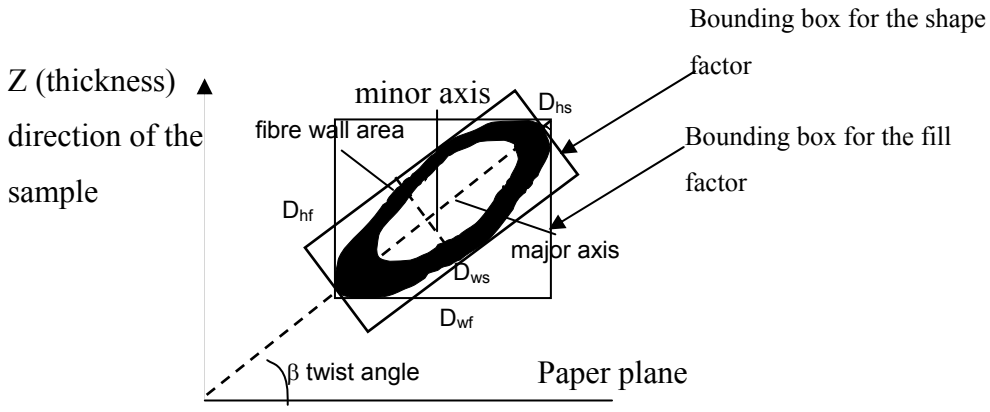

Figure 4-7 Definition of the fibre shape factor and twist angle

In order to measure f_m and the twist angle, β, we need firstly to create the smallest rectangle that encloses the irregular shape of the fibre. In practice, it is difficult to calculate this smallest rectangle. The bounding box used in this study was a rectangle with its major axis parallel and equal in length to the longest dimension of the fibre cross-section. For most types of fibre shape this bounding box is very similar to the

smallest rectangle in the definition of f_m. The measurement error is significant only for square shaped fibres. However, the square shaped fibres were rare in the pulp used in this study and were discarded during measurement. The percentage of the fibres been discarded for the particular samples will be given in Chapter 6.

The twist angle used was the measured angle between the longest dimension of the fibre cross-section and the horizontal frame of the image. This reference direction has to be used because the position of the paper plane is unknown during the measurement. However, if the horizontal frame of the image is at an angle $-\alpha$ to the paper plane, then it can be shown that, for a randomly oriented handsheet, $\overline{\beta} = \alpha$. We estimated the angle α by averaging the measured twist angles. The twist angle was also corrected by the angle, θ, that the fibre is sitting to the surface of the paper cross-section. If the fibre length axis is not perpendicular to the paper cross-section, then one axis of the fibre image will be lengthened by a factor of $1/\cos\theta$. Thus unless $\beta = 0$, this distortion of one axis will cause an error in the measured value of β. It can be shown from geometry that the true angle β is given by $\beta = \arcsin(\frac{\sin\beta_m}{\cos\theta})$, where β_m is the measured twist angle. All measured twist angles were first corrected by the angle α and then by the angle θ using the above formula.

4.4.2 Measurement of fibre-fibre contacts

The measured parameters associated with the fibre-fibre contacts included the nature of fibre contact, the number of fibre-fibre contacts, the lengths of the free fibre segments and the out-of-plane angle of each free fibre segment. These parameters were measured directly in images of paper cross-sections. For each sample, 70 frames of cross-sectional images were obtained consecutively along the sample cross-section using the confocal laser-scanning microscope and the 60x oil-immersion lens. The inspection area of each image was 200x200μm^2, and the resolution was 512x512 pixels. The 70 images were then joined together in consecutive order during the measurements, therefore a 14mm length of the sample cross-section was imaged in this way. Some fibres or fibre segments in the sample cross-section were imaged along their long axes.

These fibres were chosen as the fibre of interest for the measurements of fibre-fibre contacts. Two images of such fibres are shown in Figure 4-8. When such a fibre was chosen, the number of fibres in contact with the fibre of interest was counted, and a line was drawn between the centres of two neighbouring contacts along the fibre axis. The length of the line is the free fibre length and the angle between the line and the horizontal frame of the image is the measured out-of-plane angle of the free fibre segment. If the horizontal frame of the image is at an angle $-\alpha$ to the paper plane, then it can be shown that, for a randomly oriented handsheet, the average value of the out-of-plane angles of all the free fibre segments in the paper is equal to α. We estimated the angle α by averaging the measured out-of-plane angles and we then corrected all the measured out-of-plane angles by the angle α.

To identify fibre-fibre contacts, the cross-sectional images of the samples were first thresholded manually, and then binaried into black and white images. In the binary images, fibre-fibre contacts could easily be identified. If there is no black gap between two fibre surfaces, we defined that a contact has been made between these two fibres. Otherwise, there is no contact between them. In this project, fibre-fibre contacts were classified into full contacts and partial contacts. The cross-section of a fibre is assumed to have two long sides and two short sides. When one of the long sides is totally in contact with the fibre of interest, this contact is a full contact. Otherwise, the contact is a partial contact (see Figure 4-9). All these image analysis and measurements were conducted using the Optimas 6.1 software.

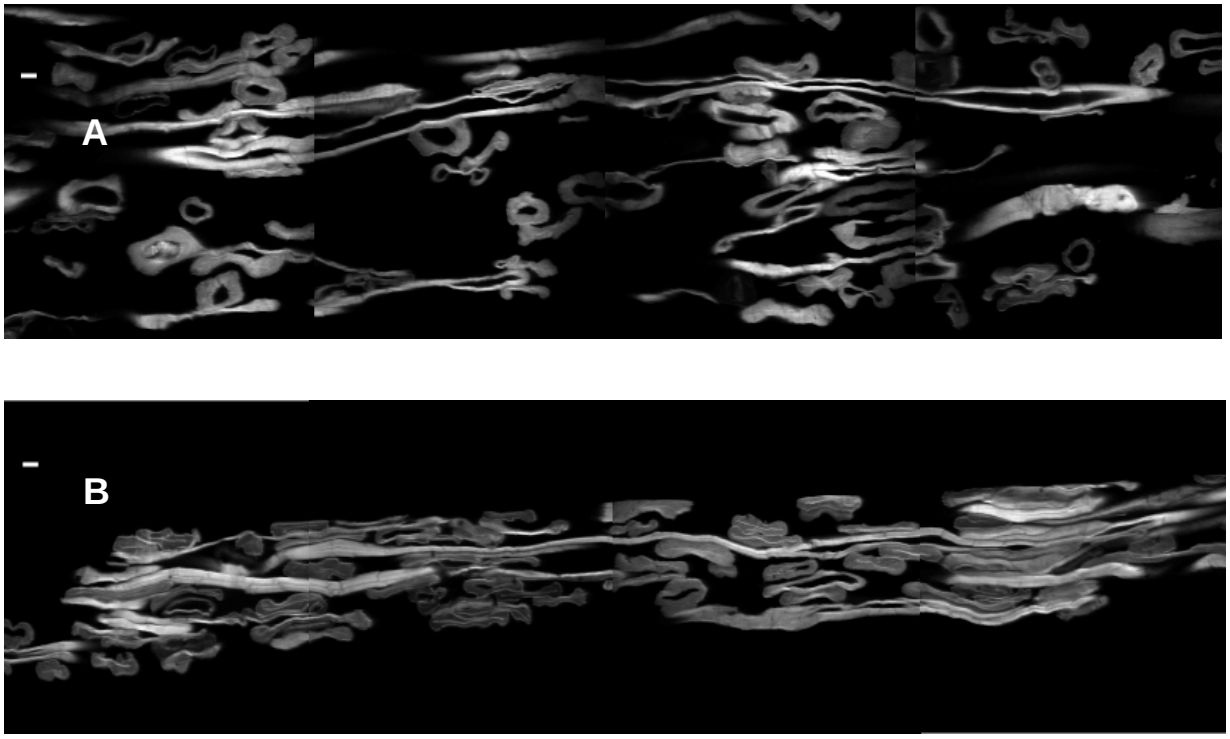

* the size bar is 10μm

Figure 4-8 Images of paper cross-sections (A is sample Rej-P_0 and B is Rej-P_H)

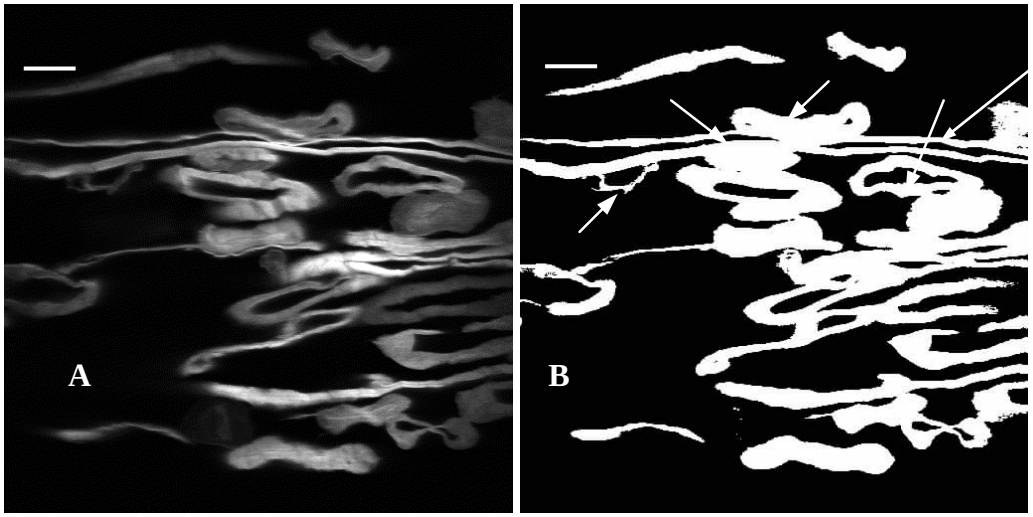

* the size bar is 20μm

Figure 4-9 Cross-section image before (A) and after (B) thresholding and binarisation. Fibre 2 and 3 in (B) make two full contacts, fibre 1 makes a partial contact, and fibre 4 is not in contact with the fibre of interest.

The measured results of fibre-fibre contacts will be discussed in detail in Chapter 7.

4.5 Validation of the new technique

The new technique for microscopic analysis of paper structure was validated by comparing the fibre dimensions measured by the new technique in paper with those measured on fibres dried on slides by the route confocal microscopy method. The validity of the new technique was further checked by comparing the measured fibre orientation with the theoretical value of a random sheet.

4.5.1 Comparison of the fibre wall area measured in paper with that measured on slide

Table 4-1 summarizes the fibre dimensions and the sheet properties measured in this study. As can been seen from Table 4-1, the average fibre wall areas of the recycled pulp samples R_0, R_L and R_H are very close to each other, especially for those measurements acquired 4μm below the sample surface. A similar situation is shown for the kraft pulp samples Kp_0, Kp_L and Kp_H. This is as expected because wet pressing should not change the wall areas of fibres in the sheets.

Table 4-1 A summary of the experimental results

Pulp Sample	Handsheet Sample Code	Apparent density (kg/m^3)	Tensile index (kNm/kg)	Fibre wall area (μm^2) (at 0μm depth)	Fibre wall area (μm^2) (at 4μm depth)	Fill factor (at cross-sectional surface)	Fill factor (at 4 μm depth)	Fibre angle to X-direction (degree)	Number of fibre measured
Recycled pulp	R_0	234	17.3	220±9*	181±9*	0.56±0.01	0.54±0.01	25.8	147
	R_L	334	22.9	223±9	179±9	0.53±0.01	0.55±0.01	24.6	146
	R_H	380	22.3	209±10	172±9	0.56±0.01	0.57±0.01	26.0	147
Recycled pulp fibres dried on slides	/	/	/	170±8	170±8	/	/	/	319
Kraft pulp	Kp_0	112	13.1	312±9	266±9	0.45±0.01	0.46±0.01	28.1	176
	Kp_L	215	29.2	295±10	256±9	0.50±0.01	0.48±0.01	25.2	192
	Kp_H	393	51.0	294±10	260±9	0.55±0.01	0.56±0.01	26.9	180
Kraft pulp fibres dried on slides	/	/	/	249±9	249±9	/	/	/	338

± is 95% confidence interval.

Comparisons were made between the fibre wall areas measured in sheets and those measured on dried fibres on glass sides for the purpose of validating the measurements of the new method. As shown in Table 4-1, for both of the pulps used in this study, when the fibre wall areas were measured in images of paper cross-sections scanned 4μm below the sample surface, the results are very close to those measured on the same pulp fibres dried on glass sides. The maximum difference between them is 11μm^2 for the recycled fibres and 17μm^2 for the kraft fibres. The frequency distributions of fibre wall areas of these measurements are given in Figure 4-10 for the recycled pulp and Figure 4-11 for the kraft pulp. From these figures, it can be seen that the distributions of fibre wall areas of samples made from the same pulp fibres but pressed at different pressing levels are not only in close agreement with each other but also in close agreement with those measured on the freely dried fibres on glass. The fibre wall areas of recycled fibres were mostly distributed between 100μm^2 and 200μm^2, and between 200μm^2 and 350μm^2 for the kraft fibres. These comparisons indicate that the measurements of fibre wall areas using the proposed new method and taking measurements from images of paper cross-sections acquired 4μm below the surface of the sample cross-sections are valid.

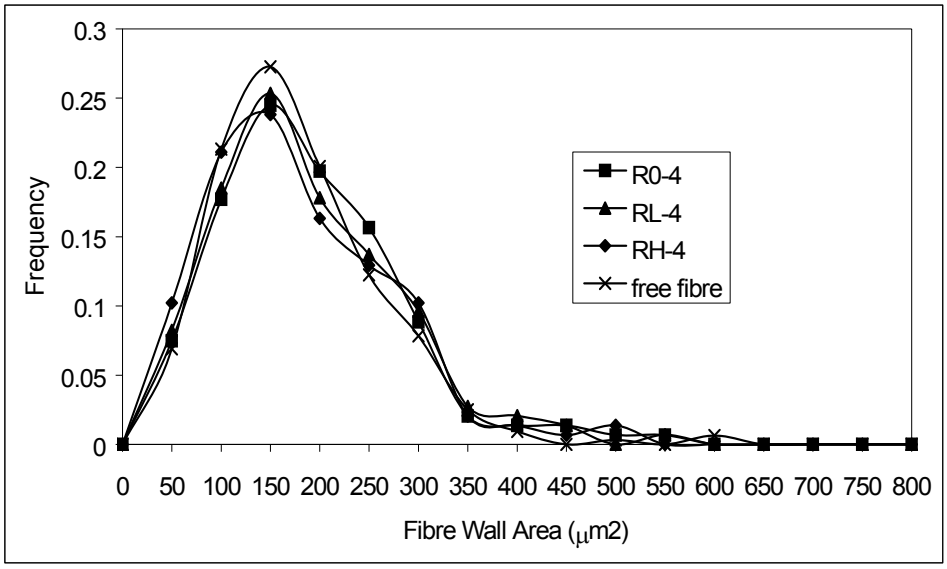

Figure 4-10 Distribution of fibre wall areas measured in paper and on slides for the recycled fibres. The fibre wall areas measured in paper were determined from images taken at 4μm depth.

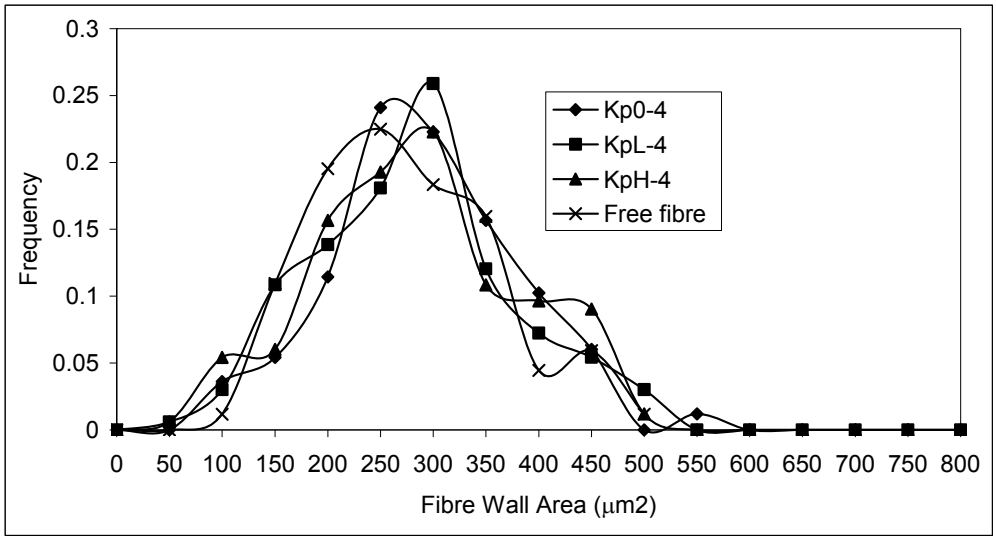

Figure 4-11 Distribution of fibre wall areas measured in the sheet and on slide for the kraft fibres. The fibre wall areas measured in paper were determined from images taken at 4μm depth.

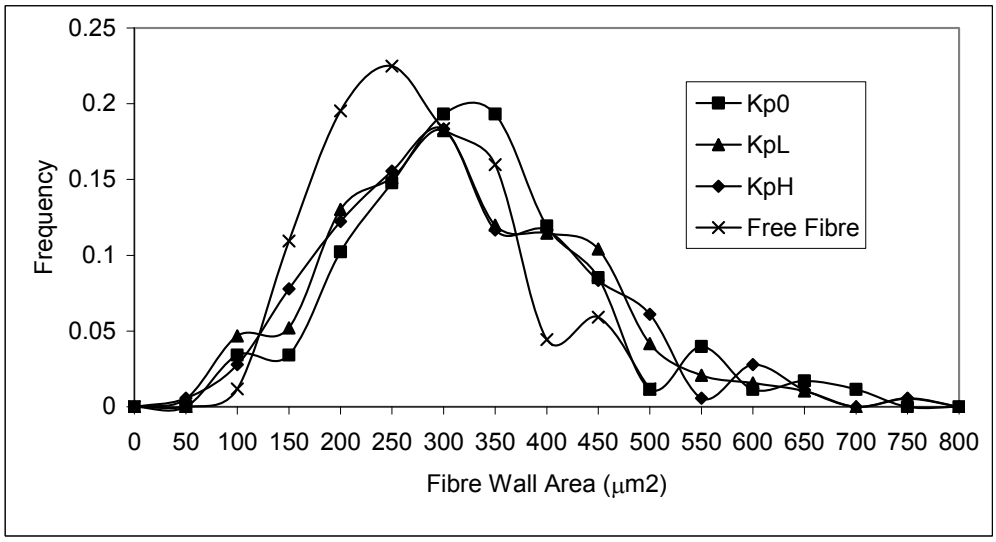

Figure 4-12 Distribution of fibre wall areas measured in the sheet and on slide for the kraft fibres. The fibre wall areas measured in paper were determined from the surface images.

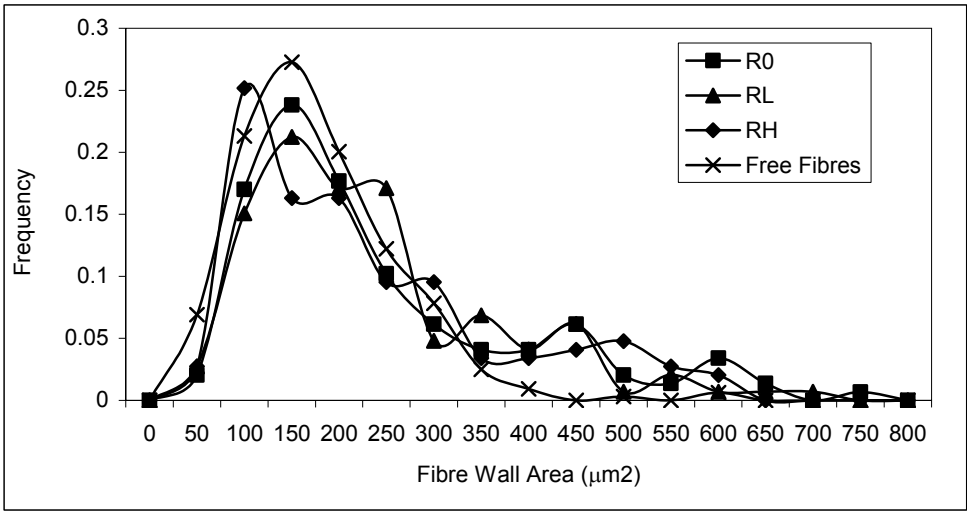

Figure 4-13 Distribution of fibre wall areas measured in the sheet and on slide for the recycled fibres. The fibre wall areas measured in paper were determined from the surface images.

When the measurements were made in the 0μm depth images of the paper cross-sections, the mean values of the fibre wall areas of both pulps are greater than those of their corresponding freely dried fibres (see Table 4-1). The average difference is 50.9μm^2 for the kraft fibres and 47.2μm^2 for the recycled fibres. Despite these relatively large differences in average fibre wall areas, the frequency distributions are still quite similar (see Figure 4-12 and Figure 4-13). It is very interesting to note that the results measured in sheets showed some large values (greater than 500μm^2), which could not be seen in the results measured on free fibres from the same pulp. It is believed that these large fibre wall area values result from artifacts produced by sample preparation. A careful observation of the images of the paper cross-sections found that there were a few fibres, especially large fibres, that seemed have been 'smeared' during grinding and polishing. The 'smeared' fibres obviously created larger images and this effect would seem to cause an overestimation of fibre wall areas when these fibres are included in the measurements. The 'smeared' effect implies that the sample structure had not been supported sufficiently by the resin block. A possible reason for this could be that the resin that penetrated into the paper structure during degassing treatment was not replaced sufficiently by the mixture of the resin and the hardener in the subsequent step. Another possibility is that the resin and hardener mixture may not have penetrated into the fibre walls. This indicates that the sample surface is not free of artifacts although

great care has been taken during sample preparation. When measurements were taken 4μm below the sample surface, there were only a few large values (as shown in Figure 4-10 and Figure 4-11) and the measured mean values of fibre wall areas were close to the results obtained for the free fibres. It appears that any artifacts at the sample cross-sectional surface are eliminated by taking measurements at 4 microns below the sample cross-section. As mentioned before, the sample embedding technique was later improved by using a vacuum impregnation rig to allow the mixture of resin and hardener to penetrate the paper structure thoroughly. Figure 4-14 gives a group of paper cross-sectional images obtained from the sample embedded by the improved technique. As can be seen in Figure 4-14, the quality of images has been improved compare with those shown in Figure 4-5, and the 'smeared' effect cannot be seen in the image acquired at the sample surface. All of the later measurements were conducted in the 0μm images acquired by the improved technique.

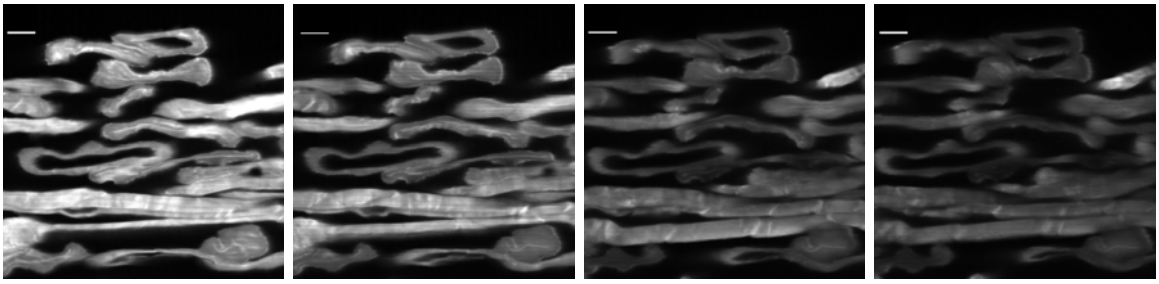

0μm 4μm depth 8μm depth 10μm depth

** The size bar is 10 μm*

Figure 4-14 Cross-sectional images of paper acquired when the vacuum impregnation rig was used for sample embedding.

4.5.2 Comparison of the measured fibre orientation with the theoretical value

The average values of the angles of fibres to the X direction (Figure 4-5) are given in Table 4 1. The fibre orientation measured in this study was actually the orientation of fibre segments. In fact it is almost impossible to properly define the fibre orientation because fibres are not straight in a sheet. However, the orientation of fibre segments might be more important for paper properties than the average orientation of entire fibres.

In this study the measurement for fibre orientation calculation included any position shift of the fibre, in any direction, between the surface and 10μm depth into the paper cross-section. The fibres measured were sampled randomly through the whole thickness of the paper. Therefore, the fibre orientation measured is an overall fibre orientation. Although the position shift of fibres in sheets are not calculated in this chapter (such calculations will be shown in Chapter 6), in fact the positions of fibres were most likely to shift in both Y and Z directions (see Figure 4-5), although the shift in the Z direction was usually very small. If the position shift in the Z direction was zero, it indicates that the fibre is in-plane with respect to paper surface. Otherwise the fibre is out-of-plane. The small shift in the Z direction indicates that the out of plane movement of the fibres in the handsheets used in this study is small.

If θ is the in-plane fibre angle to any given line within the plane in the direction perpendicular to the exposed surface (the X direction in Figure 2), then from simple geometry the average value for a randomly oriented sheet, θ_{av}, is given by Equation 4.1. Integrating equation (1) gives an average value of π/2-1, or 32.7°.

$$\theta_{av} = \frac{\int_0^{\pi/2} \theta \cos\theta \; d\theta}{\int_0^{\pi/2} \cos\theta \; d\theta} \qquad \textbf{4. 1}$$

From Table 4-1, there is about an 8° difference between the average measured value and this theoretical value of fibre orientation. This difference is considered to be reasonable because the theoretical value includes all fibres with angles between 0° and 90° but in this study fibres with high angles were excluded. After examining the raw data of fibre angles carefully, it was found that all the measured values seldom included fibres with angles over 80°. The reason for this is that the 'high angle fibres' are likely to be sectioned along the fibre axis and were treated as 90° fibres and not included in the measurements. This difference between the measured average fibre angle and the theoretical average value does not affect the validity of the angle measurements using the new technique. It appears that the effect of the out of plane movements of fibres in the sheets used in this study on the overall fibre orientation is negligible.

This study made no attempt at measuring the distribution of fibre orientation through the thickness of a sheet, however, the new technique could be used as needed to measure the distribution of fibre orientation through the thickness of a sheet.

4.6 Application of the New Technique

One possible application of the new technique is to quantify the behaviour of individual fibres in a sheet after wet pressing. Consolidation of the paper structure during pressing will occur through a combination of compressing fibres closer together and collapse of the fibres. How much the fibres are collapsed and brought closer together in wet pressing and how much these changes in individual fibres contribute to the densification of the sheet is still not clear. It is only possible to quantify these changes when the fibre dimensions in the sheet can be measured. The mechanisms of sheet densification will be studied in Chapter 6.

The new term, fibre fill factor, as defined in subsection 3.4.1 was used to quantify the collapse degree of fibres in sheets. As shown in Table 4-1, the fill factors of the recycled fibres in sheets show no significant change with increasing intensity of wet pressing. Additionally, the value of the fill factor measured in the 0μm depth images and that measured in the 4μm-depth images shows no significant difference. These results indicate that the collapse degree of the recycled fibres is not increased in wet pressing.

In the case of the kraft pulp fibres, the fill factor increases steadily as the pressing intensity is increased. This means that wet pressing has increased the degree of collapse of the kraft fibres in the sheets. The collapse behavior of the kraft fibres in wet pressing is different to that of the recycled fibres. A possible explanation for this difference is that the recycled fibres have already been collapsed to a certain degree during the previous papermaking process. It is therefore not easy to collapse these fibres further by wet pressing. The kraft pulp fibres were never dried and most of the fibres are uncollapsed. Therefore they are more likely to be collapsed in wet pressing.

The fibres in a sheet move closer together in wet pressing, forming more bonds. However other types of movement of fibres in wet pressing must still be clarified. One additional type of movement that was observed when the sheet was pressed was that the fibres were twisted so that they lay flat and became closer to each other. The new technique presented here can be used to quantify this twist of fibres in wet pressing. The twist angle defined in subsection 4.4.1.5 is used to quantifying the twist of fibres in wet pressing. The measured results of the twist angle will be discussed in Chapter 6.

Basing on the new technique, we have further developed a new technique for measuring fibre-fibre contacts in paper. The measured results will be outlined and discussed in Chapter 7.

4.7 Conclusions

Fibre dimensions, fibre orientation and fibre collapse have been measured directly in paper using a combined technique of resin embedding and confocal laser scanning microscopy. This is the first time a technique has been demonstrated for quantifying paper structure at the fibre level. Comparisons between the measured values of fibre wall areas by the new technique in paper with those measured by the routine confocal microscopy technique on free fibres show close agreement. The fibre orientation measured in the handsheets compares reasonably well with the theoretical value of fibre orientation of a random sheet. These results show that the measurements made by the new technique are valid.

Based on the new technique, new techniques for measuring fibre-fibre contacts have been developed. The new technique makes it possible to quantify the changes of individual fibres in paper in wet pressing and measure the fibre-fibre contacts directly in paper.

5 Methods used to vary fibre and sheet properties

5.1 Introduction

In order to verify the theory for tensile strength of paper, experiments were carried out trying to vary only one property of the fibres or paper and keep the other properties constant. In this project, we used hydrocyclone fractionation to generate fibre fractions with different fibre cross-sectional shape but approximately the same fibre length. We used cutting wet handsheets to generate fibre fractions with different fibre length but the same fibre cross-sectional dimensions and shape. We used wet pressing to vary the sheet density or the degree of bonding of the sheets. These experiments and the properties of the fibre fractions generated by these experiments are discussed in this chapter. The starting material for all these experiments was the never dried low kappa (30) pulp described in Appendix A2. This was a new pulp that was specially prepared for these experiments after the high kappa pulp used in Chapter 4 was found to contain too many shives.

5.2 Experimental methods

5.2.1 Wet pressing

The purpose of the wet pressing experiment is to generate sheet with different tensile strength but not to significantly affect the properties of the fibres in the sheets.

Most of the handsheets made in this project were pressed dynamically using a Sheet Roller Press. Only the handsheets from the fractions generated by cutting wet handsheets were pressed statically using a hydraulic pressing machine.

Pressing the sheets dynamically involved placing the plate, sheet and blotter between two press felts which were then passed through a roller press a number of times, as illustrated schematically in Figure 5-1. For the size of the handsheets used in this

project, the pressing load applied on the sheets can be calculated using the chart shown in Figure 5-2.

In the static pressing experiments, each handsheet, sandwiched between blotters and an iron plate, was pressed for 2 minutes so that the handsheet was transferred to the iron plate.

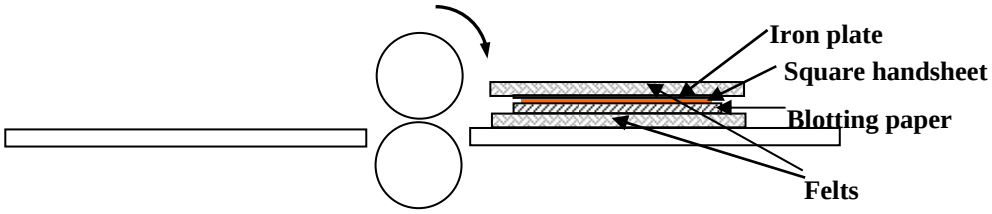

Figure 5-1 Schematic diagram of the Roller Sheet Press (drawing not to scale)

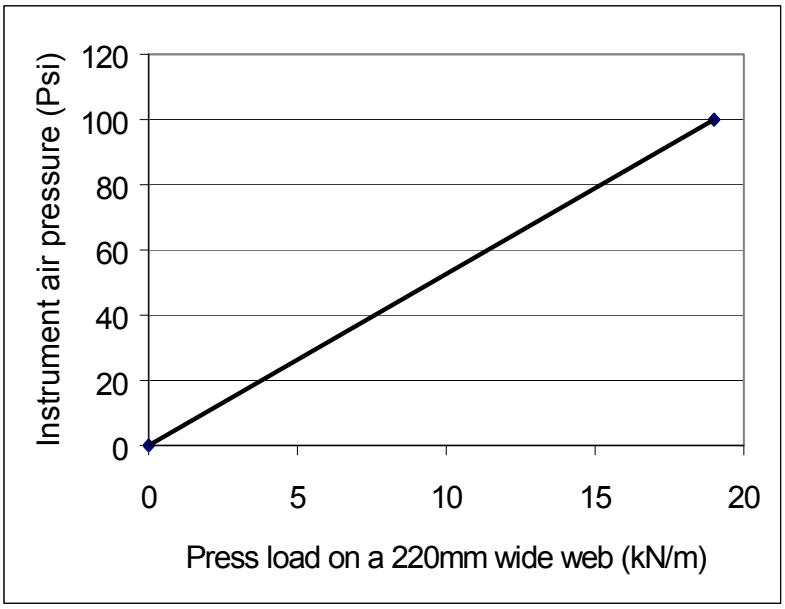

Figure 5-2 Pressure conversion from the instrument air pressure to press load on paper

In both of the dynamic and the static pressing experiments, handsheets were pressed at one of five pressing levels as given in Figure 5-1. These sheets were then dried under restraint in a conditioned test room (23ºC, 50%RH).

Table 5-1 PRESSING LOAD AND PRESSURE FOR DYNAMIC AND STATIC PRESSING

Press level	Dynamic press load (kN/m)	Static press pressure (kPa)
P_1	0*	100
P_2	3.0	200
P_3	7.0	500
P_4	3.0 + 10.0×2 passes	2000
P_5	3.0 + 10.0 + 20.0×10 passes	4000

*"0" represents pressing with no additional force applied to the rollers.

5.2.2 Fractionation – for generating fibre fractions with different cross-sectional shapes

Previous studies of hydrocyclone fractionation show that hydrocyclones can be used to separate chemical pulp effectively into accepts and rejects fractions with different cross-sectional properties (Gavelin 1991; Paavilainen 1993; Rehmat 1995; Li 1999). In earlier studies (Gavelin 1991; Rehmat 1995), fibre length and coarseness were claimed to be the key properties affecting the separation. Paavilainen (Paavilainen 1993) showed empirically that, for softwood pulps, the fibre wall thicknesses are significantly different for fibres in the accept and reject fractions from hydrocyclone fractionation. Recently, Li et al. (Li 1999) studied the mechanism of hydrocyclone fractionation systematically. They demonstrated that the 'apparent density' of fibres is the major factor controlling the hydrocyclone separation. An apparent density factor was defined and used to describe the efficiency of hydrocyclone separation. The derivation of the apparent density factor begins by idealising a fibre as a tube. The fibre wall area, A_f, for an ideal tubular-shaped fibre can be calculated from the outer diameter D_0 and the lumen diameter d_0 by the following equation.

$$A_f = \pi(D_0 - d_0)/4 \qquad \textbf{5. 1}$$

The apparent density factor is then given by the following equation.

$$AD = 4\pi A_f / P_0^2 = (D_0 - d_0)/D_0^2 \qquad \textbf{5. 2}$$

where AD is the apparent density factor and P_0 is outer perimeter.

The value of AD is can be calculated by measuring the perimeter and the wall area of the dry fibre according to its definition by Equation 5.2.

In physical terms, AD represents the fraction of the cross-sectional area of an idealized dry fibre cylinder occupied by the cell wall. When the fibre approaches a solid cylinder, AD approaches its maximum value of 1. When the fibre becomes more open AD decreases.

An AKW (Amberger Kaolinwerke Gmbh) 40mm cyclone was used to do the fractionation. The hydrocyclone test rig used in the experiment is illustrated in Figure 5-3. The rig consists of an AKW cyclone, a flow meter measuring in milli ampere, a mono pump and a stock tank. A container with a 200 mesh screen on the bottom is not shown in this Figure.

Two fractionation runs were conducted with the low kappa pulp. 100g of pulp was fractionated for each run. The mass split between the accepts and the rejects was set to be 9 to 1 for each run. The unit was running at 0.1% pulp consistency, which was found to give the best efficiency of separation by the AKW cyclone in a study by Mattson (Mattson 2001). The inlet flow rate was set at 0.2 mA, which was approximately 8 kilograms per second as one milli ampere was equal to 4 kilograms per second. The separated accept and reject fractions were each collected by drainage through a 200 mesh screen so that fines in these fractions have been removed before they were used in subsequent experiments. During the fractionation the stock tank was constantly refilled with fresh water so as to keep the level in the tank constant. A two-stage fractionation was carried out in the experiment in order to obtain good separation results. Figure 5.4 illustrates the procedure used.

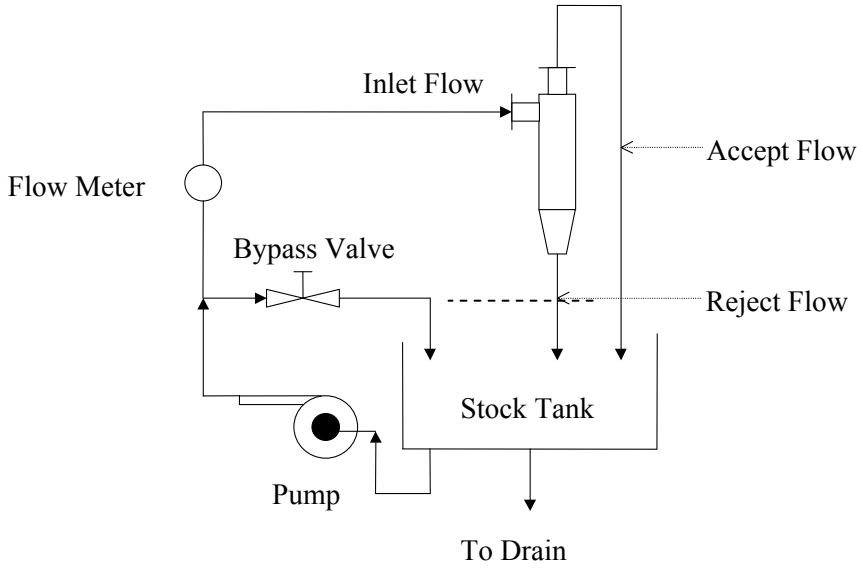

Figure 5-3 Hydrocyclone unit used in the fractionation experiment.

The final accept fraction was 'fraction AA' shown in Figure 5-4 and the reject fraction was 'fraction RR'. The fractions AA and RR were treated as the accepts and the rejects used in the subsequent experiment.

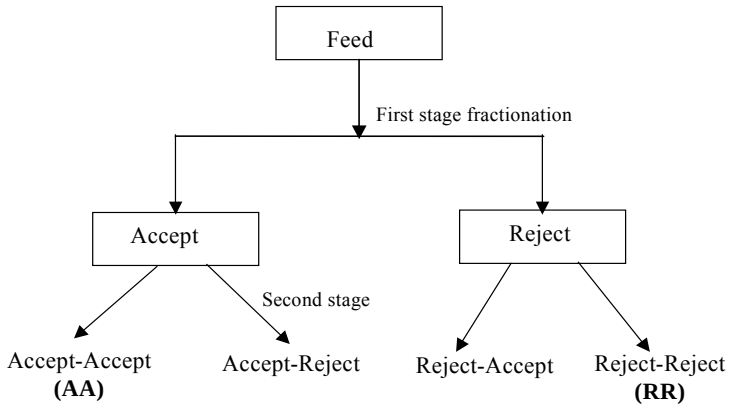

Figure 5-4 Procedure of the two-stage fractionation

AD given in Equation 5.2 was used to evaluate the fibre separation occurring in the hydrocyclone. The AD factors of the accepts and rejects were determined from measurement of the perimeter and wall area of fibres deposited on glass slides using the confocal microscope following the method described in (Li 1999). Figure 5-5 shows the cumulative distributions of the AD factors of the accepts and rejects fractions. The means of the AD factors of the accepts and the rejects are 0.50 and 0.57 respectively. Statistical analysis shows that the AD factors of the accepts and the rejects are

significantly different at a 99.5% confidence level. This indicates that the pulp fibres have been separated on the basis of different cross-sectional shape by the hydrocyclone operation. The length weighted fibre lengths of the accepts and the rejects are 2.42mm and 2.24mm. this compares with a length weight fibre length of the starting stock of mm. The fibre lengths of both accepts and rejects are somewhat higher than the starting stock due to the loss of fines in the filtering process.

Five sets of 60g/m^2 square handsheets were made from the accepts and the rejects respectively on a Moving Belt Sheet Former (see Appendix A). The apparent density of the handsheets were varied by pressing dynamically using the roller press at one of the 5 different pressing levels as shown in Table 5-1. The apparent density, as a function of pressing level, of handsheets of the accepts and the rejects from the low kappa pulp is shown in Figure 5-6. It can be seen that the sheet density of the accepts is up to 100kg/m^3 higher than handsheets made from the rejects. The difference in sheet density confirms that significant separation has been achieved in the hydrocyclone.

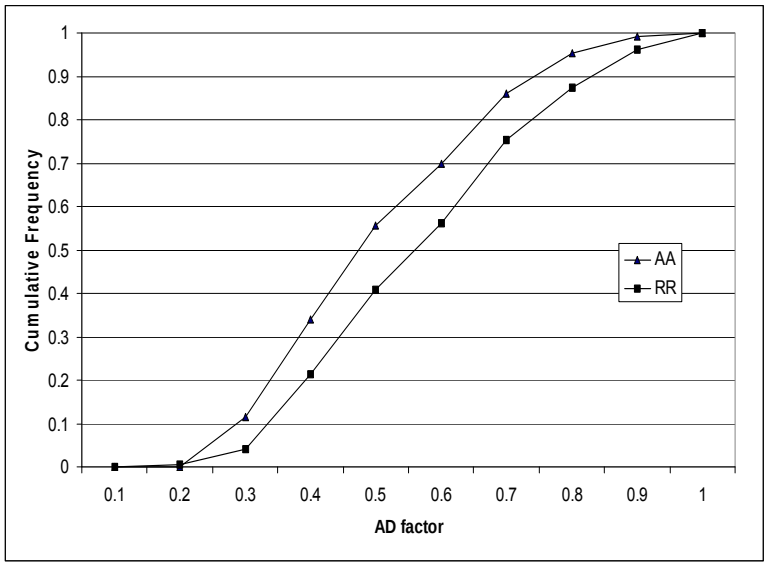

Figure 5-5 Cumulative distributions of AD factor of the accepts and the rejects

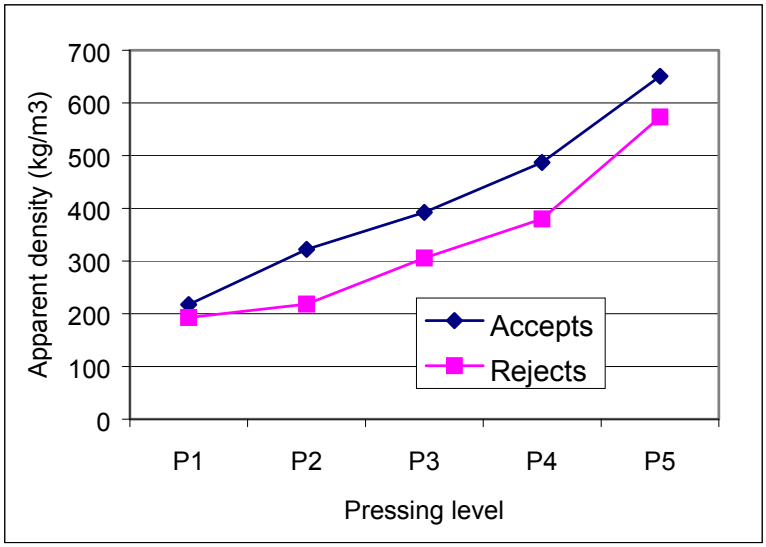

Figure 5-6 Apparent density of handsheets made from the fractionated low kappa pulp where the density has been varied by dynamic pressing at different pressing levels.

5.2.3 Cutting wet handsheets – for generating fibre fractions with different fibre length

This experiment aimed to vary fibre length only while keeping the other properties of fibre constant. Four fibre fractions with different fibre lengths were produced (L_0, L_1, L_2, L_3) with ever decreasing fibre length. The L_0 fraction was not cut and is the starting low kappa pulp from which all the other fractions were produced.

Wet handsheets were cut, immediately after they were formed on a Moving Belt Sheet Former (MBSF), using a specifically designed die (see Figure 5-7) to generate fractions of fibres differing only in the fibre length. The blades of the die are very sharp and thin so that the compression effects on the fibres during cutting have been minimized. The fibre ends generated by the cutting operation were carefully examined in the confocal microscope. As shown in Figure 5-8, no compression can be seen at the cut end.

In the cutting operation, the die was placed blade side down (Front view) on several wet sheets and impact pressed. Four fractions of fibres with different fibre length were then created as L_0: uncut fibres, L_1: cut once in one blade direction, L_2: cut twice, with the die being rotated 90º between cuts, L_3: cut wet handsheets made from L_2. The fibre

length of the four fractions was measured using a Kajaani optical fibre length analyser (see Appendix C for the full set of results).

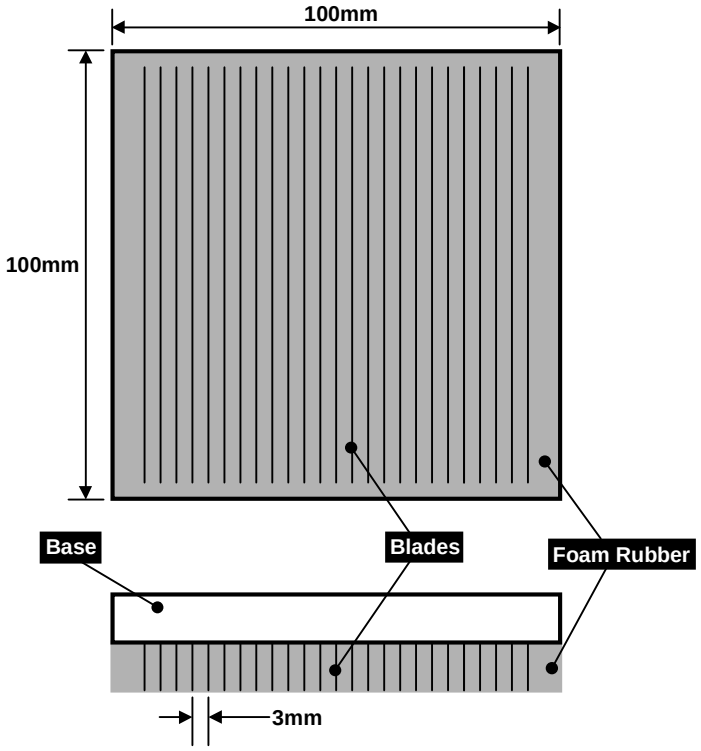

Figure 5-7 Diagram of the die used to cut wet handsheets (drawing not to scale)

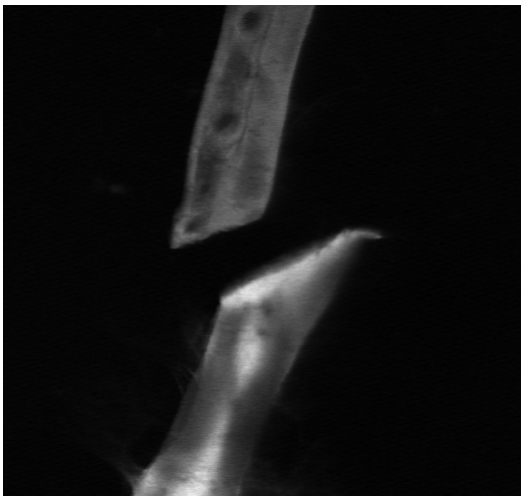

Figure 5-8 Image of fibre ends generated by the cutting operation

Figure 5-9 shows the length weighted fibre length distributions of the fibre fractions generated by cutting the wet handsheets. This method has been used in previous studies (Seth 1983; Kärenlampi 1996) and is believed to be able to change only fibre lengths while keeping other fibre dimensions constant. As shown in Figure 5-9, the length weighted fibre length distribution is shifted to a lower value range and narrowed after

the fibres were cut by the above operation. The average length weighted fibre length of L_0, L_1, L_2 and L_3 are 3.14mm, 2.53mm, 2.10mm and 1.80mm, respectively. The cut wet sheets were then reslushed and formed into handsheets. These results show that fibre length has been successfully reduced by cutting the wet handsheets.

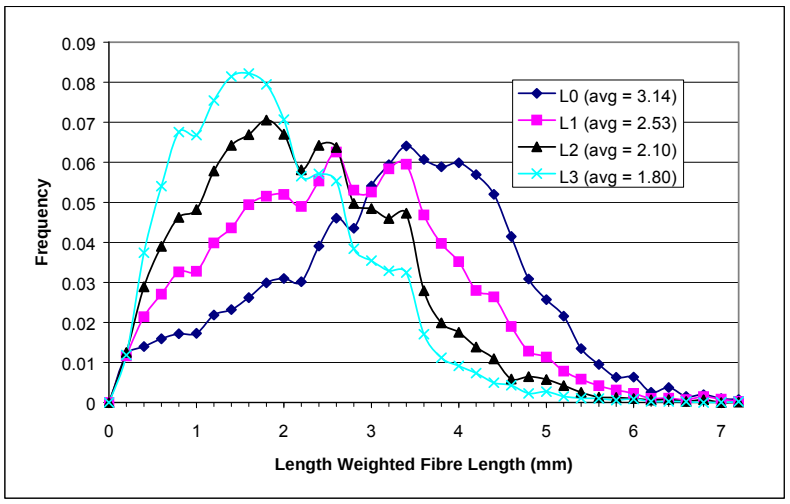

Figure 5-9 Fibre length distribution of the fractions generated by cutting wet handsheets

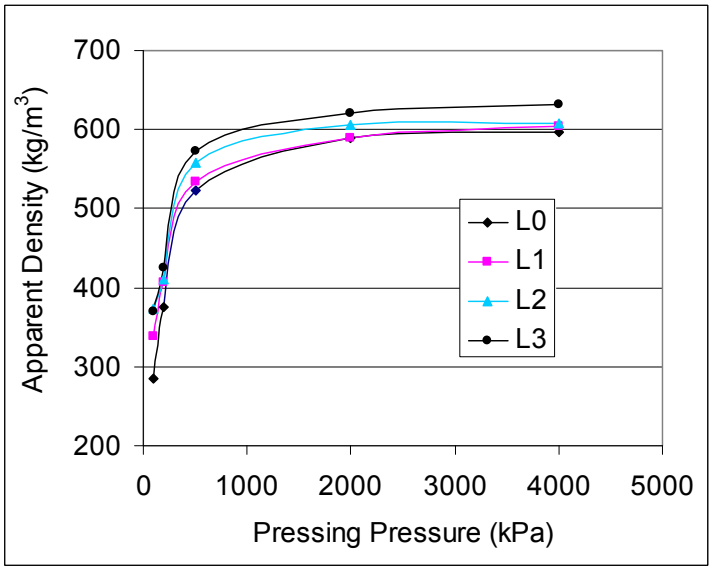

Figure 5-10 Apparent density of handsheets made from fibres with different fibre lengths where the density has been varied by static pressing at different pressing pressures.

Handsheets made from the fractions generated by cutting wet handsheets were pressed statically using a hydraulic press at one of the five pressing pressures shown in Table 5-1. The apparent density of handsheets pressed at different pressing pressures are

given in Figure 5-10. As can be seen in Figure 5-10, the apparent density of the handsheets have been varied effectively by wet pressing. The data also shows a small increase in sheet density, at a given pressing pressure, as the fibre length decreases. This probably arises because the shorter fibres are better able to pack together as the sheet formes.

5.3 Conclusions

It has been shown that fibres of the low kappa pulp have been successfully separated into fibre fractions with different fibre shape. It has also shown that fibre fractions with different fibre length have been generated by cutting the wet handsheets. Examination of the fibre ends generated by the cutting operation shows that no compression effects were induced by this operation. These fibre fractions can be used in subsequent experiments for verification of theories in this project.

6 Microscopic study of sheet densification by wet pressing

6.1 Introduction

Fibre bonded area and sheet density are strongly affected by wet pressing. A better understanding of the mechanisms of the changes of paper structure in wet pressing is of critical importance for the understanding of the fibre bonding and sheet densification. This information is also important for network modelling. In a sense wet pressing will bring fibres closer together and thus promote bonding. Wet pressing will also compress the fibres in the network and thus increase the degree of fibre collapse. However, how much these changes contribute to the sheet densification is still not clear.

Paulapuro (Paulapuro 2001) recently established that the observed effects of wet pressing on paper properties are related to changes of sheet density, the z-direction density distribution created by the pressing and surface evenness (topography). Szikla and Paulapuro (Szikla 1986; Szikla 1989) found that increasing fibre bonding is the dominant mechanism in the densifying effect of wet pressing (Szikla 1989). Gorres et al (Gorres 1993) believed that fibre collapse and deflection of free fibre segments are the predominant mechanisms at low pressing pressure, while at high pressure all spaces within the sheet which can be filled by such deflections have been filled, and therefore completion of fibre collapse and perhaps other effects then predominate. From these studies, it appears that the mechanisms in the densification effect of wet pressing on paper structure are still not completely understood.

Previous studies of fibre cross-sections measured the transverse dimensions of individual pulp fibres deposited on glass slides or embedded individually in resin (Kibblewhite 1991; Gorres 1993; Jang 1998). Gorres et al pressed very thin fibre networks (less than 0.1g/m^2) on glass slides and used a stylus profilometer to evaluate the transverse dimensions of fibres in the networks (Gorres 1993). However, no quantitative studies have been reported on the behaviour of fibre cross-sections in "true" paper in wet pressing, primarily because before the work of this thesis there was no technique to measure fibre cross-sectional dimensions directly in a sheet.

The collapse degree of fibres has been characterized in different ways, such as by the fibre aspect ratio (Kibblewhite 1991) and the fibre collapse index, which is defined either as the reduction of fibre thickness (Gorres 1993) or the reduction of fibre lumen area (Jang 1995), compared to an un-collapsed fibre. To calculate the fibre collapse index, the original fibre shape must be assumed to be either circular or rectangular in shape (Gorres 1993; Jang 1995). The collapse index cannot be measured directly and it only describes the shape of the fibre lumen area, completely neglecting the shape of fibre wall area.

One factor that has not been considered in studies of pressing is the twisting of the fibres so that their cross-sectional major axis rotates to be closer to parallel to the paper plane. The orientation of the fibre with respect to the paper plane could strongly affect the structure of the paper. Decreasing the number of twists in fibres will increase sheet strength (Mohlin, Dahlbom et al. 1996).

In this chapter, a fibre shape factor and a twist angle of the fibre cross-section are defined. These parameters are measured directly in handsheets using the cross-section preparation and analysis technique describe in Chapter 4. The results are used to quantify the changes of fibres in the handsheets in wet pressing. The mechanisms behind densification effects of wet pressing on paper structure are discussed.

6.2 Theory

6.2.1 Degree of fibre collapse in paper

For the purpose of quantifying the degree of collapse of fibres in sheets we defined the new term of shape factor, f_m, as the ratio of the fibre wall area, A_f, to the area of the smallest rectangular bounding box, A_s, that can completely enclose the irregular shape of the fibre. (Refer to subsection 4.4.5). In this section, we will examine the relationship between the shape factor and the degree of collapse of the fibre. To do this we begin by assuming that the fibre cross section before wet pressing is circular with diameter, D, and wall thickness, t, and that the fibre wall area, A_f, is constant with

wet pressing. We assume that if the thickness decreases by a distance δ_D, then the width will increase by the same amount (see Figure 6-1). Accordingly, f_m is:

$$f_m = \frac{A_f}{A_s} = \frac{A_f}{(D-2\delta_D)(D+2\delta_D)} = \frac{\pi t(D-t)}{D^2-4\delta_D^2} \qquad \textbf{6. 1}$$

Equation 6.1 can also be written as:

$$f_m = \frac{\pi^2 (t/P)(1-t/P)}{1-(\delta_D/r)^2} \qquad \textbf{6. 2}$$

where P is the fibre perimeter, and r is the fibre radius.

Following Jang (Jang 2001), the collapse index, CI, is defined as $CI = (\delta_D/r)^2$. For a thin walled fibre, $t << P$, and $(1-t/P) \approx 1$, and Equation 6.2 becomes:

$$f_m = \frac{\pi^2 (t/P)}{1-CI} \qquad \textbf{6. 3}$$

Obviously, uncollapsed fibres and fully collapsed fibres will have the minimum and the maximum values of f_m respectively. These maximum and minimum values of f_m can be used to create an approximate scale to separate fibres in a sheet into three collapse-states, viz. uncollapsed fibres, partially collapsed fibres and fully collapsed fibres (Figure 6-2). The validity of using the boundary values of f_m in describing the collapse-state of a fibre will be verified in this study.

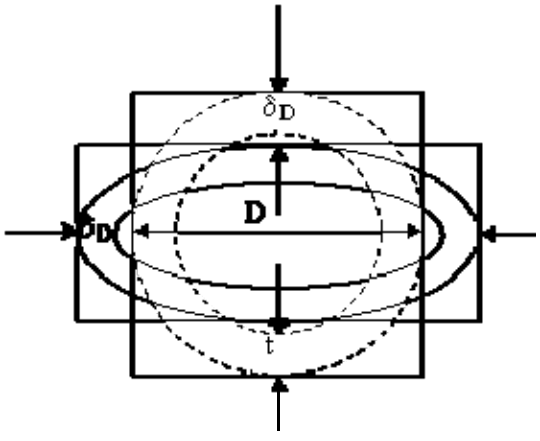

Figure 6-1 Model fibre cross-section

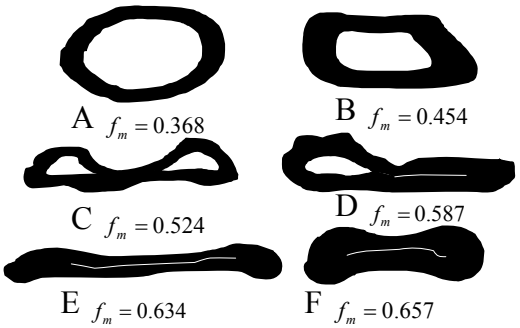

Figure 6-2 Different collapse states of fibre: uncollapsed fibres (A, B), partially collapsed fibres(C, D), and fully collapsed fibres (E, F).

6.2.2 Reduction in paper thickness by fibre twist and fibre collapse

Assuming the paper has layered structure, fibres in each layer are twisted and collapsed in wet pressing, reducing the thickness of each layer. The total reduction in the paper thickness is the sum of the thickness reduction of each layer. Figure 6-3 shows schematically the i^{th} fibre in a layer of a sheet before and after it is pressed. Before the fibre is pressed, the fibre has width, D_{wi}, thickness, D_{hi}, and twist angle, β_i. After it is pressed, the width, thickness and twist angle are D'_{wi}, D'_{hi} and β'_i respectively. If the paper has m independent layers and each layer has n fibres, the total reductions in paper thickness from the fibre twist, $\overline{\Delta T}_{twist}$, and from fibre collapse, $\overline{\Delta T}_{collapse}$, are given by Equations 6.4 and 6.5 respectively:

$$\overline{\Delta T}_{twist} = \frac{m}{n}\sum_{i=1}^{n}\left[D_{wi}\sin\beta_i - D'_{wi}\sin\beta'_i\right] \qquad \textbf{6. 4}$$

$$\overline{\Delta T}_{collapse} = \frac{m}{n}\sum_{i=1}^{n}\left[\frac{D_{hi}}{\cos\beta_i} - \frac{D'_{hi}}{\cos\beta'_i}\right] \qquad \textbf{6. 5}$$

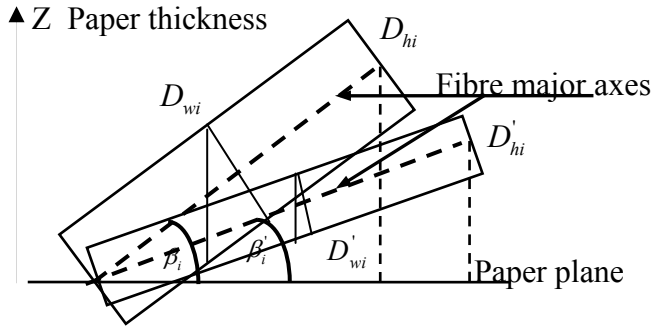

Figure 6-3 Schematic showing the reduction in paper thickness contributed by fibre twist and fibre collapse in any layer of a sheet

6.3 Sample used in this study

The low kappa pulp was used in this study (refer to Appendix A). This is the pulp labelled L_0 in subsection 5.2.3. Five sets of 60g/m^2 square handsheets were made on the Moving Belt Sheet Former. Each set of handsheets was pressed statically at one of 5 pressures, viz 100kPa, 200kPa, 500kPa, 2000kPa and 4000kPa (for details refer to subsection 5.2.1). Cross-sections of handsheets pressed at 100kPa, 500kPa and 4000kPa, which are denoted as L_0P_1 L_0P_3, and L_0P_5 respectively, were examined in a confocal microscope. The method for sample preparation for the confocal microscope has been given in subsection 4.3.2. The methods for measuring the shape factor, f_m, and the twist angle, β, have been given in Subsection 4.4.1.5.

6.4 Results and discussion

6.4.1 Changes in paper cross-section

Figure 6-4 shows typical cross-sectional images of the three samples L_0P_1, L_0P_3 and L_0P_5. The sample thickness and the void space are reduced with increasing pressing pressure. In sample L_0P_1, it can be seen that most fibres are either uncollapsed or partially collapsed, but there are also some fully collapsed fibres. In sample L_0P_3, the number of uncollapsed fibres is dramatically reduced, and around half the fibres are fully collapsed. In sample L_0P_5, most of the fibres have been fully collapsed, but a few uncollapsed fibres still can be seen.

Figure 6-4 also shows that fibres in the sheet have been rearranged in wet pressing. Some of the fibres are pressed into gaps or void space. The type of movement is called gap closure in this project.

In summary three types of movement of fibres in wet pressing have been observed in this study including collapse of fibre, twist of the fibre and gap closure. These three types of movements, which control the change in paper thickness, have been quantified in this study and the results are discussed in the following paragraphs.

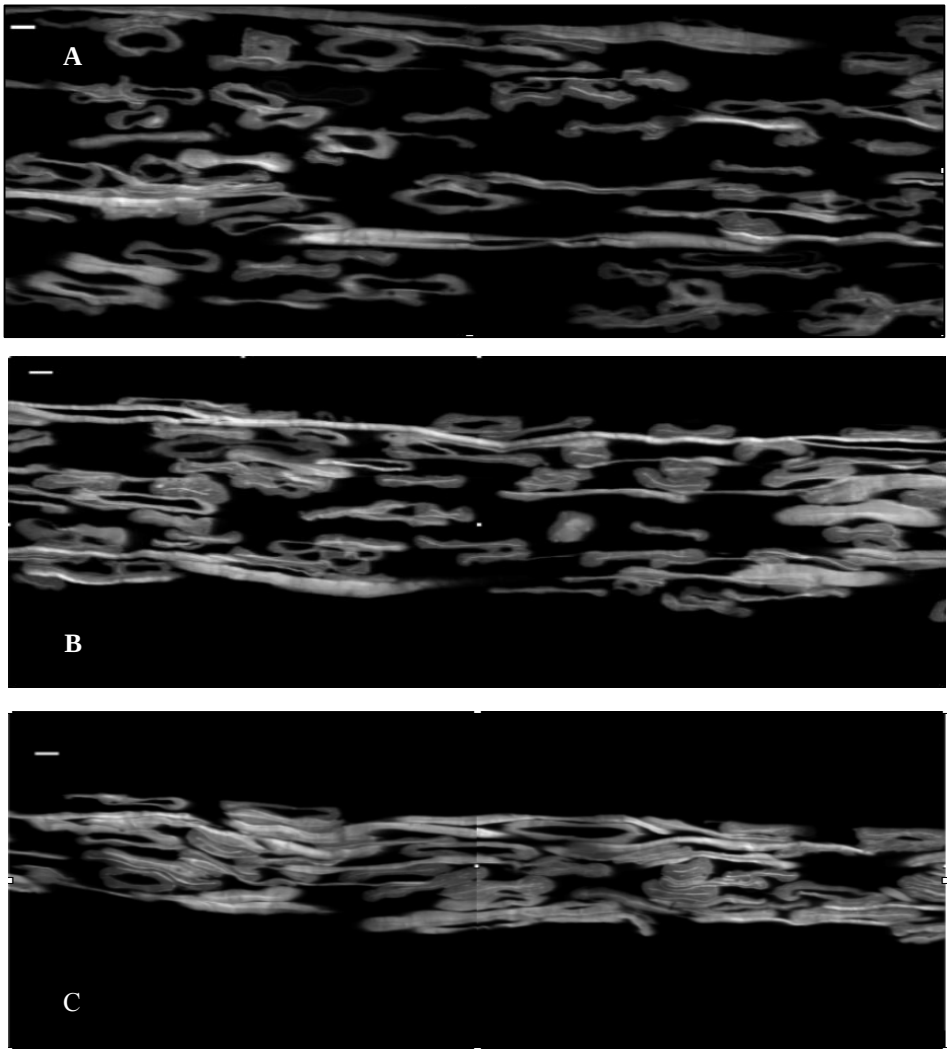

* The size bar is 10μm

Figure 6-4 Images of cross-sections of sample L_0P_1 (A), L_0P_3 (B) and L_0P_5 (C)Table 6-1 summarizes the fibre dimensions and the sheet properties measured in this work. The fibre wall area was not changed by wet pressing and the mean value of f_m increases with increasing wet pressing pressure. The twist angle falls from 9^o to 6.8^o with increasing wet pressing.

Table 6-1 Handsheet properties and mean fibre properties

Sample	Wet press pressure (kPa)	Shape factor, f_m (%)	Average twist angle	*Fibre wall area (μm^2)	Out-of-plane angle (degree)	Number of fibres measured	Sheet density (kg/m^3)	Paper thickness (μm)	Tensile index (kNm/kg)
L_0P_1	100	0.548±0.014**	9.0±1.1	206±9**	5.13±0.61	247	286	239	34.45
/	200	/	/	/	/	/	375	172	36.98
L_0P_3	500	0.589±0.013	8.2±1.0	198±9	4.49±0.48	241	522	125	45.98
/	2000	/	/	/	/	/	590	109	48.04
L_0P_5	4000	0.603±0.011	6.8±0.8	205±9	4.64±0.52	247	596	107	49.95

*Fibre wall area and fibre axes have been corrected by its angle to the surface of the paper cross-section.

** ± is 95% confidence interval.

Figure 6-5 shows the twist angle distribution of fibres in the three samples L_0P_1, L_0P_3 and L_0P_5. As the pressing pressure is increased, the number of fibres with twist angle less than 10^o increases, while the number of fibres with twist angle more than 10^o decreases. It can be seen that 67% of the fibres in sample L_0P_1 have a twist angle less than 10^o and this percentage is increased by wet pressing to 71% for sample P_3 and to 78% for sample L_0P_5. This reduction in fibre twist will reduce the amount of space taken by the fibre in the paper structure, therefore reducing the void space and increasing the density of the paper. The reduction in fibre twist could also increase the potential bonding surface area of the fibres, especially for collapsed fibres.

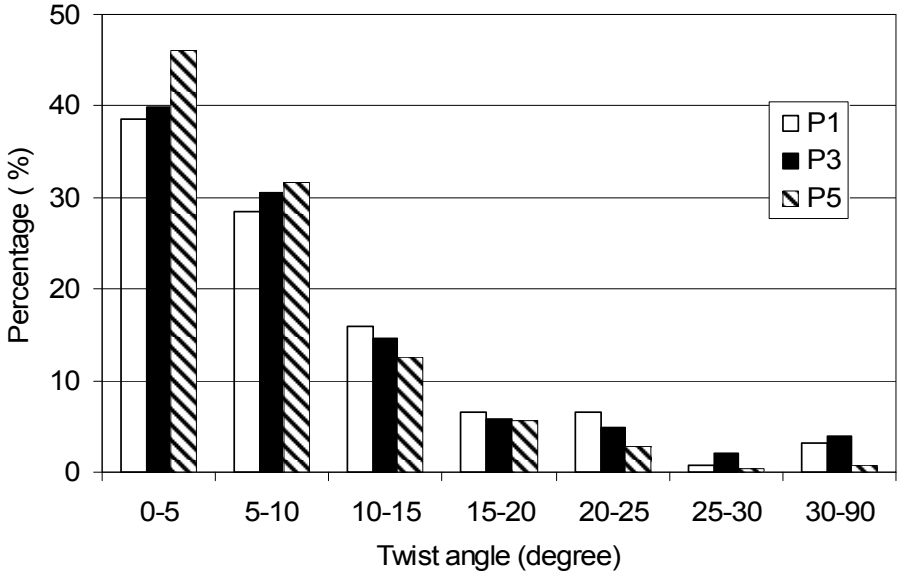

Figure 6-5 Frequency distribution of twist angle of fibre cross-section of sample L_0P_1, L_0P_3 and L_0P_5

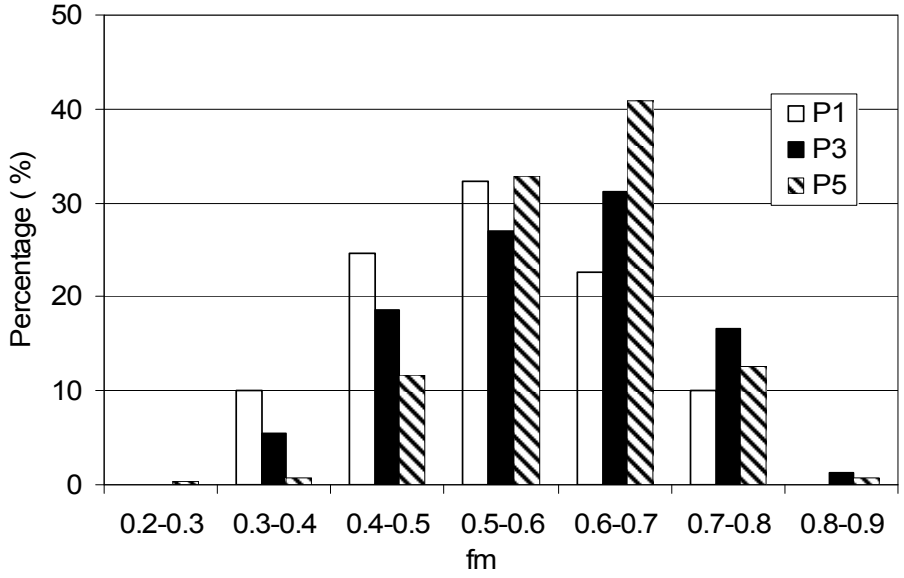

Figure 6-6 Frequency distribution of the fibre shape factor of sample L_0P_1, L_0P_3 and L_0P_5

The frequency distributions of f_m are shown in Figure 6-6. For sample L_0P_1, f_m has an almost symmetrical distribution. When the pressing pressure is increased, the distribution of f_m skews to a higher f_m range and becomes narrower. Since the three samples were made from the same pulp, fibres in the three samples should have the same wall thickness and perimeter. In that case, according to Equation 6.3, the value of f_m should be mainly affected by the degree of collapse of the fibres. The trends in f_m are therefore most likely indicative of fibre collapse.

As discussed in subsection 6.2.1, the maximum and the minimum values of f_m can be used to assign the fibres as collapsed, partially collapsed or uncollapsed. The boundary values of f_m used to do this were set somewhat arbitrarily. Fibres with f_m less than 0.50 were treated as uncollapsed fibres, fibres with f_m greater than 0.60 were treated as fully collapsed fibres and fibres with f_m in between 0.50 and 0.60 were treated as partially collapsed fibres. Using this classification 35% of fibres in the slightly pressed sample P_1 were uncollapsed and 33% were fully collapsed (Figure 6-6). After the sample was pressed at 500kPa, the percentage of uncollapsed fibres dropped to 24% and the percentage of fully collapsed fibres rose to 49%. After the sample was heavily pressed, the percentage of fully collapsed fibres increased to 54% and the percentage of uncollapsed fibres fell to 13%. The percentage of partially collapsed fibres stayed

relatively stable at around 30% in all the three samples. These quantitative results are consistent with the observations shown in Figure 6-4, but quite different from those reported by Gorres and his coworkers (Gorres 1993) who found fibres of a softwood kraft pulp can be totally collapsed at a pressing pressure of 2240kPa. This indicates that the collapse behaviour of fibres on glass slides and in paper is different.

There are two major factors that may cause the observed non-uniform collapse of fibres. Firstly, fibre collapsibility will vary between fibres and at different points along fibres. Secondly, and perhaps more importantly, the non-uniform structure of paper causes an uneven pressure transfer in the network that results in the non-uniform collapse of fibre.

6.4.2 Relationship between apparent density and the changes in fibre cross-section

The apparent density of the handsheets increased from 286 kg/m^3 to 522 kg/m^3 as the pressure increased from 100 to 500 kPa. However, pressing at 4,000 kPa increased the sheet density only slightly, to 596 kg/m^3, compared to pressing at 500kPa (Table 6-1). Gorres et al (Gorres 1993) found a similar relationship between density of paper and the wet pressing pressure. They failed to explain the continuing increase in density at high pressure where they believed that fibres are totally collapsed. One reason is that they used the measured degree of collapse of fibres pressed on glass slides to represent the degree of collapse of fibres in paper, which as discussed before is a different situation to collapse in the pressing of paper. Another reason is that they did not take account of the contribution of fibre twist to the density of paper.

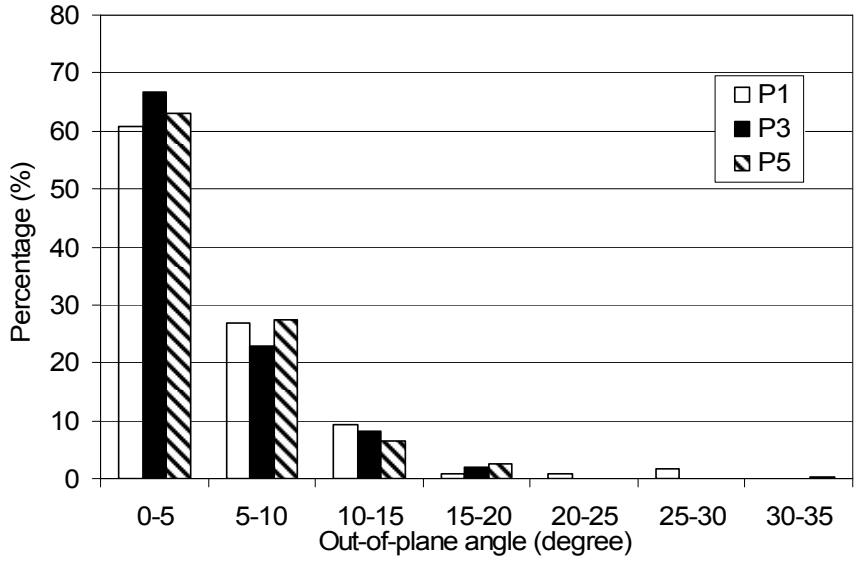

Figure 6-7 Frequency distribution of out-of-plane angle of sample L_0P_1, L_0P_3 and L_0P_5

Gorres and Luner developed a model for the apparent sheet density (Gorres and Luner 1992). The model assumed that increasing fibre deflection with increasing wet pressing pressure is a major mechanism in the densification of the paper. However, no evidence was given to prove this relationship. In this study, the out-of-plane deflection angles of fibre segments in samples L_0P_1, L_0P_3 and L_0P_5 were measured. If the sample is not arranged exactly vertically, an error will arise for the measured value of the out-of-plane deflection angle. A correction, similar to the correction for the twist angle measurements, has been done for each individual fibre to avoid this error. The results (Table 6-1) show that the average out-of-plane deflection angle of fibre segments in the three samples ranges from 4.49^o to 5.13^o, and no regular increase with wet pressing pressure can be observed. The distribution, shown in Figure 6-7, of out-of-plane defection angles, also shows no regular trends with pressing level. If the out-of-plane angle of the fibre segment stays constant, the deflecting distance of the fibre segment will be reduced as the pressing pressure is increased. This is because wet pressing will reduce the distance between fibre-fibre contacts.

To quantify, using Equations 6.4 and 6.5, the contributions of fibre twist, fibre collapse and gap closure to the measured reduction in paper thickness we assumed that the samples have 10 layers and the number of layer stays constant as the pressing pressure

is changed. These data were used to calculate the $\overline{\Delta T}_{twist}$ and $\overline{\Delta T}_{collapse}$ between samples L_0P_3 and L_0P_1 and between samples L_0P_5 and L_0P_3, and the results are given in Table 6-2. The measured total thickness reduction between samples L_0P_3 and L_0P_1 is 114μm, of which the contributions from the fibre twist and fibre collapse only accounts for 16%. We believe that the rest of the thickness reduction is caused by closing the gap between the layers. The total reduction in paper thickness between samples L_0P_5 and L_0P_3 is 18μm which is mostly contributed by fibre twist and fibre collapse. These findings clearly show that fibre twist, fibre collapse and gap closure occur simultaneously at low pressing pressures and the gap closure is the predominant mechanism in paper structure densification at low pressures. When the pressing pressure was increased from 500 to 4000kPa, the density increased only slightly. This density increase was mainly due to the additional twist and collapse of the fibres at the high pressure.

Table 6-2 Reduction in paper thickness

	* L_0P_3- L_0P_1	* L_0P_5- L_0P_3
$\overline{\Delta T}_{twist}$ (μm)	7	3
$\overline{\Delta T}_{collapse}$ (μm)	11	10
** $\overline{\Delta T}_{gapclosure}$ (μm)	96	5
*** $\overline{\Delta T}_{measured}$ (μm)	114	18

* L_0P_3- L_0P_1 and L_0P_5- L_0P_3 represents thickness reduction between those samples.

** $\overline{\Delta T}_{gapclosure} = \overline{\Delta T}_{measured} - \overline{\Delta T}_{twist} - \overline{\Delta T}_{collaspe}$. *** $\overline{\Delta T}_{measured}$ is the measured total reduction in paper thickness.

6.5 Conclusions

A fibre shape factor and twist angle of fibre cross-section in paper have been defined for the purpose of quantifying the changes in the transverse dimensions of fibres in paper in wet pressing. It was found that fibre twist, fibre collapse and gap closure are the major types of movement of fibres in paper in wet pressing. In particular, fibre twist has been found and quantified for the first time. The results show that the number of fibres with twist angles greater than 10^o is reduced by wet pressing and that the average twist angle decreases as the pressing pressure was increased. The fibre shape factor of fibres in the

lightly pressed handsheets showed an almost symmetrical distribution, which indicates that the degree of collapse of fibres in the handsheets is symmetrically distributed. The distribution was narrowed and skewed to the high value range when the handsheets were pressed at 500kPa or at 4000kPa. These results show that fibres in the handsheets cannot be totally collapsed by wet pressing even when the very high pressing pressure (4000kPa) is used. The experimental data also suggest that out of plane fibre deflection angle is independent of wet pressing pressure.

Fibre twist, fibre collapse and gap closure occur simultaneously at low pressing pressures, and the gap closure is the predominant mechanism in paper structure densification at low pressing pressures (less than 500kPa). Increasing pressing pressure beyond 500kPa only increases the apparent density slightly and the density increase is mainly contributed by the additional twist and collapse of the fibres at the higher pressing pressure.

7 Study of fibre-fibre contacts and verification of the model for number of fibre-fibre contacts and expressions for relative bonded area *(RBA)*

7.1 Introduction

In Chapter 3, we have presented a new model for the number of fibre-fibre contacts (Equation 3.11). This model has been further extended to derive expressions for Relative Bonded Area (RBA). In this chapter, we will present the experimental verification of the model.

Chapter 2 has reviewed that no technique is available for measuring the number of fibre-fibre contacts directly in paper. For the first time a new technique that can measure fibre-fibre contacts directly in paper has been developed in this project. The new technique involves resin embedding and confocal laser scanning microscopy and has been detailed in Chapter 4. Using the new technique, we obtained high quality cross-sectional images of the samples in which some fibres or fibre segments were imaged along their long axes. These fibres were chosen as fibres of interest for the measurements of fibre-fibre contacts. The measured results, including the nature of each fibre contact, the number of fibre-fibre contacts, the lengths of the free fibre segments and the out-of-plane angle of each free fibre segment, will be discussed in this chapter. The effects of fibre length and fibre cross-sectional shape on the properties of fibre fibre contacts are also studied. It is shown that a two parameter Weibull probability density function provides a good fit to the measured distribution of free fibre length. The measured number of fibre-fibre contacts will be used to verify the model for number of fibre-fibre contacts presented in Chapter 3.

Chapter 2 has also reviewed that measurement of RBA is always problematic. In this chapter, we will present two methods for measuring RBA, viz. by measuring the BET area of the sheets by nitrogen adsorption technique (RBA_{N_2}) and by measuring scattering coefficients of the sheet (RBA_{sc}). The measured results of RBA will be used to further check the correctness of the model for the number of fibre-fibre contacts.

7.2 Sample used in this study

The low kappa pulp (see Appendix A2) was used in this study. Sets of handsheets were made from pulps that had been made from the starting pulp either by hydrocyclone fractionation (see subsection 5.2.2) or by forming sheets, wet cutting them and reslushing (see subsection 5.2.3). For each set of handsheets the density was changed by wet pressing (see subsection 5.2.1).

7.3 Results and discussion

7.3.1 Average results for fibre-fibre contacts

Table 7-1 summarizes the average results of the measured fibre-fibre contacts. As shown in Table 7-1, for the accepts and rejects, as the pressing pressure increases the number of fibre-fibre contacts per unit fibre length increases. This means new contacts of fibres are formed in wet pressing. Associated with this is a reduction in the free fibre length. It also shows that the percentage of full contacts increases as the pressing pressure is increased. For a given pressing level, the sample of the accepts and that of the rejects have almost the same values of the average free fibre length and number of fibre-fibre contacts per unit fibre length. As discussed in 5.2.2, the accepts and the rejects have different fibre cross-sectional dimensions (different AD factor). However, the two sets of handsheets made from these pulps have almost the same properties of fibre-fibre contacts, for a given level of wet pressing, although handsheets from the accepts always have higher density than the rejects. It should be emphasised that the above results do not necessarily mean that fibre shape has no effect on fibre-fibre contacts because, as indicated in our model (Equation 3.11), number of fibre-fibre contacts is affect by the fill factor, fibre width, fibre density and sheet density. At this stage it is still difficult to make paper with fibres with different shapes while still keeping the other factors constant. Further study is needed for drawing a conclusion on the effect of fibre shape on number of fibre-fibre contacts.

Table 7-1 also shows that sample $AccP_1$ has higher percentage of full contacts than sample $RejP_1$. This is because the accept fibres, which are thin walled fibres, are more

flexible than the reject fibres, the thick walled fibres, therefore show a higher ability for bonding. After wet pressing, full contacts in samples from both fractions are increased dramatically, indicating, in another aspect, the increase in the degree of fibre bonding. We should also note that each full contact in the accept samples has higher contact area in average than that of a full contact in the reject samples.

Table 7-1 Summary of the average results of the geometrical parameters of paper structure

Sample	N_c * (no./mm)	Full contact (%)	Partial contact (%)	Free fibre length* (μm)	Out-of-Plane angle* (degree)	Total length of fibre segment measured (μm)	Fibre width** (μm)	Fibre height** (μm)	Sheet Density (kg/m^3)
$AccP_1$	13.0±1.5	24	76	73.8±7.7	4.39±0.67	10563	31.6±1.3	13.7±0.7	218
$AccP_3$	20.8±2.0	35	65	45.4±5.1	5.36±0.71	9594	34.3±1.4	11.9±0.6	392
$AccP_5$	27.7±2.1	47	53	35.7±3.0	5.76±0.56	9504	36.6±1.5	9.7±0.4	651
$RejP_1$	12.9±4.8	18	82	82.6±11.9	7.41±1.30	9225	29.5±1.2	15.8±0.8	193
$RejP_3$	19.5±2.0	34	66	50.3±5.5	6.07±0.86	9281	32.7±1.3	14.0±0.7	306
$RejP_5$	28.8±2.6	44	56	35.8±4.1	6.75±0.96	6862	34.9±1.3	11.2±0.4	510
***L_0P_3	23.4±2.4	48	52	42.1±4.2	4.30±0.63	8794	31.0±1.2	11.2±0.5	522
L_1P_3	22.2±1.9	53	47	45.6±5.2	4.62±0.65	7528	31.8±1.2	12.3±0.6	535
L_2P_3	22.5±2.1	50	50	45.4±5.0	6.35±2.27	8212	33.2±1.3	10.2±0.4	434

* ± is 95% confidence interval. ** fibre width and height were measured in sheets and fibre width has been corrected by the angle that the fibre sitting to the cross-sectional surface of the sample. ***these samples were statically pressed.

For samples with different fibre length but pressed at the same pressing pressure (samples L_0P_3, L_1P_3, and L_2P_3), the number of fibre-fibre contacts, the percentage of the full contacts and the free fibre length are almost the same. This indicates that fibre length has no effect on the properties of fibre-fibre contacts.

The out-of-plane deflection angles of all the fractions used in this study show no regular trend with the pressing intensity (Table 7-1). It can also be shown that the distributions of the out-of-plane deflection angle of samples made from the same pulp fraction but pressed at different pressing levels are very similar and show no regular trends with pressing intensity. These results are consistent with the results shown in Table 6-1, where the out-of-plane deflection angles were measured in a different way, but are inconsistent with what was assumed in a Gorres and Luner's study (Gorres and Luner 1992), in which they assumed that the fibre deflection increases with increasing pressing pressure. If the out-of-plane deflection angle of the fibre segment stays

constant, the deflecting distance of the fibre segment will be reduced as the pressing intensity is increased because the free fibre segment length has been reduced as the pressing intensity is increased. This movement provides a densification effect for the paper structure in wet pressing (for details see Chapter 6).

7.3.2 Frequency distribution of free fibre length

Different quantities have been defined as the free fibre length. The free fibre length has been defined as the distance between the centres of fibre crossings (Kallmes and Corte 1960); as the intercrossing distance represented by the distance between the centres of bonded crossings (Kallmes 1963); as the projected interbond distance, which is the distance between the projection of the bonds on the fibre axis (Page 1962). Kallmes and Bernier (Kallmes 1963) have shown that these three definitions of free fibre length will have different absolute values but will produce the same distribution of the free fibre length. In this study we define the free fibre length as the distance between the centers of two neighbouring contacts or bonds, which is the same definition as that used in (Kallmes 1963).

Kallmes et al (Kallmes and Corte 1960; Kallmes 1963) proposed that the free fibre length of a random sheet has a negative exponential distribution as $f(g) = (1/\overline{g})e^{g/\overline{g}}$, where g is the free fibre length and $\overline{g}$ is the mean of the free fibre length. They found this equation to hold for 2-dimensional sheets that are almost completely bonded, but bias arises for normal sheets (Kallmes 1963).

In this thesis we used a two-parameter Weibull probability density function (PDF), as shown by equation 7.1, to describe the distribution of the free fibre length.

$$f(g) = \frac{c}{b}\left[g/b\right]^{c-1} \exp\left[-(g/b)^{c}\right] \qquad \textbf{7. 1}$$

where b and c are constants, and $b, c > 0$, and $g \geq 0$.

The Weibull parameter b is scale parameter, and c is the shape parameter. The Weibull parameter is more general than the negative exponential distribution. When the

shape parameter, c, is equal to 1, the Weibull PDF becomes negative exponential distribution. In this thesis, the values of b and c for different samples were determined through the best-fit by non-linear least-squares curve fitting.

Different fit lines with different values of c for sample $AccP_3$ are shown in Figure 7-1. As can be seen in Equation 7.1, when c is equal to 1, the Weibull PDF becomes negative exponential distribution and does not fit the experimental results in Figure 7.1 well. This indicates that the free fibre length does not take the negative exponential form proposed by Kallmes and Bernier (Kallmes and Corte 1960; Kallmes 1963). The distributions of free fibre length measured in this study, as shown in Figure 7.1 and in later figures, are very similar in shape to the measurements reported by Page et al (Page 1962).

Dent (Dent 2001) showed, about the same time as this part of work was being carried out, that a random sheet of fibres of finite length has a general gamma distribution of the free fibre length. Dent has also provided good theoretical basis for using the general gamma distribution to describe the free fibre length distribution. It is recommended to use the data in this thesis to test the gamma distribution proposed by Dent in the future work.

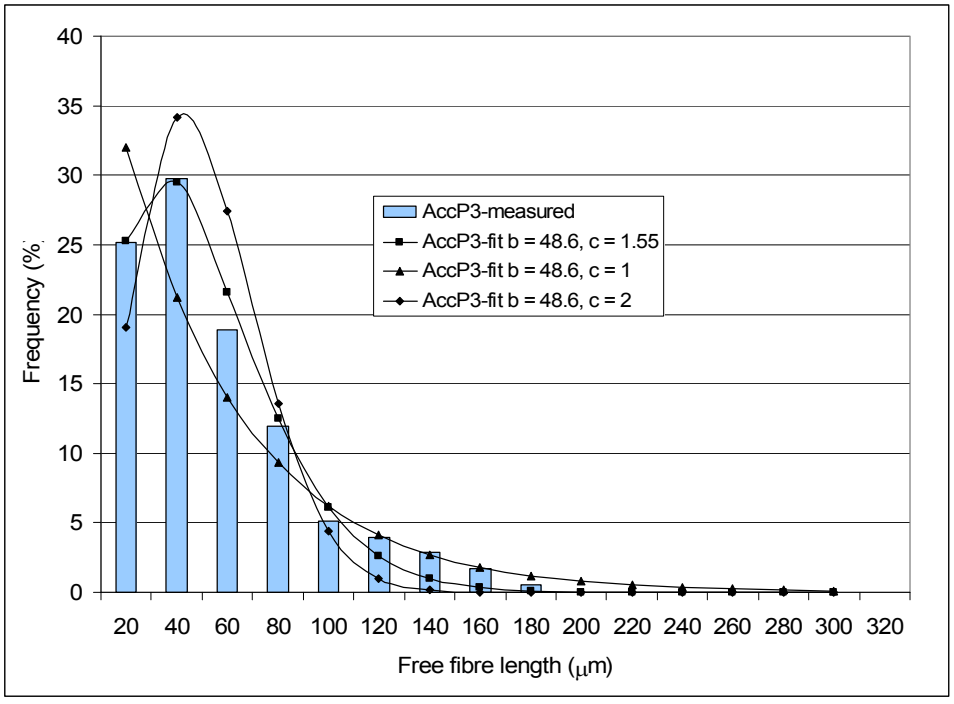

Figure 7-1 Fit lines with constant b value but different c values for sample $AccP_3$

The distributions of free fibre length of the samples made from the accepts and the rejects are given in Figure 7-2 and 7-3 respectively. The lines shown in these figures are the best fit of the Weibull PDF. The values of parameters of b and c are also given in these figures. The values of b are each about 10μm higher than the corresponding mean values of the free fibre length (see Table 7-1) The best-fit lines of Weibull PDF for these samples have values of c greater than 1, and the values of c for these samples except $RejP_1$ decrease as the wet pressing intensity is increased. We believe that the value of c for a normal sheet is in the range of 1 to 2.

The interval size at which the measured free fibre length was grouped significantly influences the "smoothness" of its frequency distribution. The greater the interval size, the smoother the distribution, but this will also reduce the points available for the comparison with the predictions made by Equation 7.1. In this study we chose arbitrarily a 5μm interval to group the measured free fibre lengths to do the fit with the Equation 7.1. A 20μm interval was used when the distributions were plotted in order to smooth the lines. As shown in Figure 7-2 and 7-3, Equation 7.1 can fit distributions of the free fibre lengths well

At a given pressing level, the free fibre length of the accepts sample shows a very similar distribution to that of the corresponding sample of the rejects fraction. This further suggests that for the sheets made from these pulps, the cross-sectional dimensions of the fibres have no effect on the frequency distribution of the free fibre length and the number of fibre-fibre contacts per unit fibre length. Kallmes and Bernier (Kallmes 1963) have shown that the free fibre length distribution is independent of fibre width, which is in agreement with the results obtained in this study. Page et al (Page 1962) claimed that the free fibre length and the frequency of bonding are highly sensitive to the fibre width and to the fibre flexibility, but no particular experimental data were provided to support these claims. The main reason for the apparent discrepancy is that the definition used in this study, which completely ignores the influence of fibre width on the free fibre length, is different from the definition used by Page et al (Page 1962), which considers the free fibre length as the lengths of fibre not covered by bonds. We believe that the fibre width and fibre flexibility mainly affects the bonded area of each bond. However, it is necessary to perform further experiments to draw a final conclusion.

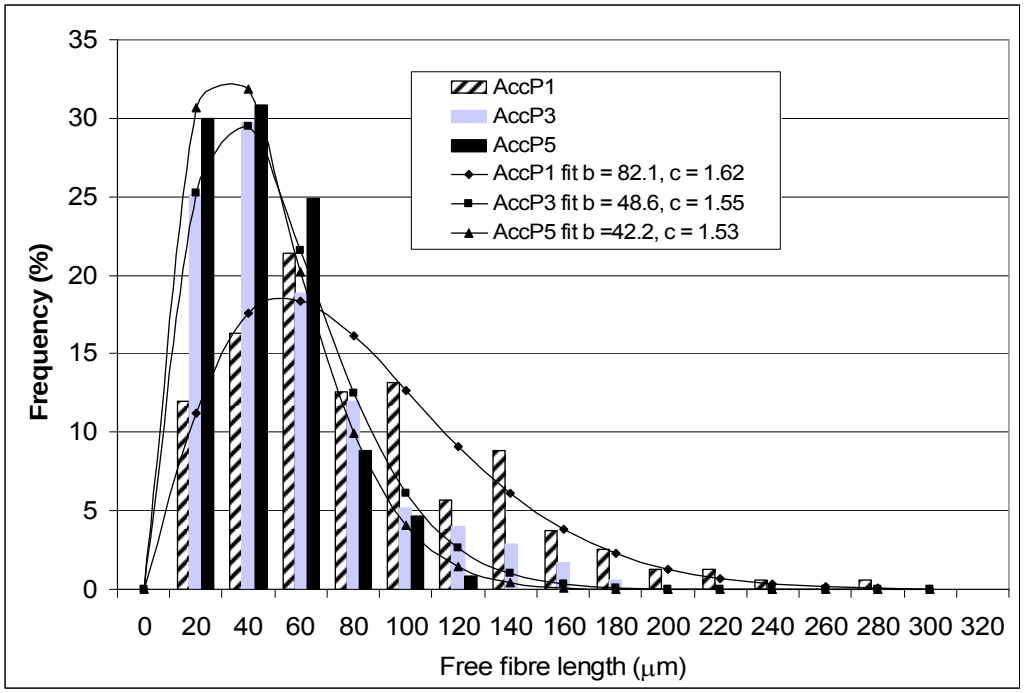

Figure 7-2 Frequency distribution of free fibre length of samples of the accepts

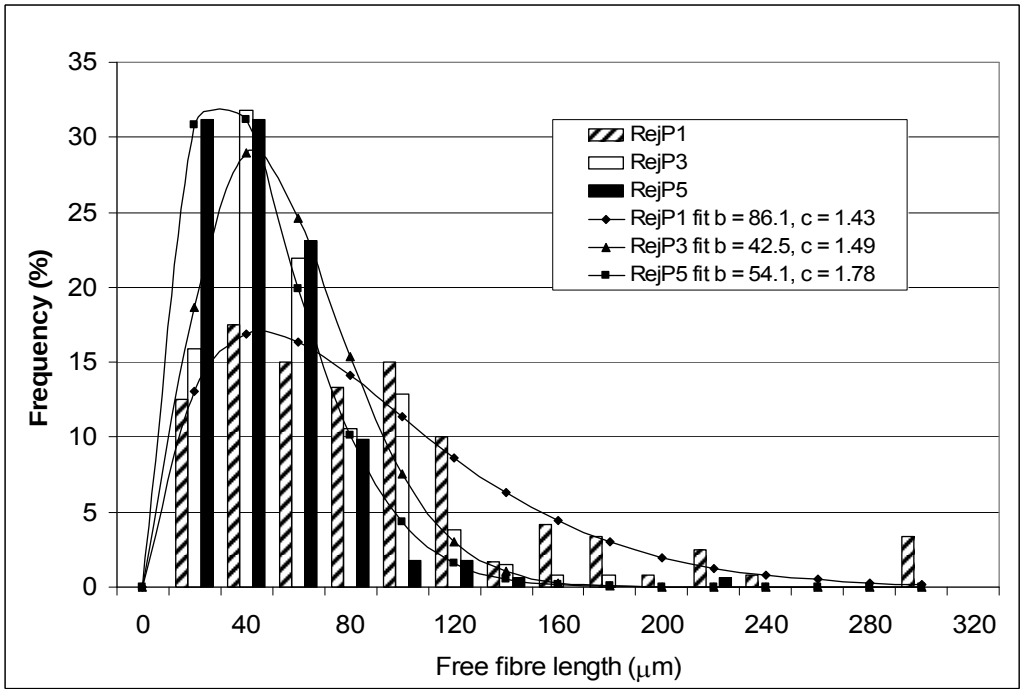

Figure 7-3 Frequency distribution of free fibre length of samples of the rejects

Both the accepts and rejects reponse to wet pressing in a similar manner. The free fibre length distributions were skewed to a lower value range and narrowed when the samples were pressed (see Figure 7-2 and 7-3), resulting in decreases in the mean value of free

fibre length and increases in the number of fibre-fibre contacts per unit length of fibre (Table 7-1). The broad distributions of free fibre length in $AccP_1$ and $RejP_1$ imply that the bonding structure along fibres in these sheets is non-uniform, which will produce a non-uniform load distribution along the fibres and will lead to less efficient load transfer between fibres when the sheet is loaded. Wet pressing can narrow the distribution of free fibre length in the sheet, which therefore improves the uniformity of load transfer between fibres when the sheet is loaded.

The distributions of the free fibre length of the samples made from fractions with different fibre lengths are also almost the same as each other, indicating that the fibre length has no effect on the distribution of free fibre length in a sheet (see Figure 7-4). As discussed before, the mean values of the free fibre length and the number of fibre-fibre contacts per unit length of fibre are also independent of fibre length (see Table 7-1). Page (Page 1962) believed that fibre length would have strong influence on the frequency of fibre bonding, but no evidence was given. Kallmes and Bernier's (Kallmes and Corte 1960) theory was based on fibres with infinite length, but their theory was partial verified with data obtained with normal sheets.

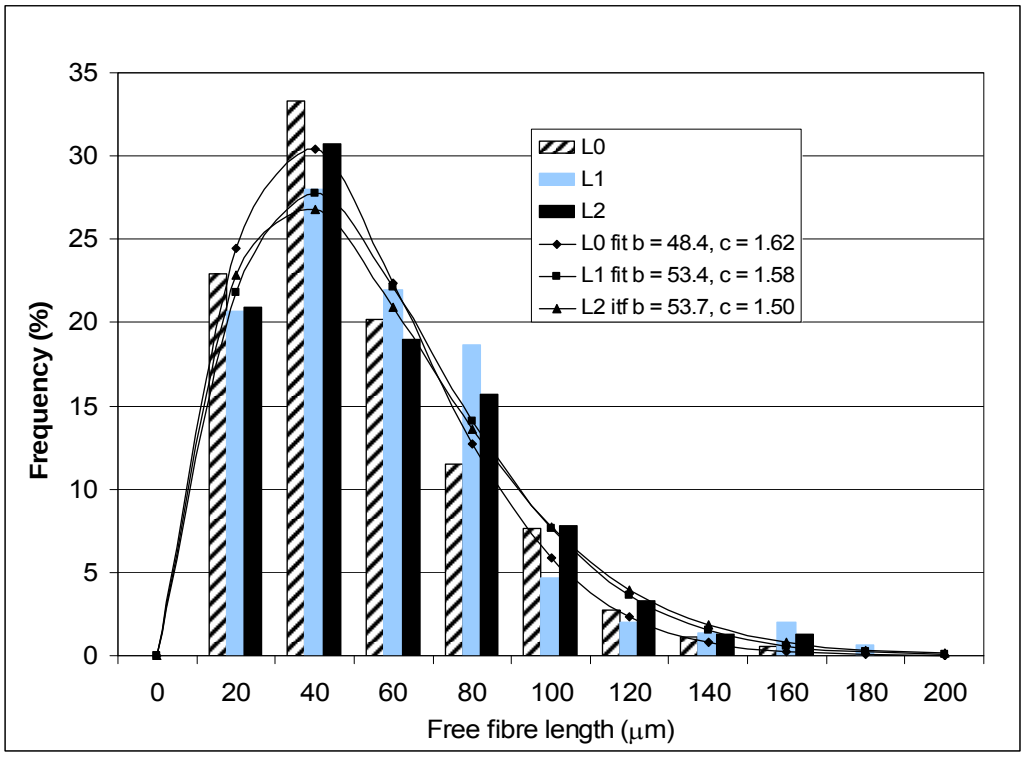

Figure 7-4 Frequency distribution of free fibre length of samples of fractions with different fibre length (these samples were pressed statically at P_3)

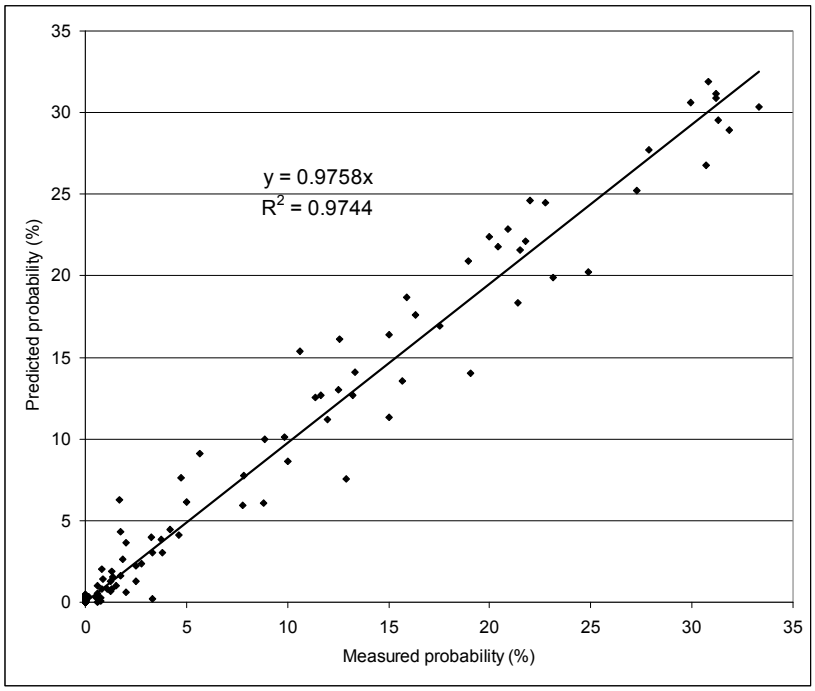

Figure 7-5 The correlation plot of all of the samples used in this study

The measured probability in each interval (interval size is 20μm) for all of the samples used in this study is plotted against the corresponding predicted probability in Figure 7-5. As shown in Figure 7-5, the measured values and predicted values show very good correlation with a correlation equation of $y = 0.97x$. This means that Equation 7.1 can describe the distribution of the free fibre length very well.

Although we can not justify theoretically the use of the two-parameter Weilbull PDF to fit to the experimental data, both the graphic comparison and the check of correlation between the experimental results and the predictions show that the two Weibull PDF can fit the distribution of the free fibre length well and will be used to build model structures of fibre-fibre contacts in simulations of load distributions in fibres in Chapter 8.

7.3.3 Reconstruction of the fibre-fibre contacts

Based on the experimental results of the distribution of the free fibre length, the number of fibre-fibre contacts per unit length of fibre, the nature of the contacts and the distribution of the out-of-plane angle, a model structure of fibre-fibre contacts for a fibre segment of any of these samples can be reconstructed. Examples of such model structures for samples $RejP_1$ and $RejP_5$ are illustrated in Figure 7.6, in which the small

circles along the fibre axes represent points between which the free fibre lengths were measured. The drawing here is to scale. The position of each contact and the out-of-plane angle of each free segment were calculated using their frequency distributions, respectively. The nature of the contacts was randomly assigned to each contact according to the percentage of fully and partial contacts for each fibre sample. The fibre segments shown in Figure 7-6 are 1mm in length. Clearly, in sample $RejP_1$, the arrangement of fibre-fibre contacts along the fibre segment is not uniform. There are some long free fibre segments. After it was pressed, the number of fibre-fibre contacts increased and arrangement of the contacts become more uniform. The number of long free fibre segments was reduced dramatically. These model structures provide a direct view and better understanding of the structure of fibre-fibre contacts in paper, and these data can also provide important information for simulation studies of the load distribution along a fibre.

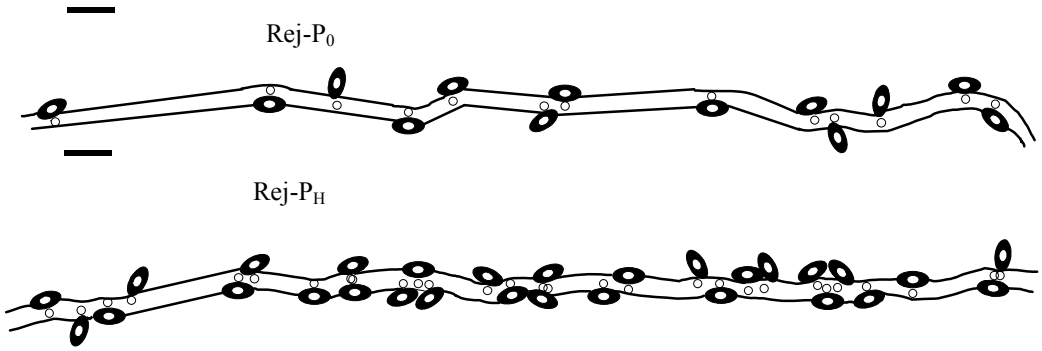

*** the size bar is 50μm.**

Figure 7-6 Model structure of fibre-fibre contacts

7.4 Verification of the model for number of fibre-fibre contacts

7.4.1 Direct comparison between measured number of fibre-fibre contacts and predictions by Equation 3.11

As discussed above, the number of fibre-fibre contacts has been measured directly in the cross-section of paper. The measured data is now ready for comparison with the predictions made by the new model for number of fibre-fibre contacts given by Equation 3.11 in Chapter 3.

Several points need to be clarified here. Firstly, Equation 3.11 assumed that all of the contacts in paper are identical and are full contacts. However, as shown in Subsection 4.4.2, the fibre-fibre contacts measured in the handsheets can be divided into two types, viz. full contacts and partial contacts. There is no theoretical basis for determining how many partial contacts are equivalent to one full contact. However, the 'converting factor' is most likely to be within the range between 1 and 2. Secondly, to use Equation 3.11, we need first of all to determine the value of the packing factor, β, in the Equation. By using data from literature, we have shown in Subsection 3.3.3 that the packing factor appears to be a constant. In this study, we allowed the 'converting factor' to be adjustable between 1 and 2, and then calculated the values of β for each sample by bringing the converted number of fibre-fibre contacts and other parameters into Equation 3.11. The best value for the converting factor was determined by assessing how close to each other the calculated values of β are. It was found that the value of such a 'converting factor' was 1.5. The calculated values of β are given in Table 7-2. As shown in Table 7-2, the calculated β by equation 3.11 is constant within errors for all samples. In all following calculations, we used an average value of $\beta = -0.29$.

Table 7-2 Determination of β using the measured results of fibre-fibre contacts in paper (converting factor was 1.5)

Sample	D_w (μm)	f_h	N_{cm} (No./m)	β
L_0P_3	30.68	0.55	19375±4008	-0.31±0.14
L_1P_3	34.45	0.52	18710±4215	-0.31±0.15
L_2P_3	33.11	0.55	18725±4074	-0.33±0.15
$AccP_1$	30.19	0.43	9743±1710	-0.36±0.17
$AccP_3$	34.08	0.45	16309±2509	-0.31±0.12
$AccP_5$	36.38	0.51	22784±3521	-0.29±0.12
$RejP_1$	28.03	0.46	9377±1992	-0.31±0.16
$RejP_3$	32.22	0.49	15757±3141	-0.16±0.20
$RejP_5$	34.71	0.54	23482±4584	-0.21±0.14

A comparison between the measured number of fibre-fibre contacts and the prediction made by the new model are shown in Figure 7-7. When the trend line is forced to pass the origin, the slope (0.99) is very close to 1 and the correlation coefficient R^2 is 0.93. This means that the predictions made by the new model and the measurements are very close to each other indicating the model with best fit parameters can predict number of fibre-fibre contacts very well.

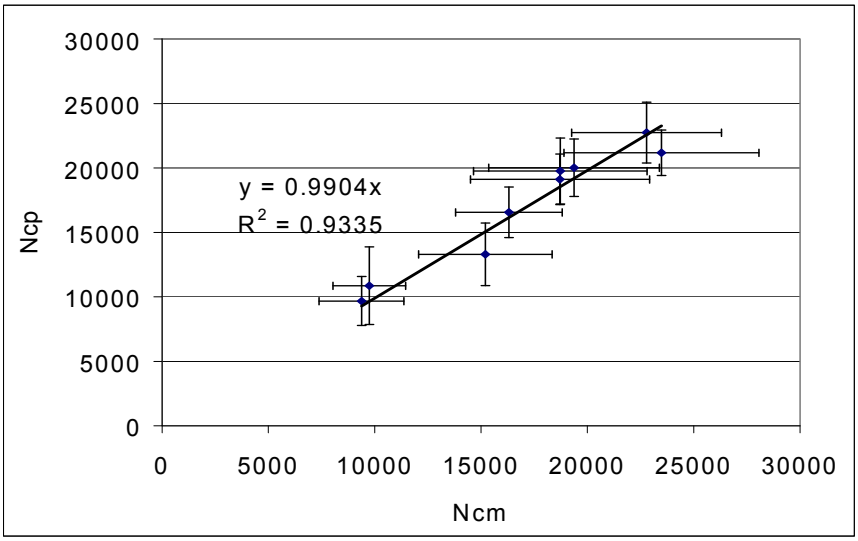

Figure 7-7 Correlation of measured equivalent number of fibre-fibre contacts per unit fibre length against the predictions made by Equation 3.11 using $\beta = -0.29$.

7.5 Verification of the expressions for *RBA*

7.5.1 Measurement of *RBA* with nitrogen adsorption

As reviewed in Chapter 2, the measurement for *RBA* is always problematic. In this study, the nitrogen adsorption method was used to determine *RBA* for all of the samples used and denoted as RBA_{N2} (see Appendix C). The surface area of unbonded sheets was determined by measuring the free surface of spray dried fibres. A fibre suspension with very low consistency (0.04%) was sprayed on a teflon surface and left to dry in the air. The dried fibres were then collected carefully avoiding losing material. Since fibres dried in this way rarely are in contact one another, no bonds should formed between fibres when they dry and the fibres should have an equivalent free fibre surface to a unbonded sheet made from the same pulp fibres. The free fibre surface area of

these spray dried fibres were then measured by the nitrogen adsorption method and used as the free fibre surface area of unbonded sheets to calculate RBA by:

$$RBA = (A_u - A) / A_u \qquad \textbf{7. 2}$$

where A_u is the free surface area of unbonded sheets and A is the free surface area of normal sheets.

The measured surface areas of unbonded sheets for samples L_0, L_1, L_2 and L_3 were 905m^2/kg, 920 m^2/kg, 921 m^2/kg and 927 m^2/kg respectively, and for the accepts and the rejects were 993 m^2/kg and 1063 m^2/kg, respectively. According to Braaten (Braaten 2000), if fibres are cylindrical with perfect smooth surfaces, and the fibre wall density is always 1.5g/cm^3, then the total surface area (includes the external surface and the lumen surface) per unit weight of such fibres can be estimated by $SA = 2/1.5t$, where t is the fibre wall thickness. For fibres used in this study, the wall thickness is in the range of 2μm to 3μm. The estimated SA is within 667 m^2/kg to 444 m^2/kg. These values are comparable with the measured results of the fibre surface area of unbonded sheets. The difference is reasonable because the calculation assumes that the surface of the fibres is perfectly smooth, which is not true in reality. Therefore, the measured results of the surface area of unbonded sheets are acceptable.

7.5.2 Comparison between the measured RBA_{N2} and the predicted RBA_{N2} by Equation 3.13

A comparison between the measured RBA_{N2} and the predicted RBA_{N2} is given in Figure 7.8. The predicted RBA_{N2} was calculated by Equation 3.13. The R factor in this equation considers the difference between the contact area of a real contact and an ideal contact. The factor R in Equation 3.13 was determined by fitting the measured values with predicted values of RBA_{N2} and using R as a variable. The value of R for the best fit was found to be 1.35, which is greater than 1 indicating that the actual bond width is greater than D_w. This may be true, as fibres tend to flatten when they are bonded together to form a skirt shape of bonding region (Nanko 1989). The value of 1.35 for R implies that each bond has expanded the width of the fibre by about 15%.

Figure 7-8 includes all of the data for samples used in this thesis. The best fit line, shown in Figure 7-8, shows an intercept close to zero and slope close to 1. It shows a reasonably good correlation ($R^2 = 0.88$) between the measurements and the predictions. All these indicate that Equation 3.13 can predict *RBA* well. This indirectly also proves that the model for the number of fibre-fibre contacts, Equation 3.11, is correct.

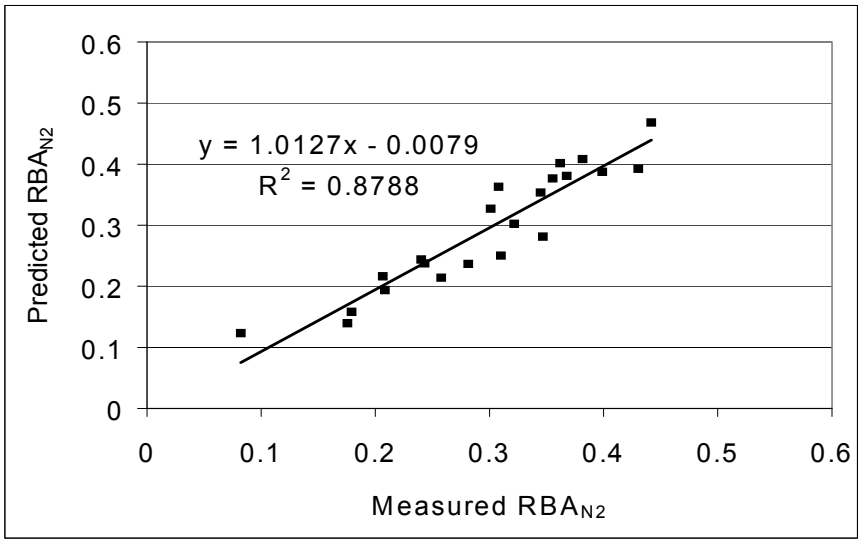

Figure 7-8 The correlation between the measured RBA by N2 adsorption and the predicted RBA by Equation 3.13.

7.5.3 Calculation of *RBA* with scattering coefficient

Traditionally, the Ingmanson and Thode pressing/beating extrapolation method (Ingmanson and Thode 1959) is the most widely used method for *RBA* measurement. In this method the light scattering coefficient for an unbonded sheet is determined by extrapolating the plot between tensile strength and the light scattering coefficient to determine the scattering coefficient, S_0, corresponding to zero tensile strength of paper. *RBA* is then calculated from $RBA = (S_0 - S)/S_0$. In this thesis, different S_0 for samples with different fibre lengths were obtained by using this extrapolation. The values of S_0 determined by this method of extrapolation for the L_0, L_1, L_2 and L_3 are 42.0 m^2/kg, 34.1 m^2/kg, 33.1 m^2/kg and 28.6 m^2/kg (Figure 7-9). These results are unreasonable because these fibre fractions only differ in fibre length and should have almost the same S_0. The Ingmanson and Thode extrapolation may have worked for their data because they were able to obtain data over a large range of tensile strength. Their

extrapolation showed a highly non-linear curve. Thus if only a limited range of tensile strength vs scattering coefficient is available, it is not surprising that the extrapolation does not work. The results suggest that this extrapolation should not be used to determine S_0 and therefore the RBA. Obviously, an alternative method should be used for determining S_0.

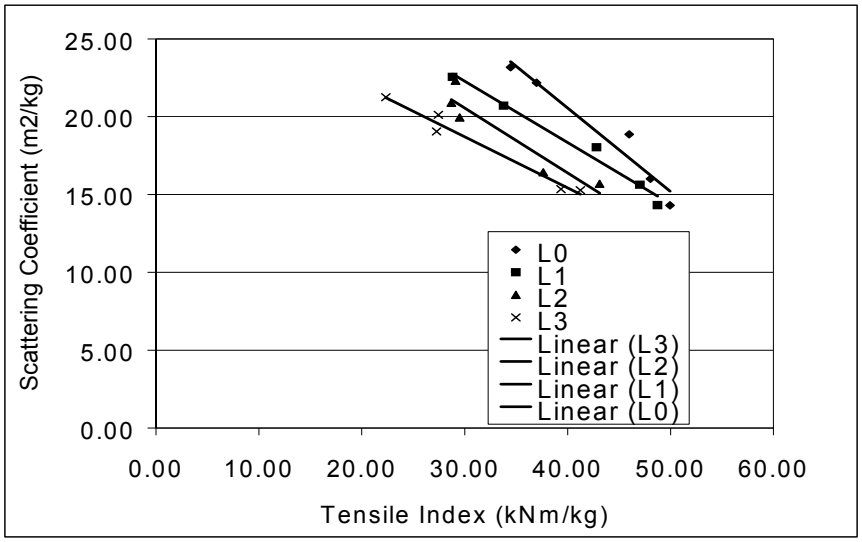

Figure 7-9 Plot between tensile index and light scattering coefficient of samples made from cut fibres pressed at different pressing levels

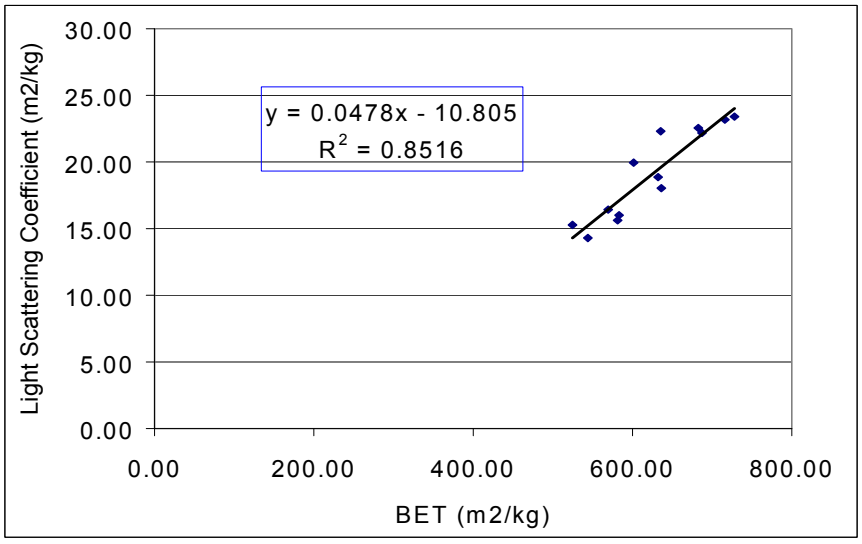

Figure 7-10 The relationship between the BET area and the light scattering coefficient for samples made from fibres with different length and pressed at different pressing levels

A linear relationship was found between the light scattering coefficient and the BET area for samples made from fibre fractions generated by cutting wet handsheets (see Figure 7-10). Similar relationships have previously been reported (Haselton 1955; Swanson 1959). S_0 was determined by using the linear equation shown in Figure 7-10 to calculate the scattering coefficient corresponding to the BET area of the spray dried sheets. The S_0 obtained using this method was 32.4 m^2/kg for L_0, 33.1 m^2/kg for L_1, 33.2 m^2/kg for L_2 and 33.5 m^2/kg for L_3. These values were then averaged and used as S_0 for RBA calculation for all of the four different fibre length fractions. It is important to note that S_0, calculated in this manner, does not change as the fibre length is decreased. This is as expected because the cutting process does not change the cross-sectional dimensions of the fibres.

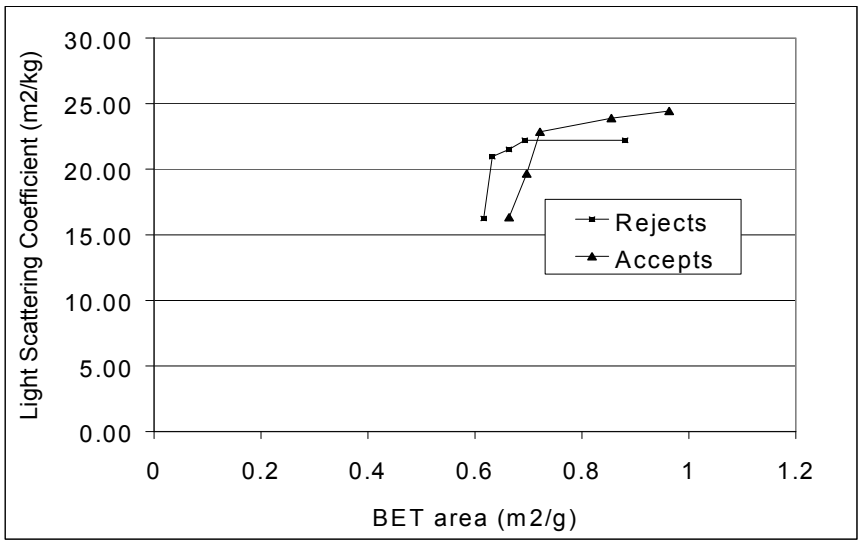

Figure 7-11 The relationship between the BET area and the light scattering coefficient for samples made from the accepts and the rejects pressed at different pressing levels

It was also found that the relationship between the BET area and the light scattering coefficient was non-linear for samples made from the rejects and also for samples made from the accepts (as shown in Figure 7-11). Currently, we have no good explanation for this non-linear relationship. A possible reason is that the accepts and the rejects were fines free pulps and formed sheets having "pin holes", which seemed to have a significant effect on the measurement of the light scattering coefficient.

7.5.4 Comparison between the measure RBA_{sc} and the predicted RBA_{sc} by Equation 3.14

A comparison between the measured RBA_{sc} and the predicted RBA_{sc} by Equation 3.14 is shown in Figure 7-12. The value of R in Equation 3.14 was also determined by fitting the measured RBA_{sc} with the calculated RBA_{sc} using R as a fitting parameter. Interestingly, the value of R was 1.39 that is almost equal to the value of R determined in Figure 7-8. This means R is a constant as is assumed in Equations 3.13 and 3.14. As can be seen in Figure 7-12, the trend line shows an intercept very close to zero and slope close to 1 and very high R^2 statistic of 0.94 indicating that Equation 3.14 can predict RBA very well. This further proves that the new model for number of fibre-fibre contacts is valid.

It is also interesting to estimate the maximum values of RBA_{N2} and RBA_{sc} by setting ρ_a, f_h, and δ in Equations 3.13 and 3.14 to limiting values. For a sheet made from heavily refined pulp and pressed at high pressure, the reasonable maximum value for ρ_a is 750kg/m^3, for f_h is 0.6 and for δ is 1/4. When these values were brought into Equations 3.13 and 3.14, the calculated maximum values for RBA_{N2} and RBA_{sc} are 0.49 and 0.61 respectively, which are quite reasonable.

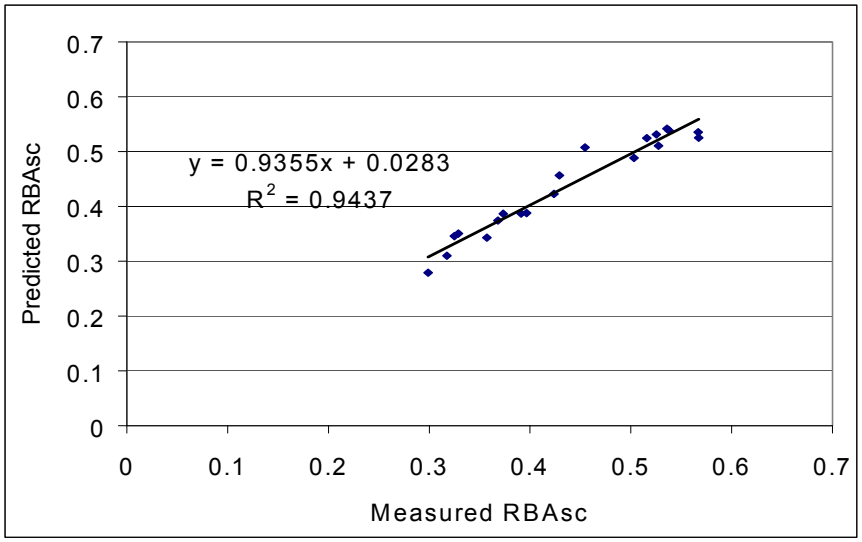

Figure 7-12 Correlation between the measured *RBA* by scattering coefficient and the predicted *RBA* by Equation 3.14 (The handsheets were made by fibres with different fibre lengths generated by cutting wet handsheets)

7.6 Conclusions

The main conclusions from this chapter are:

- A new technique for measuring the properties of fibre-fibre contacts directly in paper has been proposed and has been used successfully. It is the first technique that can determine all of the parameters associated with the fibre-fibre contacts simultaneously.
- It has been shown for the first time that fibre length seems to have no effect on the properties of fibre-fibre contacts. Fibre cross-sectional shape has no significant effect on the frequency of fibre bonding along a fibre and the distribution of the free fibre length. However, the accepts fibres (the thin walled fibres) tend to form a higher percentage of full contacts in a sheet.
- The out-of-plane deflection angles of the free fibre segments have no regular trend with the pressing intensity for both the handsheets of the accepts and of the rejects. However, the out-of-plane deflection distance has been reduced by wet pressing since the free fibre length has been reduced.
- The distribution of free fibre length for a normal sheet is not negative exponential. It seems to fit a two-parameter Weibull probability density function.
- The distribution of the free fibre length is narrowed and shifted to a lower value range by wet pressing. The bonding frequency along a fibre is increased, while the free fibre length is reduced as the pressing intensity is increased. There is no significant difference in the behavours of the fibre-fibre contacts of the handsheets made from the accepts and those made from the rejects.
- It has been demonstrated that model structures of fibre-fibre contacts can be reconstructed using the data measured by the new technique.
- The model for the number of fibre-fibre contacts per unit fibre length has been verified directly by using the data of fibre-fibre contacts measured in paper. The comparison between the measurements and the predictions made by the new model shows a very good correlation, indicating that the model is valid.
- It has been shown that both of the two expressions can predict *RBA* well. This further proves that the new model for fibre-fibre contacts is valid.

8 Verification of models for tensile strength of paper

8.1 Introduction

An important aspect of modelling tensile strength is to fully verify the model with experimental data. Verification of a model is at least equally important as the development of the model. It is well known that fully verifying models for tensile strength is usually very difficult because it requires a wide range of data and some parameters, as discussed in Chapter 2, are difficult or extremely difficult to measure in practice. A wide range of paper and fibre properties have been measured in this project.

A very important part of this project has been to develop new techniques for measuring the difficult parameters so as to obtain a full range of data for fully testing the important models developed in previous studies and the new model developed in this project. In this project we have developed new techniques to measure some of these difficult parameters including fibre dimensions in a sheet and the number of fibre-fibre contacts in paper. These techniques have been presented in Chapter 4. The experimental data measured by these new techniques have been discussed in Chapters 6 and 7. Cutting wet handsheets and hydrocyclone fractionation were employed to vary only fibre length and fibre cross sectional properties, respectively. These experiments have been discussed in Chapter 5. For the first time, such comprehensive sets of data are available for testing models of paper tensile strength.

In this Chapter, we will first test the Page equation, which is the most commonly used model for tensile strength, by using experimental data obtained in this project. The key parameter in the simple fracture model, r, is the ratio of peak load in a fibre to the average load in the fibre (see Chapter 3). This is first calculated by using the shear lag model. Several types of shear lag models will be examined for this purpose. This will be followed by discussion of a newly developed direct stress transfer theory. The stress distribution in a fibre is simulated based on the new theory. The peak average load in the fibre is used to calculate the tensile strength and compared with the measured tensile strength of paper.

8.2 Verification of the Page equation

As discussed in Chapter 2, the Page equation (as given in Equation 8.1) is the most commonly used model for the tensile strength of paper. However, this equation has never been fully verified with experimental data.

$$\frac{1}{T} = \frac{9}{8Z} + \frac{12A\rho g}{bPL(RBA)} \qquad \textbf{8. 1}$$

In Equation 8.1, T is the tensile strength (km), Z is the zero span breaking length (km), A is the average fibre cross sectional area (m^2), ρ is the density of the fibre (g/m^3), g is the acceleration due to gravity (m/s^2), P is the perimeter of the fibre cross section (m), L is the length of the fibre (m) and RBA is the relative bonded area

In the work in this thesis, all of the parameters in Equation 8.1 except the fibre-fibre bond strength and the fibre wall density have been measured. The fibre wall density was assumed to be $\rho = 1500 kg/m^3$. According to Page (Page 1969) the length weighted fibre length should be used for this calculation. The perimeter was calculated by $2(D_w + D_h)$. The fibre-fibre bond strength was used as a fitting parameter. The calculated tensile strength by Equation 8.1 was then fit to the measured tensile strength using a least squares method. The data of two series of samples were used for the fits. One series of samples was made from fibres with different fibre length, which was changed by wet cutting the fibres with a die (refer to subsection 5.2.3). The other series of samples was made from fibres with different cross-sectional dimensions, which was altered by hydrocyclone fractionation (the accepts and rejects see subsection 5.2.2). For each set of sheets, the density and strength were altered by wet pressing at different pressing pressures. The details about the pressing pressures used and the sheet preparation techniques are described in subsection 5.2.1).

It was found that the bond strength for the best fit for the cut fibres is 3.0×10^6 N/m^2, compared to 2.0×10^6 N/m^2 for the accepts and 1.9×10^6 N/m^2 for the rejects. These values of bond strength are of the same order of the previous measurements in the literature. Mayhood, Kallmes and Cauley (Mayhood 1962) reported that the bond strength of 2.9×10^6 N/m^2 for spruce sulfite fibres and 3.6×10^6 N/m^2 for spruce sulfate

fibres. In the work here, the fitted values for the rejects (mainly summer wood fibres) and the accepts (mainly springwood fibres) bond strengths show about the same value. This conflicts with previous measurements by McIntosh (McIntosh 1962) who measured the bond strength between fibre and shive as 2.7×10^6 N/m^2 for springwood fibres and 7.1×10^6 N/m^2 for the summerwood fibres.

It is also difficult to explain why the bond strengths of the rejects and accepts are lower than the whole pulp. One possible reason why the bond strength might be lower is that both accepts and rejects were screened to thicken the stock after fractionation. This will have the effect of removing some of the fines from the stock. However, the effect of the removal of the fines on the bond strength is likely to be minimal. This is because the samples were unrefined and so it was likely that fine material made up only a small fraction of the total stock. Certainly it is hard to see how the removal of these fines in the accepts and rejects could reduce the shear bond strength by 50%.

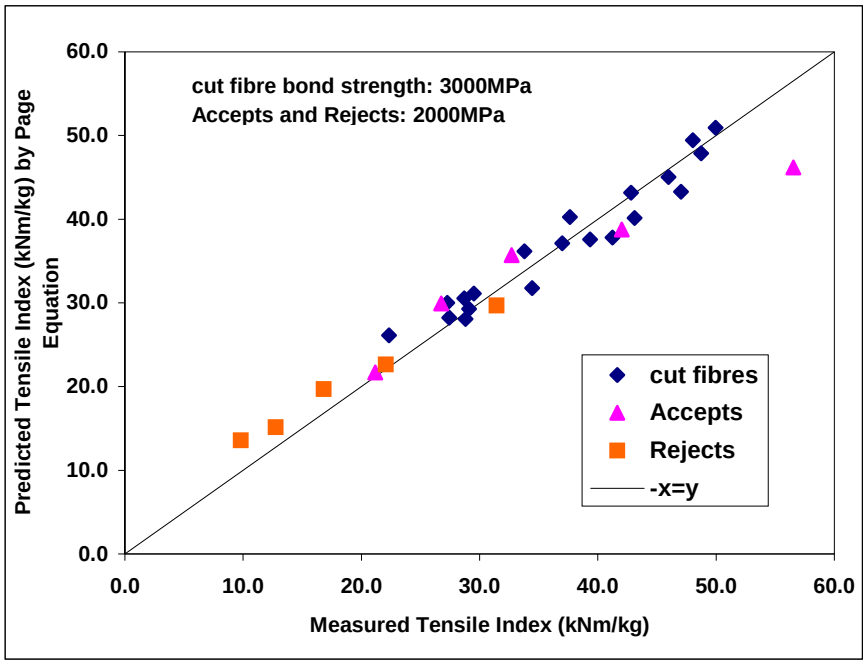

Figure 8-1 Correlation between the measured and predicted tensile strength by Page equation using different shear bond strengths

Figure 8-1 shows the correlation between the measured tensile strength and the predicted tensile strength by the Page equation when the bond strength was set to be 3.0×10^6 N/m^2 for the cut fibres and 2.0×10^6 N/m^2 for the fractionated fibres. It shows a very good correlation between the measurements and the predictions. If a single bond

strength was used in the fit between the measurements and the predictions, the best fit bond strength for all of the samples was 2.6×10^6 N/m^2 and the correlation between the measurements and the predictions is much poorer as shown in Figure 8-2.

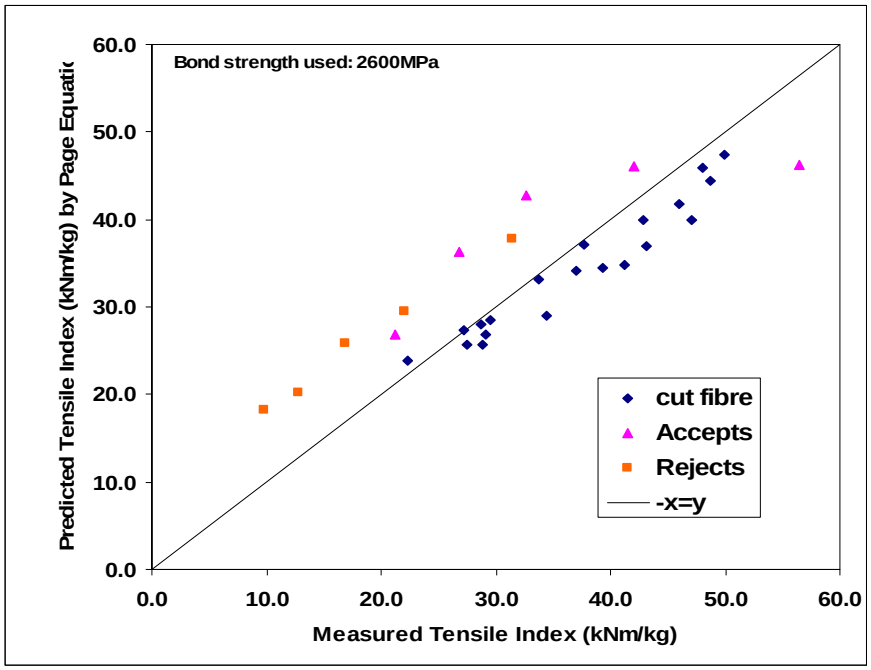

Figure 8-2 Correlation between the measured and predicted tensile strength by Page equation using same shear bond strength

In deriving the equation, Page assumed that all fibre-fibre bonds act cooperatively along the length of a fibre and the fibre-fibre bond strength, β, is given by:

$$\beta = bP(RBA)l_f / 4 \qquad \textbf{8. 2}$$

where b is shear bond strength per unit bonded area, and the other parameters are the same as in Equation 8.1.

The calculation seems to consider that all types of fibres would bond in the same manner if they have the same length and perimeter. This might be reasonable for one type of fibre but not necessarily correct for different types of fibres. This equation also assumes that the bonds act co-operatively. That is the contribution of the bonds is the same whether they are at the end of the fibre or in the middle. This assumption also contradicts the shear lag model, which assumes that the bonds at the end of the fibre are the most heavily loaded.

Thus it seems from our data that the Page equation can provide a reasonable prediction for paper strength only if the bond strength is used as a fitting parameter for each set of data. The explanation for this is that the Page equation is probably not correctly accounting for the effect that changes in fibre morphology has on paper strength. Given that all the fibre morphology variables appear together with the fibre-fibre bonding in the right hand term in the Page equation, then any inadequacies in the way that the Page equation takes fibre morphology effects into account can be compensated for by adjusting the bond strength.

The above discussion suggests that the Page equation gives only a reasonable qualitative description of how trends in fibre and sheet properties will affect paper strength and that it cannot be relied upon for quantitative predictions. Thus the need for a quantitative model for paper strength remains.

8.3 Examination of Fibre Fracture Model

The fracture of paper can be triggered either by the fracture of fibre or the failure of fibre-fibre bonds. As reviewed in Chapter 2, it is still not quite clear what triggers the fracture of a sheet of paper. The first premise of Page equation proposes that fibre fracture initiates the fracture of the paper. The tests of the Page equation have shown that this premise is acceptable. In this project we also believe that the fracture of paper is triggered by the fracture of fibres that are aligned with the applied stress. A simple fibre fracture model has been developed as discussed in Chapter 3. This model is written as:

$$T = \frac{1}{r}\frac{8}{9}Z \qquad \textbf{8. 3}$$

where T is tensile index, Z is zero span tensile index and r is a constant for a given paper

To test the fibre fracture model (Equation 8.3), we need first to determine the value of r in the equation. The key variable, r, in Equation 8.3 is defined as the ratio of peak load to the average load in a fibre at the point of fracture (refer to 3.3.5 for details of the definition). The value of r is determined by the mechanism of load transfer from fibre

to fibre in a sheet. The literature review (Chapter 2) shows that the shear lag model has been the most commonly used theory for load transfer in paper.

According to the shear lag theory, the load distribution along a fibre can be expressed as (Räisänen 1997):

$$\sigma_f(x,k) = E\varepsilon_x\left(1-\frac{\cosh kx}{\cosh(kl_f/2)}\right) \qquad \textbf{8. 4}$$

where E is the elastic modulus of the sheet, ε_x is the strain of the sheet in the direction of the fibre, l_f is the fibre length and k is an adjustable parameter, the value of which is determined by the assumed stress transfer mechanism.

The average load in the fibre can be calculated by integrating Equation 8.4. The value of r is then calculated by:

$$\frac{1}{r} = \left[1-\frac{2\tanh kl_f/2}{kl_f}\right] \qquad \textbf{8. 5}$$

The shear lag model for the network elastic modulus, E_n, is given by (Räisänen 1997; Räisänen, Heyden et al. 1997):

$$E_n = \frac{3qD_w^2E_f}{8}\left[1-2\frac{\tanh kl_f/2}{kl_f}\right] \qquad \textbf{8. 6}$$

In the high density limit, the shear lag model for a 2-D network is also written as:

$$E_n = \frac{3}{8}E_fD_w^2[q-Kq_c] \qquad \textbf{8. 7}$$

Here $q_c = 5.71/l_f$ is the percolation density (the smallest number of fibres per unit area for forming a fibre network (Pike 1974) and D_w is fibre width. In a 2-D network, the density, q, is defined as the total fibre length per unit area, whereas in a 3-D network (real paper), of course, density is given by the total mass per unit volume. The correspondence between the two densities is best established through the number of bonds per fibre. This was approximately given by $q/q_c \approx \pi l_f/11.42l_s$, in which $l_s = 1/N_c$ is the average length of free fibre segments (Corte 1962; Pike 1974) and N_c

has been previously defined by us as the number of bonds per unit fibre length. Thus q and N_c are related by:

$$q \approx \pi l_f q_c N_c / 11.42 \qquad \textbf{8. 8}$$

Comparing Equation 8.6 with Equation 8.7 and substituting N_c for q by using Equation 8.8, we can get:

$$k = \frac{\pi}{5.71}\frac{N_c}{K} \qquad \textbf{8. 9}$$

Bringing Equation 8.9 into Equation 8.5 then yields:

$$\frac{1}{r} = 1 - \frac{K}{0.275 N_c l_f} \qquad \textbf{8. 10}$$

The question for determination of the value of r becomes the determination of the value of K, which is referred to as the coefficient of load transfer in the literature (Aström, Saarinen et al. 1994; Räisänen 1997), and the number of fibre-fibre contacts per unit length of fibre, N_c, in the sheet. In Chapter 3 we have presented a model for number of fibre-fibre contacts in paper and the model has been fully verified in Chapter 7. Here we calculate N_c by using the model for number of fibre-fibre contacts. The value of K can be determined by different types of shear lag analysis. In the following subsections, we will discuss different types of shear lag analysis for determining the value of K and then r.

8.3.1 Determination of r by fitting elastic modulus data to shear lag model

Substituting Equation 8.8 into Equation 8.7 and rearranging yields the following expression:

$$\frac{8}{3}\frac{E_n l_f}{5.71 D_w^2 E_f} = 0.275 N_c l_f - K \qquad \textbf{8. 11}$$

We then plot $E_n l_f / D_w^2 E_f$ against $0.275 N_c l_f$. As shown in Figure 8-3, a very good linear relationship is found for each sample group. The same linear relationship has been found from simulations by Aström et al (Aström, Saarinen et al. 1994) and Räisänen et al (Räisänen 1997). Linear extrapolation from high densities down to

$E_n = 0$ gives $K = 1.82$ for cut fibres, $K = 4.29$ for the rejects and $K = 4.80$ for the accepts. These values are very close to those obtained by simulations in the work of Räisänen et al and Aström et al (Aström, Saarinen et al. 1994). Räisänen et al reported that the value of K was in the range of 3.5 to 4.3 for networks with flexible bonds. For networks with rigid bonds, Aström et al found K was in the range of 2.1 to 2.8.

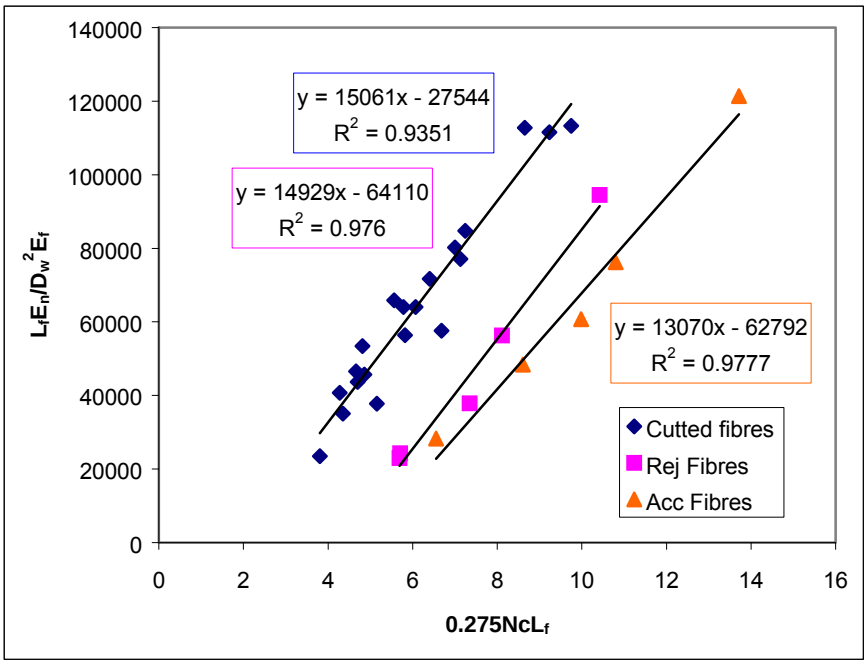

Figure 8-3 Plot between $E_n l_f / D_w^2 E_f$ and $0.275 N_c l_f$

The values of K for the cut fibres, accepts and rejects were then brought into Equation 8.9 to calculate values of r for these samples. The calculated values of r are plotted in Figure 8-4 against sheet density for the accepts, rejects and cut fibres. It can be seen from the figure that the calculated values of r slowly decrease with sheet density. The values of r range from 4.1 for the lowest density sheets to 1.2 for the denser sheets. These values of r were then used to calculate the tensile strength with Equation 8.3. Figure 8-5 compares the calculated tensile index with the measured tensile strength for these samples.

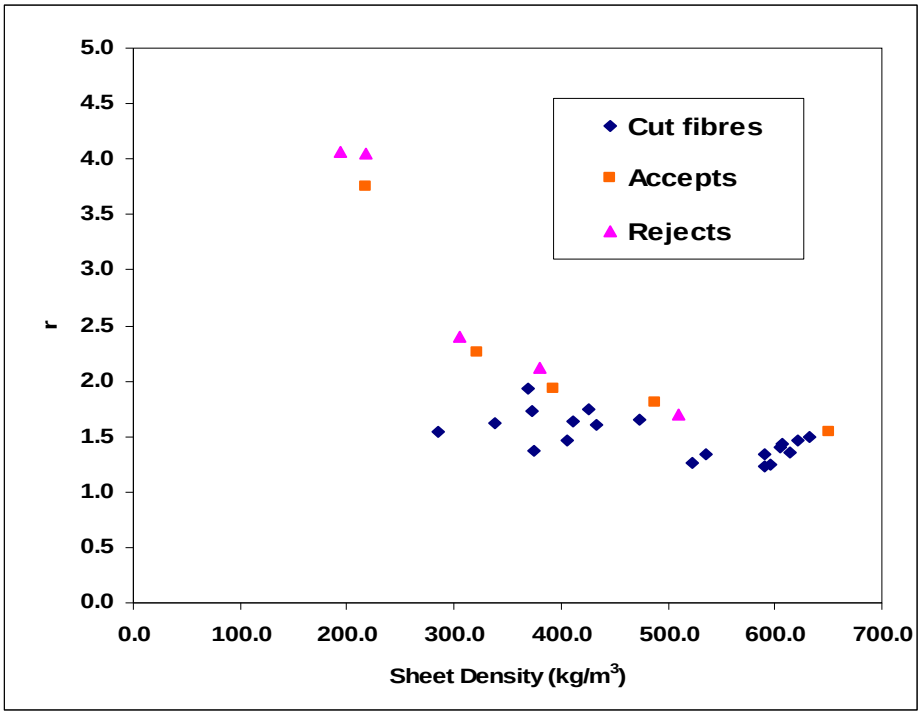

Figure 8-4 Relationship between sheet density and the value of r determined from elastic modulus data

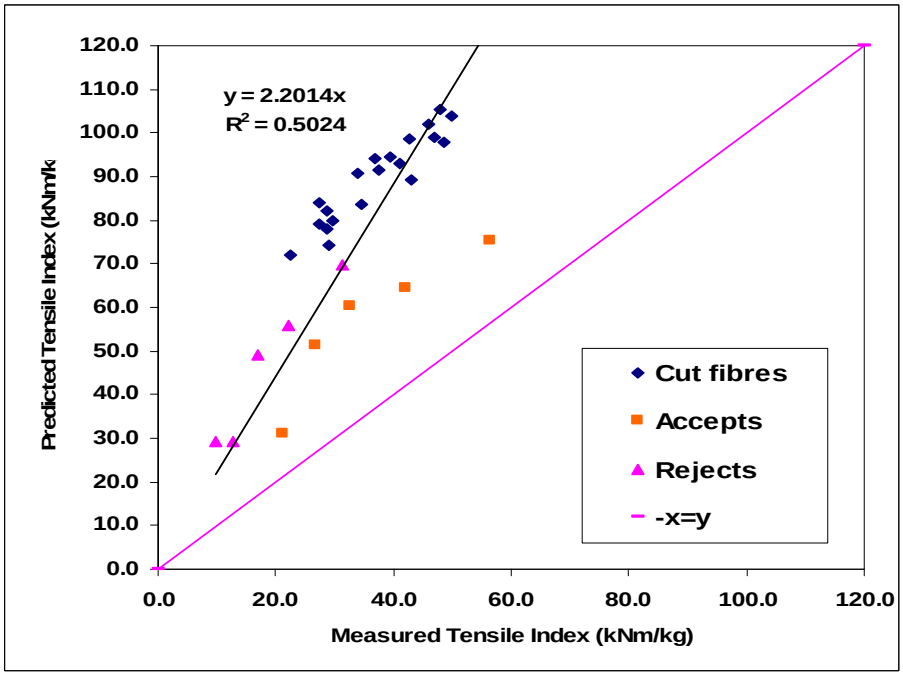

Figure 8-5 Comparison between the measured and predicted tensile index by the fibre fracture model, with r determined from the elastic modulus data.

As can be seen in Figure 8-5, there is a reasonable correlation between measured and predicted tensile index with an R^2 of 0.5. However, the slope of the correlation is 2.2, indicating either that the simple fibre fracture model for paper strength is not correct or

that the shear-lag formulation for the elastic properties does not apply to the fracture of paper.

8.3.2 Determination of r by Räisänen et al shear lag analysis

(Räisänen 1997) et al extended Cox's shear lag model to flexible bonds. From their work, K is given by:

$$K = \frac{\pi}{5.71}\sqrt{1+\nu+R_f\frac{11.4}{\pi}\frac{q}{q_c}} \qquad \textbf{8. 12}$$

where $R_f = (l_b E_f D_w^2 / l_f E_b D_b^2)$ is the ratio of the spring constants of the whole fibre and the bond. The spring constants are defined as $k_i = E_i D_i^2 / l_i$ ($l_i = length$, $E_i = modulus$ and $D_i = width$, $i = w,b$ for fibres and bonds, respectively). Substituting $q/q_c \approx \pi l_f / 11.4 l_s$ and $l_s = 1/N_c$ into equation 8.9, produces:

$$K = \frac{\pi}{5.71}\sqrt{1+\nu+R_f N_c l_f} \qquad \textbf{8. 13}$$

Bringing Equation 8.12 into Equation 8.9, and then into the fibre fracture model for tensile strength (Equation 8.3), we get:

$$T = \frac{8}{9}\left[1-\frac{2\tanh\dfrac{N_c l_f}{2\sqrt{1+\nu+R_f N_c l_f}}}{\dfrac{N_c l_f}{\sqrt{1+\nu+R_f N_c l_f}}}\right] * T_z \qquad \textbf{8. 14}$$

This is the final form of the model for tensile strength if the value of r is determined by Räisänen et al shear lag analysis. In Equation 8.13, R_f is determined by the rigidity of the bonds in the sheet. For the rigid bond case, $R_f \to 0$. Very flexible bonds give a large value for R_f. As mentioned before, $R_f = (l_b E_f D_w^2 / l_f E_b D_b^2)$. There is no way to measure the bond length l_b. In the simulation work by Räisänen et al (Räisänen, Heyden et al. 1997), a bonding element was inserted with a fixed length of

$l_b = 5 \times 10^{-5} l_f$ and width $D_w = D_f$. In this way it was determined that $R_f = 5 \times 10^{-5}$ for rigid bonds and $R_f = 5 \times 10^{-3}$ for flexible bonds.

For this work, we treated R_f as an adjustable parameter. The value of R_f was determined by optimising the fit of the measured tensile index with the calculated tensile index by Equation 8.14. The best fit result is shown in Figure 8-6 and the corresponding r values are shown in Figure 8-7. As can be seen in Figure 8-6, the predictions do not fit the measurements well. The optimised value of R_f was 5.1, which is far greater than that in the simulations by Räisänen et al (Räisänen, Heyden et al. 1997). This large value of R_f implies that the bonds in the network are so flexible that they will not break under any strain, which is physically unreasonable. It appears that the shear lag analysis by Räisänen et al cannot calculate correctly the value of r. Similar to the tensile strength, the correlation between sheet density and the value r is also poor (Figure 8-7).

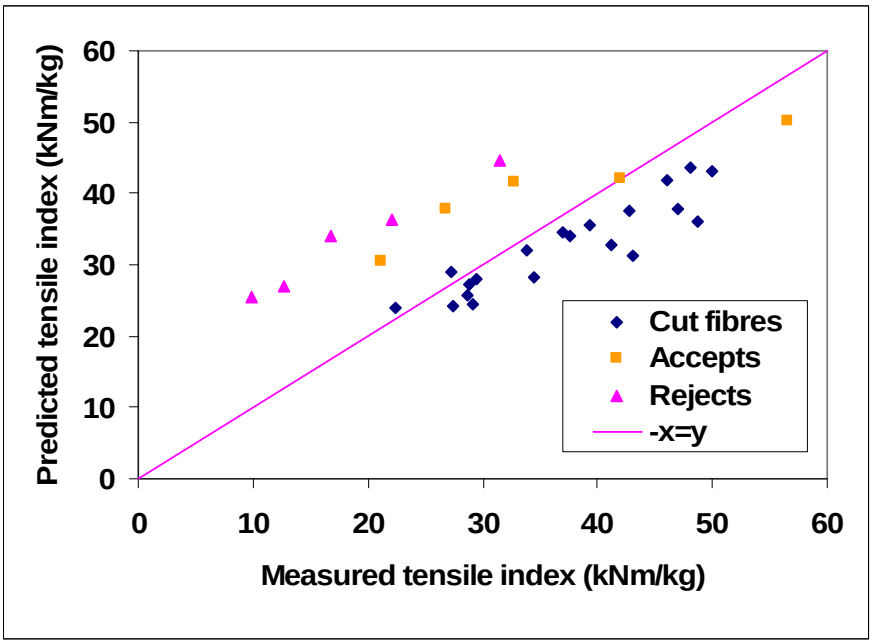

Figure 8-6 Comparison between the measured and the predicted tensile index by the fibre fracture model. r determined from Räisänen et al. shear lag analysis.

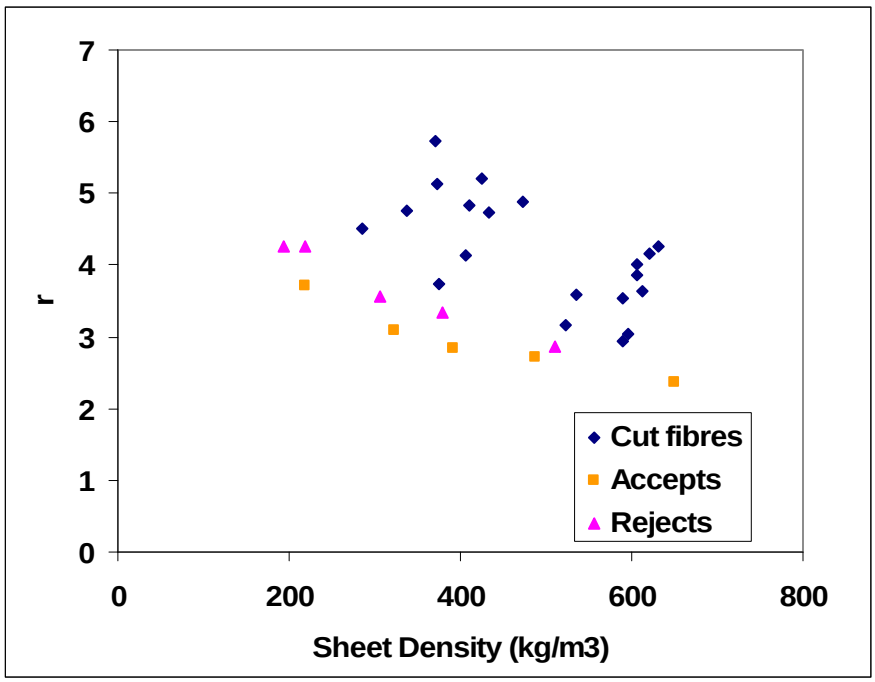

Figure 8-7 The plot of sheet density against the value of r determined from Räisänen et al shear lag analysis

8.3.3 Determination of r by Aström et al shear lag analysis

Aström et al (Aström, Saarinen et al. 1994) presented the following ad hoc relationship from summarising their simulations:

$$k \approx (a + bD_w / l_f) * q / q_c \qquad \textbf{8. 15}$$

Where a and b are constants. This expression can also be written as:

$$k \approx \frac{\pi}{11.42} * \frac{l_f}{l_s} * (a + bD_w / l_f) = \frac{\pi}{11.42} * N_c l_f * (a + bD_w / l_f) \qquad \textbf{8. 16}$$

This shows that the value of k is determined by the number of fibre-fibre contacts per fibre and the aspect ratio of the fibre. Bringing Equation 8.15 into Equation 8.8, and then into the model for tensile strength (Equation 8.3), we get the final form of the model for tensile strength with the Aström shear lag analysis as:

$$T = \frac{8}{9} * \left[1 - \frac{2 \tanh \frac{\pi}{11.42} * N_c l_f * (a + bD_w / l_f) / 2}{\frac{\pi}{11.42} * N_c l_f * (a + bD_w / l_f)} \right] * T_z \qquad \textbf{8. 17}$$

We allowed a, and b to be adjustable parameters and varied them to find the best fit between the predicted tensile index and the measured tensile index. For the best fit, $a = 0.08$ and $b = 11.2$. This corresponds $K = 11.7$, which is much higher than that obtained from the elastic modulus data and the values from literature (Aström, Saarinen et al. 1994; Räisänen, Heyden et al. 1997).

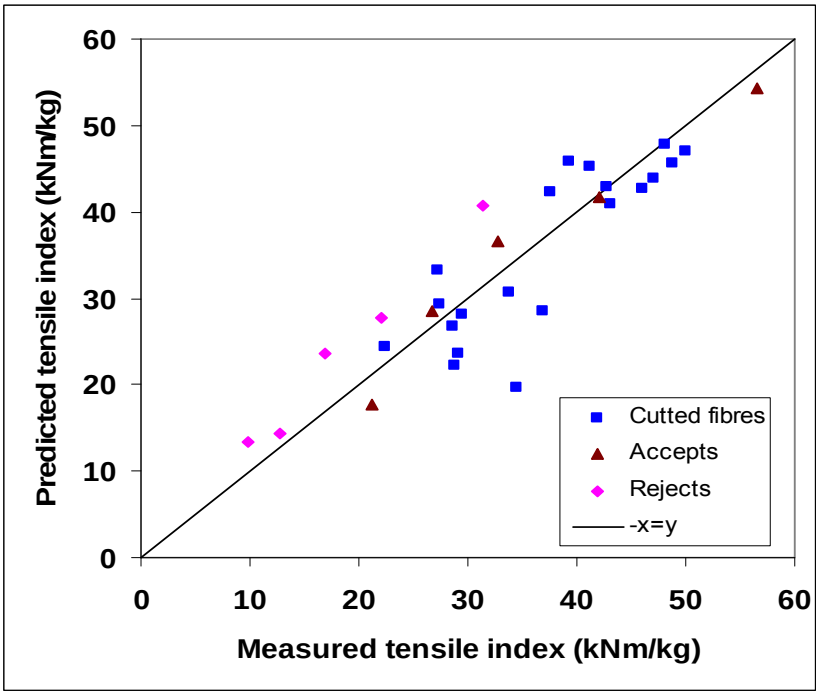

Figure 8-8 Comparison between the measured and the predicted tensile index by Equation 8.17. r was determined from Aström et al. shear lag analysis.

As shown in Figure 8-8, the data points lie much closer to the x-y line compared to that obtained by Räisänen et al shear lag analysis. The measurements and the predictions have a correlation coefficient of $R^2 = 0.79$ and a slope = 0.96. Also a good correlation was seen between the sheet density and the value of r determined from Aström et al shear lag analysis for the different samples (see Figure 8-9). The good correlation does not necessarily mean that the Aström et al shear lag analysis provides a physically reasonable value of r. It is not surprising that a good correlation can be generated as two fitting parameters are available in Equation 8.16.

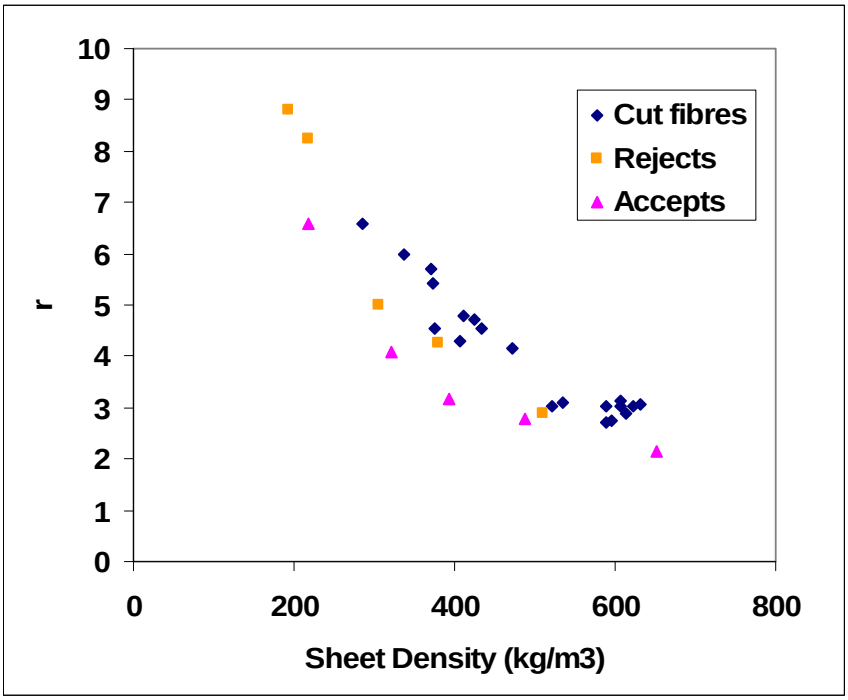

Figure 8-9 The plot of sheet density against value of r determined from Aström et al. shear lag analysis

The high value of K produced from this fit, in comparison to the much lower values obtained from fitting the elastic modulus data (refer to Figure 8-3) has the physical meaning that the stress transfer in the fibre was much less efficient at fracture than it was under elastic loading. The most reasonable explanation for this is bond failure within the samples before fracture starts. This has been experimentally observed in the literature (Niskanen, Alava et al. 1999). Bond failure will decrease the number of crossings of which a fibre can be loaded and thus increase the distance from the fibre end required to obtain the maximum load. However, such bond failure decreases the validity of shear-lag model itself, as the model assumes that stress transfer into the fibre is controlled by one parameter, k, which is uniform along the length of the fibre. Obviously some means of analytically accounting for fibre bond breakage is required. An initial attempt doing this is described in the next section.

8.4 Direct load transfer theory

8.4.1 The theory and network model

Räisänen et al (Räisänen, Heyden et al. 1997) believed that most stress-transfer along a fibre is by direct axial transfer of stress. However, no explicit expression or any kind of mathematical method was given for calculating the stress-transfer. Batchelor has recently developed a method for calculating stress-transfer based on the direct load transfer theory (see Appendix E). The main achievement of this theory is that it allows for the stress transfer to vary from point to point. Thus distributions in the properties of the crossing fibres can be modelled as well as different modes of stress transfer. The theory applies for linear transfer between the local displacement of the fibre and the displacement of the surrounding matrix. The theory assumes the fibre and fibre network to be purely elastic. The theory is based on a different type of approach where all displacements at contacts can be expressed in terms of the next displacement at the next contact along.

Figure 8-10 shows half the fibre of interest and crossing fibres. Each of the crossing fibres is then attached to the paper network. If the network is strained, then force will be transmitted into the fibre of interest from the crossing fibres. If the force delivered at the j^{th} contact is F_j, then assuming the fibres are linear elastic, it can be shown that the displacement from straining the first segment from the fibre mid-point is (see Appendix E for detailed derivation):

$$\delta_1 = \frac{1}{EA} x_1 \sum_{j=1}^{j=i} F_j - \varepsilon x_1 \qquad \textbf{8. 18}$$

where E and A are the elastic modulus and cross-sectional area, respectively, of the fibre.

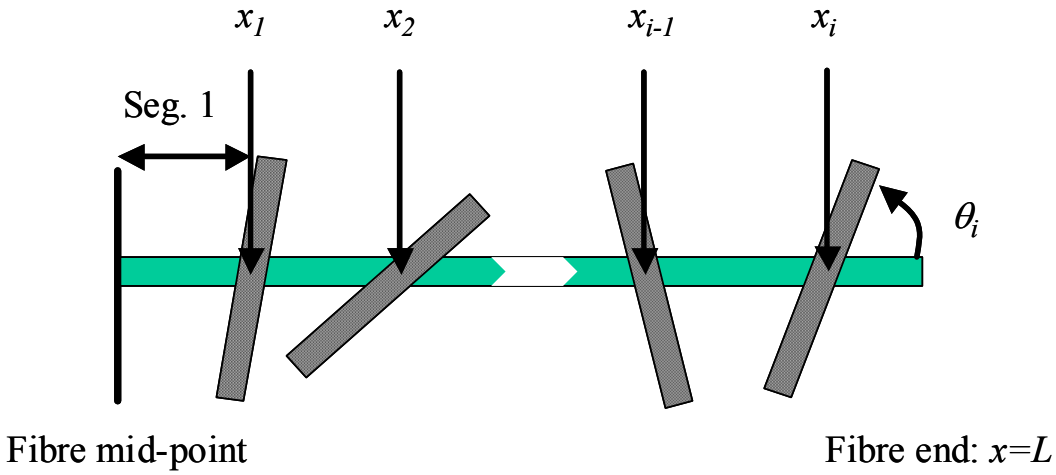

Figure 8-10 Unstrained half fibre of length, L, with i crossing fibres

The displacement at the second contact is

$$\delta_2 = \frac{1}{EA}\left(x_1 \sum_{j=1}^{j=i} F_j + (x_2 - x_1) \sum_{j=2}^{j=i} F_j \right) - \varepsilon x_1 - \varepsilon (x_2 - x_1) \qquad \textbf{8. 19}$$

which simplifies to

$$\delta_2 = \frac{1}{EA}\left(x_1 F_1 + x_2 \sum_{j=2}^{j=i} F_j \right) - \varepsilon x_2 \qquad \textbf{8. 20}$$

Extending this process it can be shown that for n^{th} and $n-1^{\text{th}}$ contacts that

$$\delta_n = \frac{1}{EA}\left(\sum_{j=1}^{j=n-1} x_j F_j + x_n \sum_{j=n}^{j=i} F_j \right) - \varepsilon x_n \qquad \textbf{8. 21}$$

$$\delta_{n-1} = \frac{1}{EA}\left(\sum_{j=1}^{j=n-2} x_j F_j + x_n \sum_{j=n-1}^{j=i} F_j \right) - \varepsilon x_{n-1} \qquad \textbf{8. 22}$$

and Equation 5 can be rewritten as

$$\delta_{n-1} = \delta_n + (x_n - x_{n-1}) \left(\varepsilon - \frac{1}{EA} \sum_{j=n}^{j=i} F_j \right) \qquad \textbf{8. 23}$$

Thus the displacement at each contact can be expressed in terms of the forces (which in turn are a function of the displacements) developed at all the contacts further along the fibre towards the end as well as the displacement of the next contact along the fibre.

Thus δ_{i-1} can be written in terms of δ_i; δ_{i-2} can be written in terms of δ_{i-1} and thus in terms of δ_i, and a similar chain can be developed such that each of the displacement can be expressed in terms of δ_i, the displacement at the final crossing nearest the fibre end. The displacements at all the fibre crossings can be expressed in terms of δ_i and as δ_i is given by

$$\delta_i = \frac{1}{EA}\left(\sum_{j=1}^{j=i} x_j F_j\right) - \varepsilon x_i \qquad \textbf{8. 24}$$

It is possible to solve this equation to determine δ_i and thus to uniquely determine the displacements at all crossings, provided that F can be expressed as a function of displacement.

The model assumes that stress transfer takes place directly from direct transfer of axial loads in the crossing fibres and that the crossing fibre has a distance, l_c, before it is rigidly bonded into the surrounding network or matrix. Figure 8-11 shows such a single fibre contact, before and after the matrix is strained. For this analysis, the reference point, $x = 0$, is set at the position of the crossing point in the unstrained system. We need to note that for the rest of the analysis $x = 0$ corresponds to the mid-point of the fibre.

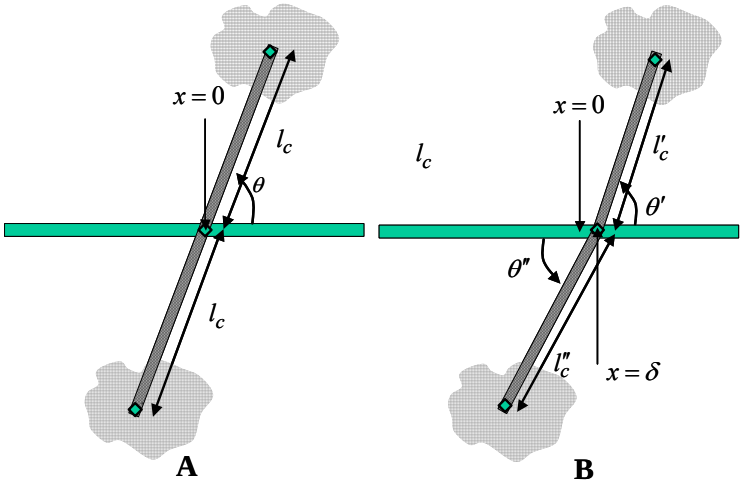

Figure 8-11 Part A: A crossing fibre, with a crossing angle of θ and a distance of l_c until it is firmly bonded into the surrounding matrix. The point at which the fibre crosses is $x = 0$. Part B: The same fibre crossing after the matrix has been strained by ε and the crossing point has also moved a distance of δ from $x = 0$.

By using the above fibre-fibre contact model, it has been shown that F can be expressed as:

$$F = -2E_c A_c \cos^2(\theta)\delta / l_c \qquad \textbf{8. 25}$$

where E_c and A_c are the modulus and cross-sectional area of the crossing fibre, respectively and θ is the crossing angle.

It should be noted that the result, that the force is linearly proportional to the displacement of the contact relative to the applied strain, is the same assumption made in the shear-lag model. The force function, Equation 8.25, is for direct load transfer only and ignores the effect of shear in fibre (see Appendix E for details)

Before doing any calculation of load distribution, a model for a fibre connected with the fibre network, as shown in Figure 8-10, has to be constructed first. As discussed in Chapter 7, the free fibre length has a Weibull distribution as given by Equation 7.1. The cumulative density function for Equation 7.1 is:

$$F(g) = 1 - e^{-(g/b)^c} \qquad \textbf{8. 26}$$

where b is the scale parameter, and c is the shape parameter for the Weibull density function, and $b, c > 0$, and $g \geq 0$ is the free fibre segment length. $F(g)$ ranges from 0 to 1. The values of b and c for some samples in this project have been determined experimentally, as presented in subsection 7.3.2.

Rearranging Equation 8.26, the free fibre segment length can be given as:

$$g = b\left[\left(-\ln(1 - F(g))\right)^{\frac{1}{c}}\right] \qquad \textbf{8. 27}$$

Equation 8.27, in which $F(g)$ is a random number between 0 and 1, can be used to generate the free fibre length.

Similarly, in a random sheet, the angles of the fibres crossing the fibre of interest can be calculated by the follow equation:

$$\theta = \arcsin\left(F(\theta)\right) \qquad \textbf{8. 28}$$

where $F(\theta)$ is a random number between 0 and 1.

The crossings for the fibre of interest were then constructed using the following scheme. As the method itself only considers the strain from the middle of the fibre ($x = 0$), this was taken as the start point. The position of the first crossing fibre was then calculated by generating a random number for F, calculating g using Equation 8.28 and dividing this by half for the first contact only. The next fibre crossing position was generated by calculating the next free fibre length and then adding this to the first position. This process was repeated until the end of the fibre is reached. A crossing angle was generated for each of the crossing fibres by using Equation 8.29.

The above calculations were conducted by using a programme written in Matlab software (see Appendix D for details). We assumed that no fibres were broken and did not consider the non-uniformity of the paper.

8.4.2 Simulations without bond breakage

The simulations show that if we do not allow bond breakage, the value of r is independent of external strain and is a constant for a given fibre. The calculated r values are plotted against the sheet density in Figure 8-12 showing a weak negative correlation. The r values for no bonds failure were brought into the fibre fracture model (Equation 8.3) to calculate the tensile index for samples of the cut fibres, the accepts and rejects and the results are compared with the corresponding measurements in Figure 8-13. Each point in Figure 8-13 is an average of ten simulations. Clearly, the calculations significantly overestimate the tensile index. This suggests the existence of bond breakage before fracture of the paper and its strong influence on the value of r.

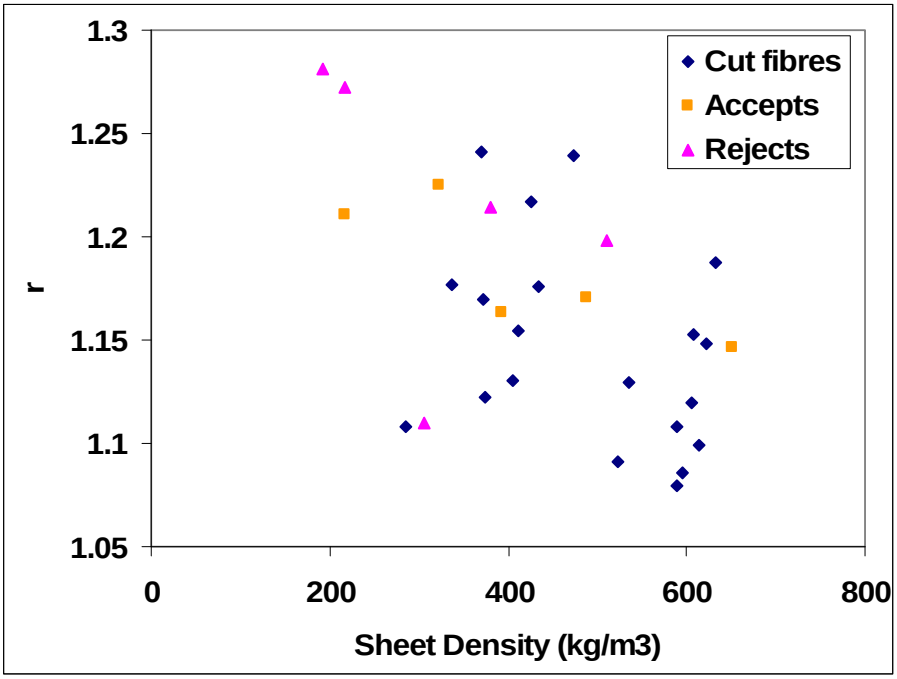

Figure 8-12 The plot of sheet density against value determined by simulations allowing no bonds breakage.

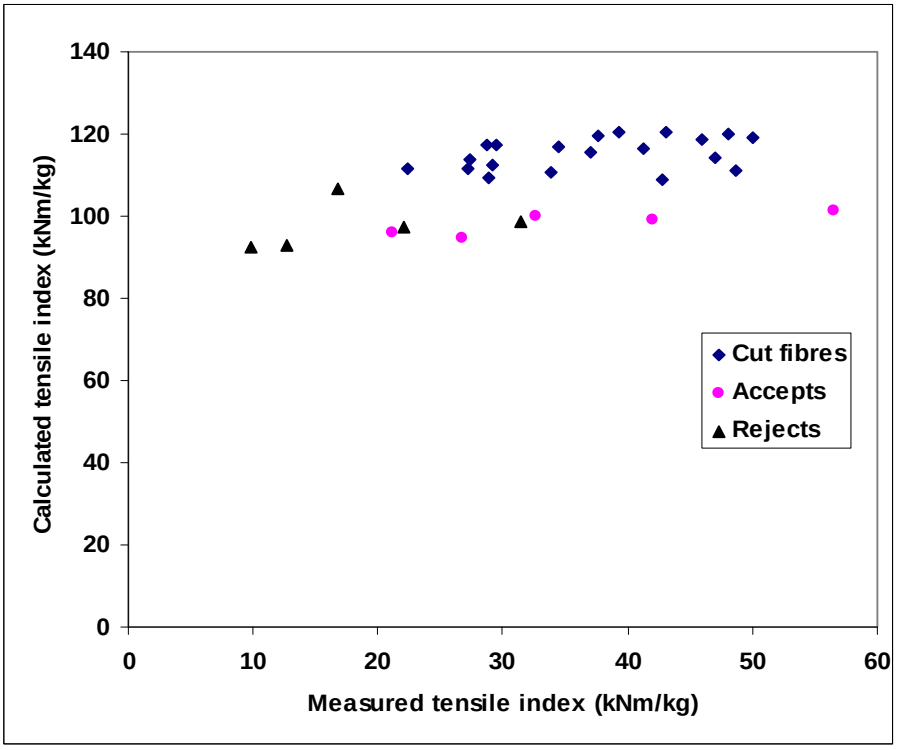

Figure 8-13 Comparison between measured tensile index and calculated tensile index by the fibre fracture model where r is determined by simulations allowing no bonds break.

8.4.3 Summary of values of r calculated by different methods

The values of r calculated from the above different methods are summarised in Table 8-1. Clearly, the r values significantly differ from method to method. As discussed above, the r values calculated by Aström et al shear-lag analysis with two fitting parameters gave the best correlation between the measured tensile strength and the predicted tensile strength. The good correlation do not necessarily mean that the Aström et al shear-lag analysis is better than the others. However, it is probably true that the r values of the samples used here are in the range of 2.1 to 8.8, which is the prediction by Aström et al shear-lag analysis.

Table 8-1 Summary of values of r calculated by different methods

Sample	Aström Shear lag analysis	Räisänen Shear lag analysis	Elastic Modulus Fitting	Simulation (no bond breakage)
L_0P_1	6.6	4.5	1.5	1.1
L_0P_2	4.6	3.7	1.4	1.1
L_0P_3	3.0	3.2	1.3	1.1
L_0P_4	2.7	2.9	1.2	1.1
L_0P_5	2.8	3.0	1.2	1.1
L_1P_1	6.0	4.8	1.6	1.2
L_1P_2	4.3	4.1	1.5	1.1
L_1P_3	3.1	3.6	1.3	1.1
L_1P_4	3.0	3.5	1.3	1.1
L_1P_5	2.9	3.6	1.4	1.1
L_2P_1	5.4	5.1	1.7	1.2
L_2P_2	4.8	4.8	1.6	1.2
L_2P_3	4.6	4.7	1.6	1.2
L_2P_4	3.0	3.9	1.4	1.1
L_2P_5	3.1	4.0	1.4	1.2
L_3P_1	5.7	5.7	1.9	1.2
L_3P_2	4.7	5.2	1.7	1.2
L_3P_3	4.2	4.9	1.6	1.2
L_3P_4	3.0	4.2	1.5	1.1
L_3P_5	3.1	4.3	1.5	1.2
AcP_1	8.8	3.7	3.8	1.2
AcP_2	8.3	3.1	2.3	1.2
AcP_3	5.0	2.8	1.9	1.2
AcP_4	4.3	2.7	1.8	1.2
AcP_5	2.9	2.4	1.5	1.1
$RejP_1$	6.6	4.3	4.1	1.3
$RejP_2$	4.1	4.3	4.0	1.3
$RejP_3$	3.2	3.6	2.4	1.1
$RejP_4$	2.8	3.3	2.1	1.2
$RejP_5$	2.1	2.9	1.7	1.2

8.4.4 Simulations with bond breakage

In the following simulations, we included bonds failure. The loads in the bonds were calculated and compared with the strength of the bonds. The bond was broken and removed from the fibre of interest if the load in the bond was greater than the strength of the bond. The bond strength was estimated to be 3000kN/m^2 according to the prediction made by Page equation (refer to subsection 8.2).

Figure 8-14 shows an example of load distribution in a half fibre. This is one simulation for sample SL0. As can be seen in Figure 8-14, the load in the fibre increases as the external strain is increased from 0.001 to 0.003. Over this range no bonds have failed and the load distribution scales directly with strain. The first bonds failed in the simulation when the external strain was increased to 0.004. Successive simulations are shown for this strain. This is because the simulation proceeds in an iterative manner. Whenever bond fracture occurs the stress distribution in the fibre is then recalculated and the loads in the bonds rechecked against bond strength. Frequently it is found that the redistribution in the load has caused bond failure in the nearby bonds. Bond failure tends to start at the ends of the fibres and move inwards. This can be observed in the simulation shown in Figure 8-14, where the data set with the solid squares represents the last simulation. Interestingly, it can be seen that while the maximum load in the fibre changes very little, the average load across the fibre has dropped sharply. These results dramatically increase the r value. The simulations showed that the r value is a 'dynamic value' which was significantly affected by the bond breakage. For the simulation in Figure 8-14, the r value gradually increased from 1.1 to 3.0 as the number of bonds broken was increased by increasing the external strain. Although the values of r can be calculated during the whole process, these values cannot be applied to our simple fibre fracture model because no fibre breakage occurs during the process.

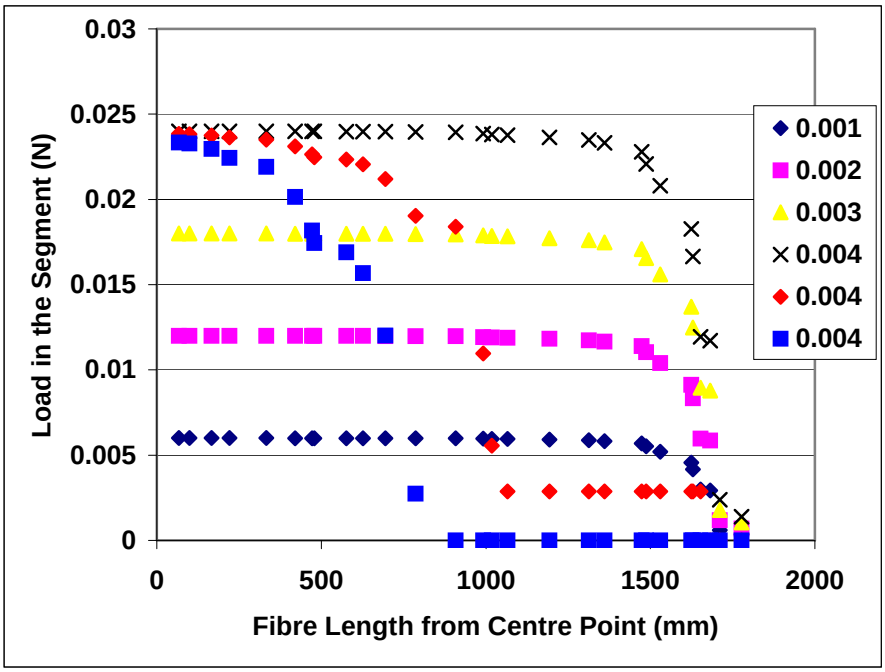

Figure 8-14 Load distribution in a fibre of interest as the global strain is increased

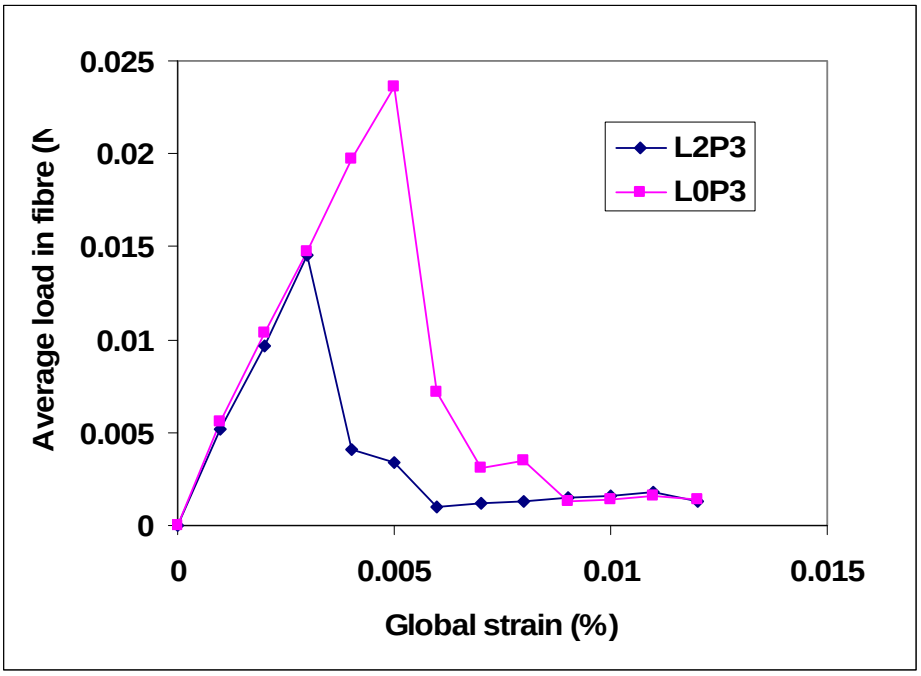

Figure 8-15 The relationship between the global strain and the average load in the fibre of interest.

Interestingly, when the average load was plotted against the global strain, it was found that the average load in the fibre increases to a peak point and then drops abruptly as the

global strain is increased (see Figure 8-15). We then define the average load in the fibre just before the abrupt drop of the load in the fibre as the peak average load. This peak average load represents the maximum load holding the fibre under the simulation conditions. It is assumed that the abrupt drop of average load corresponds to the breakage of the sheet. The peak average load was then used to calculate the tensile strength of the sheet. The calculation is shown as follows.

The number of fibres per unit width of the sheet can be written as:

$$n_f = \frac{\cos\theta * G}{A_{ap} * \rho} \qquad \textbf{8. 29}$$

where θ is the overall angle a fibre made to the cross-section of the sheet, G is grammage, A_{ap} is the apparent fibre wall area, which is the wall area cut in the cross-section, ρ is the density of the fibre wall.

The tensile strength of the sheet breaks as the average load in the fibre reaches the peak can be calculated by:

$$T_b = \frac{3}{8} * \frac{n_f * F_{ave}}{G} \qquad \textbf{8. 30}$$

where F_{ave} is the peak average load in the fibre as indicated in Figure 8-15 and 3/8 is the constant which applies for a randomly oriented sheet.

Table 8-2 Calculated tensile index by using peak average load from simulations with bond breakage summarises the calculated tensile index by using the peak average load from simulations with bond breakage.

Table 8-2 Calculated tensile index by using peak average load from simulations with bond breakage

	Apparent Fibre Wall Area (μm^2)	Grammage (g/m^2)	N0.of fibre (no. per unit sheet width)	F_{ave} (N)	Calculated Tensile Index (kNm/kg)	Measured Tensile Index (kNm/kg)
L_0P_1	235	66	156734	0.015	13.11	34.45
L_0P_2	229	65	158318	0.019	17.91	36.98
L_0P_3	223	64	161618	0.024	23.15	45.98
L_0P_4	228	64	156845	0.020	18.13	48.04
L_0P_5	233	64	154345	0.026	23.43	49.95
L_1P_1	247	65	147380	0.012	9.88	29.11
L_1P_2	221	65	166354	0.015	14.63	28.70
L_1P_3	236	64	152057	0.011	10.25	29.52
L_1P_4	238	64	151251	0.021	18.73	37.63
L_1P_5	236	63	150401	0.022	19.99	43.11
L_2P_1	226	64	158940	0.018	16.31	28.82
L_2P_2	230	66	161809	0.017	15.15	33.78
L_2P_3	234	66	157754	0.023	21.00	42.82
L_2P_4	233	66	157846	0.022	20.22	47.03
L_2P_5	232	65	158464	0.027	24.85	48.74
L_3P_1	226	65	161363	0.011	9.78	22.34
L_3P_2	230	66	160255	0.013	12.12	27.43
L_3P_3	234	66	157630	0.015	13.44	27.25
L_3P_4	233	65	157066	0.020	18.41	39.34
L_3P_5	232	65	157113	0.021	19.17	41.23
AcP_1	221	64	162936	0.008	7.84	21.17
AcP_2	224	68	169873	0.013	11.81	26.75
AcP_3	218	70	179809	0.016	15.85	32.70
AcP_4	231	72	174361	0.022	19.88	42.02
AcP_5	228	70	171332	0.027	25.07	56.52
$RejP_1$	259	62	135260	0.007	5.76	9.80
$RejP_2$	260	63	135744	0.006	4.94	12.77
$RejP_3$	270	68	141160	0.008	6.35	16.82
$RejP_4$	262	67	144192	0.013	10.64	22.06
$RejP_5$	254	69	152749	0.017	14.34	31.42

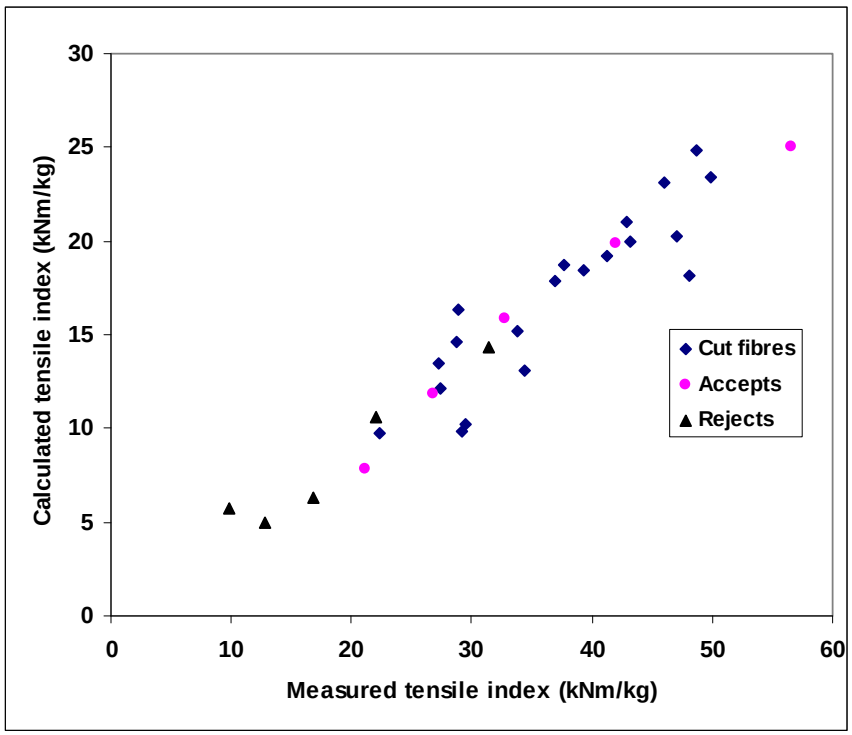

Figure 8-16 Comparison between measured tensile index and predicted tensile index by the peak average load.

Figure 8-16 compares the predicted tensile indices with the measurements. Each of the points is the average of ten simulations. It shows a very good correlation between the calculations and the measurements, and all the data points for the different series seem to fall on the same straight line. However, the calculations significantly underestimated the tensile index. The calculated strength is only about 1/3 of the measured strength. These results show that the bond break model significantly underestimates the tensile strength.

Not only do the simulations predict sheet strength of around 1/3 of the measured strength, but they also predict that the sheet will fail entirely through bond breakage. This is shown in Figure 8-17, which plots the estimated fibre strength calculated from the zero-span tensile strength against the peak load in the fibre. It can be seen that peak load in the fibre is always much less than the fibre strength.

The model provides an exact analytical solution to the stress-distribution along the fibre but depends for its accuracy on the expressions for the stress-transfer into the fibre from the surrounding matrix. These are clearly under-estimating the load transfer.

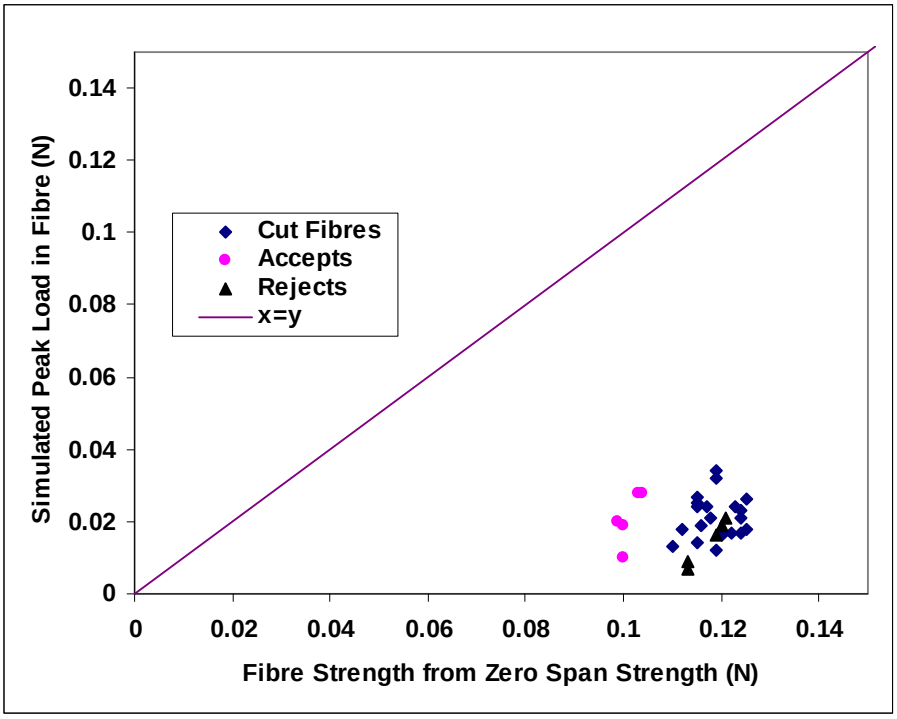

Figure 8-17 Fibre strength calculated from zero span strength against simulated peak load in the fibre

The previous discussion has shown that the fibre fracture model without bond breakage significantly overestimated tensile strength. The bond break model presented here significantly underestimates the tensile strength. It appears that to successfully predict the fracture of paper, the bond breakage model will need to be modified to increase maximum loads and strain at break. The following factors will need to be considered:

- Allowing fibres crossing at 90^{o} to contribute to load transfer via shear mechanism. The major difficulty here is how to treat the shear contribution of fibres not crossing at 90^{o}.
- Allowing crossing fibres at broken bonds to continue to contribute force to fibre via a friction mechanism. In the current model, it is assumed that once a bond breaks then that crossing fibre is completely removed from the simulation. In reality, such fibres are likely to continue to transfer some load by fibre-fibre friction even after they have broken.
- Introducing plastic deformation into the fibre of interest. This will reduce the load at the fibre-fibre bonds for a given level of external strain.
- Including fibre fracture in the simulation.

The result will be a model in which bonds will break but at higher loads, allowing the fibre to be loaded until fracture. It is beyond the scope of this PhD to do this, but the data make it clear such a model combining both fibre and bond breakage is likely to deliver the model that we have sought.

8.5 Conclusions

The following conclusions are drawn from the work in this chapter:

- The Page equation can provide a reasonable prediction for paper strength only if the bond strength is used as a fitting parameter. The reason probably is that the Page equation is not correctly accounting for the effect that changes in fibre morphology has on paper strength.
- The value of r in the simple fibre fracture model of the tensile strength of paper has been determined by fitting elastic modulus data to shear lag model, by using Räisänen et al shear lag analysis and Aström et al shear lag analysis, respectively. The tensile strength of paper calculated by the simple fibre fracture model using the values of r determined by each of the shear lag analysis has been compared with the measured tensile strength of paper. Only when the r values determined by Aström et al shear lag analysis were used, did the predicted tensile strength showed a good correlation with the measured tensile strength. Given that two fitting were available parameters in the Aström et al shear lag analysis, the good correlation does not necessarily mean that the Aström et al shear lag analysis provides a physically reasonable value of r. The above findings suggest that the shear-lag formulation for the elastic properties does not apply to the fracture of paper.
- For the first time, an explicit expression of direct load transfer theory is available for calculation of the load distribution in a fibre in a strained network. It has been demonstrated that a model structure of a fibre connected to a fibre network can be constructed by using the two parameter Weibull density function. The load distribution in the model fibre has been simulated by using the direct load transfer theory. The simulations show that, when there is no bond breakage, the load distribution in the fibre shows a similar pattern to that predicted by the

shear-lag model and the peak load and the average load increase at the same rate as the global strain is increased. In other words, the value of r for a given fibre is independent of the external strain. When bond breakage is included, the simulations show that bonds start to break from the ends of the fibre as the external strain is increased. It has also been shown that the tensile strength calculated from the peak average load in the fibre has a very good correlation with the measured tensile strength although the predictions significantly underestimate the measurements. Further modifying the bond breakage model is likely to deliver the model for tensile strength that we have sought.

- Although great efforts have been made in this thesis to test the simple fibre fracture model for the tensile strength of paper, this has not been possible because none of the methods used can calculate the value of r in the model correctly. However, it has been shown in the bond breakage model (simulation) that the r value is a 'dynamic value', which is significantly affected by the breakage of bonds before the sheet breaks. Further modifying the bond breakage model by including fibre fracture is expected to provide better prediction of the sheet fracture and therefore better calculation of r value for testing the simple fibre fracture model. It is beyond the scope of this PhD to do this but will be done in the future work.

9 Conclusions and Recommendations for Future Work

9.1 Conclusions

A new combined technique of resin embedding and confocal laser scanning microscopy has been developed for quantitative analysis of paper structure at the fibre level. Fibre dimensions, fibre orientation and fibre collapse have been measured simultaneously in paper by using the new technique and image analysis. Comparisons between the measured values of fibre wall areas by the new technique in paper with those measured by the routine confocal microscopy technique on free fibres show close agreement. The fibre orientation measured in the handsheets compares reasonably well with the theoretical value of fibre orientation of a random sheet. It is concluded that the measurements made by the new technique are valid. For the first time, a technique is available for quantitative analysis of paper structure at the fibre level.

This technique has been used to study the mechanisms of densification of the paper structure in wet pressing. A fibre shape factor and twist angle of fibre cross-section in paper have been defined for the purpose of quantifying the changes in the transverse dimensions of fibres in paper in wet pressing. It was found that fibre twist, fibre collapse and gap closure are the major types of movement of fibres in paper in wet pressing. In particular, fibre twist has been found and quantified for the first time. The results show that the number of fibres with twist angles greater than 10^{o} is reduced by wet pressing. The degree of collapse of fibres in the handsheets is symmetrically distributed at the low pressing pressure. The fibres in the handsheets cannot be totally collapsed by wet pressing even when the very high pressing pressure (4000kPa) is used. The experimental data also suggest that out of plane fibre deflection angle is independent of wet pressing pressure.

Fibre twist, fibre collapse and gap closure occur simultaneously at low pressing pressures, and the gap closure is the predominant mechanism in paper structure densification at low pressing pressures (less than 500kPa). Increasing pressing pressure only increases the apparent density slightly and the density increase is mainly

contributed by the additional twist and collapse of the fibres at the high pressing pressure (greater than 500kPa).

Based on the above new technique, a new technique for measuring properties of fibre-fibre contacts has been developed. Properties of fibre-fibre contacts, including the free fibre segment length, number and nature of fibre-fibre contacts and out-of-plane angle of fibre segments have been measured in paper. It is the first technique that can determine all of the parameters associated with the fibre-fibre contacts simultaneously in paper. For the first time, data of fibre-fibre contacts in 'real' paper is available for testing models of fibre-fibre contacts. It has been found that fibre length seems to have no effect on the properties of fibre-fibre contacts. Fibre cross-sectional shape has no significant effect on the frequency of fibre bonding along a fibre and the distribution of the free fibre length. This study shows again that the out-of-plane deflection angles of the free fibre segments have no regular trend with the pressing intensity. However, the out-of-plane deflection distance has been reduced by wet pressing since the free fibre length has been reduced. The experimental data has shown that the distribution of free fibre length for a normal sheet is not negative exponential. It seems to fit a two-parameter Weibull probability density function, even if no theoretical basis is given for using the Weibull density function. It has been demonstrated that model structures of fibre-fibre contacts can be reconstructed using the data measured by the new technique. Such model structures are important for simulations of load distribution along the length of a fibre.

This thesis presents a new model that relates the fibre cross-sectional dimensions and the apparent density of paper to the number of fibre-fibre contacts per unit length of fibre. It is the first model that considers the effects of fibre cross-sections on the fibre-fibre contacts and it is also the first time such a model has been fully verified with experimental data. The model has also been converted into two expressions for RBA, which have been verified with measured results by two different methods. It has been shown that both of the two expressions can predict RBA well. It has also been demonstrated that the RBA can be measured by using the combined technique of nitrogen adsorption and spray dry fibres on a teflon surface.

This thesis also presents a new analytical model for tensile strength of paper based on the assumption that the macroscopic fracture of paper is trigger by the failure of fibres lying in the direction of the applied load. The new model relates the tensile strength to the zero-span strength of the component fibres through a factor r. The value of r is the ratio of the peak load and the average load in the fibres. It is the first analytical model that attempts to predict the start point of paper failure under load. It has been shown that the shear lag analysis does not seem to apply to the fracture of paper.

Model structures of a fibre of interest connecting the fibre network matrix were constructed by using the experimental data and the Weibull density function. Simulations of load distribution on the fibre of interest have been done for situations of no bond breakage, as well as with bond breakage. The simulations suggest that the value of r is a 'dynamic value', which is determined by the way that the fracture of paper is triggered. It has been shown that bond breakage occurs before the sheet fracture, and it significantly affects the value of r. The simulation model is still at very preliminary stage. It has not included the fracture of fibres, which is believed to be the trigger of the fracture of paper. Therefore, it is not surprising that the preliminary simulations can not predict the correct values of r. However, a very good correlation has been shown between the tensile index calculated by the peak average load from the bond breakage model and the measured tensile index, although the predicted value was still only 1/3 of the measured value. This indicates the promise of the bond breakage model. Further modifying the bond breakage model by including fibre fracture is expected to provide better prediction of the sheet fracture and therefore better calculation of r value for testing the simple fibre fracture model. It is beyond the scope of this PhD to do this and will be done in the future work.

9.2 Recommendations for Future Work

9.2.1 Further study on the fibre-fibre contacts

In this thesis, although the nature of fibre-fibre contacts was classified into full and partial contacts, there is no theoretical basis for doing this. The type of the contacts was

determined by the operator by examining the cross sections of fibre-fibre contacts. A contact that had about the same distance as the fibre width then this was defined as a full contact. A contact about half or less of the fibre width was defined as partial contact. How to define the partial and full contacts in a more scientific way is a question to be answered in future work. For doing this, a series cross-sectional images at different depth of a sheet cross section can be obtained by using the new technique developed in this thesis. Then the series of images can be used to reconstruct the 3-D image of the paper structure using new image analysis software, such as ImagePro. The 3-D image will show more information of fibre-fibre contacts.

Dent (Dent 2001) has shown that from theoretical analysis the free fibre length should be a general gamma distribution. It is recommended to use the data in this thesis to test the gamma distribution in the future work.

It has been shown that some fibre-fibre bonds break before the fracture of paper. The bond strength affects the bond breakage and therefore the load transfer between fibres and the value of r. This is how the bond strength comes into the simple fibre fracture model for the tensile strength of paper. The bond strength in this thesis was estimated by fitting the experimental data to the Page equation where the bond strength was treated as a fitting parameter. The literature has shown that there is no technique available to measure the bond strength so far. Development of techniques for measuring the bond strength is an important topic in the future work in this area.

It has been shown that the bond breakage simulation model is very promising. Refining the bond breakage model by including the fracture of fibre and other factors as discussed in Chapter 8 is expected to be able to predict the fracture of paper and therefore to generate correct values of r in the simple fibre fracture model of the tensile strength of paper. This can be done by:

- Allowing fibres crossing at 90^o to contribute to load transfer via shear mechanism. Major difficulty here is how to treat the shear contribution of fibres not crossing at 90^o.
- Allowing crossing fibres at broken bonds to continue to contribute force to fibre via a friction mechanism. In the current model, it is assumed that once a bond

breaks then that crossing fibre is completely removed from the simulation. In reality, such fibres are likely to continue to transfer some load by fibre-fibre friction even after they have broken.

- Introducing plastic deformation into the fibre of interest. This will reduce the load at the fibre-fibre bonds for a given level of external strain.
- Including fibre fracture in the simulation.

References

Allan, G. G. and A. N. Neogi (1974). "Fundamental of Fiber Assemblages: A Unifying Theory for the Tensile Strength of Paper and Nonwoven." Cellulose Chemistry and Technology **8**: 297.

Aström, J. and K. Niskanen (1991). "Simulation of Network Fracture". Proceedings of the Internatinal Paper Physics Conference, Kona, Hawaii.31

Aström, J., S. Saarinen, et al. (1994). "Microscopic mechanics of fiber networks." Journal of Applied Physics **75**(5): 2383-2392.

Batchelor, W., Westerlind, B.S., Hagglund, R., and Gradin, P. (2003). "Effect of test conditions on measured loads and displacements in zero and short span testing". 2003 International Paper Physics Conference, Canada.115-120

Baum, G. A. (1993). "Subfracture mechanical properties". Transactions of the Tenth Fundamental Research Symposium, PIRA International.1-126

Bentley, R. G., Scudamore, P., and Jack, J. S. (1994). "A Comparison Between Fibre Length Measurement Methods." Pulp & Paper Canada **95**: 41.

Boucai, E. (1971). "The zero-span test: its relation to fibre properties". International Paper Physics Conference, Mont Gabriel, QC.3-5

Braaten, K. R. (2000). "Fibre and Fibril Properties Versus Light Scattering and Surface Smoothness for Mechnical Pulps." Pulp & Paper Canada **101**(5): T122-T126.

Brunauer, S., Emmett, P.H., and Teller, E. (1938). "Adsorption of gases in multimolecular layers." J. Am. Chem. Soc. **60**: 309-319.

Button, A. (1979). "Fibre-Fibre Bond Strength: A Study of a Linear Elastic Model Structure. Ph.D. thesis" Ph. D.Inst. of Paper Chemistry, Appleton, Wisconsin

Campbell, W. B. (1959). Tappi **42**(12): 999.

Christine, A., Per, N., Weiby, N., Rune, H., Timm, W., and Christoph, R. (2002). "3D images of paper obtained by phase-contrast X-ray microtomograph: image quality and binarisation." Nuclear Instruments and Methods in Physics Research Section A: Accelerators, spectrometers, detectors and associated equipment(409 (1-2)): 392-402.

Clark, J. d. A. (1943). "Factors Influencing Apparent Density of Paper." Paper Trade J. **116**(1): 9-13.

Clark, J. d. A. (1985). "Pulp Technology and Treatment for Paper"

Conn, A., and Parker, I. (1999). "Fibre Wall Thickness Measurement Using the Distance Transform". Clayton, APPI, Monash University**:** 10.

Corte, H., and Kallmes, O.J., (1962). "Statistical Geometry of a Fibrous Network. In The Formation and Structure of Paper, Trans. IInd Fund. Res. Symp., (F. Bolam, ed.), Tech. Sect. BPBMA, London." 13-52.

Corte, H., Kallmes, O.J., and Jarrot, D. (1961). "Mechanical Failure of Ideal 2-D Fibre Networks." Paper Maker **142**(1): 61-68,72.

Cox, H. L. (1952). "The Elasticity and Strength of Paper and Other Fibrous Materials." British J. Applied Physics **3**(3): 372.

Denis, E. S. (1996). "Creep and Dynamic Mechanical Properties of Eucalypt Single Fibres and Handsheets" M.Eng.Sc.M.Eng.Sc., Chemical Engineering.Monash.220

Dent, R. W. (2001). "Inter-fibre Disdances in Paper and Nonwovens." J. Text. Inst., **92**(Part1, 1): 65-74.

Dickson, A. R. (2000a). "Quantitative Analysis of Paper Cross-Sections." Appita Journal **53**(4): 292-295.

Dickson, A. R. (2000b). "The Quantitative Microscopic Analysis of Paper Cross-Sections: Sample Preparation Effects." Appita Journal **53**(5): 362-366.

Dodson, C. T. J. (1996). "Fiber Crowding, Fiber Contacts, and Fiber Flocculation." TAPPI Journal **79**(9): 211-216.

Dumbleton, D. F. (1972). "Longitudinal Compression of Individual Pulp Fibres." TAPPI J. **55**(6): 461-467.

El-Hosseiny, D. H. (1979). "Light Scattering and Sheet Density." Tappi **62**(10): 127-129.

El-Hosseiny, F. and D. Abson (1983). "A critical examination of theories of paper tensile strength." Paper Technology and Industry **24**(6): 209-213.

El-Hosseiny, F. and K. Bennett (1985). "Analysis of the Zero-Span Tensile Strength of Paper." J. Pulp Paper Sci. **11**(4): J121-J126.

Elias, T. G. (1967). "Investigation of the Compression Response of Ideal Unbonded Fibrous Structures." TAPPI J. **50**(3): 125-132.

Erikkila, A. L., Pakarinen, P. and Odell, M. (1998). "Sheet Forming Studies Using Layered Orientation Analysis." Pulp Paper Can **99**(1): 81-85.

Feldman, H., K. Jayaraman, et al. (1996). "A monte carlo simulation of paper deformation and failure." Journal of Pulp & Paper Science **22**(10): J 386-J 392.

Fellers, C., Anderson, H. and Hollmark, H. (1986). "The Definition and Measurement of Thickness and Density." in Paper Structure and Properties, Bristow, J.A. and Kolseth, P., eds., Marchel Dekker, Inc., New York: 151-167.

Forseth, T., and Helle, T. (1997). "Effect of moistening on cross-sectional details of calendered paper containing mechanical pulp." Journal of Pulp & Paper Science **23**(3): J 95-J 100.

Gavelin, G., and Backman, J. (1991). "Fractionation with Hydrocyclones". TAPPI Pulping Conf., Orlando.753-774

Giertz, H. W., and Roedland, H. (1979). "Elongation of Segments - Bonds in the Secondary Regime of the Load/Elongation Curve". International Paper Phyiscs Conference, Harrison Hot Spring, CPPA,129-136

Gorres, J., Amiri, R., Grondin, M., and Wood, J.R. (1993). "Fibre Collapse and Sheet Structure". Products of Papermaking: Transactions of the Tenth Fundamental Research Symposium, Oxford, UK, Pira International, Leatherhead.285

Gorres, J. and P. Luner (1992). "An Apparent Density Model of Paper." J. Pulp Paper Sci. **18**(4): J127-J130.

Haselton, W. R. (1954). "Gas Adsorption by Wood, Pulp and Paper (1)." Tappi **37**(9): 404-412.

Haselton, W. R. (1955). "Gas Adsorption by Wood, Pulp and Paper (2)." Tappi **38**(12): 716-723.

Hasuike, M., Kawasaki, T. and Murakami, K. (1992). "Evaluation Method of 3-D Geometric Structure of Paper Sheet." Journal of Pulp & Paper Science **18**(3): J114-J120.

Heyden, S. and P. J. Gustafsson (1998). "Simulation of fracture in a cellulose fibre network." Journal of Pulp & Paper Science **24**(5): 160-165.

Ingmanson, W. L. and E. F. Thode (1959). "Factors Contributing to the Strength of a Sheet of Paper." Tappi **42**(1): 83-93.

Jang, H. F. (2001). "A Theory for the Transverse Collapse of Wood Pulp Fibres." Transactions of the 12th Fundamental Research Symposium held at Oxford: September 2001, edited by C.F Baker, Pira International, Leatherhead, UK **1**: 193-210.

Jang, H. F., and Seth, R. S. (1998). "Using confocal microscopy to characterize the collapse behavior of fibers." TAPPI Journal **81**(5): 167-174.

Jang, H. F., Howard, R.C. and Seth, R.S. (1995). "Fiber Characterization Using Microscopy-Effects of Recycling." TAPPI J. **78**(12): 131.

Jang, H. F., Robertson, A.G. and Seth, R. S. (1992). "Transverse Dimensions of Wood Pulp Fibres by Confocal Laser Scanning Microscopy and Image Analysis." Journal of Materials Science **27**: 6391-6400.

Jayaraman, K. and M. T. Kortschot (1998). "Closed-form network models for the tensile strength of paper - a critical discussion." Nordic Pulp and Paper Research Journal **13**(3): 233-242.

Johnston, R. E. (1995). "A simplified shear-lag model of paper as a long fibre reinforced material." Proc. 49th Apptia Annual General Conference: 405-409.

Johnston, R. E., Li, M. L. and Waschl, R. (1997). "Eucalypt fibre size fractions - modelling and measuring their effect on sheet properties." Appita Journal **50**(4): 307 ff.

Kallmes, O. J., and Bernier, G. (1963). "The Paper Structure, 4. The Free Fibre Length of a Multiplanar Sheet." TAPPI J. **46**(2): 108-114.

Kallmes, O. J., Bernier, G.A. and Perez. M (1977). "A mechanistic theory of the load-elongation properties of paper-in four parts." Paper Technology and Industry **18**(part1 -7,222; part2 -8,243; part3 -9,283; part4 -10,328).

Kallmes, O. J., Bernier, G.A. and Perez. M (1978). "A mechanistic theory of the load-elongation properties of paper-A descriptive summary." Paper Technology and Industry **19**(9): 311.

Kallmes, O. J. and H. Corte (1960). "The Structure of Paper, 1. The Statistical Geometry of An Ideal two Dimensional Fibre Network." TAPPI J. **43**(9): 737-752.

Kallmes, O. J., Corte, H. and Bernier, G. (1961). "The Structure of Paper, 2. The Statistical Geometry of A Multiplanar Fibre Network." TAPPI J. **44**(7): 519-528.

Kallmes, O. J. and M. Perez (1965). "A New Theory for the Load/Elongation Properties of Paper". Consolidation of Paper, Transactions of the Third Fundamental Research Symposium, Cambridge, British Paper and Board Makers Association, London, U.K.,.779

Kane, M. W. (1959a). "The Effect of Beating on Fiber Length Distribution-Part 1." Pulp and Paper Magazine of Canada **60**(10): T308.

Kane, M. W. (1959b). "Beating, Fiber Length Distributions and Tensile Strength-Part 2." Pulp and Paper Magazine of Canada **60**(12): T359.

Kärenlampi, P. (1995). "Effect of distributions of fibre properties on tensile strength of paper - a closed-form theory." Journal of Pulp & Paper Science **21**(4): J 138-J 143.

Kärenlampi, P. (1995). "Tensile strength of paper - a simulation study." Journal of Pulp & Paper Science **21**(6): J 209-J 214.

Kärenlampi, P., Suurhamari, H. T. , Alava, M. J., and Niskanen, K. J. (1996). "The effect of pulp fibre properties on the in-plane tearing work of paper." TAPPI Journal **79**(5): 203-210.

Keeny, F. C. (1952). "Physical Properties of Slash Pine Semichemical Kraft Pulp and of Its Fully Chlorited Component." Tappi **35**: 555-563.

Kibblewhite, R. P. (1993). "Effects of refined softwood:eucalypt pulp mixtures on paper properties". Products of Papermaking, Transactions of the Tenth Fundamental Research Symposium, Oxford, PIRA International, Leatherhead, U.K.127-157

Kibblewhite, R. P., and Bailey, D. G. (1988). "Measurement of Fibre Cross-Section Dimensions Using Image Processing." Appita J. **41**(4): 297-303.

Kibblewhite, R. P., and Bawden, A.D. (1991). "Fibre and Fibre Wall Response to Refining in Softwood and Hardwood Pulps." PIRA conference on "Current and Future Technologies of Refining," Birmingham, UK, December paper 6.

Komori, T. and M. Itoh (1994). "A Modified Theory of Fiber Contact in General Fiber Assemblies." Textile Res. J. **64**(9): 519-528.

Komori, T. and K. Makishima (1977). "Numbers of Fiber-to-Fiber contacts in General Fiber Assemblies." Textile Res. J. **47**(1): 13-17.

Laivins, G. V., and Scallan, A.M. (1993). "The mechanism of hornification of wood pulps". Transactions of the Tenth Fundamental Research Symposium, Oxford, PIRA International.1235-1260

Lehto, H. J. (2004). "Charaterization of mechanical and chemical pulp fibres". Proceedings of the 58th Appita Annual Conference: 349-356., Canberra

Li, M., Johnston, R., Xu, L., Filonenko, Y. and Parker, I. (1999). "Characterization of Hydrocyclone-Separated Eucalypt Fibre Fractions." Journal of Pulp & Paper Science **25**(8): 299-304.

Li, X., and Parker, I. (1999). "Correction of Fluorescence Attenuation with Depth in Fibre and Paper Images Collected by Confocal Laser Scanning Microscopy." Appita J. **52**(1): 41-44.

Li, X., Parker, I. and Osborne, C. (1997). "Technique for Determing the Fibre Distribution in the Z-Direction Using Confocal Microscopy and Image Analysis." Appita J. **50**(4): 325-328.

Luner, P., Karna, A.E.U. and Donofrio, C.P. (1961). "Studies in Interfibre Bonding of Paper. The Use of Optical Bonded Area with High Yield Pulps." TAPPI J. **44**(6): 409-414.

Lyne, L. M., and Gallay, W. (1954). "Fibre Properties and Fibre-Water Relationships in Relation to the Strength on Rheology of Wet Webs." Tappi **37**(12): 694.

Mark, R. E., and Gillis, P.P. (1994). "Handbook of Physical and Mechanical Testing of Paper and Paperboard". New York, Marcel Dekker.Chapter 10

Mattson, E. (2001). "Towards a Understanding in Paper Strength." A thesis for the degree of Masters of Science Programme, Department of Chemical and Metallurgical Engineering, Lulea University of Technology.

Mayhood, C. H., Kallmes, O.J., and Cauley, M.M. (1962). "The mechanical properties of paper Part II: Measured shear strength of individual fiber to fiber contacts." TAPPI J. **45**(1): 69-73.

McIntosh, D. C., and Leopold, B. (1962). "Bonding Strength of Individual Fibres". The Formation and Structure of Paper. F. Bolam. London, Brit. Paper&Board Makers Assn.**:** 265-275.

Merchant, M. V. (1957). "A Study of Water-Swollen Cellulose Fibres Which Have Been Liquid-Exchanged and Dried From Hyrocarbon." Tappi **40**: 771-781.

Mohlin, U. B. (1974). "Cellulose Fibre Bonding. Determination of Interfiber Bond Strength." Svensk Papperstid **77**(4): 131-137.

Mohlin, U. B., J. Dahlbom, et al. (1996). "Fiber deformation and sheet strength." TAPPI Journal **79**(6): 105-111.

Moss, P. A., and Retulainen, E. (1997). "The Effect of Fines on Fiber Bonding: Cross-Sectional Dimensions of TMP Fibres at Potential Bonding Sites." J. Pulp Paper Sci **23**(8).

Nanko, H., and Ohsawa, J. (1989). "Mechanisms of Fibre Bond Formation." Transactions of the Ninth Fundamental Research Symposium Cambridge, Brander, J., Ed., Mechanical Engineering Publications, Lit., London U.K.: 783-830.

Niskanen, K. (1993). "Strength and Fracture of Paper". Transactions of the tenth fundamental research symposium, Oxford, Pira International, Leatherhead.641-725

Niskanen, K. (1998). "Paper Physics". Helsinki, Fapet Oy

Niskanen, K. (1998). "Paper Physics", Finish Paper Engineers' Association and TAPPI.46-47

Niskanen, K., and Rajatora (2002). "Statistical Geometry of Paper Cross-Sections." Journal of Pulp & Paper Science **28**(7): 228-233.

Niskanen, K., Nilsen, N., Hellen, E. and Alava, M. (1997). "KCL-Pakka: Simulation of the 3D Structure of Paper". 11th Fundamental Research Syposium, Cambridge, Pira International.1273-1291

Niskanen, K. J., M. J. Alava, et al. (1999). "Fracture energy in fibre and bond failure." Journal of Pulp & Paper Science **25**(5): 167-169.

Nordman, L., Aaltonen, P. and Makkonen, T. (1965). "Relationships Between Mechanical and Optical Properties of Paper Affected by Web Forming Variables". Transactions of the Third Fundamental Research Symposium, Cambridge, British Paper and Board Makers Association, London, U.K.909-927

Nordman, L., and Gustafsson, C. (1951). Paper and Timber **33**(2): 36-41.

Nordman, L. S. (1957). "Bonding in Paper Sheets". Transactions of the Second Fundamental Research Symposium Held at Cambridge,, London, U.K., British Paper and Board Makers Association.333

Ochiai, S., and Hojo, M. (1994). "Stress distribution in discontinuous fibres in a model composite." J. Mat. Sci. **29**: 2754-2760.

Paavilainen, L. (1993). "Importance of Cross-Dimensional Fibre Properties and Coarseness for the Characterisations of Softwood Sulfate Pulp." Paperi Ja Puu-Paper & Timber **75**(5): 343-351.

Paavilainen, L. (1994). "Bonding Potential of Softwood Sulphate Fibres." Paperi ja Puu **76**(3): 162-173.

Page, D. H. (1969). "A method of determining the fibrillar angle in wood tracheids." Journal of Microscopy **90**(2): 137-143.

Page, D. H. (1969). "A Theory for the Tensile Strength of Paper." TAPPI J. **52**(4): 674-681.

Page, D. H. (2002). "The Meaning of Nordman Bond Strength." Nordic J. Pulp Paper Res. **17**(1): 39-44.

Page, D. H., and Sargent, J.W. (1962). "The Fine Structure of Fibre Bonding". The Formation and Structure of Paper. F. Bolam, Brit. Paper & Board Makers Assn., London**:** 195-203.

Page, D. H., Sargent, J.M. and Nelson R (1965). "Structure of Paper in Cross-Section". Transactions of Symposium, Cambridge, British Paper and board Industry Res. Assoc., Kenley, Surrey.313-352

Page, D. H. and R. S. Seth (1980). "The elastic modulus of paper II. The importance of fiber modulus, bonding, and fiber length." Tappi **63**(6): 113-116.

Page, D. H. and R. S. Seth (1980). "The elastic modulus of paper III. The effects of dislocations, microcompression, curl, crimps and kinks." Tappi **63**(10): 99-102.

Page, D. H., R. S. Seth, et al. (1979). "The elastic modulus of paper I. The controlling mechanisms." Tappi **62**(9): 99-102.

Page, D. H., Seth, R.S., Jordan B.D., and Barbe M.C. (1985). "Curl, crimps, kinks and microcompressions in pulp fibres - their origin, measurement and significance". Papermaking Raw Materials, Oxford, Mechanical Engineering Publications.183-227

Page, D. H., Tydeman, P.A., and Hunt, M. (1962). "A Study of Fibre-to-Fibre Bonding by Direct Observation". The Formation and Structure of Paper. F. Bolam, Brit. Paper & Board Makers Assn., London**:** 171-193.

Pan, N. (1993). "A Modified Analysis of the Microstructural Characteristics of General Fiber Assemblies." Textile Res. J. **63**(6): 336-345.

Parsons, R. S. (1942). "Optical Characteristics of Paper as a Function of Fibre Classification." Paper Trade J. **115**(25): 34-42.

Paulapuro, H. (2001). "Wet Pressing - Present Understanding and Future Challenges." Transactions of the 12th Fundamental Research Symposium held at Oxford: September 2001, edited by C.F Baker, Pira International, Leatherhead, UK **1**: 639-678.

Perkins, R. W., and Mark, R.E. (1981). "Some New Concepts of the Relation Between Fibre Orientation, Fibre Geometry, and Mechanical Properties". The Role of Fundamental Research in Paper Making, Mech. Eng.Publ., London.479-525

Pike, G. E., and Seager, C.H (1974). Physical Review B **10**: 1421-1426.

Quackenbush, D. W. (1971). "Faults in Paper Coatings and Their Relationship to Base Sheet Structure." Tappi **54**(1): 47-52.

Radvan, B. (1980). "Forming the Web of Paper". Elsevier, Netherlands

Räisänen, V. I., Alava, M. J., Niskanen, K. J. and Nieminen, R. M. (1997). "Does the shear-lag model apply to random fiber networks." Journal of Materials Research **12**(10): 2725-2732.

Räisänen, V. I., Alava, M.J., Nieminen, R. M., and Niskanen, K.J. (1996). "Elastic-plastic behaviour in fibre network." Nordic J. Pulp Paper Res. **11**(4): 243-248.

Räisänen, V. I., S. Heyden, et al. (1997). "Simulation of the effect of a reinforcement fiber on network mechanics." Nordic Pulp Paper Research J. **12**(3): 162-166.

Ratliff, F. T. (1949). "The Possible Corrrelation Between Hemicelluloses and the Physical Properties of Bleached Kraft Pulps." Tappi **32**: 357-367.

Rehmat, T., and Branion, R. (1995). "Fibre Fractionation in Hydrocyclones." Preprints 81st Ann. Matg., Tech. Sect., CPPA(B105-125).

Retulainen, E. and K. Ebeling (1993). "Fibre-fibre bonding and ways of characterizing bond strength." Appita Journal **46**(4): 282-288.

Rigdahl, M., Andersson, B.W. and Hollmark, H. (1983). "Elastic Behaviour of Low Density Paper Described by Network Mechanics." Fibre Sci. Technol. **19**(2): 127-144.

Rigdahl, M., Westerlind, B., Hollmark, H. (1984). "Analysis of cellulose network by finite element method." Journal of Materials Science **19**: 3945-3952.

Roberts, J. C. (1996). "The Chemistry of Paper". Cambridge, The Royal Society of Chemistry

Robertson, G., J. Olson, et al. (1999). "Measurement of fiber length, coarseness, and shape with the fiber quality analyzer." TAPPI Journal **82**(10): 93-98.

Ruvo, D. A., Fellers, C. and Kolseth, P. (1986). "Descriptive Theories for the Tensile Strength of Paper", Marchel Dekker, Inc., New York.267-279

Schniewind, A. P., Nemeth, L.J., and Brink, D.L. (1964). "Fibre and Pulp Properties. I. Shear Strength of Single Fiber Crossings." Tappi **47**(4): 244-248.

Seth, R. S. (1990). "Fiber Quality Factors in Papermaking - II. The Importance of Fiber Coarseness". Materials Interaction Relevant to the Pulp, Paper and Wood Industries, San Francisco, California, USA, Materials Research Society.143-161

Seth, R. S. (1990). "Fibre Quality Factors in Papermaking - 1 The Importance of Fibre Length and Strength". Materials Interaction Relevant to the Pulp, Paper and Wood Industries, San Francisco, California, USA, Materials Research Society.125 -141

Seth, R. S., and Chan, B. K. (1997). "Measurement of fiber coarseness with optical fiber length analyzers." TAPPI J. **80**(5): 217-221.

Seth, R. S., and Page, D H (1983). "The Stress-Strain Curve of Paper". The Role of Fundamental Research in Papermaking - Transactions of the Seventh Fundamental Research Symposium, Cambridge, Mechanical engineering publications, Ltd., London, U.K. p.421.421

Seth, R. S., Jang, H. F., Chan, B. K. and Wu, C. B. (1997). "Transverse dimensions of wood pulp fibers and their implications for end use". Fundamentals of Papermaking Materials, Transactions of the Fundamental Research Symposium, 11th,, Cambridge, UK,, Pira International, Leatherhead, UK.473-503

Seth, R. S. and D. H. Page (1975). "Fracture resistance: a failure criterion for paper." Tappi **58**(9): 112-117.

Shallhorn, P. M. and A. Karnis (1979). "The tear and tensile strength of mechanical pulps". International Mechanical Pulping Conference, Technical Section, Canadian Pulp and Paper Association.25-36

Skowronski, J. (1991). "Fibre-to-fibre bonds in paper. Part II: Measurement of the breaking energy of fibre-to-fibre bonds." J. Pulp Paper Sci. **17**(6): J217-222.

Stratton, R. A. (1990). "Dependence of Fiber/Fiber Bonding on Some Papermaking Variables". Material Interactions Relevant to the Pulp, Paper and Wood Industries, Pittsburgh, Materials Research Soc.173-181

Stratton, R. A., and Colson, N. L. (1993). "Fibre Wall Damage During Bond Failure." Nordic Pulp & Paper Research Journal **8**(2): 245.

Struers "www.struers.com.au."

Swanson, J. W., and Steber, A. J. (1959). "Fiber Surface Area and Bonded Area." Tappi **42**(12): 986-994.

Szikla, Z., and Paulapuro, H. (1986). "Z - Directional Distribution of Fines and Filler Material in the Paper Web Under Wet Pressing Condition." Paperi ja Puu **68**: 654-658.

Szikla, Z., and Paulapuro, H. (1989). "Changes in Z-Direction Density Distribution of Paper in Wet Pressing." J. Pulp Paper Sci **15**(1): J11-J17.

Taylor, D. L. (1964). "Thichness and Apparent Density of Paper." Tappi **47**(7): 165A.

Ting, T. H. D., Chiu, W.K. and Johnston, R. E. (1997). "Network Changes in Paper Under Compression in the Z-Direction - The Effect of Loading Rate and Fibre Wall Thickness." Appita Journal **50**(3): 223-229.

Uesaka, T. (1984). Handbook of Physical and Mechanical Testing of Paper and Paperboard. R. E. Mark, and Murakami, K. New York, Marcel Dekker**:** 379-402.

Van Den Akker, J. A. (1962). London, Brit. Paper&Board Maker Assn.205-245

Van Den Akker, J. A., Lathrop,A.L., Voelker, M.H. and Dearth, L.R. (1958). "Importance of Fiber Strength to Sheet Strength." TAPPI J. **41**(8): 416-425.

Weise, U. and H. Paulapuro (1996). "Relation between fibre shrinkage and hornification [german]." Papier **50**(6): 328-333.

Williams, D. G. (1983). "The Page equation- a limiting form of the Kallmes-Bernier-Perez theory of the load elongation property of paper." Tappi **66**(1): 100.

Williams, G. J., and Drummond, J.G. (2000). "Preparation of Large Sections for the Microscopical Study of Paper Structure." J. Pulp Paper Science **26**(5): 188-193.

Williams, G. J., Drummond, J.G. and Cisneros, H.A. (1994). "A Microscopical Approach for Examining Fiber and Paper Structures." J.Pulp Paper Science **20**(4): J110-114.

Xu, L., A. B. Conn, et al. (1998). "Quantification of Wood Pulp Fibres by Confocal Microscopy." Proceedings of the 10th International Conference on Confocal Microscopy, Sydney, 14-17th, April.

Xu, L., Y. Filonenko, et al. (1997). "Measurement of Wall Thickness of Fully Collapsed Fibres By Confocal Microscopy and Image Analysis". 51st Appita Annual General Conference Proceedings.551-555

Xu, L. and I. Parker (2000). "Simulating the forming process with the Moving Belt Drainage Former." Appita Journal **53**(4): 282-286.

Yamauchi, T. (1987). "Measurement of Paper Thickness and Density." Appita **40**(5): 359.

Yang, C. F., Eusufzai, A.R.K., Mark, R.E., Sankar, R.E. and Perkins Jr. R.W. (1978). "Measurements of Geometrical Parameters of Fiber Networks Part 1. Bonded Surfaces, Aspect ratios, Fiber Moments of Inertia, Bonding State Probability." Svensk Papperstidning **13**: 426-433.

Appendix. A Pulping, Handsheet Formation and Physical Testing

Appendix A.1 Fibre raw material

Laboratory made pulps were used in this project. Firstly, it is easier to control the quality of the laboratory made pulp compare to commercial pulp. It can also avoid any effects on the pulp that may result from commercial pulping process. Radiata pine, which is the major long fibre resource used in Australia, was chosen as the fibre raw material for this project. In the preliminary experiment, recycled fibres from commercial plaster board were also used. The recycled pulp was washed in a container with a 200 mesh screen on its bottom to remove fines and fillers before it was used for making handsheets and doing fibre analysis. This pulp was a mixture of different fibre resources and only for the purpose of demonstration of the new technique for measuring fibre cross-sectional dimensions directly in paper. It was not used any more in later experiment.

Wood chips of radiata pine, collected from a pulp mill in Australia, were mixed, air dried and stored in a laboratory of Australian Pulp and Paper Institute. These woodchips were cooked using kraft batch pulping process to obtain pulps with different kappa number.

The wood chips selected for this project were cooked in the Australian Pulp and Paper Institute laboratory pulping rig using the kraft cooking process. Pulps with two different kappa number were cooked.

Appendix A.2 Pulping for low kappa pulp

The cooking conditions used for cooking low kappa pulp are presented in TableA.1. The kappa number was tested in accordance with AS201m-86: 1990. Figure A.1 gives the cooking temperature profile used for making the low kappa pulp.

Table A.1. Cooking conditions for low kappa pulp

Wood chips (O.D)	4530g (each batch)
Liquid ratio	8.35
EA	18% (on wood, as Na_2O)
Sulfidity	30%
Yield	45.6%
Kappa No.	30

Figure A.1 Cooking temperature profile

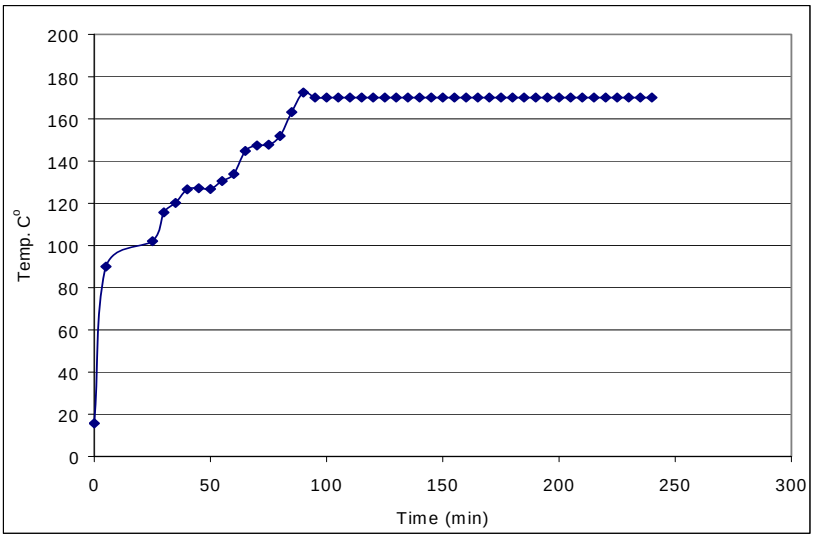

Appendix A.3 Pulping for high kappa pulp

A two-stage cooking process, which simulates the cooking conditions of the pulp mill, was used for making high kappa pulp. The chemicals were split into two equal portions as shown in Table 3.2. Figure A.2 gives the cooking temperature profile used for making the high kappa pulp. This pulp was not used in further experimental work because there were a large quantity of shives in it.

Table A.2 Cooking conditions for high kappa pulp

Wood chips (O.D)	4530g (each batch)
Liquid ratio	9.01
EA	7.5% (on wood, as Na_2O, for initial and second stages)
Sulfidity	30%
Yield	65.8%
Kappa No.	95

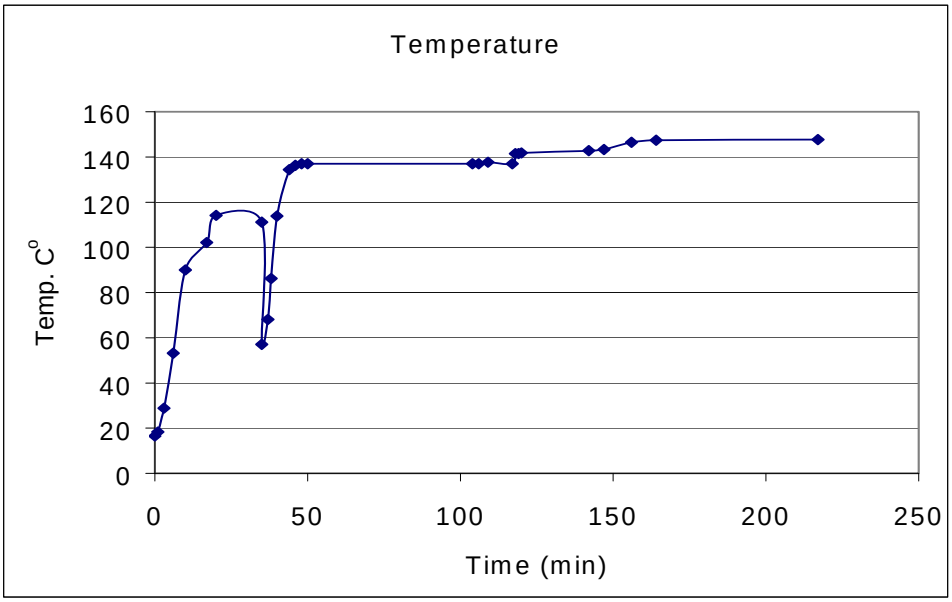

Figure A. 2 Temperature profile for cooking the high kappa pulp

Appendix A.4 Handsheet formation

Handsheets of 60g/m^2 from different pulp fractions were made on a Moving Belt Sheet Former {Xu, 2000 #840}. The handsheets were formed at a very low pulp consistency (0.06%) in order to get good formation of the paper. The size of the square handsheets used is 220mm×220mm. All of the handsheets were dried under restrained in a conditioned room (23 C^o and 50% humidity).

Appendix A.5 Physical property test

- The sheet grammage was tested following AS/NZS 1310. 405s-92: 1991.
- The tensile strength of paper with normal strength was tested using a Lorentzen & Wettre, Alwetron TH1 following AS/NZS 1301.404s-81: 1991.
- The tensile strength of paper made from the unrefined high kappa pulp and the fractionated fractions from this pulp was too low to be able to test using the Lorentzen & Wettre, Alwetron tensile tester. The tensile strength of handsheets from these pulp fractions was tested using an Instron Tensile Tester at a constant elongation of 0.166mm/sec.
- The sheet thickness and apparent density were tested following AS/NZS 1301.426s-94: 1992.
- The zero span tensile strength of paper was tested using a Pulmac Zero Span tester in accordance with the method comes with the machine.
- The scattering coefficient of paper was measured at two different light wavelengths, viz. 557nm and 700nm, using a Colortouch Brightness tester.

Table A.3. Summary of physical properties of handsheets from the low kappa pulp

Sample	Apparent density (kg/m^3)	Tensile index (kN.m/kg)	Zero span tensile index (kN.m/kg)	Scattering coefficient (m^2/kg)	RBA_{N2}	RBA_{sc}
L_0P_1	286	34.5	143.1	23.17	0.21	0.30
L_0P_2	375	37.0	145.7	22.19	0.24	0.33
L_0P_3	509	46.0	148.6	18.87	0.30	0.43
L_0P_4	590	48.0	143.8	16.00	0.36	0.52
L_0P_5	596	50.0	147.3	14.30	0.40	0.57
L_1P_1	338	29.8	145.5	22.56	0.26	0.32
L_1P_2	406	33.8	149.2	20.71	/	0.37
L_1P_3	541	42.8	151.9	18.03	0.31	0.45
L_1P_4	590	47.0	151.4	15.62	0.37	0.53
L_1P_5	613	48.7	147.7	14.32	/	0.57
L_2P_1	373	29.1	141.2	22.31	0.31	0.33
L_2P_2	411	28.7	140.1	20.89	/	0.37
L_2P_3	434	29.5	148.4	19.95	0.35	0.40
L_2P_4	609	43.1	148.2	15.69	/	0.53
L_2P_5	573	37.6	141.5	16.43	0.38	0.50
L_3P_1	370	22.3	154.3	21.25	/	0.36
L_3P_2	425	27.4	142.2	20.12	/	0.39
L_3P_3	473	27.3	158.8	19.05	/	0.42
L_3P_4	621	39.3	165.6	15.35	/	0.54
L_3P_5	632	41.2	158.0	15.28	0.43	0.54
AcP_1	218	21.2	127.5	24.43	0.18	/
AcP_2	322	26.8	131.8	23.90	0.24	/
AcP_3	392	32.7	132.2	22.85	0.32	/
AcP_4	487	42.0	127.9	19.66	0.34	/
AcP_5	651	56.5	134.3	16.34	0.44	/
$RejP_1$	193	9.8	121.4	22.21	0.08	/
$RejP_2$	218	12.8	129.4	22.21	0.18	/

$RejP_3$	306	16.8	136.1	21.51	0.21	/
$RejP_4$	380	22.1	136.2	20.96	0.28	/
$RejP_5$	574	31.4	142.9	16.25	0.36	/

Appendix B Measurement of fibre cross-section on glass slides

Appendix B 1 Slide preparation

A drop of diluted suspension of pre-stained pulp fibres was taken and placed on a clean glass slide. The slide was then put into an oven for 2 minutes to dry the fibres. A few drops of immersion oil were placed on the dried fibres and a cover slip was placed on top. The slide assembly was put into a container where a vacuum was then applied for about 1 hour to expel the air trapped in the fibre and allow the immersion oil thoroughly penetrate into the fibre structure. The slide assembly was then taken out of the container and put another drop of immersion oil on top of the cover slip, and it is ready for analysis in the confocal microscope.

Appendix B 2 Imaging and image analysis

A 60×oil immersion lens was used to capture the image. The cross-sectional images of fibres were scanned perpendicular to the longitudinal axes of the fibres to avoid elongation of the image. The image frame acquired was 50×50 μm with a resolution of 512×512 pixels.

The images of fibre cross-sections were then analyzed using a custom macro written in the software OPTIMAS 6.1. {Xu, 1997 #213} (see Appendix A2). The macro performs the following steps for each fibre to determine the cross-section dimensions:

(1) Locates a fibre in the multi-image file.

(2) Extracts the region of interest (ROI) around the fibre.

(3) Applies filtering operations to the ROI to improve image quality. A variation of the algorithm by {Xu, 1997 #213} was used to reduce the amout of change to the original image associated with using averaging filters and threshold {Conn, 1999 #1136}.

(4) Reduction of the image from 256 bit grey scale image to a binary (black and white) image where the fibre is classed as white and the background black.

(5) Direct measurements of total fibre cross-section area, fibre wall cross-section area, outside fibre perimeter, fibre wall thickness, fibre width and fibre thickness.

Appendix. C Other Measurement

Appendix C.1 Measurement of fibre length

The fibre length of the pulp samples used in this project was measured using a Kajaani FS200 optical fibre length analyser. The Kajaani fibre length analyzer measures single fibres that are drawn from a diluted 0.01% consistency through a narrow capillary, under suction. The fibres pass through a beam of polarized light. These fibres, being birefringent to polarized light, create an interval of birefringence as they pass through. This interval is related to the fibre length of the fibres. This method is fast as it can measure thousands of fibres in a short space of time. Up to 35 length categories can be measured and the software produces statistical information on the fibre distributions.

Table C.1. Summary of fibre length of different pulp fibres measured by Kajaani FS 200

Pulp Fibre			Mathematic length	Weighted length	Fines (<0.1mm)	
					P (%)	W (%)
Low kappa pulp		L_0	1.78	3.14	10.06	0.29
		L_1	1.44	2.53	7.01	0.25
		L_2	1.22	2.10	6.18	0.27
		L_3	1.08	1.80	4.48	0.22
		Accepts (AA)	2.41	3.34	2.59	0.05
		Rejects (RR)	2.22	2.98	1.09	0.03
High kappa	Pine 1		2.16	3.10	2.78	0.06
	Pine 2	Feed	2.28	3.10	2.60	0.06
		Accepts	2.29	3.17	2.23	0.05
		Rejects	2.38	3.42	0.81	0.02

Appendix C.2 Measurement of free surface area of paper

The nitrogen adsorption is an important technique has been used to measure fibre surface area. Haselton [Haselton, 1954 #1079][Haselton, 1955 #1080] is the first to propose the use of gas adsorption as a method of measurement of the surface area and bonded area of papers. After comparing bonded areas calculated by four methods he concluded that a value closest to the true bonded area could be obtained by applying a correction factor to the regular optical values. When nitrogen adsorption is employed for area studies, the surface area accessible to nitrogen molecules of approximately 4.3Å thickness (N2 diameter is 16.3 sq A) is determined. The bonded area in the external and internal portions of fibres is believed to be separated by distances of 4 to 5 Å or less. Therefore, it is reasonable to believe that nitrogen is not absorbed on areas involved in bonding and that adsorption methods may provide an excellent tool for the measurement of the unbonded internal and external area of cellulosic materials. The Brunauer, Emmett and Teller (B.E.T.) theory [Brunauer, 1938 #1082] was used to calculate the volume of gas required to form a monolayer on a given adsorbent. The BET equation is given as:

$$\frac{p/p_0}{v(1-p/p_0)} = \frac{1}{v_m c} + \frac{c-1}{v_m c}(p/p_0) \qquad \textbf{C. 1}$$

where p/p_0 is relative pressure, v is the volume of adsorbed gas (cm^3/g STP) per gram of adsorbent at a certain relative pressure, v_m (cm^3 STP) is the volume of gas per gram sample required to form a monolayer, c is a constant.

The plot of $\frac{p/p_0}{v(1-p/p_0)}$ against p/p_0 should therefore be a straight line with slope $s=(c-1)/v_m c$ and intercept $i=1/v_m c$. Solution of the two simultaneous equations gives v_m and c. Multiplying the number of gas molecules corresponding to v_m by the cross-sectional area of each molecule gives the area of the solid accessible to the gas.

$$A = \frac{Nv_m L}{22{,}400} x10^{-20} \qquad \textbf{C. 2}$$

Where A (m^2/g) is the specific area of the sample, N is Avogadro's number and L (m^2) is the molecular cross-sectional area of the gas absorbed.

The isotherm for this calculation was obtained by the nitrogen adsorption method using a Micromeritics ASAP (Accelerated Surface Area and Porosimetry) 2010. The sample weight for each measurement was about 2g. Each data point of the BET area was the average of two duplicate measurements.

Table C.2. Summary of BET area for handsheets and spray dried fibres

Sample	BET area of sheets (m^2/kg)	BET area of spray dried fibres (m^2/kg)
L_0P_1	716	905
L_0P_2	687	
L_0P_3	632	
L_0P_4	583	
L_0P_5	544	
L_1P_1	683	920
L_1P_3	636	
L_1P_5	582	
L_2P_1	636	921
L_2P_3	602	
L_2P_5	570	
L_3P_5	525	/
AcP_1	873	950
AcP_2	805	
AcP_3	722	
AcP_4	697	
AcP_5	594	

$RejP_1$	872	1064
$RejP_2$	783	
$RejP_3$	754	
$RejP_4$	683	
$RejP_5$	606	

Appendix.D-Macro used in this thesis

Appendix D.1 Optimas macro for measuring mass centre of fibre in paper cross-section

```
/*****************************************************************
Optimas macro for calculating the position of a fibre
in a paper X-section by describing with the mouse.

author: A. Conn
APPI (c) 2000
25-Oct-2000
*****************************************************************/

/* set pixel scale here */
REAL COM_rMicron_per_pixel = 100.0/512.0;

/* Open configuration file */
OpenConfiguration("c:/optimas6/Config/JiHong.cfg");
Calibrate (One_Pixel_per_Micro);

/* clear screen of lines, areas etc. */
/* set ROI to full screen */
SelectFullScreen();
ClearScreen();

/* user creates area to get the centre of mass */
SetExport(ArCenterOfMass,1,TRUE); /* set "To DDE" */
CreateArea(); /* user creates an area */
Extract();        /* get the data object */
CreatePoints(ArCenterOfMass); /* create a point at the center */
```

```
FSP_Centre = ArCenterOfMass*COM_rMicron_per_pixel;

/* write results to screen */
MacroMessage("\nFibre Centre (um) = ",FSP_Centre);

/* write results to center.dat file */
                fh = OpenFile ("c:/optimas6/center.dat");
                PositionFile (fh, 0L, 2); /* position to end of file */
                a = ToText (FSP_Centre): "\n";
                WriteFile (fh, a);
                CloseFile (fh);
/* end with clean up */
ObjectWildCardList("COM_.*", 2);
```

Appendix D.2 Optimas macro for measuring fibre dimensions in paper cross-section

```
/*****************************************************************
Optimas macro for calculating the Area, position and bounding
box of a fibre in a paper X-section via thresholding.

author: A. Conn
APPI (c) 2000
25-Oct-2000
*****************************************************************/

/* set pixel scale here */
REAL FSP_rMicron_per_pixel = 100.0/512.0;

/* Open configuration file */
OpenConfiguration("c:/optimas6/Config/JiHong.cfg");
Calibrate (One_Pixel_per_Micro);
```

```
/* set ROI to full screen */
SelectFullScreen();
ClearScreen();

/* save image to List */
ROItoList(, "Xsection");

/* user selects Region of interest to be processed */
StatusBar = "Select a Region of Interest around a single fibre Xsection ...";
SelectROI();

/* image filtered to improve contrast and smoothness */
Filters( SharpenMed );
MedianFilter(,5);

/* Automatic threshold - Search for threshold in minimum near region of mean  */
BOOLEAN FSP_bLightObjects = TRUE;        /* find light objects          */
INTEGER FSP_iForegroundLimits = 1 : 95;  /* ignore bottom 1% and top 5% */
REAL FSP_rEndPercents =
(REAL)( FSP_iForegroundLimits[0] : (100 - FSP_iForegroundLimits[1]) );
if (FSP_bLightObjects)
FSP_rEndPercents = FSP_rEndPercents[1:0];
Histogram();   /* force update of ArROIHistogram */
REAL FSP_rAutoThresh =
GetAutoThreshold(ArROIHistogram,5,,FSP_rEndPercents,ActiveLuminanceRange);
Threshold( FSP_rAutoThresh[FSP_bLightObjects+1,]); /* set new threshold */

/* fine tune threshold manually */
StatusBar = "Manually fine tune the threshold ...";
Threshold();
```

```
/* Binarise to bitmap */
INTEGER FSP_hInitialBitmap = BitmapCreate();

/* auto create areas */
CreateArea(,,TRUE);  /* clear existing, autocreate areas */

/* user selects area (outside of fibre) of interest */
StatusBar = "Select the outside boundary of the fibre ...";
AutoExtract = FALSE;          /* no auto extract on select */
MultipleMode = FALSE; /* single mode is better for simple selecting */
/* while user does not select one */
while ( !(FSP_hID = Select( , FALSE)) ) /* prevent edit/deletes */
        if ( !Prompt("None selected, try again?") )     /* give more tries */
                pause();          /* if user cancels, stop the macro */

/* reset extract modes */
//AutoExtract = TRUE;          /* no auto extract on select */
//MultipleMode = TRUE; /* single mode is better for simple selecting */

/* clear other Areas */
ClearProtect( FSP_hID, TRUE); /* protect 'em */
ClearScreen();
ClearProtect( FSP_hID, FALSE); /* unprotect 'em */

/* Screen Area to Bitmap  - process to give fibre of interest*/
INTEGER FSP_hAreaBitmap = ActiveImage.BitmapCreate(,,,0);
BitmapProcess (FSP_hAreaBitmap, FSP_hInitialBitmap, 8, );        /* AND Bitmaps */
BitmapProcess (FSP_hAreaBitmap, , 22,);    /* copy result to image */
ClearScreen();

/* calculate Area from white pixels */
Histogram();
```

```
FSP_Area = (REAL)ArROIHistogram[255] *
FSP_rMicron_per_pixel*FSP_rMicron_per_pixel;

/* Create Area and Points */
SetExport( mArBoundingROI,1,TRUE); /* set "To DDE" */
SetExport(mArCenterOfMass,1,TRUE); /* set "To DDE" */
CreateArea(, , TRUE);
MultipleExtractAll (TRUE);
FSP_Centre =  mArCenterOfMass[0..2]* FSP_rMicron_per_pixel;
CreatePoints(mArCenterOfMass[0..2]);

/* set ROI to full screen */
SelectFullScreen();

/* replace original image */
ArithmeticOp("copy", "Xsection");

/* draw BoundingROI around Area and calculate sides*/
ROI = mArBoundingROI[0..4];
FSP_Width = (mArBoundingROI[2] - mArBoundingROI[0])*FSP_rMicron_per_pixel ;
FSP_Height = (mArBoundingROI[1] - mArBoundingROI[3])*FSP_rMicron_per_pixel ;

/* calculate % of fibre area in boundingbox */
FSP_AreaPercent = FSP_Area/FSP_Width/FSP_Height*100.0;

/* write results to screen */
MacroMessage("Fibre Area (um2) = ",FSP_Area,"\nFibre Centre (um) =
",FSP_Centre,"\nWidth (um) = ",FSP_Width,"\nHeight (um) = ",FSP_Height,"\nArea
(%) = ",FSP_AreaPercent);

/* write results to sp.dat file */
                fh = OpenFile ("c:/optimas6/sp.dat");
```

```
        PositionFile (fh, 0L, 2); /* position to end of file */
        a = ToText (FSP_Area) :"\t":ToText (FSP_Centre):"\t":ToText
(FSP_Width):"\t":ToText (FSP_Height):"\t":ToText (FSP_AreaPercent): "\n";
        WriteFile (fh, a);
        CloseFile (fh);


/* end with clean up */
ObjectWildCardList("FSP_.*", 2);
```

Appendix D.3 Optimas macro for calculating major axis bounding box

```
/*****************************************************************
Optimas macro for calculating the Area, position and bounding
box of a fibre in a paper X-section via thresholding.

author: A. Conn and Jihong He
APPI (c) 2001
25-July-2001
*****************************************************************/

/* set pixel scale here */
REAL FSP_rMicron_per_pixel = 100.0/512.0;

/* Open configuration file */
OpenConfiguration("c:/optimas6/Config/JiHong.cfg");
Calibrate (One_Pixel_per_Micro);

/* set ROI to full screen */
SelectFullScreen();
ClearScreen();
```

```
/* save image to List */
ROItoList(, "Xsection");

/* user selects Region of interest to be processed */
StatusBar = "Select a Region of Interest around a single fibre Xsection ...";
SelectROI();

/* image filtered to improve contrast and smoothness */
Filters( SharpenMed );
MedianFilter(,5);

/* Automatic threshold - Search for threshold in minimum near region of mean  */
BOOLEAN FSP_bLightObjects = TRUE;        /* find light objects          */
INTEGER FSP_iForegroundLimits = 1 : 95;  /* ignore bottom 1% and top 5% */
REAL FSP_rEndPercents =
(REAL)( FSP_iForegroundLimits[0] : (100 - FSP_iForegroundLimits[1]) );
if (FSP_bLightObjects)
FSP_rEndPercents = FSP_rEndPercents[1:0];
Histogram();   /* force update of ArROIHistogram */
REAL FSP_rAutoThresh =
GetAutoThreshold(ArROIHistogram,5,,FSP_rEndPercents,ActiveLuminanceRange);
Threshold( FSP_rAutoThresh[FSP_bLightObjects+1,]); /* set new threshold */

/* fine tune threshold manually */
StatusBar = "Manually fine tune the threshold ...";
Threshold();

/* Binarise to bitmap */
INTEGER FSP_hInitialBitmap = BitmapCreate();

/* auto create areas */
```

```
CreateArea(,,TRUE);  /* clear existing, autocreate areas */

/* user selects area (outside of fibre) of interest */
StatusBar = "Select the outside boundary of the fibre ...";
AutoExtract = FALSE;          /* no auto extract on select */
MultipleMode = FALSE; /* single mode is better for simple selecting */
/* while user does not select one */
while ( !(FSP_hID = Select( , FALSE)) ) /* prevent edit/deletes */
        if ( !Prompt("None selected, try again?") )    /* give more tries */
                pause();          /* if user cancels, stop the macro */

/* reset extract modes */
//AutoExtract = TRUE;          /* no auto extract on select */
//MultipleMode = TRUE; /* single mode is better for simple selecting */

/* clear other Areas */
ClearProtect( FSP_hID, TRUE); /* protect 'em */
ClearScreen();
ClearProtect( FSP_hID, FALSE); /* unprotect 'em */

SetExport(mArBoundingBox,1,TRUE); /* set "To DDE" */
SetExport(mArMajorAxisAngle,1,TRUE); /* set "To DDE" */
MultipleExtractAll(TRUE); /* get the data object */
CreateArea(mArBoundingBox);

ClearProtect( FSP_hID, TRUE); /* protect 'em */

Box = mArBoundingBox[0..7];
Box_Width = Sqrt(Pow((ArBoundingBox[2] -
ArBoundingBox[0]),2)+Pow((ArBoundingBox[3] -
ArBoundingBox[1]),2))*FSP_rMicron_per_pixel ;
```

```
Box_Height = Sqrt(Pow((ArBoundingBox[0] -
ArBoundingBox[6]),2)+Pow((ArBoundingBox[7] -
ArBoundingBox[1]),2))*FSP_rMicron_per_pixel ;

/* clear other Areas */
ClearProtect( FSP_hID, TRUE); /* protect 'em */
ClearScreen();
ClearProtect( FSP_hID, FALSE); /* unprotect 'em */

/* Screen Area to Bitmap  - process to give fibre of interest*/
INTEGER FSP_hAreaBitmap = ActiveImage.BitmapCreate(,,,,0);
BitmapProcess (FSP_hAreaBitmap, FSP_hInitialBitmap, 8, );        /* AND Bitmaps */
BitmapProcess (FSP_hAreaBitmap, , 22,);    /* copy result to image */
ClearScreen();

/* calculate Area from white pixels */
Histogram();
FSP_Area = (REAL)ArROIHistogram[255] *
FSP_rMicron_per_pixel*FSP_rMicron_per_pixel;

/* Create Area and Points */
SetExport( mArBoundingROI,1,TRUE); /* set "To DDE" */
SetExport(mArCenterOfMass,1,TRUE); /* set "To DDE" */
CreateArea(, , TRUE);
MultipleExtractAll (TRUE);
FSP_Centre =  mArCenterOfMass[0..2]* FSP_rMicron_per_pixel;
CreatePoints(mArCenterOfMass[0..2]);



/* set ROI to full screen */
SelectFullScreen();
```

```
/* replace original image */
ArithmeticOp("copy", "Xsection");


/* draw BoundingROI around Area and calculate sides*/
ROI = mArBoundingROI[0..4];
FSP_Width = (mArBoundingROI[2] - mArBoundingROI[0])*FSP_rMicron_per_pixel ;
FSP_Height = (mArBoundingROI[1] - mArBoundingROI[3])*FSP_rMicron_per_pixel ;

/* calculate % of fibre area in boundingbox */
FSP_AreaPercent = FSP_Area/FSP_Width/FSP_Height*100.0;
Box_AreaPercent = FSP_Area/Box_Width/Box_Height*100.0;


/* write results to screen */
MacroMessage("Fibre Area (um2) = ",FSP_Area,"\nFibre Centre (um) =
",FSP_Centre,"\nWidth (um) = ",FSP_Width,"\nHeight (um) = ",FSP_Height,"\nArea
(%) = ",FSP_AreaPercent,"\nBoxWidth (um) = ",Box_Width,"\nBoxHeight (um) =
",Box_Height,"\nBoxArea (%) = ",Box_AreaPercent,"\ MajorAxisAngle (degree) =
",ArMajorAxisAngle);

/* write results to sp.dat file */
                fh = OpenFile ("c:/optimas6/sp.dat");
                PositionFile (fh, 0L, 2); /* position to end of file */
                a = ToText (FSP_Area) :"\t":ToText (FSP_Centre):"\t":ToText
(FSP_Width):"\t":ToText (FSP_Height):"\t":ToText (FSP_AreaPercent):"\t": ToText
(Box_Width):"\t": ToText (Box_Height):"\t": ToText (Box_AreaPercent):"\t":ToText
(ArMajorAxisAngle):"\n";
                WriteFile (fh, a);
                CloseFile (fh);
```

```
/* end with clean up */
ObjectWildCardList("FSP_.*", 2);
```

Appendix D.4 MatLab macro for simulation of load distribution along the fibre with bond breakage

```
%Evaluate n contacts direct stress transfer
clear

syms  d1 d2 d3 d4 d5 d6 d7 d8 d9 d10 d11 d12 d13 d14 d15 d16 d17 d18 d19 d20 d21 D
sum1;
syms  d22 d23 d24 d25 d26 d27 d28 d29 d30 d31 d32 d33 d34 d35 d36 d37 d38 d39 d40
d41 d42 d43 d44 d45 d46 d47 d48 d49 d50 d51 d52 d53 d54 d55 d56 d57 d58 d59 d60;
syms d61 d62 d64 d64 d65 d66 d67 d68 d69 d70
add=0  %Counter for separating different simulation sets in excel spreadsheet. Later to
set to no. of fibres+2
bdd=0 %conter for r position
Favmax=0 %max average load
%Sample identifiers and comments
SampleID='SL0'
Comment='Increase strain, remove broken bonds random angle and position. Force=-
2(d/lc)EAcos2th'
nsimulations=2 % no. of separate simulations

%constants for calculation
fibrelength=1572;
b=48.4;
c=1.62; %Weibull distribution parameters

lc=5*b; %length before crossing fibres bonded into matrix
```

```
E=40*10^9; %Fibre elastic modulus
A=200*10^-12; %Fibre cross-sectional area
halfc=0.52; %Fraction of partial contacts
Width=31.0e-6; %fibre width
sbs=3e6; %shear bond strength per unit area
R=1.35; %Fractional spreading on contact
spread=ddeinit('excel','data.xls'); %Write the calculation constants to the data file
ddepoke(spread,'r1c1',Comment);
ddepoke(spread,'r2c1','Half fibre length (microns)');
ddepoke(spread,'r3c1',fibrelength);
ddepoke(spread,'r4c1','Crossing fibre length until locked in matrix');
ddepoke(spread,'r5c1',lc);
ddepoke(spread,'r6c1',strcat('Sample: ',SampleID));
ddepoke(spread,'r7c1','Weibull contact distribution parameters');
ddepoke(spread,'r8c1',b);
ddepoke(spread,'r8c2',c);
ddepoke(spread,'r9c1','Shear bond strength per unit area');
ddepoke(spread,'r10c1',sbs);

ddepoke(spread,'r2c6','Fibre elastic modulus');
ddepoke(spread,'r3c6',E);
ddepoke(spread,'r4c6','Fibre cross-section area');
ddepoke(spread,'r5c6',A);
ddepoke(spread,'r6c6','Fibre width');
ddepoke(spread,'r7c6',Width);
ddepoke(spread,'r8c6','Percentage of fractional contacts');
ddepoke(spread,'r9c6',halfc);
ddepoke(spread,'r2c11','Spreading of bonded area');
ddepoke(spread,'r3c11',R);


%Generate fibres with random positions, angles and full or partial contacts
```

```
%Generate positions from Weibull distributions
x(1)=b*(-log(1-rand))^(1/c)/2; %Generates the first fibre
%Division by 2 as calculating from middle of fibre
sum2=x(1);
for j=2:60;
  sum2=sum2+b*(-log(1-rand))^(1/c);
  if sum2<fibrelength; % Generate fibre until latest fibre exceeds fibre length, then stop. i
is total fibre no.
        x(j)=sum2;
    i=j;
  end;
end;
%Generate random anglees
for j=1:i;
  th(j)=pi/2-asin(rand);
end;

%Generate full or partial contacts
for j=1:i;
  if rand<halfc;
    bondstrength(j)=0.5*R*Width^2/sin(th(j))*sbs;
  else;
    bondstrength(j)=R*Width^2/sin(th(j))*sbs;
  end;
end;

for j=1:i
  bondbreak(j)=0;
end

count=1
interval=0.001;
```

```
eps=0;

while eps<0.013; %network/matrix strain
eps

  'Simulation No.:',count
  clear  Dr F Fseg D sum1 sum2
  D=[d1 d2 d3 d4 d5 d6 d7 d8 d9 d10 d11 d12 d13 d14 d15 d16 d17 d18 d19 d20 d21
d22 d23 d24 d25 d26 d27 d28 d29 d30 d31 d32 d33 d34 d35 d36 d37 d38 d39 d40 d41
d42 d43 d44 d45 d46 d47 d48 d49 d50 d51 d52 d53 d54 d55 d56 d57 d58 d59 d60 d61
d62 d64 d64 d65 d66 d67 d68 d69 d70];

for j=1:i;
  fv(j)=-2/lc*cos(th(j))^2; %multiply these values by displacement to get force
end;

for j=i-1:-1:1;
    sum1=0;
  for k=i:-1:j+1;
    sum1=vpa(sum1+fv(k)*D(k));
  end;
  D(j)=vpa(D(j+1)+(x(j+1)-x(j))*(eps-sum1));
  end

sum1=0;

for j=1:i;
  sum1=vpa(sum1+x(j)*fv(j)*D(j));
end;

z=vpa(sum1-eps*x(i)-D(i));
```

```
y=solve(z,'D(i)');
double(y)
Dr(i)=double(y);
for j=i-1:-1:1;
    sum2=0;
  for k=i:-1:j+1;
    sum2=sum2+fv(k)*Dr(k);
  end;
  Dr(j)=Dr(j+1)+(x(j+1)-x(j))*(eps-sum2);
end;
%resubstitution to obtain expressions for the D(j) Dr is now the real expression

for j=1:i;
  F(j)=Dr(j)*fv(j)*E*A;
end;
%Calculate the forces applied at each contact point.



for j=1:i;
   sum2=0;
  for k=j:i;
    sum2=F(k)+sum2;
  end;
  Fseg(j)=sum2;
end;
%Calculate the force applied to each segment

%'check of calculation'
Fseg(1)*x(1)/E/A-eps*x(1);
Dr(1);
```

```
fibrestrain=double((eps*x(i)+Dr(i))/fibrelength);
Fav=fibrestrain*E*A;


if Fav>Favmax
   Favmax=Fav;
end
Favmax;
r=Fseg(1)/fibrestrain/E/A;
%r calculated from maximum load in first segment divided by average load along whole
fibre.


xr=rot90(x,3);
thr=rot90(th,3);
Drr=rot90(Dr,3);
bsr=rot90(bondstrength,3);
Fr=rot90(F,3);
Fsegr=rot90(Fseg,3);
Datamat=[xr thr bsr Drr Fr Fsegr];


%Write the results of the simulation to the Excel spreadsheet
ddepoke(spread,strcat('r',num2str(11+add),'c',num2str(11)),'External matrix strain');
ddepoke(spread,strcat('r',num2str(12+add),'c',num2str(11)),eps);

ddepoke(spread,strcat('r',num2str(13+add),'c',num2str(11)),'Check of calculation');
ddepoke(spread,strcat('r',num2str(14+add),'c',num2str(11)),'Displacement of first contact,
d1');
ddepoke(spread,strcat('r',num2str(15+add),'c',num2str(11)),double(Dr(1)));
ddepoke(spread,strcat('r',num2str(16+add),'c',num2str(11)),'Total force in 1st segment');
```

```
ddepoke(spread,strcat('r',num2str(17+add),'c',num2str(11)),Fseg(1));
ddepoke(spread,strcat('r',num2str(18+add),'c',num2str(11)),'Displacement due to force');
ddepoke(spread,strcat('r',num2str(19+add),'c',num2str(11)),Fseg(1)*x(1)/E/A);
ddepoke(spread,strcat('r',num2str(20+add),'c',num2str(11)),'d1=Force-segment1*x1-
globalstrain*x1');
ddepoke(spread,strcat('r',num2str(21+add),'c',num2str(11)),Fseg(1)*x(1)/E/A-eps*x(1));
ddepoke(spread,strcat('r',num2str(22+add),'c',num2str(11)),'Difference between two
calculations of d1');
ddepoke(spread,strcat('r',num2str(23+add),'c',num2str(11)),double(Dr(1))-
(Fseg(1)*x(1)/E/A-eps*x(1)));

ddepoke(spread,strcat('r',num2str(25+add),'c',num2str(11)),'r: cald from max load in first
segment divided by avg. load along whole fibre');
ddepoke(spread,strcat('r',num2str(26+add),'c',num2str(11)),r);
ddepoke(spread,strcat('r',num2str(27+add),'c',num2str(11)),'Fibre strain');
ddepoke(spread,strcat('r',num2str(28+add),'c',num2str(11)),fibrestrain);

ddepoke(spread,strcat('r',num2str(11+add),'c',num2str(3)),strcat('Simulation no.:
',num2str(count)));
ddepoke(spread,strcat('r',num2str(12+add),'c',num2str(3)),'Contact position');
ddepoke(spread,strcat('r',num2str(12+add),'c',num2str(4)),'angle');
ddepoke(spread,strcat('r',num2str(12+add),'c',num2str(5)),'Bond strength');
ddepoke(spread,strcat('r',num2str(12+add),'c',num2str(6)),'Displacements');
ddepoke(spread,strcat('r',num2str(12+add),'c',num2str(7)),'force at contact');
ddepoke(spread,strcat('r',num2str(12+add),'c',num2str(8)),'Force in segment');
ddepoke(spread,strcat('r',num2str(13+add),'c',num2str(3),':r',num2str(i+13+add),'c',num2s
tr(8)),Datamat);
ddepoke(spread,'r10c20','r');
ddepoke(spread,'r10c21','Fav');
ddepoke(spread,'r10c22','Favmax');
ddepoke(spread,'r10c23','strain');
ddepoke(spread,'r10c24','Simulation No.');
```

```
broken=0
%Check for broken fibres
for j=1:i;
  if bondstrength(j)>0;
    if bondstrength(j)<F(j);
      bondbreak(j)=1;
      th(j)=acos(0);
       bondstrength(j)=0;
       broken=1;
    end
  end
end
bondbreakr=rot90(bondbreak,3);
ddepoke(spread,strcat('r',num2str(12+add),'c',num2str(9)),'Bonds broken');
ddepoke(spread,strcat('r',num2str(13+add),'c',num2str(9),':r',num2str(i+13+add),'c',num2s
tr(9)),bondbreakr);
ddepoke(spread,strcat('r',num2str(11+bdd),'c',num2str(20)),r);
ddepoke(spread,strcat('r',num2str(11+bdd),'c',num2str(21)),Fav);
ddepoke(spread,strcat('r',num2str(11+bdd),'c',num2str(22)),Favmax);
ddepoke(spread,strcat('r',num2str(11+bdd),'c',num2str(23)),eps);
ddepoke(spread,strcat('r',num2str(11+bdd),'c',num2str(24)),count);


if broken==0
  eps=eps+interval
end
if Fav<0.5*Favmax
eps=0.013
end
broken=0
```

```
if i<19 %calculates how much to displace write statements so each simulation is
separated in excel
   add=22+add;
else
   add=i+3+add;
end

count=count+1;
bdd=bdd+1;

end
end
```

Appendix E. Direct Load Transfer Theory

An analytical solution for the load distribution in a fibre in a network

Warren Batchelor

Australian Pulp and Paper Institute, Department of Chemical Engineering, PO Box 36, Monash University, 3800 Victoria Australia

Abstract

A new method is presented which allows the load-distribution in one fibre in a loaded network to be analytically calculated. Only the case of a fibre oriented in the direction of the applied load is considered. The method assumes that the force applied to the fibre at a fibre-fibre contact (a crossing point) arises from the displacement of the fibre crossings compared to the external strain field. This paper shows that the displacements at all the contacts can be expressed in terms of the displacement at the final contact and consequently how this can be used to calculate the displacement at the final crossing point. An expression for force transfer at a contact is developed, which assumes that force is transferred into the fibre of interest by direct axial loading, rather than shear. Each crossing fibre is assumed to be rigidly connected into the surrounding matrix after a given distance. The expression for force and the new analytical solution was used to derive force distributions along a fibre for a number of examples. The calculated force distribution along the fibre is sensitive to the exact geometry, for example, the number, location, orientation of the set of crossing fibres.

Introduction

An important factor affecting the mechanical properties of a fibre network under load is the stress-distribution along the length of a fibre in a network. This distribution has been solved analytically only for the relatively simple case of the shear lag model [1-3], where all of the fibres are assumed to be the same and to cross each other at 90^{o}. The force on the fibre from a contact is assumed to be proportional to the difference between the local displacement of the contact point and the overall displacement due to the applied strain.

However, the stress-distribution along a fibre has not been solved analytically for a network with distributions of fibre properties and orientation, although it is possible to calculate using finite element models. The problem is difficult to analyse because force can be applied at any or all fibre crossings and any force both produces and is caused by displacement relative to the applied strain. The force distribution along the fibre will also depend on the exact geometry of the crossing fibres

This purpose of this paper is to present an analytical solution to this problem. A simple model of stress transfer at a fibre crossing is also developed and the model and the analytical solution will be combined to calculate some stress-distributions for some specific examples.

Theory Part 1 Stress Distribution along a fibre in a network

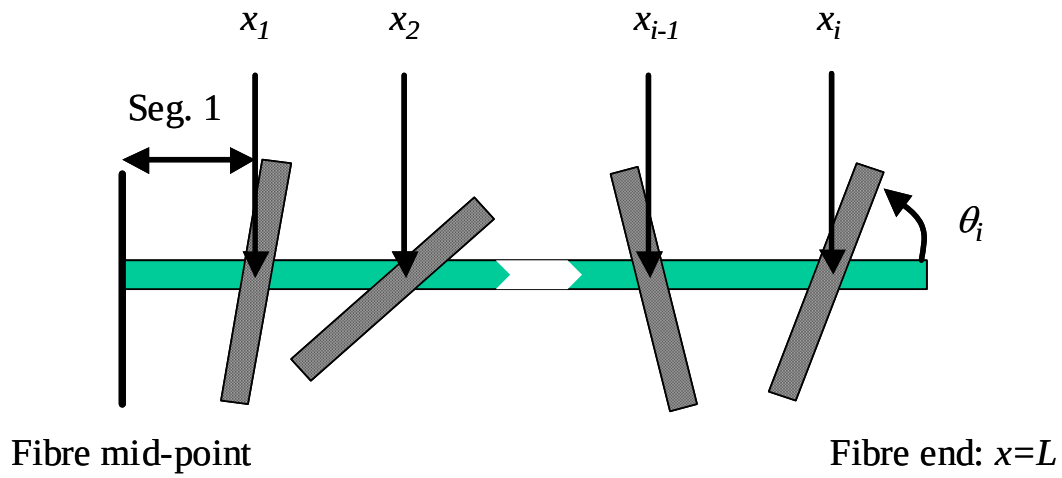

Figure 1 Unstrained half fibre of length, L, with i crossing fibres.

Figure 1 shows half of a fibre, which is connected to a fibre network by i crossing fibres. The centre of the fibre at $x=0$ set as the reference point. A strain of ε is applied to external network in the direction of the fibre axis. It is assumed that force is transferred into the fibre by displacements of the fibre-crossings from their equilibrium position for the applied network strain. The displacement of the j^{th} crossing fibre is designated δ_j. The forces that develop at the j^{th} crossing are some function of δ_j and the angle of the crossing fibre to the fibre axis, θ_j.

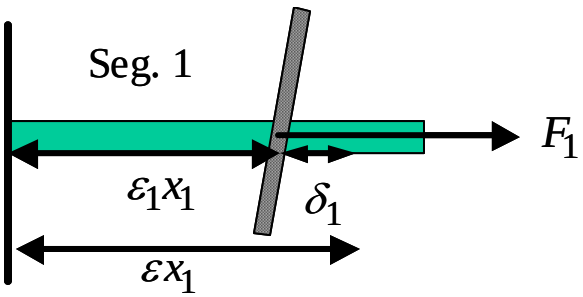

Figure 2. Displacement of crossing point from equilibrium position in the applied global strain field.

The idea is illustrated in Fig. 2, which shows segment 1 of the loaded fibre from Fig. 1. This has a strain in the first segment of ε_1 which differs from the network strain, ε, displacing the crossing point from the equilibrium position by $\delta_1 = (\varepsilon_1 - \varepsilon) x_1$. The force which has produced the strain ε_1 is the sum of the forces developed at all i crossing fibres and therefore

$$\delta_1 = \frac{1}{EA} x_1 \sum_{j=1}^{j=i} F_j - \varepsilon x_1 \qquad 1$$

where E and A are the elastic modulus and cross-sectional area, respectively, of the fibre. The forces that develop each contact point are some function of δ and the angle of the crossing fibre to the fibre axis, θ.

The displacement at the second contact is

$$\delta_2 = \frac{1}{EA}\left(x_1 \sum_{j=1}^{j=i} F_j + (x_2 - x_1) \sum_{j=2}^{j=i} F_j \right) - \varepsilon x_1 - \varepsilon (x_2 - x_1) \qquad 2$$

which simplifies to

$$\delta_2 = \frac{1}{EA}\left(x_1 F_1 + x_2 \sum_{j=2}^{j=i} F_j \right) - \varepsilon x_2 \qquad 3$$

Extending this process it can be shown that for n^{th} and $n-1^{\text{th}}$ contacts that

$$\delta_n = \frac{1}{EA}\left(\sum_{j=1}^{j=n-1} x_j F_j + x_n \sum_{j=n}^{j=i} F_j \right) - \varepsilon x_n \qquad 4$$

$$\delta_{n-1} = \frac{1}{EA}\left(\sum_{j=1}^{j=n-2} x_j F_j + x_n \sum_{j=n-1}^{j=i} F_j \right) - \varepsilon x_{n-1} \qquad 5$$

and eqn. 5 can be rewritten as

$$\delta_{n-1} = \frac{1}{EA}\left(\sum_{j=1}^{j=n-1} x_j F_j + x_n \sum_{j=n}^{j=i} F_j \right) - \varepsilon x_n + \left(x_n - x_{n-1} \right)\left(\varepsilon - \frac{1}{EA} \sum_{j=n}^{j=i} F_j \right) \qquad 6$$

or

$$\delta_{n-1} = \delta_n + \left(x_n - x_{n-1} \right)\left(\varepsilon - \frac{1}{EA} \sum_{j=n}^{j=i} F_j \right) \qquad 7$$

Thus the displacement at each contact can be expressed in terms of the forces (which in turn are a function of the displacements) developed at all the contacts further along the fibre towards the end as well as the displacement of the next contact along the fibre. Thus δ_{i-1}, can be written in terms of δ_i; δ_{i-2} can be written in terms of δ_{i-1} and thus in terms of δ_i, and a similar chain can be developed such that each of the displacement can be expressed in terms of δ_i, the displacement at the final crossing nearest the fibre end. The displacements at all the fibre crossings can be expressed in terms of δ_i and as δ_i is given by

$$\delta_i = \frac{1}{EA}\left(\sum_{j=1}^{j=i} x_j F_j \right) - \varepsilon x_i \qquad 8$$

then it is possible to solve this equation to determine δ_i and thus to uniquely determine the displacements at all crossings, provided that F can be expressed as a function of displacement.

In the next section, a simple expression for force is developed assuming direct axial stress transfer from the crossing fibres. This expression and eqns 7 and 8 are then used to calculate stress distributions for several examples of sets of crossing fibres.

However, it should be emphasised that equations 6 and 7 apply to any mode of stress transfer and the work that follows is included to illustrate how the solution is applied.

Theory Part 2- A model for force transfer at fibre contacts

The model assumes that stress transfer takes place directly from direct transfer of axial loads in the crossing fibres and that the crossing fibre has a distance, l_c, before it is rigidly bonded into the surrounding network or matrix. Figure 3 shows such a single fibre contact, before and after the matrix is strained. For this analysis, the reference point, $x = 0$, is set at the position of the crossing point in the unstrained system.

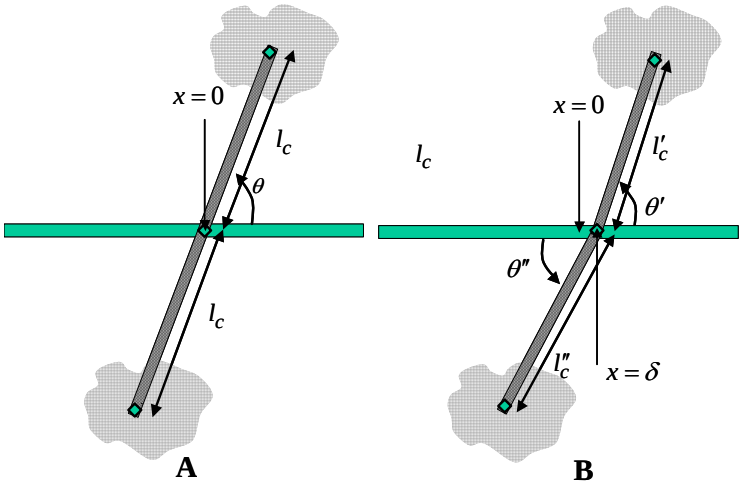

Figure 3 Part A: A crossing fibre, with a crossing angle of θ and a distance of l_c until it is firmly bonded into the surrounding matrix. The point at which the fibre crosses is $x = 0$. Part B: The same fibre crossing after the matrix has been strained by ε and the crossing point has also moved a distance of δ from $x = 0$.

A network strain of ε, in the direction of the fibre axis is applied to the crossing fibre's contacts in the surrounding matrix. To keep the calculation simple, it is assumed that the matrix is rigid, except under the application of the external strain, ε.

This means that loads developed in the crossing fibre will not cause the anchor points in the matrix to move.

Under the matrix strain of ε, the RHS and LHS contacts into the matrix are displaced by $+\varepsilon l_c \cos\theta$ and $-\varepsilon l_c \cos\theta$, respectively. As a result of other strains in the fibre of interest, the contact point is also displaced by δ. Following this displacement, the length of the RHS and LHS of the crossing fibre are not the same. If the new lengths are denoted l_c' (RHS) and l_c'' (LHS), then

$$l_c'^2 = l_c^2 \sin^2(\theta) + \left(l_c \cos(\theta)(1+\varepsilon) + \delta\right)^2 \qquad 9$$

$$l_c''^2 = l_c^2 \sin^2(\theta) + \left(l_c \cos(\theta)(1+\varepsilon) - \delta\right)^2 \qquad 10$$

and the forces in the two crossing fibre segments are $F_a' = (l_c'/l_c - 1)E_c A_c$ and $F_a'' = (l_c''/l_c - 1)E_c$, where E_c is the modulus of the crossing fibre and A_c is the cross-sectional area. The net force along the fibre of interest is

$F = F_a' \cos(\theta') - F_a'' \cos(\theta'')$ which is equal to

$$F = -2E_c A_c \cos^2(\theta)\delta / l_c \qquad 11$$

provided that $\varepsilon << 1$ and $\delta << l_c$. This equation does not imply that the crossing fibre is not under load if $\delta = 0$. Rather, both segments are under load, but if $\delta = 0$, then the two forces exactly cancel each other out.

Calculation of sample stress distributions

To illustrate the application of eqns. 7 and 8, the equations for three fibre crossings will now be given in combination with the force expression given by eqn. 11. To

simplify these equations it is assumed that the fibre and the crossing fibres are identical and thus $E_c = E$ and $A_c = A$. The three fibres crossing the fibre of interest do so at positions x_1, x_2 and x_3 and at angles θ_1, θ_2 and θ_3, respectively. The relevant equations then become:

$$\delta_2 = \delta_3 + (x_3 - x_2)\left(\varepsilon + 2(\delta_3 / l_c)\cos^2\theta_3\right) \quad 12$$

$$\delta_1 = \delta_2 + (x_2 - x_1)\left(\varepsilon + 2(\delta_3 / l_c)\cos^2\theta_3 + 2(\delta_2 / l_c)\cos^2\theta_2\right) \quad 13$$

$$\delta_3 = 2x_3(\delta_3 / l_c)\cos^2\theta_3 + 2x_2(\delta_2 / l_c)\cos^2\theta_2 + 2x_1(\delta_1 / l_c)\cos^2\theta_1 - \varepsilon x_3 \quad 14$$

and both δ_1 and δ_2 can ultimately expressed in terms of δ_3 and eqn. 14 is solvable to obtain δ_3 in terms of x_1, x_2, x_3, θ_1, θ_2 and θ_3. Therefore the displacement at each contact (and the corresponding force) can be calculated.

Figure 5 shows calculated force distributions for several cases for a half fibre with 10 fibre crossings. In each case the following constants were used for the calculation: $E = E_c$=30 GPa, $A = A_c$ =200x10^{-12}m^2, a half fibre length, L, of 1000 μm and a network strain of 3%. Also common to each case is that the 10 contacts are spaced 100μm apart at 100, 200, 300…1000 μm from the fibre mid-point. In each example in Figure 5, the load is plotted at the mid-point between contacts. Straight lines link the points from the same series as a guide to the eye, although these are not strictly correct, as the load actually changes in steps at each fibre crossing.

In Case 1, l_c =300 μm and the angle of fibre crossing is 57.3^o, which is the average crossing angle for randomly distributed fibre network. The calculated average strain along the fibre is 2.45%. The fibre would have a uniform strain equal to the external

matrix strain of 3% if the entire length of the fibre had a tensile load of 0.18N. It can be seen from Figure 5, that the force on the fibre only approaches this load near the middle of the fibre ($x = 0$) and that the load imparted to the fibre by each contact smoothly increases, the further the crossing fibre is from the centre. Case 2, uses the same conditions as above, except that l_c = 150 μm. The overall calculated strain in the fibre of interest has then risen to 2.65% and the cumulative force at each crossing point is higher than in Case 1, although the overall shape of the distribution is the same. The shape of the distribution is also similar to what would be produced by the shear-lag model.

Case 3, uses the same conditions as case 1, except that the fibre angles are varied and for the fibres 1-10 are [57.3^o, 57.3^o, 57.3^o, 90^o, 57.3^o, 57.3^o, 10^o, 80^o, 90^o]. The calculated overall strain in the fibre is then 2.12%. Figure 5 shows that over half of the final maximum load in the fibre is applied at the 8th fibre crossing. Case 4 is then calculated by assuming that this stress concentration has caused this bond to break. The overall calculated strain has then fallen to 1.62%. It can be seen that with the 8th fibre crossing removed, the other load-bearing crossing fibres have partially compensated for the missing fibre as the load applied at each of these other crossings has increased. The data calculated for case 3 and 4 shows that if the fibre properties and orientations are randomly distributed, then the development of stress will be quite non-uniform.

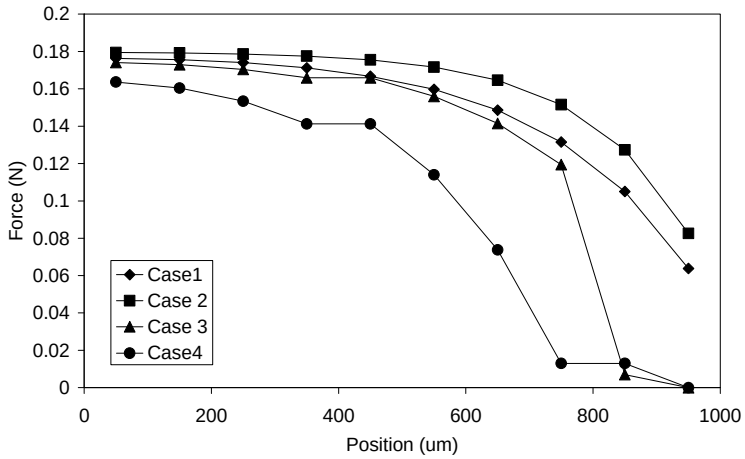

Figure 4. Calculated force distributions along the fibre length

Conclusions

A new solution has been developed which allows the displacements, compared to the applied strain field, at different bonds along a fibre of interest to be all expressed in terms of the displacement at the last bond before the end of the fibre. This allows, provided force is known as a function of the displacement, the displacement of the final crossing to be calculated, from which the force distribution along the whole length of the fibre can be determined. A model for direct force transfer from axial loading of the crossing fibre was also developed. The crossing fibres in this model were connected to a matrix, which was assumed to be rigid except for the strain due to the applied stress. The new method was used to derive the stress distribution along the length of the fibre of interest for several cases. It was shown that the exact geometry of the set of crossing fibres has a strong influence on the calculated stress field.

References

[1] COX, H.L., "The Elasticity and Strength of Paper and Other Fibrous Materials", *British Journal of Applied Physics*, 3(3):72-79 (1952).

[2] PAGE, D.H. and SETH, R.S., "The Elastic Modulus of Paper Ii. The Importance of Fiber Modulus, Bonding, and Fiber Length", *Tappi*, 63(6):113-116 (1980).

[3] ASTROM, J., SAARINEN, S., NISKANEN, K., and KURKIJARVI, J., "Microscopic Mechanics of Fiber Networks", *Journal of Applied Physics*, 75(5):2383-2392 (1994).